Tampere University

Paula Puistola

NOVEL BIOINK DESIGN FOR 3D BIOPRINTING OF HUMAN PLURIPOTENT STEM CELL DERIVED CORNEAL EPITHELIAL CELLS

Master of Science Thesis
Faculty of Medicine and Health Technology
September 2020

ABSTRACT

Paula Puistola: Novel bioink design for 3D bioprinting of human pluripotent stem cell derived corneal epithelial cells
Master of Science Thesis
Tampere University
Degree Programme in Bioengineering, MSc (Tech)
September 2020
Examiners: Professor Minna Kellomäki and PhD Anni Mörö

Objectives: The correct function and structure of cornea is essential for vision. Cornea is maintained by limbal epithelial stem cells (LESCs), and the lack of functional LESCs in a disease called limbal stem cell deficiency (LSCD) can lead to blindness. The traditional treatment for corneal blindness is a corneal transplant. However, there is a severe shortage of cornea donors and the transplants lack functional LESCs. Thus, a corneal transplant cannot be used as a treatment for LSCD. The field of tissue engineering aims to restore, replace and regenerate damaged native tissues, such as develop artificial corneas. Yet, the conventional methods fail to mimic the native-like cellular variety and specific microstructure. Moreover, they lack the ability for precise positioning of cells and materials into a three-dimensional (3D) environment. 3D bioprinting offers a possibility to overcome these issues due to its better control, accuracy and customizability. The main challenge in 3D bioprinting is the lack of bioprintable, cell-laden bioinks with suitable properties to guide the desired cell behaviour. The aim in this thesis was to design and optimize a novel bioink and bioprinting conditions in order to 3D bioprint human pluripotent stem cell (hPSC) -derived corneal epithelium mimicking tissue.

Materials and methods: A novel bioink composition was done combining human and recombinant sourced extracellular matrix proteins. The native human cornea was used as a source of inspiration in the development. Moreover, two crosslinking strategies were combined. First, the printability of the bioink and the printing parameters for extrusion-based bioprinting were tested and determined. The hPSC-derived LESCs (hPSC-LESCs) were produced, and the bioprinting conditions, including the ultra violet (UV) light exposure and printing substrate, were optimized. The response to different bioprinting conditions and behaviour of the bioprinted hPSC-LESCs were analysed with phase contrast microscopy, proliferation and live/dead assays, and immunofluorescence analysis. Finally, the bioink was characterized by analysing its swelling behaviour, transparency and rheological properties.

Results and conclusions: Overall, the developed bioink was well extrudable and had good transparency. The bioink supported the proliferation and maturation of the hPSC-LESCs. UV exposure did not decrease the cell viability (> 88%), however, it was observed to affect the crosslinking density and the stiffness of the material considerably. The bioprinted hPSC-LESCs preferred softer, highly viscous material, and bioprinting without UV exposure resulted in the most stratified epithelium. From the printing substrates, Matrigel™ coating provided the best results in regards to the cell proliferation and adhesion. However, due to the softness of Matrigel™, the bioprinted epithelium showed shrinkage leading to partially ruptured epithelium. Therefore, further optimization of the printing substrate is required. Furthermore, due to the low crosslinking degree of the bioink without UV, rheological measurements were challenging to perform, and require further optimization in the future. This was the first study in which the stratification of hPSC-LESCs was observed after extrusion-based 3D bioprinting. Thus, the novel bioink showed great potential for 3D bioprinting corneal epithelium mimicking structures and should be further studied in ocular surface reconstruction.

Keywords: cornea, corneal epithelium, corneal tissue engineering, 3D bioprinting, bioink, human pluripotent stem cell, limbal epithelial stem cell

TIIVISTELMÄ

Paula Puistola: Uudenlainen biomuste sarveiskalvon epiteelin 3D biotulostukseen ihmisen pluripotenteista kantasoluista
Diplomityö
Tampereen yliopisto
Biotekniikan diplomi-insinöörin tutkinto-ohjelma
Syyskuu 2020
Tarkastajat: Professori Minna Kellomäki ja tutkijatohtori Anni Mörö

Tutkimuksen tavoitteet: Virheetön sarveiskalvon toiminta ja rakenne ovat näkökyvyn kannalta oleellisia. Sarveiskalvon toiminnallisuutta ylläpitävien limbaalisten kantasolujen puutos voi johtaa sokeutumiseen. Perinteinen hoitomuoto sarveiskalvon vaurioitumisesta johtuvaan sokeuteen on sarveiskalvon kudossiirre kuolleelta luovuttajalta, mutta kudossiirteistä on vakava puute, eikä siirteissä ole toiminnallisia limbaalisia kantasoluja. Siksi kudossiirre ei ole toimiva hoitokeino limbaalisten kantasolujen puutoksesta johtuvaan sokeuteen. Kudosteknologian tavoitteena on palauttaa, korvata ja uudistaa vaurioitunutta kudosta, kuten kehittää keinotekoisia sarveiskalvoja. Nykyiset menetelmät eivät kuitenkaan pysty mimikoimaan alkuperäisen kudoksen solutason tarkkaa rakennetta. Lisäksi perinteisillä 3D-biovalmistustekniikoilla ei ole mahdollista saavuttaa solujen ja materiaalien yhtäaikaista sijoitusta kolmiuloitteiseen (3D) ympäristöön. 3D-biotulostus tarjoaa tähän ratkaisun ja mahdollistaa sarveiskalvon kaltaisten, kolmiulotteisten kudosten valmistuksen. Suurin haaste 3D-biotulostuksessa on puute biotulostettavista, soluja sisältävistä biomusteista, jotka tukevat solujen kypsymistä ja järjestäytymistä toiminnalliseksi yksiköksi. Tämän työn tavoite oli suunnitella ja optimoida uudenlainen biomuste ja biotulostusolosuhteet ihmisen erittäin monikykyisistä kantasoluista valmistetun sarveiskalvon epiteelin kaltaisen kudoksen 3D-biotulostukseen.

Materiaalit ja menetelmät: Uudenlainen biomuste valmistettiin yhdistämällä ihmislähtöisiä rekombinanttisoluväliaineproteiineja. Lisäksi biomusteessa yhdistettiin kaksi erilaista ristisilloitustekniikkaa. Ensin biomusteen soveltuvuus paineavusteiseen ekstruusio-biotulostukseen tutkittiin. Ihmisen erittäin monikykyisistä kantasoluista erilaistetut limbaaliset kantasolut tuotettiin, ja biotulostuksen olosuhteet, kuten tulostuspaine ja -nopeus sekä ultraviolettisäteilyn (UV) määrä ja tulostusalusta, optimoitiin. Biotulostettujen kantasolujen vaste tulostusolosuhteisiin analysoitiin optisella mikroskoopilla, proliferaatio- ja elävyys/kuolleisuus-analyysien sekä immunofluroesenssivärjäysten avulla. Lopuksi ristisilloittamaton biomuste karakterisoitiin analysoimalla sen turpoamista, läpinäkyvyyttä sekä reologisia ominaisuuksia.

Tulokset ja johtopäätökset: Biomuste tulostui hyvin ja oli läpinäkyvää, eikä biotulostusprosessi vaikuttanut kantasolujen proliferaatio- tai erilaistumiskykyyn. UV-altistuksen määrä ei vaikuttanut elävien solujen osuuteen (> 88%), mutta sillä oli huomattavia vaikutuksia musteen ristisilloittumisen tiheyteen ja materiaalin jäykkyyteen. Biotulostetut kantasolut suosivat pehmeää, nestemäistä materiaalia, ja eniten kerrostunutta epiteeliä saavutettiin biotulostamalla ilman UV-alistusta. Tulostusalustoista Matrigeeli-pinnoituksella saatiin paras soluadheesio ja proliferaatio. Matrigeeli oli kuitenkin pehmeää, jonka vuoksi biotulostettu kerrostunut epiteeli kutistui ja osittain repeytyi viljelyssä. Siksi tulostusalustan optimointia tarvitaan tulevaisuudessa lisää. Lisäksi biomusteen nestemäisen rakenteen vuoksi reologisten ominaisuuksien määrittäminen oli haastavaa, joten reologiset mittaukset vaativat myös lisää tutkimusta ja optimointia. Tämä oli ensimmäinen tutkimus, jossa ihmisen erittäin monikykyisistä kantasoluista erilaistetut limbaaliset epiteelin kantasolut saatiin kerrostumaan extruusio-biotulostuksella. Siksi tutkimuksessa käytetyllä uudenlaisella biomusteella on potentiaalia sarveiskalvon epiteelin kaltaisen kudoksen biotulostuksessa ja koko sarveiskalvon rekonstruktiossa.

Avainsanat: sarveiskalvo, sarveiskalvon epiteeli, sarveiskalvon kudosteknologia, 3D-biotulostus, biomuste, ihmisen erittäin monikykyinen kantasolu, limbaalinen epiteelin kantasolu

PREFACE

This Master of Science thesis was done in the Eye group at the Faculty of Medicine and Health Technology at Tampere University. First, I would like to thank Professor Heli Skottman, the group leader, for the opportunity to do the thesis in the field of ophthalmology, tissue engineering and 3D bioprinting. This thesis project further developed my passion for 3D bioprinting, of which I am extremely excited and grateful.

Furthermore, I am forever grateful to my supervisor PhD Anni Mörö for valuable guidance and excellent supervision throughout the project, and for the encouragement for my future career. I would also like to thank MSc Maija Kauppila for the guidance and advice regarding the rheology in the thesis, and the whole Eye group for advice and support.

Finally, I would like thank my family and friends, who have always supported me throughout my studies, and especially during this project

Tampere, August 2020

Paula Puistola

CONTENTS

LIST OF ABBREVIATIONS

‘ene’	A carbon-carbon double bond
2D	Two-dimensional
3D	Three-dimensional
AM	Amniotic membrane
AMT	Amniotic membrane transplantation
BLP	Bordland Package Library
BMP	Bone morphogenic proteins
BSA	Bovine serum albumin
$CaCl_2$	Calcium chloride
CIJ	Continuous inkjet
CLAU	Conjunctival-limbal autograph
CLET	Cultured limbal epithelial transplantation
ColI	Collagen Type I
ColIV	Collagen Type IV
COMET	Cultured oral mucosal epithelial transplantation
CT	Computed tomography
DOD	Drop-on-demand
DTT	Dithiothreitol
EBM	Epithelial basement membrane
ECM	Extracellular matrix
EDC/NHS	N-(3-dimethylaminopropyl)-N’-ethylcarboiimide/N-hydroxysuccinimide coupling reaction
EDTA	Ethylenediaminetetraacetic acid
FDA	U.S. Food and Drug Administration
FGF	Fibroblast growth factor
G’	Storage modulus
G’’	Loss modulus
GelMA	Gelatin methacrylate
HA	Hyaluronic acid
HAMA	Hyaluronic acid methacrylate
hASCs	Human adipose-derived stem cells
hAVICs	Human aortic valve interstitial cells
hAVSSMCs	Human aortic valve sinus smooth muscle cells
hCEnCs	Human corneal endothelial cells
hCEpCs	Human corneal epithelial cells
hCSCs	Human corneal stromal cells
hCSKs	Human corneal stromal keratocytes
hECFCs	Human endothelial colony-forming cells
hESCs	Human embryonic stem cells
hiPSCs	Human induced pluripotent stem cells
hPSC-LESCs	Human pluripotent stem cell derived limbal epithelial stem cells
hPSCs	Human pluripotent stem cells
hTMSCs	Human turbinate-derived MSCs
hUVECs	Human umbilical vein endothelial cells
Igracure 2959	2-hydroxy-1-[4-hydroxyethoxyphenyl]-2-methyl-L-propanone
KLAL	Keratolimbal allograft
LAP	Lithium phenyl-2,4,6-trimethylbenzoylphosphinate
LESCs	Limbal epithelial stem cells
LGDW	Laser-guided direct writing
LIFT	Laser-induced forward transfer
LN521	Laminin 521
LSCD	Limbal stem cell deficiency

LVE	Linear viscoelastic region
MRI	Magnetic resonance imaging
MSCs	Mesenchymal stem cells
NIPAAm	N-isopropylacrylamide
PBS	Phosphate buffered saline
PCL	Polycaprolactone
PDMS	Polydimethylsiloxane
PED	Persistent epithelial defect
PEG	Polyethylene glycol
PEGDA	Polyethylene glycol diacrylate
PET	Polyethylene terephthalate
PFA	Paraformaldehyde
PGS	Poly glycerol sebacate
PHEMA	Poly-(2-hydroxyethyl-methacrylate)
PI	Polyimide
PLGA	Poly(lactic-co-glycolic acid)
PLLA	Poly L-lactic acid
PMCs	Post-mitotic cells
PMMA	Polymethyl methacrylate
Ru	Tris(2,2-bipyridyl) dischlororuthenium(II) hexahydrate
SLATEs	Self-Lifting Auto-generated Tissue Equivalent
SLET	Simple limbal epithelial transplantation
STL	Stereolithography
TACs	Transient-amplifying cells
TDCs	Terminarry differentiated cells
TE	Tissue engineering
TGFβ1	Transforming growth factor β-1
UV	Ultra-violet light
VA-086	2,2’-azobis[2-methyl-n-(2-hydroxyethyl)propionamide]

.

1. INTRODUCTION

As the outermost, transparent layer of the eye, the cornea has a key role in vision. The corneal epithelium is the smooth surface of the cornea, and together with the tear film, it provides most of the refractive power. Moreover, the epithelium acts as a barrier against chemicals and microbes. (Sridhar, 2018) Due to its critical role, corneal epithelium requires constant maintenance, which is done by limbal epithelial stem cells (LESCs). The most superficial cells of the epithelium are shed from the surface and replaced by differentiating LESCs. If this stem cell pool is lost or damaged, the maintanance of the corneal epithelium, and thus vision, is jeopardized. Subsequently, the dysfunction of LESCs can result in limbal stem cell deficiency (LSCD), which can lead to blindness (Jackson et al., 2020). In Europe, LSCD is caused by ocular burns in 30 people per million (Medicines Agency, 2015), and other less common causes include infections and autoimmune diseases, such as Stevens-Johnson syndrome (Jackson et al., 2020)

Severe LSCD requires surgical treatment, however, a traditional corneal transplant cannot be used as a treatment option due to lack of functional LESCs in the transplant (Baylis *et al.*, 2011). In addition, there is a severe shortage in donor material, and it is estimated that there is only one cornea available for 70 people who needs the corneal transplantation (Gain et al., 2016). Thus, there is a huge need for artificial corneas, which is the main problem corneal tissue engineering (TE) is aiming to solve (Fernández-Pérez and Ahearne, 2020). Boston keratoprosthesis is the most common artificial cornea (Ahearne et al., 2020), however, its poor adhesion to the host tissue (Mobaraki et al., 2019) is only one of its limitations. Subsequently, there are several different stem cell -based therapies used to treat LSCD, which usually include harvesting tissue from the healthy eye of the patient. This type of treatment causes two surgical operation sites and it cannot be used to treat bilateral LSCD, where both of the eyes are damaged. Moreover, the stem cell -based treatments using allogous donor tissue have the risk of rejection. (Jackson et al., 2020)

The conventional TE methods cannot mimick the native environment of the cells because the cells are cultured on flat substrates as monolayers (Torras et al., 2018). Moreover, when the cells are seeded afterwards on a prefabricated substrate, the precise positioning of cell types and components of the native tissue is not achieved.

Subsequently, three-dimensional (3D) bioprinting have gained interest in the field of TE to mimic the complexity and organization of the native tissue (Cui et al., 2020). With 3D bioprinting, it is possible to fabricate personalized artificial corneas with high precision and controllability (Ahearne et al., 2020). Combined with the use of human pluripotent stem cells (hPSCs) with unlimited self-renewal capacity, 3D bioprinting offers a possibility to create tissues with the native-like cellular variety and cytoarchitecture (Salaris and Rosa, 2019) as well as to overcome the donor shortage (Ahearne et al., 2020).

The aim of this thesis was to design a novel bioink for extrusion-based 3D bioprinting of stratified corneal epithelial tissue by using human pluripotent stem cell -derived limbal epithelial stem cells (hPSC-LESCs). The thesis began by optimizing the novel bioink composition and the printing parameters in order to achieve convenient printability. In addition to the bioink composition, the printing conditions were optimized based on the reaction of the bioprinted hPSC-LESCs. The printing conditions included the printing substrate and the UV exposure time. Subsequently, the bioink was characterized with transmittance and rheological measurements. The viability, proliferation, differentiation and maturation of the bioprinted hPSC-LESCs were analyzed with phase contrast microscope and with LIVE/DEAD, PrestoBlue and immunofluroescence analyses.

The thesis consists of theoretical and experimental parts, and begins with providing background information of the physiology of the human cornea, LESCs, LSCD, hPSCs and corneal TE. Thereafter, the thesis introduces 3D bioprinting, its main strategies and the commong components used in bioinks. Moreover, the main crosslinking strategies for hydrogel bioinks are described. The theoretical part concludes by introducing state-of-the-art 3D bioprinting of ocular tissues. In the experimental part, the materials and methods used in this thesis are described in detail, and finally, the results of the performed study are reported, discussed and concluded.

2. HUMAN CORNEA

The cornea is the anterior part of the eye forming a primary protective coat for it. The main function of the cornea is to provide protection from for example microbes, and act as a refractive surface, which is enabled by its structural properties described next. (DelMonte and Kim, 2011) This chapter begins with describing the basic anatomy and physiology of the human cornea with the focus on the corneal epithelium. Next, the LESCs and how they are involved in the corneal epithelial defects are discussed. Since human pluripotent stem cell -derived cells are used in this thesis, they are shortly described in this chapter. Finally, the most common corneal TE methods are introduced.

2.1 Structure of the cornea

The cornea is avascular and consists of three parts, the central, paracentral and peripheral zones (B. Zhang, Xue, Li, et al., 2019). Around the cornea, there is the limbus and the conjunctiva. The cornea has curved shape and is horizontally oval with the thickness increasing from the central zone towards the peripheral zone (Sridhar, 2018). Moreover, the cornea is transparent tissue with light transmittance varying from 80% to 96% at wavelengths 400 – 900 nm (Beems and Van Best, 1990).

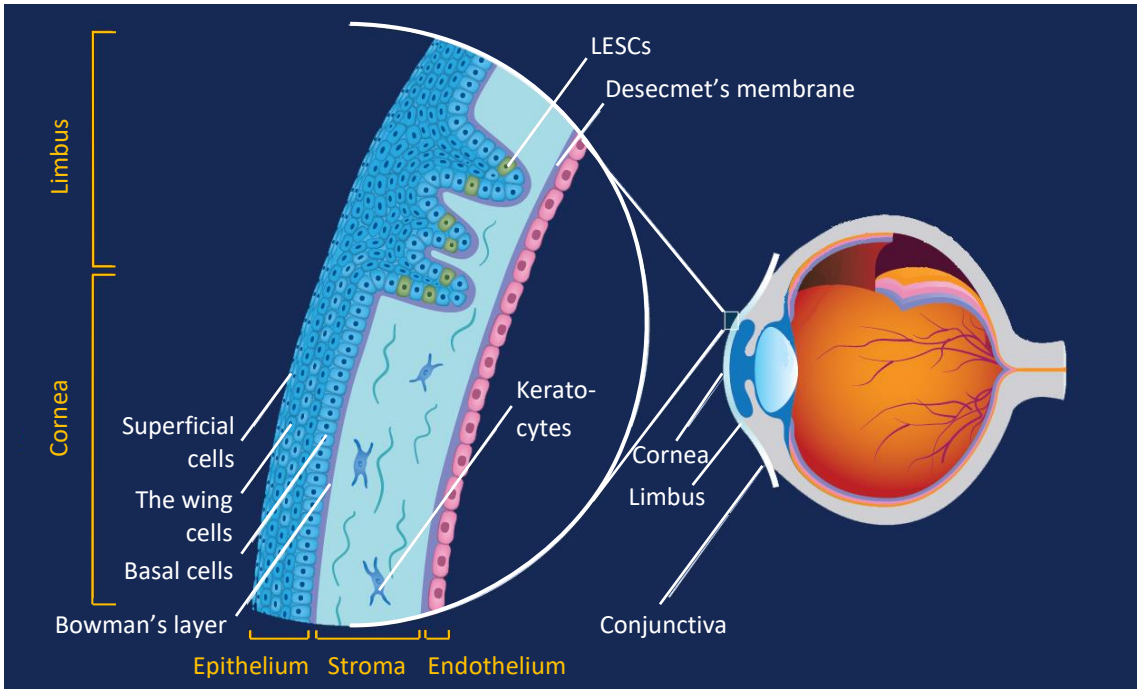

Figure 1. The structure of the cornea and limbus. LESCs = Limbal epithelial stem cells. Modified from https://discovery.lifemapsc.com/library/images/the-anatomy-and-structure-of-the-adult-human-cornea, 21.07.2020.

The cross section of the cornea consists of different layers, which are epithelium, stroma, endothelium and two acellular interfaces, Bowman's membrane and Descement's membrane (Figure 1). The epithelium is the outermost layer of the cornea and consists of 5 – 7 layers of non-keratinized, stratified squamous epithelial cells, which create about 50 µm thick structure and have a lifespan of 7 to 10 days. In the peripheral cornea, the epithelium is slightly thicker, 7 – 10 layers. The epithelium is composed of three types of epithelial cells with different structures, attached to each other through desmosomes. The 2 – 6 µm thick, flat superficial cells form 2 – 3 layered structure with tight junctions between the cells and have microvilli on the surface increasing the surface area. Beneath the superficial cell layer is the wing cells, which have a wing-like shape. The most deepest layer of the epithelium is composed of a single layer of 20 µm tall basal cells, which can undergo mitosis, and thus act as a source of wing and superficial cells. The basal cells in the central cornea are columnar, whereas in the peripheral cornea they are cuboidal. (Sridhar, 2018)

On the top of the superficial epithelial cells is a tear film, which covers the corneal epithelium, providing a smooth optical surface and most of the refractive power (DelMonte and Kim, 2011), and protects the cornea from dehydration (Sridhar, 2018). As the epithelium, the gel-like tear film is composed of three layers, the lipid, aqueous and mucin layers. The superficial lipid layer preventing evaporation is secreted by the meibomian glands on the eyelid. The aqueous middle layer is produced by the lacrimal gland located in the upper part of the eye socket. The deepest mucin layer is produced by conjunctival goblet cells. (Gipson, 2007)

Below the basal cells of the epithelium, there is the basement membrane, where the basal cells are attached to the membrane through hemidesmosomes (Sridhar, 2018). The epithelial basement membrane (EBM) is an important structure for epithelial cells, as it is involved in regulation of tissue development, function and repair. It gives the cells support as they proliferate, migrate and differentiate, and in addition, it regulates the polarity of epithelial cells. The EBM consists mainly of collagen type IV (ColIV) and laminins. ColIV provides structural stability for the EBM, and it has six α chains, which can assembly into different heterotrimers. Laminins are heterotrimeric glycoproteins and composed of three different chains, α, β and γ. Currently, there are five α, three β and three γ peptides known in humans, and the identification of laminin isoforms can be done according to the chains. (Wilson, Torricelli and Marino, 2020) For example, a nomenclature laminin 521 means that the laminin is composed of five α chains, two β chains and one γ chain.

The ColIV and laminins self-polymerize into networks, which are crosslinked with proteins called perlecan and nidogens 1 and 2. Perlecan is a proteoglycan which regulates the cell migration, proliferation and differentation by controlling the availability of different growth factors, such as fibroblast growth factors (FGF), bone morphogenic proteins (BMP), and transforming growth factor β-1 (TGFβ1). Nidogens 1 and 2 are sulfated glycoproteins creating links between other components and seem to compensate each other if other one is deficient. (Wilson, Torricelli and Marino, 2020)

Beneath the corneal epithelium and the EBM is the 15 µm thick Bowman layer, which maintains the shape of the cornea (DelMonte and Kim, 2011). It is composed of Type I and V collagens (ColI and ColV) and proteoglycans (Sridhar, 2018). Beneath, there is the stroma, which comprises the most of the cornea, 80 – 85%. The stroma is composed of ColI, ColV, proteoglycans and keratocytes. It povides mechanical strength and transparency due to the organized arrangement of the collagen fibrils into parallel bundles embedded in hydrated matrix. (DelMonte and Kim, 2011) In addition, the keratocytes contain crystallins, which reduce backscattering of light, and thus provide transparency (Jester et al., 1999).

Descement membrane is an elastic, 7 µm thick structure located beneath the stroma and consisted of ColIV and laminin. Beneath the Descement membrane, there is the endothelium, which is a 5 µm thick, honeycomb-like monolayer. Its main function is to regulate the water content of the cornea. The hexagonal endothelial cells are attached to the Descement membrane through hemidesmosomes, and their density decreases from 3000 to 4000 cells/mm^2 to 2600 cells/mm^2 throughout adult life. (Sridhar, 2018)

The cornea is surrounded by the conjunctiva, which is 1-2 cell layers thick (Dua et al., 2000). Between the conjunctiva and the peripheral cornea is the limbal zone, the limbus, which prevents the conjunctiva and its blood vessels to overgrow onto the cornea (Osei-Bempong, Figueiredo and Lako, 2013). The limbus contains limbal epithelial stem cells (LESCs) in its basal layer. These cells maintain the cornea and differentiate into corneal epithelial cells when migrating out from the stem cell niche. (Gesteira et al., 2017)

2.2 Limbal epithelial stem cells

LESCs are located at the limbus (Figure 1), and their proliferation, migration and differentiation depends on the limbal niche, which is the specialized microenvironment for LESCs. In the limbal niche, there are ridges called palisades of Vogt, where the epithelium extends deeper in the limbus creating limbal epithelial crypts in the basal layer (Figure 2). In addition to LESCs, the limbal niche contains other cell types, such as

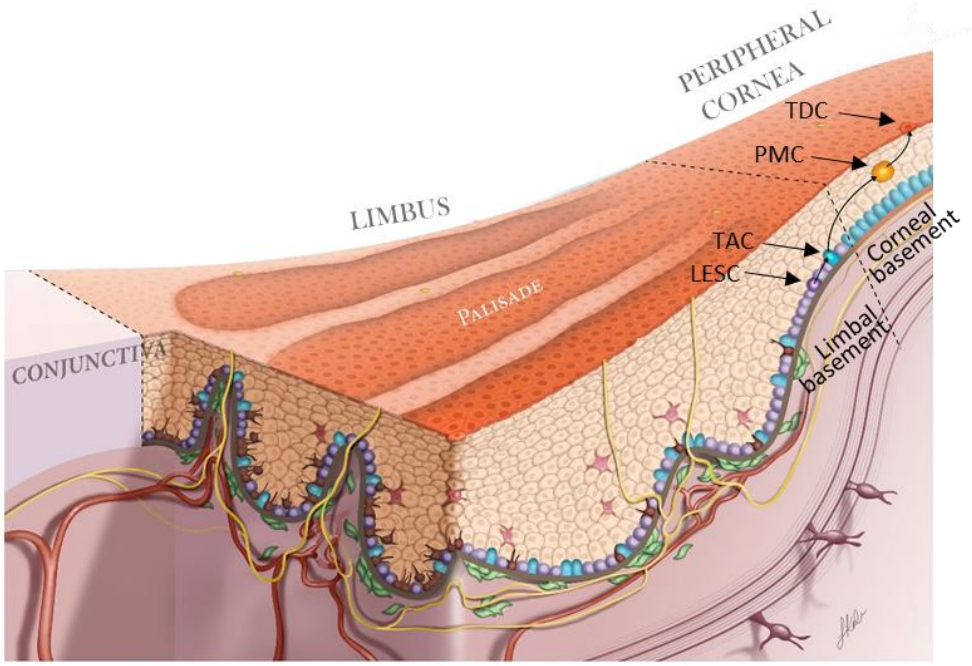

Figure 2. Schematic of the limbal niche and the maintanance of cornea by LESCs. The corneal epithelium extends deeper in in the limbus, creating Palisades of Vogt and limbal epithelial crypts. In the Palisades, LESCs undergo asymmetric division into stem-like daughter cells (another LESC) and transient amplifying cells (TACs). TACs migrate towards the the peripheral cornea and divide into post-mitotic cells (PMCs), which then are differentiated into terminally differentiated cells (TDCs) and shed from corneal surface. Modified from (Yazdanpanah *et al.*, 2019).

melanocytes, Langerhans cells, nerve cells and mesenchymal stem cells (MSCs). (Yazdanpanah et al., 2019)

The main role of LESCs is to maintain the cornea by replacing the cells on the corneal surface, and thus, deficiency of these cells has a significant effect on the renewal of the cornea (Dua et al., 2000). The theory of maintaining corneal homeostasis is the XYZ hypothesis proposed in 1983. According to this theory, the basal cells proliferate (X), cells migrate towards the center (Y) and cells are lost from the surface (Z). (Thoft and Friend, 1983) At the limbus, LESCs undergo asymmetric division into stem-like daughter cells (other LESCs) and transient-amplifying cells (TACs), which represents the X. TACs then migrate towards the centre of the cornea, undergoing mitosis and differentiating into post-mitotic cells (PMCs) (Y). PMCs migrate through the basal epithelium of the cornea, differentiating into terminally differentiated cells (TDCs) (Figure 2). TDCs are superficial squamous epithelial cells, which exfoliate and shed from the surface (Z), and thus new cells are needed constantly. (Yazdanpanah et al., 2019)

The cells are constantly sensing and reacting to their environment through mechanotransduction, which means converting mechanical stimulus into biochemical activity (Iskratsch, Wolfenson and Sheetz, 2014). Intraocular pressure, eyelid and tear

film motion and eye rubbing are examples of mechanical stimuli the cells experience in the corneal epithelium in vivo (Masterton and Ahearne, 2018). Therefore, the conditions in vitro and the mechanical properties of biomaterials can be used to affect the behaviour of LESCs. It has been demonstrated that the substrate stiffness affects the migration, proliferation and stratification of LESCs in vitro, stiffer substrate promoting migration and softer substrate promoting proliferation and stratification. Softer matrix has been shown to promote the expression of limbal markers, whereas the expression of differentation markers is decreased. (Gouveia, Lepert, et al., 2019) This information can be utilized in the design of biomaterials for LESCs and corneal tissue engineering.

2.3 Corneal epithelial defects and current treatments

Since the cornea is the outermost layer of the eye, it is vulnerable to external damage or organisms, such as bacteria. If the epithelium, the protective barrier of the eye, is damaged, it can cause infections, perforation, scarring and decreased vision. The epithelial defect can be acute, which heals within 7 – 14 days. However, if the normal healing process does not occur, the epithelial defect becomes persistent. There, the stroma is affected in addition to the epithelium, the epithelial cells cannot migrate to the damaged area and the basement membrane becomes thinned. Persistent epithelial defect (PED) can be caused by for example defective epithelial adhesion to the basement membrane, over-activity of inflammatory cytokines or recurrent mechanical damage. (Vaidyanathan et al., 2019)

If the LESCs maintaining the corneal epithelium are damaged or lost, it can lead to LSCD, which is one of the conditions resulting in PED (Vaidyanathan et al., 2019). The main causes for LSCD are physical or chemical burns, infections (trachoma) and autoimmune diseases, such as Stevens-Johnson syndrome. (Utheim, 2013; Jackson et al., 2020), and it can be aquired or hereditary (Yazdani et al., 2019) LSCD is caused by ocular burns in 30 people per million in Europe (Medicines Agency, 2015). In LSCD, the function of the limbus is lost completely or partially due to insufficient stromal microenvironment or external damage which destroys the LESCs. Subsequently, the barrier function of the limbus is lost, and the conjunctival epithelium invades the cornea. (Osei-Bempong, Figueiredo and Lako, 2013) The corneal epithelium is replaced with conjunctival epithelium, and scarring and vascularization occur. This decreases the transparency of the cornea, and therefore can lead to corneal blindness. (Samoila and Gocan, 2020) Limbal basal cell density decreases (Chan et al., 2015), and moreover, LSCD causes corneal stiffening (Gouveia, Lepert, et al., 2019). The stiffening affects the ability of LESCs to maintain their phenotype, as the expression of limbal markers decrease and

the expression of differentiation markers increase (Gouveia, Lepert, et al., 2019). Depending the extent of the damaged LESCs, LSCD can be partial or total. In addition, it can be bilateral or unilateral, depending if the both eyes are damaged or just the other one. (Samoila and Gocan, 2020)

Traditionally, corneal blindness is treated with corneal transplantation (keratoplasty) from a donor. The successive rate of a donor cornea is higher than many other tissues due to the reduced risk of immune rejection, because there are no vascular or lymphatic vessels in the cornea (Ahearne et al., 2020). However, for every 70 people in need there is only one donor cornea available (Gain et al., 2016). Moreover, corneal transplantation cannot be used to treat LSCD due to the lack of functional LESCs in the transplant (Baylis *et al.*, 2011). Subsequently, alternative options to develop artificial corneas have been studied. The most common artificial cornea is the Boston keratoprosthesis (Ahearne et al., 2020), which has been used for treating LSCD (Shanbhag et al., 2018).

The Boston keratoprosthesis is a device, which consists of a front and back plates made of polymethyl methacrylate (PMMA). A donor cornea is placed between the plates and a titanium ring locks them in place, and the device is implanted to replace the damaged cornea. (Mobaraki et al., 2019) The Boston keratoprosthesis had the U.S. Food and Drug Administration (FDA) approval in 1992, and over 12 000 devices have been implanted since then (Saeed, Shanbhag and Chodosh, 2017). However, a major disadvantage in Boston keratoprosthesis is the poor adhesion between the PMMA and the host tissue (Mobaraki et al., 2019). Other limitations of keratoprosthesis include discomfort, complex transplantation process, limited visual field and unsatisfying appearance (B. Zhang, Xue, Li, et al., 2019)

Due to the poor long-term outcomes of corneal transplants and problems of the previous artificial corneas, the development of alternative treatments with successful transplantation of functional stem cells is important. Subsequently, there are different cell-based surgical techniques currently available for the treatment of LSCD. However, most of these treatment options use autologous limbal tissue (Jackson et al., 2020), which means the tissue is harvested from the same individual, or in this case, the healthy or less damaged eye. Therefore, these techniques can be used only for unilateral LSCD. The first technique using autologous tissue was introduced in 1989 by Keivyon and Tseng and is called conjunctival-limbal autograph (CLAU). In CLAU, two conjunctival-limbal biopsies are harvested from the healthy eye and transferred into the damaged eye, without the need for any transplant substrate (Keivyon and Tseng, 1989). In the second technique, cultured limbal epithelial transplantation (CLET) introduced by Pellegrini et al. in 1997, the harvested biopsies are cultured to produce cell sheets, which

are then transplanted (Pellegrini et al., 1997). CLET technique includes the first stem cell -based theraphy for LSCD called Holoclar, which has been approved by the European Union in 2015 (Pellegrini et al., 2018).

However, these techniques have challenges, such as the expensive and time-consuming ex vivo cultivation in CLET and possible risks due to taking two large biopsies in CLAU. Therefore, Sangwan et al. introduced the third treatment option for LSCD in 2012, called simple limbal epithelial transplantation (SLET). In SLET, a small biopsy is harvested from the healthy eye of the patient, and the biopsy is cut into eight pieces. A human amniotic membrane (AM) is fixed with fibrin glue onto the damaged eye, and the biopsy pieces are placed onto the AM and fixed with fibrin glue. (Sangwan et al., 2012)

If LSCD is bilateral, it is not possible to use tissue from the patient's own eye, and therefore other techniques have been studied. In 1994, Tsai and Tseng introduced keratolimbal allograft (KLAL), where the tissue is harvested from deceased donors or living relatives. However, the use of allogous tissue requires immunosuppression to prevent rejection. (Holland, 2015) Cultured oral mucosal epithelial transplantation (COMET) is an alternative, autologous technique for treating bilateral LSCD (Jackson et al., 2020). In COMET, autologous oral epithelial cells are harvested and cultured on a denuded human AM carrier, and after 2-3 weeks, the resultant cell sheet is transplanted onto the damaged eye (Nakamura et al., 2004). COMET overcomes the challenges of risk of rejection and large biopsies, however, the production of the cell sheets is the main challenge, as in CLET (Jackson et al., 2020). In addition, peripherical corneal vascularization have been reported in many cases (Prabhasawat et al., 2016). Moreover, the number of functional LESCs in these treatments is low. For example, the commercially available treatment for LSCD, Holoclar, has only 3.5% of functional LESCs on average (European Medicines Agency, 2019). Therefore, better techniques for treating LSCD are studied to overcome these challenges.

2.4 Human pluripotent stem cells

Stem cells are responsible for constructing every tissue in the human body, and they are defined with two main characteristics. Stem cells need to have unlimited ability to proliferate into cells, which are the same as the stem cell itself, in a phenomenon called self-renewal. Moreover, stem cells need to give rise to one or more differentiated cell type. The self-renewal can be symmetric, meaning one stem cell divides into two daughter stem cells increasing the stem cell pool, or asymmetric, meaning one stem cell divides into one daughter stem cell and one differentiated daughter cell. If the stem cell does not divide or differentiate, it remains quiescent maintaining the stem cell pool. The

fourth option for the stem cell is to divide into two differentiated daughter cells without self-renewal, however, this results in a decrease in stem cell pool. (Bozdağ, Yüksel and Demirer, 2018)

Stem cells can be divided into categories based on their differentiating potency. Totipotent stem cells can differentiate into any cell type, including embryonic and extraembryonic tissues. Pluripotent stem cells can differentiate into all cell types in embryonic tissue, such as the three germ layers, endo-, meso- and ectoderm. Multipotent stem cells can differentiate only into cell types of one germ layer. Unipotent stem cells can differentiate only into a specific cell type. (Bozdağ, Yüksel and Demirer, 2018) Human pluripotent stem cells (hPSCs) can self-renew and differentiate into all cell types, and they mainly include human embryonic stem cells (hESCs) and induced pluripotent stem cells (hiPSCs). (Rehakova, Souralova and Koutna, 2020)

First hESCs were derived from human blastocysts in 1998 by Thomson (Thomson et al., 1998). In 2007, the first hiPSCs were derived from adult human somatic cells by reprogramming them with specific transcription factors (Takahashi et al., 2007; Yu et al., 2007). The ethical issues and limited supply of hESCs are avoided due to the possibility to reprogram adult somatic cells into hiPSCs, and in addition, the use of autologous cells enables personalized cell therapies (Ortuño-Costela et al., 2019). Due to their capabilities to proliferate and differentiate into any cell type in the human body, hPSCs are advantageous in cell-based therapies and overcome the limitations of using other stem cells, such as mesenchymal stem cells, which can differentiate only into a few specific cell types and have limited proliferation capacity. (Rehakova, Souralova and Koutna, 2020) Therefore, the use of hPSC have gained attention in corneal cell therapy as they reduce the need of donor corneas and provide almost unlimited source of cells due to the ability to self-renew (Chakrabarty, Shetty and Ghosh, 2018). The LESCs derived from hPSCs are shown to be similar to the native LESCs, and thus they offer an alternative cell supply for LSCD treatments (Mikhailova et al., 2015).

The challenge of using hPSCs rises from the reproducibility issues and variability for example in methodologies and cell lines (Salaris and Rosa, 2019). To produce clinical-grade hPSCs, careful characterization, standardization and quality control are required. There are several methods for characterization of hPSCs, such as determining the genetic stability with karyotype analysis and pluripotency with flow cytometry, as well as ensuring their sterility and viability. (Rehakova, Souralova and Koutna, 2020) In addition, the production of clinical-grade autologous hiPSCs is expensive, up to 40-80 times more costly than the production of research-grade hiPSCs (Bravery, 2015). Despite of the challenges, there have been clinical trials using hPSCs derived cells. In 2010, Geron

was able to proceed to the first clinical trial using hESCs in the treatment of acute spinal cord injury. The first clinical trial using hiPSC-derived cells was launched in 2013 by a Japanese company RIKEN CBD. (Ilic et al., 2015) In May 2019, a clinical trial of hiPSCs derived corneal epithelial cell sheet transplantation for patients with LSCD was started in Japan (ICTRP Search Portal, 2020).

2.5 Corneal tissue engineering

The main target of tissue engineering (TE) is to restore, replace or regenerate defective tissues (Ovsianikov, Khademhosseini and Mironov, 2018). Therefore, the field of corneal TE aims to develop artificial corneas to overcome the corneal transplant shortage and immune response, which can lead to rejection of the transplant (Fernández-Pérez and Ahearne, 2020). In addition to the biocompatibility, biodegradability, and the physical structure, such as porosity, the main aspects to consider when developing a TE cornea are the transplant location and its cell type as well as the transparency of the scaffold material (Ahearne et al., 2020).

There are two main approaches to fabricate the TE construct. In scaffold-based approach, the goal is to fabricate a biomimetic structure which supports the cells until the new tissue is formed. Scaffold-free, or cell-based, approach has an opposite point of view, as there the cellular construct is fabricated from prefabricated cell sheets, spheroids or tissue strands. (Ovsianikov, Khademhosseini and Mironov, 2018) In corneal tissue engineering, the scaffold-free approach be can used to produce cell sheets on a substrate and transplant them without an additional carrier (Syed-Picard et al., 2018). The structure of the desired tissue affects the selection of the TE approach. For example, the corneal epithelium mainly consists of cells associated to the EBM and there is only a little ECM, whereas the corneal stroma has only 10 % of its volume composed of cells. Therefore, the cell-based approach is better choice for the epithelium and the scaffold-based for the stroma. (Matthyssen et al., 2018)

In many TE approaches, such as using a hydrogel scaffold or electrospun polymers, the cells are seeded afterwards on the fabricated scaffold. This multistep process is time-consuming and results flat 2D structures, and thus other approaches to mimic the native tissue better are under research.

2.5.1 Hydrogels

Hydrogels are widely studied group of biomaterials for TE due to their hydrophilic and cell-friendly properties as well as the large range of material and modification options. Hydrogels are formed through chemical or physical crosslinking, which creates a highly hydrophilic polymeric network with ability to swell, and in fact, from 70 % to 99 % of hydrogels can consist of water (Chimene, Kaunas and Gaharwar, 2020). Hydrogels can consist of natural or synthetic polymers and can be fabricated as films, sponges and gels (Chen et al., 2018). Moreover, hydrogels are biodegradable and provide a 3D environment (Mahdavi, Abdekhodaie, Mashayekhan, *et al.*, 2020), which is desired in tissue engineering. Because hydrogels usually have too weak mechanical properties, different reinforcement strategies have been studied (Chimene, Kaunas and Gaharwar, 2020). For example, combining hydrogels and with polymer electrospinning can be used to reinforce hydrogels (Tonsomboon, Strange and Oyen, 2013). In addition, different nanofibers and nanotopographies have been studied in order to provide highly porous 3D framework and to better mimick the native environment of corneal cells (Sahle et al., 2019).

There are several hydrogel materials studied in corneal TE, and especially hydrogel-forming ECM components are the common choice. Collagen is the most abundant ECM component in the cornea, and thus, it has gained popularity as a material choice (Matthyssen et al., 2018; Ahearne et al., 2020). Collagen can be fabricated as films, sponges or hydrogels, or compress it to reduce the water content of the hydrogel and improve the mechanical properties. (Ahearne et al., 2020) It has been fabricated as films and membranes (Ye et al., 2014; Chae et al., 2015; Y. Liu et al., 2019), or as compressed gel to improve the mechanical strength of the scaffold (Rafat et al., 2016; Cen and Feng, 2018; Miotto et al., 2019). Corneal substitutes of collagen have been tested in phase I clinical trials (Fagerholm et al., 2010).

Silk fibroin is a natural polymer with good biocompatibility, mechanical strength and transparency. It can be formed as hydrogels, sheets, fibers and sponges, which makes it an interesting material for corneal TE. (Ahearne et al., 2020) To produce a hydrogel, silk fibroin solution can be crosslinked with riboflavin (Applegate et al., 2016) or genipin (H. Zhou et al., 2019). Silk fibroin has been used to fabricate film substrates for corneal epithelial cells (Higa et al., 2011; Liu et al., 2012; Li et al., 2017), stromal cells (Wu et al., 2014; Bhattacharjee, Fernández-Pérez and Ahearne, 2019) and endothelial cells (Vázquez et al., 2017; Song et al., 2019), as well as a co-culture for corneal epithelial and stromal cells with innervating neurons at an air-liquid interface (Wang et al., 2017).

In addition, silk fibroin films can be stacked after culturing stromal cells on single films to mimic the native physiology of corneal stroma (Ghezzi et al., 2017)

Gelatin is a low-cost, natural polymer, which has been used as a hydrogel scaffold material in corneal TE (Ahearne et al., 2020). For example, gelatin has been used to prepare cell substrates (Goodarzi et al., 2019), blended membranes (Xu et al., 2018) or cell loaded slabs for in vivo study (Kilic Bektas et al., 2019). In addition, it can be modified, for example by acrylation or thiolation, which enhances its mechanical properties and provides variability and control in crosslinking (Li et al., 2018).

Another common ECM component, hyaluronic acid (HA), has gained attention as a hydrogel biomaterial for corneal TE due to its hydrophilicity and possibility to tailor its properties, even though it is not yet as widely studied (Yazdani et al., 2019). HA has been shown to regulate differentiation of LESCs (Gesteira et al., 2017), and thus it has been studied in the treatment of LSCD (Yazdani et al., 2019). For example, HA-based hydrogel substrates have been used for human epithelial limbal cells, replacing AM as the carrier (Fiorica et al., 2011), and co-culturing human adipose stem cells (hASCs) with human corneal epithelial cells (hCECs), resulting in enhanced growth and differentiation of hCECs (Kiiskinen, 2016). Later, HA has been shown to support the expansion of hCECs in a xeno-free culture, resulting in stratified epithelium (Chen et al., 2017).

2.5.2 Decellularized cornea

Decellularized tissue means removing the cells and their debris, which results a ECM scaffold and thus reduces the risk of rejection. Since the scaffold is composed of native ECM, it mimics well the native environment of the cells with a suitable composition and organization. However, there is batch-to-batch variation, which is a common disadvantage when using natural materials. (Ahearne et al., 2020)

There are several methods to decellularize tissue, and they can be divided into three categories. Physical decellularization can be done with freeze-thawing or supercritical carbon dioxide, usually combined with mechanical agiation. Chemical decellularization can be done for example with different detergents, such as sodium dodecyl sulphate, or hypertonic solutions of sodium chloride. Biological decellularization is done with enzymes, such as trypsin, and an additional incubation with nucleases to degrade the released DNA. (Fernández-Pérez and Ahearne, 2020) The use of chemicals creates a risk of chemical residues in the scaffold, which is one disadvantage of this method (Ahearne et al., 2020).

In cornea TE, decellularized porcine cornea is the most commonly studied. It is well available and has similarities in the anatomy with the human cornea. However, there is a risk of rejection, if the decellularization is insufficient. To overcome the problems of using xenogenic tissues, human corneas unsuitable for corneal transplantation have been decellularized. (Fernández-Pérez and Ahearne, 2020)

2.5.3 Amniotic membrane

AM can be used together with the cell-based surgical techniques, such as SLET, to treat LSCD. AM is a semi-transparent, the innermost layer of the placenta, which consists of the monolayered epithelium, a basement membrane rich in collagen types IV and VII, fibronectin, laminins and HA, and the avascular stroma (Jirsova and Jones, 2017). AM can be transplanted alone, however, usually it is combined with the surgical techniques described above. There, it is used as a substrate for ex vivo LESC expansion and as a carrier of the cell sheet to provide physical support when it is transplanted onto a damaged ocular surface. (Le and Deng, 2019)

AM can be applied directly onto the damaged eye by a surgeon and fixed with sutures or glue. There, it either acts as a basal membrane for the corneal epithelial cells or protective cover for the ocular defect, depending on the surgical technique. Fresh AM can be used, however, to rule out the possibility of disease transmission, it is usually preserved. Typical methods are lyophilization (drying under vacuum and rehydrating when used) and cryopreservation at - 80 °C. (Lacorzana, 2020) The common long term complications of using AM alone to treat ocular surface are eyelid-related and dry eye (Shanbhag et al., 2020). In addition, the availability of AM is limited and mouse fibroblast feeder cells are used in co-culture when using AM as a stem cell carrier, which is why other carriers are under research (Oliva, Bardag-Gorce and Niihara, 2020). Other disadvantages include batch-to-batch variation, difficulties in storage, costly donor screening and possibile immunological rejection (Nguyen et al., 2018).

2.5.4 Electrospinning

Electrospinning has been used in corneal TE to fabricate and study alternative scaffolds for corneal constructs (Kong and Mi, 2016; Ahearne et al., 2020), and it has been used as a technique to fabricate nanofiber scaffolds for corneal TE (Sahle et al., 2019). In electrospinning, the scaffold is fabricated from thin fibers, which are drawn from a syringe due to high voltage (Ortega et al., 2012), ranging from 5 to 50 kV (Kong and Mi, 2016). Electrospinning technology uses an electrostatic field for the repulsive force between particles to overcome the solution surface tension. This results the solution droplet to

stretch and finally jet from the syringe as a fiber when the solvent evaporates, and the fiber is then collected on a collector slide. (Kong and Mi, 2016)

The syringe containing the polymer solution is typically a hypodermic syringe needle (Kong and Mi, 2016), however, there are different options for collectors. For example, the collector can be a plate wrapped in aluminium foil (Aslan et al., 2018; Fernández-Pérez et al., 2020; Sanie-Jahromi et al., 2020) a polymeric structure produced by stereolithography (Ortega et al., 2012) or a pre-treated glass plate (Alexander et al., 2019). To obtain the curved shape of cornea, a hemispherical collector has been studied (Kim, Kim and Park, 2018). In addition, the collector can be static (Z. Zhou et al., 2019) or rotating (Sanie-Jahromi et al., 2020). Whereas the fiber orientation is usually random, by altering the electrical potential on the collector, it is possible to orientate the fibers radially or perpendicularly (Montero et al., 2012; Fernández-Pérez et al., 2020).

In addition to the collector design, other electrospinning parameters, such as the applied voltage, the polymer solution and the humidity, can be altered to fabricate different kind of fibers and scaffolds (Kong and Mi, 2016). For example, the fiber can have smooth of rough surface (Cui et al., 2008). In addition, by varying the collector height, it is possible to affect the diameter of the electrospun fibre as well as the density and thickness in the inner and outer areas of the scaffold (Ortega et al., 2012). The electrospun polymer mat can be post-processed for example with laser perforation to regulate its mechanical strength and transparency, and combine with collagen gel to increase biocompatibility and enchance the mechanical strength of the collagen alone (Kong et al., 2017).

Electrospinning has been used to fabricate nanofiber scaffolds with highly porous structure for corneal regeneration (Sahle et al., 2019). Moreover, due to the possibility of controlling the fiber orientation, electrospinning can be used to mimic for example the organization of collagen fibrils in the corneal stroma (Ahearne et al., 2020). Several different synthetic polymers have been used to fabricate scaffolds for corneal constructs by electrospinning, such as poly(lactic-co-glycolic acid) (PLGA) (Ortega et al., 2012; Kong et al., 2017; H. Liu et al., 2018), poly L-lactic acid (PLLA) (Aslan et al., 2018) and polycaprolactone (PCL) (Sharma et al., 2011; Z. Zhou et al., 2019; Fernández-Pérez et al., 2020; Sanie-Jahromi et al., 2020).

In addition to synthetic polymers, natural polymers have been studied in electrospinning due to their better biocompatibility (Ahearne et al., 2020). For example gelatin (Montero et al., 2012; Sanie-Jahromi et al., 2020) and silk fibroin (Biazar et al., 2015) have been used to fabricate corneal scaffolds, however, the mechanical properties are usually too weak for the use of natural polymers alone.Therefore, a more common method is to

electrospin blends, such as PCL and PLLA copolymer with silk fibroin (Chen et al., 2015), or PCL with chitosan (Stafiej et al., 2017) or collagen (Kim, Kim and Park, 2018). In addition to blends, natural polymers can be electrospun together with a synthetic polymer without blending, such as electrospinning collagen in between electrospun PLGA (Arabpour et al., 2019). Table 1 provides examples of the recent study of fabricating scaffolds by electrospinning for corneal regeneration.

Table 1. Examples of electrospun scaffolds for corneal regeneration.

Electrospun material	Cells	Target corneal tissue	Reference
PCL with chitosan **PCL with poly glycerol sebacate (PGS)**	Human corneal epithelial cells Human corneal keratocytes	Epithelium	(Stafiej *et al.*, 2017)
PCL with PGS	Human corneal endothelial cells Human conjunctival epithelial cells	Endothelium Epithelium	(Salehi *et al.*, 2017)
PCL, PLA and PLGA on decellularized AM	Rabbit limbal stem cells	Epithelium	(Liu *et al.*, 2018; Z. Zhou *et al.*, 2019)
PCL with decellularized cornea	Human corneal stromal cells	Stroma	(Fernández-Pérez *et al.*, 2020)
PCL with gelatin	Human LESCs	Epithelium	(Sanie-Jahromi *et al.*, 2020)
PLLA	Bovine stromal keratocytes	Stroma	(Aslan *et al.*, 2018)
PLLA-PCL copolymer with silk fibroin	Human corneal endothelial cells	Endothelium	(Chen *et al.*, 2015)
Silk fibroin	Human LESCs	Epithelium	(Biazar *et al.*, 2015)
PLGA layered with collagen type I	Human endometrial stem cells	Whole cornea	(Arabpour *et al.*, 2019)

2.5.5 Scaffold-free cell sheets

During the development of the body, the cells are organized into appropriate 3D structures without scaffolds. Thus, a scaffold-free approach is gained attention in TE, as cell sheets are first cultured as a monolayer on a substrate and then removed physically or chemically. For example, surface-patterned polydimethylsiloxane (PDMS) can be used as a substrate for corneal stromal cells, which form a mechanically removable and transplantable tissue sheet. (Syed-Picard et al., 2018) Even though the cell sheet culturing is done as monolayers, 3D structure can be created by stacking the cell sheets layer-by-layer (Priyadarsini, Nicholas and Karamichos, 2018). The advantages of using scaffold-free technique are that there is usually more uniform cell distribution and no harmful degradation products are produced, which may occur during the biodegradation of some scaffold materials. (Li et al., 2019)

As ECM has a major role in connecting and holding the cells together in a scaffold-free cell sheet, enzymatic treatment for cell sheet removal should be avoided due to its ECM-damaging effect (Li et al., 2019). A common method for producing and harvesting cell sheets is to culture the cells on temperature-sensitive substrate (Kobayashi et al., 2013; Madathil, Kumar and Kumary, 2014; Kasai et al., 2020; Venugopal et al., 2020). Typical substrate material is N-isopropylacrylamide (NIPAAm), which is hydrophilic at higher temperatures (> 32 °C), enabling cell adhesion. At lower temperatures (< 32 °C), the cells cannot adhere due to rapid hydration and swelling of the NIPAAm, which results in detachment of the cell sheet. (Li et al., 2019)

In addition to the thermo-responsitivity, the response of the substrate and ermoval of the cell sheet can be caused for example by electrical activation, light, the change in pH or magnetic force, depending on the substrate material and its modification (Li et al., 2019). Recently, peptide amphiphile -coated substrates have been studied in corneal TE to fabricate removable, scaffold-free cell sheets. These cell sheets are called Self-Lifting Auto-generated Tissue Equivalents (SLATEs), and they were fabricated by using human corneal epithelial and stromal cells. (Gouveia, González-Andrades, et al., 2017)

3. 3D BIOPRINTING

In many conventional TE methods, the cells are typically cultured on a flat substrate to grow as monolayers to create a two-dimensional (2D) structure. However, in the body, most of the cells grow in a 3D environment, and therefore, the 2D systems lack the specific 3D structure of the native tissue. (Torras et al., 2018) In addition, the prefabricated substrates, where cells are seeded afterwards, cannot to mimic the precise positioning of cell types and components of the native 3D structure, which is why layer-by-layer additive manufacturing techniques have gained interest in the field of TE (Cui et al., 2020).

3D bioprinting offers a high-precision method to position biomaterials, molecules and cells in a predefined 3D model layer-by-layer, and the use of several printer heads enables the deposition of multiple materials and cell types in the same structure. In addition, due to the use of computer-aided process, 3D bioprinting offers better control and reproducibility. As the desired geometry is designed with a software beforehand, 3D bioprinting provides great customizability. (Selcan Gungor-Ozkerim et al., 2018) Moreover, 3D bioprinting overcomes the challenge with the traditional techniques enabling the fabrication of structures with interconnected pores, and thus sufficient exchange of gas and nutrients (Matai et al., 2020).

3D bioprinting can offer a method to reduce animal tests, as it can provide a more accurate model of human physiology and its responses to drug and material testing (Matai et al., 2020). In addition, patient-specific treatments and precision medicine are potential fields for utilizing 3D bioprinting (Prendergast and Burdick, 2020), and by combining it with stem cell therapy, the possibilities to create personalized therapies is unlimited (Ong et al., 2018). As there is a constant shortage of donor organs, 3D bioprinting has a great potential as a solution for the crisis, and has increasingly gained attention over the years (Vijayavenkataraman et al., 2018). In fact, from 2000 to 2015, the number of research publications related to 3D bioprinting has increased 3300% (from 24 to 792) (Rodríguez-Salvador, Rio-Belver and Garechana-Anacabe, 2017), and the market potential of 3D bioprinting is estimated to grow from USD 411.4 million in 2016 to USD 1332.6 million by 2021 (MarketsandMarkets™ INC, 2017). Thus, in addition to the potential in regenerative medicine and TE, there is a considerable market potential in the field of 3D bioprinting.

3.1 3D bioprinting strategies

3D bioprinting is an additive manufacturing method, where cells embedded in biomaterial are bioprinted layer-by-layer on a substrate or into a supportive bath/matrix by an automated dispensing system (Matai et al., 2020). In 3D bioprinting, the desired geometry is first designed with a software, and then the structure is fabricated from a bioink containing biomaterials and cells. Typically, a computer-aided design (CAD) software is used to create the 3D model and to design its characteristics in detail. In addition to creating the design from the beginning, it can be based on imaging of real tissue or organ using computed tomography (CT), magnetic resonance imaging (MRI), ultrasound imaging or optical microscopy. The model is converted into stereolithography (STL) format for the 3D bioprinter, and it is processed to design the internal structure of the model. (Vijayavenkataraman et al., 2018) After designing the 3D structure, the components for creating the structure are selected, combined together as a bioink and printed (Prendergast and Burdick, 2020). The printing movement and bioink deposition as well as the possible crosslinking are controlled by the software (Selcan Gungor-Ozkerim et al., 2018), and this step requires optimization of the bioink components and concentrations along with the printing parameters. There are several different 3D bioprinting strategies with differences in working principles, and the most common technologies are described next.

3.1.1 Inkjet-based bioprinting

Inkjet-based bioprinting is a non-contact method, where droplets of bioink are positioned on a substrate. The volume of the droplet is usually 1 – 100 pl and contains 10^4 – 30^4 cells. Inkjet-based bioprinting is divided into drop-on-demand (DOD) bioprinting and continuous inkjet (CIJ) bioprinting. In CIJ, printing is done with a continuous stream of electrically conductive bioink drops, which are steered with an electric or magnetic field to form the desired structure. In DOD, the drops are created and ejected only when needed. The major advantages of DOD compared to CIJ are that there is no need for conductive bioinks and the waste of the bioink is greatly reduced. (Matai et al., 2020)

There are different approaches in DOD bioprinting depending on the method to create and eject droplets, including thermal and piezoelectric approaches (Figure 3). In thermal approach, the bioink chamber is heated with an electric pulse, which creates a bubble into the printing nozzle. When the heat is removed after the pulse ends, the bubble inflates. The change between expansion and inflation ejects the droplets out from the nozzle. In piezoelectric approach, a pressure pulse instead of electric is created by

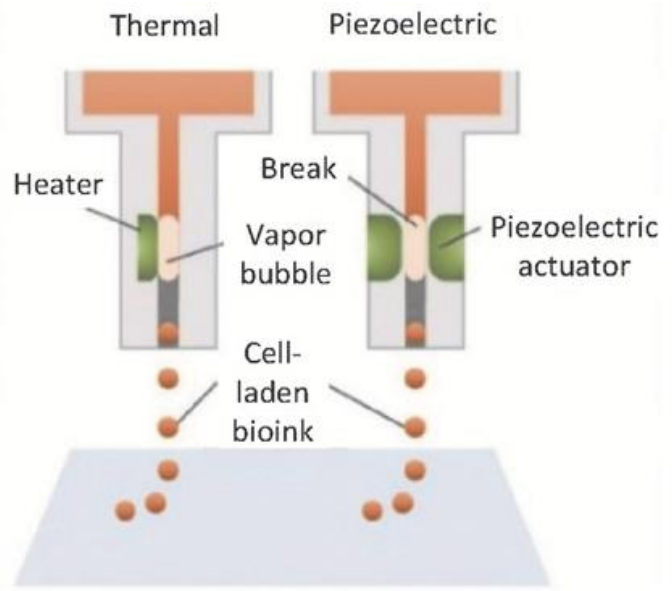

Figure 3. The two DOD bioprinting techniques, thermal and piezoelectric. Bioink bubbles are ejected either by increased temperature or mechanical actuation created by piezoelectric material. Modified from (Cui *et al.*, 2020)

mechanical actuation of piezoelectric material, and the pressure ejects the droplets out from the nozzle. (Matai et al., 2020)

There are specific aspects, which are important to consider in inkjet-based bioprinting. Inkjet-printable bioinks require rheopectic characteristic, which causes the droplets to thicken when they are jetted. In addition, the printing substrate and its coatings will affect the spreading and deformation of the droplet, which will affect the printing result. (Morgan, Moroni and Baker, 2020) The advantages of inkjet-based bioprinting are its affordability, speed and high resolution (50 µm) (Derakhshanfar et al., 2018). However, it can be used only for bioinks with low viscosity (< 10 mPa·s), which limits the used cell density (< 10^6 cells/ml) (Hölzl et al., 2016). Moreover, the vertical printing ability is poor (Derakhshanfar et al., 2018), which limits the size of the 3D bioprinted structure (Prendergast and Burdick, 2020).

Inkjet-based bioprinting has been used for example to create neural networks (Tse et al., 2016), and bone (Gao et al., 2015; Duarte Campos et al., 2016), cartilage (Gao et al., 2015; Nguyen et al., 2017), skin (B. S. Kim et al., 2018) and liver tissue (Faulkner-Jones et al., 2015). In addition, inkjet technology has been used to bioprint endothelial cells to create vascular-mimicking structures with capillary networks (Kreimendahl et al., 2017) and endothelialized lumen (Tröndle et al., 2019). Moreover, it has been used to fabricate photocurable drugs (Acosta-Vélez et al., 2017) and hierarchical porous scaffolds (Ng et al., 2018).

3.1.2 Extrusion-based bioprinting

Extrusion-based bioprinting is well-known and widely used strategy in 3D bioprinting. It is a widely available and affordable, and currently there are several commercially available extrusion-based 3D bioprinters, such as 3D-Bioplotter (EnvisionTEC, Germany), BioX and INKREDIBLE (CELLINK, Sweden), 3DDiscovery (RegenHU, Switzerland), NovoGen MMX (Organovo, USA), BioScaffolder (GeSiM, Germany) and Brinter (3DTech Oy, Finland). In addition to their good availability, they offer compatibility with a wide range of different materials and cells, which is a notable advantage compared to other 3D bioprinting technologies (Prendergast and Burdick, 2020)

In extrusion-based bioprinting, the filament is extruded continuously into a 3D structure and solidified after printing. Pneumatic pressure or mechanical force is used to extrude the bioink from a disposable plastic syringe onto a substrate (Figure 4), and the 3D bioprinted structure can be crosslinked after extrusion. The mechanical force can be generated with a piston or a rotating screw. (Matai et al., 2020) When using pneumatic dispensing system, the air pressure acts as the driving force for the extrusion, whereas in mechanical dispensing systems, the piston or the screw create mechanical force, which extrudes the filament (Derakhshanfar et al., 2018). The crosslinking of a hydrogel bioink can be done before, after or during the bioprinting process (Lim et al., 2020), which increases the flexibility of the technology.

Compared to other 3D bioprinting strategies, the resolution of extrusion-based bioprinting is relatively low, around 100 µm (Zhang *et al.*, 2017). The range of extrudable bioinks is wide (Lim *et al.*, 2020), however, the bioinks for extrusion-based bioprinting require specific rheological properties, such as shear-thinning characteristics, which

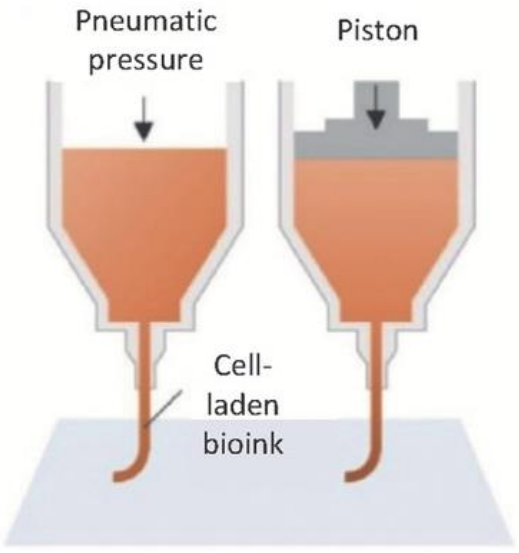

Figure 4. The two extrusion-based bioprinting techniques, pneumatic and mechanical. The bioink is extruded from the syringe onto a substrate. Modified from (Cui *et al.*, 2020).

prevents cell damage by protecting them from shear stress and provides control during printing (Cui *et al.*, 2020). Moreover, it is important that the bioink does not solidify before extrusion. The method enables bioprinting of bioinks with high viscosities, up to 6 x 10^7 mPa·s, which is a major advantage of this 3D bioprinting strategy as bioinks with high cell densities can be printed (Derakhshanfar *et al.*, 2018). High viscosity of the bioink can enhance the result of extrusion-based 3D printing, as it prevents the collapse of the printed structure, however, this increases the risk of nozzle clogging (Cui *et al.*, 2020).

In addition to the properties of the bioink, extrusion-based bioprinting has specific printing parameters, which affect the printability and cell viability. For example, the nozzle diameter, the printing pressure and the speed of the nozzle and the dispenser head affect the quality of the extruded fiber (Van Hoorick *et al.*, 2019). The printing resolution can be increased by using smaller diameter, however, higher pressure might be necessary (Kyle *et al.*, 2017). Moreover, an increase in the printing speed decreases the filament diameter (Liu *et al.*, 2017), and an increase in pressure increases the flow rate of the bioink, which consequently increases the shear stress, and thus the damage for the cells (Cui *et al.*, 2020). The cell viability of extrusion-based bioprinting is relatively low compared to other 3D bioprinting techniques, ranging from 40 – 80% (Cui *et al.*, 2020), however, due to the possibility to use high cell density bioinks, the amount of viable cells remain sufficient after printing (Matai *et al.*, 2020).

There are several techniques of extrusion-based bioprinting, of which the simpliest is the direct extrusion on a substrate (Figure 5 A). This technique enables simple and repeatable extrusion of highly concentrated bioinks, however, pronounced shear-thinning behaviour is required. Instead of extruding the bioink directly on a substrate, it

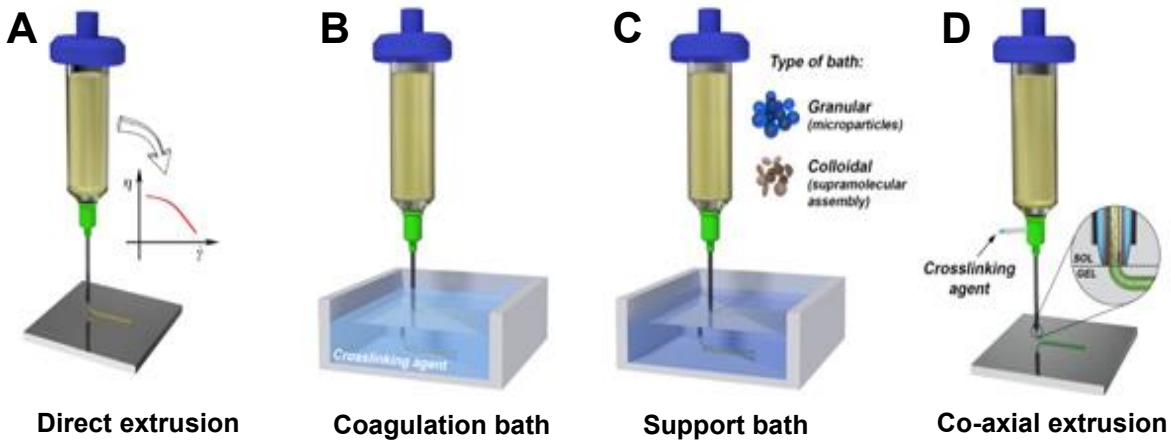

Figure 5. Different techniques for extrusion-based bioprinting. **(A)** Direct extrusion of bioink on a substrate. **(B)** Extrusion in a coagulation bath, which triggers the gelation. **(C)** Extrusion in a granular or colloidal bath, which acts as a support for the bioprinted 3D structure. **(D)** Co-axial extrusion, where bioink and crosslinking agent are dispensed simultaneously with a co-axial needle assembly. Modified from (Costantini *et al.*, 2019).

is possible to use liquid coagulation bath, which acts as a trigger for the gelation of the bioink (Figure 5 B). This requires fast gelation ability, which can clog the nozzle during printing. In addition, as liquid bath is used, the turbulence and buoyancy affect the adhesion and precision of the printed filament. However, the advantage of using coagulaton bath is the independency of printability from the rheological properties. (Costantini et al., 2019)

Freeform reversible embedding is a technique which uses a granular or colloidal bath with soft micro/nanoparticles at high volume fraction instead of the coagulation bath (Figure 5 C). The granular or colloidal bath provides structural support for the extruded bioink and the 3D structure, as the bath locally fluidises around the nozzle tip, while the bioink is extruded, and solidifies fast, when the nozzle moves on. This techniques enables more freedom in the bioink composition than the techniques described above, however, the surface roughness of the printed construct decreases the resolution and the removal of the bath can be complicated. (Costantini et al., 2019)

Due to the limitations and drawbacks of the described techniques, new extrusion-based bioprinting techniques are studied. Co-axial extrusion combines the extrusion of the bioink and the dispension of the crosslinking solution by using a co-axial needle assembly (Figure 5 D). Here, the needle has a core and shell filled with the bioink and the crosslinking agent, which are then simultaneously extruded on a substrate. The dispension of both solutions can be controlled individually, which provides better tunability. In addition, this techniques enables printing of a bulk fiber (bioink in the core and crosslinking agent in the shell) or a hollow fiber (bioink in the shell and crosslinking agent in the core). (Costantini et al., 2019)

Extrusion-based bioprinting has been used for example in cardiac (Zhang et al., 2016; Kang et al., 2017), muscle (Kim and Kim, 2019), bone (Ojansivu et al., 2019), neural (Salaris et al., 2019) and adipose TE (Tytgat et al., 2019), to create vascular-mimicking constructs (Jia, Gungor-Ozkerim, et al., 2016; Ding and Chang, 2018) and to bioprint osteochondral tissue (J. Liu et al., 2019; Kilian et al., 2020). In addition, extrusion-based technology has been used to print multiple bioinks into different layers to create gradient scaffolds (Frost et al., 2019; J. Liu et al., 2019; Kilian et al., 2020) or to use coaxial extrusion to print different bioinks simultaneously (Duchi et al., 2017; W. Liu et al., 2018). Duchi et al. developed a handheld device, Biopen, for cartilage repair. Moreover, extrusion has been used to bioprint hiPSCs for post-printing expansion and differentiation (Gu et al., 2017) and to create aligned collagen structures to provide topographical cues for cell differentiation (Kim and Kim, 2019).

3.1.3 Laser-based bioprinting

Laser-based bioprinting uses laser radiation to pattern bioink with the cells, and the most common type of laser-based method is laser-induced forward transfer (LIFT). In LIFT, there are two coplanar substrates, donor- and collector-slides (Vijayavenkataraman et al., 2018). The donor-slide is a laser-transparent substrate, usually glass or quarzt, coated with a layer of laser-absorbing metal, usually gold or titanium. The bioink is deposited onto the metal layer of the donor-slide. (Matai et al., 2020) As the laser pulse comes through the donor-slide, the metal layer absorbs it, which generates pressure. The pressure causes the bioink droplets to leave the donor-slide and attach to the collector-slide (Figure 6). (Vijayavenkataraman et al., 2018)

Another laser-based bioprinting technique is laser guided direct writing (LGDW), however, the size of the 3D structure and the scalability are limited (Morgan, Moroni and Baker, 2020), and it is not as widely studied and used as LIFT. In LGDW, laser is focused onto a target area containing the cell-laden bioink. The laser beam generates force in the cell-media interface, causing the bioink droplets to leave the suspension. When coupled with a hollow fiber, the droplets can be deposited through the fiber as a steady stream onto a substrate. (Odde and Renn, 1999)

Laser-based bioprinting is a nozzle-free approach, and thus there are no clogging problems (Vijayavenkataraman *et al.*, 2018). In addition, it can be used for bioinks with different viscosities, ranging from 1 to 300 mPa·s, and with high cell density (10^8 cells/ml) (Matai *et al.*, 2020). It offers high resolution (10-100 µm), however, to reach the high resolution, the bioink used for laser-based bioprinting requires compatibility of working

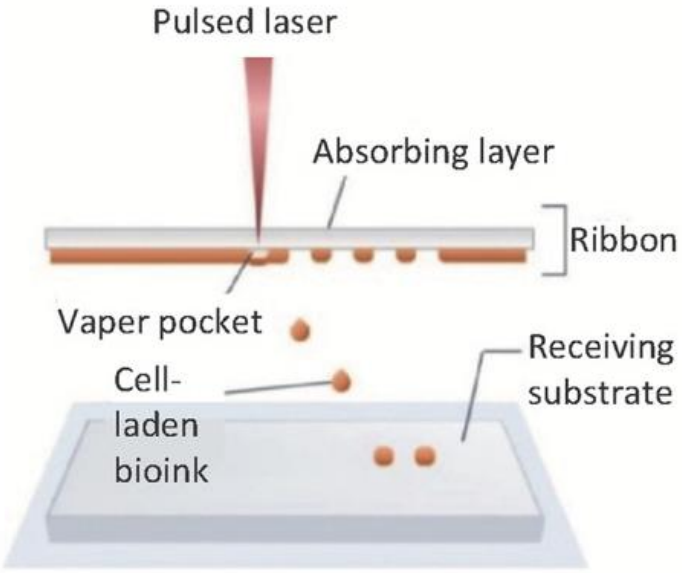

Figure 6. Laser-induced forward transfer method, where a laser pulse is used to generate pressure, causing the bioink droplets to leave from the donor-slide (ribbon) onto a collector-slide (receiving substrate). Modified from (Cui *et al.*, 2020)

wavelengths, fast gelation (Matai *et al.*, 2020), and adhesion to the printing substrate (Morgan, Moroni and Baker, 2020). The viscoelasticity of the bioink is required for the ejected droplets to keep their shape (Morgan, Moroni and Baker, 2020). Moreover, the printing speed is low (Prendergast and Burdick, 2020), the method is costly and complex (Vijayavenkataraman *et al.*, 2018), and thus it is not commercially as easily available.

LIFT technology has been used in cardiac (Gaebel *et al.*, 2011) and skin regeneration (Koch *et al.*, 2010), as well as for creating vascular-like network (Gruene *et al.*, 2011). LGDW technology has been used to bioprint multipotent adult progenitor cells (Nahmias, Gao and Odde, 2004) and endothelial cells (Nahmias *et al.*, 2005; Nahmias and Odde, 2006) (Nahmias and Odde, 2006).

3.1.4 Lithography-based bioprinting

Lithography-based bioprinting uses light to cure the 3D structure, and thus requires the use of light-sensitive bioinks. This method is divided into two main techniques, stereolithography (SLA) and digital light processing (DLP) (Figure 7). In SLA, the bioink is cured with a laser beam, which is focused onto the bioink from above. In DLP, the bioink is cured by light projected from below onto a build stage, which moves vertically upward, creating the 3D structure layer-by-layer. (Lim et al., 2020) DLP has been used to bioprint for example vascular structures (Zhu et al., 2017), and cardiac (Yu et al., 2019), cartilage (Lam et al., 2019; Chen et al., 2020) and liver tissue (Ma et al., 2016; Yu et al., 2019; Mao et al., 2020).

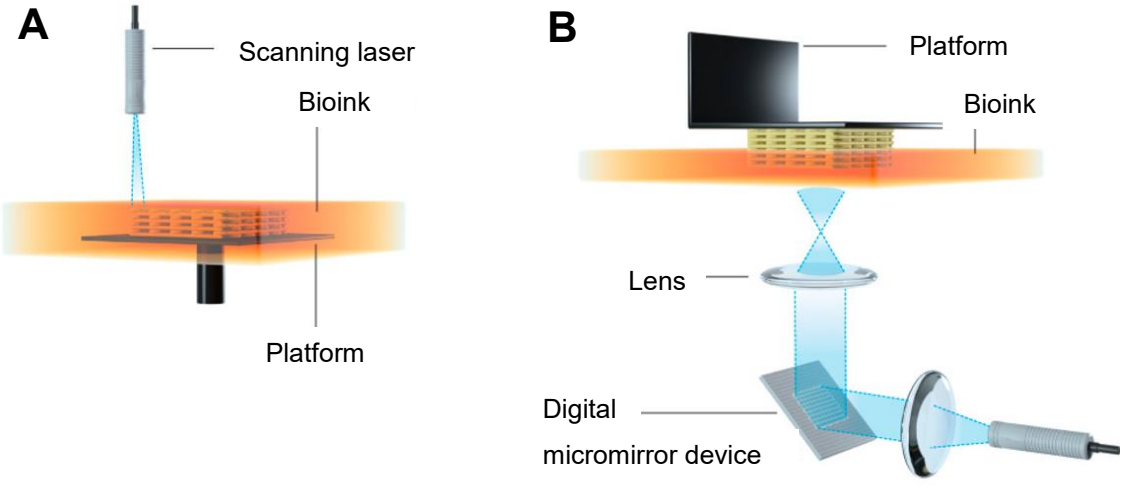

Figure 7. Two techniques for lithography-based bioprinting. **(A)** Stereolithography, where a scanning laser is used to cure the bioink on a platform. **(B)** Digital light processing, where projected light is used to cure the bioink on a vertically moving platform. Modified from (Lim *et al.*, 2020).

Lithography-based bioprinting is a nozzle-free approach (Vijayavenkataraman *et al.*, 2018), and the printing time is independent of the complexity of the structure (Matai *et al.*, 2020), resulting in efficient printing process with good ratio of spatial resolution to the time required (Prendergast and Burdick, 2020). The resolution is high (25 – 50 µm), and lithography-based tecnology offers possibilities to create structures, which are not possible with extrusion-based bioprinting (Lim *et al.*, 2020). However, as the technique requires light radiation, only inks with photo-crosslinkable polymers can be used (Prendergast and Burdick, 2020).

3.2 Bioinks

The term bioink was first introduced in 2003 in the context of organ printing, and it originally reffed to cellular components which were in 3D on or within hydrogels (Groll et al., 2018). Today, a bioink is defined as a cell-laden, printable biomaterial (Matai et al., 2020; Morgan, Moroni and Baker, 2020), and it is distinct from the term biomaterial ink, in which the cells are not a mandatory component as they are seeded afterwards on within the pre-printed scaffold (Groll et al., 2018). Even though there are increasing number of studies done in 3D bioprinting, the development of a printable, cell-laden bioink remains a challenge due to several bioink requirements discussed next.

The main objectives of a bioink are to maintain the cell viability, to direct the desired cell behaviour and to be bioprintable (Morgan, Moroni and Baker, 2020), which make designing bioinks the key in the development of 3D bioprinting tissues. Cells are sensing and responding to their environment through mechanotransduction, and depending on the tissue type, the cells are subjected to different forces (Williams et al., 2018), and different tissues have different mechanical properties (Handorf et al., 2015). The mechanical stimuli of the environment and surrounding ECM guide the proliferation and differentiation of the cells, and if there occurs a change in the mechanical properties of the ECM, such as in stiffness, the homeostasis might be shifted, leading in disease (Handorf et al., 2015). Thus, in addition to the bioprintability of the bioink, the properties of the bioprinted structure, such as the stiffness or composition of the bioink, need to mimic the microenvironment of the target cell niche (Williams et al., 2018).

The physical and rheological properties of the bioink affect greatly its bioprintability as well as the environment the cells experience (Morgan, Moroni and Baker, 2020), which makes them important for the design and characterization of the bioink. Moreover, the properties of the bioink and the printing parameters can have cooperative effects on the printability. For example, when using temperature-sensitive bioink components, such as

gelatin, the temperature of the cartiridge and the printing platform affect the printability and the cell viability (Gu et al., 2018).

The physical properties, such as the viscosity, surface tension and density, can be altered for example by changing the composition and concentration of the bioink components or modifying it chemically (Morgan, Moroni and Baker, 2020). The viscosity describes fluid's resistance to flow (Zimmerman Jones, 2019), and if the viscosity is too low, the printed structure does not keep its shape, however, with too high viscosity the shear stress increases, which is harmful for the cells (Chimene, Kaunas and Gaharwar, 2020). The rheological properties of the material describe its flow behaviour, and include for example yield stress or shear-thinning characteristics. Yield stress means the minimum stress, which is needed for the material to flow, and for the material to be fluid-like, its need to be higher than the shear stress. (Chimene, Kaunas and Gaharwar, 2020) Shear-thinning means the viscosity is decreased when the material is subjected to shear stress (Morgan, Moroni and Baker, 2020).

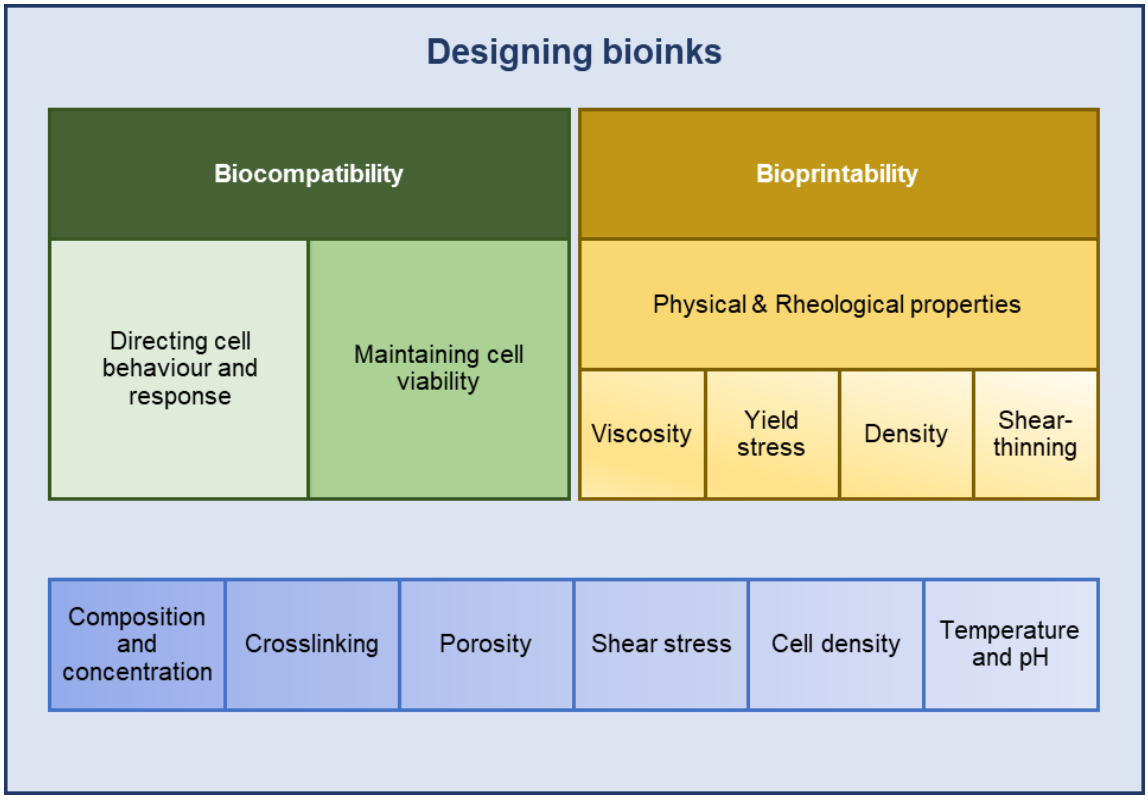

Figure 8. The main aspects to consider when designing bioinks. The bioink has two roles from the biocompatibility side, to direct cell behaviour and response, and to maintain cell viability. The third role of the bioink is to be bioprintable, which is affected by its physical and rheological properties, such as viscosity, yield stress, density and shear-thinning behaviour. All these aspects are affected by the composition and concentration of the bioink components, the crosslinking method and density, porosity, shear stress, cell density and the temperature and pH.

Figure 8 summarizes the main properties guiding the design of bioinks considering the cell and biology aspect and the bioprintability aspect. Extrusion-based bioprinting has special requirements for properties of bioinks, as these properties are essental for printability and shape fidelity. Table 2 summarizes these properties presented by Cui et al. 2020.

Table 2. The summary of bioink criteria for extrusion-based bioprinting.

Property	Explanation	Determined by	Impacts
Viscosity	The fluid's resistance to flow under applied stress	Polymer concentration and molecular weight Solubility Shear rate Temperature	High viscosity prevents the printed structure from collapsing and the bioink dropping from the nozzle, however, the risk of nozzle clogging increases
Shear thinning	Viscosity decreases under increased stress due to disentanglement of polymer chains	The ability of polymer chains to reorganize	Affects printability and structural integrity after printing Protects cells from shear stress Essential in direct extrusion
Yield stress	The minimum value of stress which is required for the fluid to flow	Shear thinning behaviour Crosslinking mechanism	Affects printability Prevents the cells from settling in the bioink solution Prevents printed structure from collapsing
Shear recovery	The recovery of mechanical properties after shear thinning	Bioink composition	Stabilizes the printed filament
Gelation or crosslinking mechanism	Solidification of the bioink solution Creation of physical or chemical crosslinks which link polymer chains together	Composition of the bioink Crosslinking strategy	Affects the density and stiffness of the printed structure Stabilizes the printed filament Affects the cell viability and functionality

The biomaterial component of a bioink can be a natural polymer, synthetic polymer or a composite, and usually it is in hydrogel form (Matai *et al.*, 2020). The advantages of hydrogels are their aqueous environment and porosity, which enable sufficient oxygen and nutrient diffusion as well as the cell migration. A single component bioink is not capable of meeting the bioink requirements, which is why most of the bioinks combine multiple materials (Cui *et al.*, 2020). In addition, the possibility of adding proteins and other ECM components to hydrogel bioinks allow them to mimic the native microenvironment of the bioprinted cells and guide the stem cell growth (Chimene, Kaunas and Gaharwar, 2020).

Even though hydrogels have become a popular choice for cell-laden bioinks, many hydrogels alone are mechanically too weak to support the bioprinted structure. Subsequently, their polymer content and crosslinking density are modified, or other components are added to the bioink as rheological modifiers. In addition to these more conventional techniques, hydrogel bioinks can be reinforced by polymer functionalization, nanocomposites and thermoplastic reinforcement. (Chimene, Kaunas and Gaharwar, 2020)

The cells are an important component of the bioink, and in the field of 3D bioprinting, the number of recent studies using hPSCs is increasing due to the possibility to mimic the native cellular variety and cytoarchitecture. Yet, they have specific characteristics, which makes them challenging to use in bioprinting. Even though cell spheroids can be bioprinted with specific method called Kenzan method, most of the bioprinting techniques require the cells to be dissociated as single cells for 3D bioprinting. However, hPSCs survive poorly as singe cells, and thus, they tend to form clusters. This can cause challenges with nozzle-based bioprinting approaches, such as extrusion-based bioprinting. In addition, because hPSCs are highly sensitive to their environment and its cues, the composition and properties of the bioink need careful research and design. (Salaris and Rosa, 2019)

There are several different biomaterials studied in developing bioinks, however, this thesis can cover only few of them. Moreover, there is research done to 3D bioprint cells as shperoids without any biomaterial (Moldovan *et al.*, 2017; Ong *et al.*, 2017), however, this thesis concentrates on bioinks combining cells and biomaterials. Table 3 presents a summary of different bioink components, crosslinking and 3D bioprinting techniques as well as the bioprinted cell types. The common biomaterial components used in bioinks are discussed next.

Table 3. Summary of recent research in the field of 3D bioprinting. Col = Collagen, hMSCs = Human mesenchymal stem cells, GelMA = Gelatin methacrylate, HA = Hyaluronic acid, HAMA = Hyaluronic acid methacrylate, hACS = Human adipose stem cells, hUVECs = Human umbilical vein endothelial cells, PEG = Polyethylene glycol.

Bioink	Crosslinking	3D bioprinting technique	Cell type	Reference
Alginate – Carboxymethyl chitosan – Agarose	Ionic	Extrusion	hiPSCs	(Gu *et al.*, 2017)
Alginate	Ionic	Inkjet	hiPSCs	(Faulkner-Jones *et al.*, 2015)
Alginate – Matrigel	Ionic	Extrusion	hiPSC-derived neurons and glial cells	(Salaris *et al.*, 2019)
Alginate – Gelatin – Fibrinogen	Ionic Covalent	Extrusion	hMSCs	(Henrionnet *et al.*, 2020)
Alginate – GelMA	Ionic Photocrosslinking	Extrusion	hUVECs	(Zhang *et al.*, 2016)
Alginate – Methylcellulose – O_2-sensitive luminescent nanoparticles	Ionic	Extrusion	hMSCs	(Trampe *et al.*, 2018)
Alginate – Nanocellulose **Tyramine-functionalized HA – Nanocellulose**	Ionic Covalent	Inkjet	hiPSCs	(Nguyen *et al.*, 2017)
Alginate – Nanocellulose	Ionic	Extrusion	Human fibroblasts Human nasal chondrocytes	(Thayer, Orrhult and Martínez, 2018)
Alginate – Methylcellulose	Ionic	Extrusion	Human chondrocytes	(Kilian *et al.*, 2020)
Alginate – nanocellulose – carboxymethyl cellulose	Ionic	Extrusion	Human skin fibroblasts	(Zidarič *et al.*, 2020)

Col type I – Alginate	Ionic	Extrusion	Human preosteoblasts and hACS	(Lee *et al.*, 2015)
Col type I – Agarose **Fibrinogen - Agarose**	Thermal	Inkjet	hUVECs and human fibroblasts	(Kreimendahl *et al.*, 2017)
Col type I - Agarose	Thermal	Inkjet	hMSCs	(Duarte Campos *et al.*, 2016)
Col type I	Thermal Covalent	Extrusion	Myoblasts	(Kim and Kim, 2019)
Decellularized liver tissue	Thermal	Extrusion	Human hepatocellular carcinoma cells	(Lee *et al.*, 2017)
Decellularized cardiac tissue – GelMA **Decellularized liver tissue – GelMA**	Photocrosslinking	Digital light processing	hiPSC-derived cardiomyocytes and hepatocytes	(Yu *et al.*, 2019)
Decellularized liver tissue - GelMA	Photocrosslinking	Digital light processing	hiPSC-derived hepatocytes	(Mao *et al.*, 2020)
Decellularized skin tissue	Thermal	Extrusion Inkjet	Human fibroblasts and keratinocytes hMSCs Human endothelial progenitor cells	(B. S. Kim *et al.*, 2018)
Decellularized pancreatic tissue	Thermal	Extrusion	Primary islet cells from rat pancreas	(J. Kim *et al.*, 2019)
GelMA	Photocrosslinking	Extrusion	Human fibroblasts	(Kolesky *et al.*, 2014)
GelMA – Glycidal methacrylate HA	Photocrosslinking	Extrusion	hiPSC-derived hepatic progenitor cells	(Ma *et al.*, 2016)
GelMA **HAMA**	Photocrosslinking	Digital light processing	Porcine chondrocytes	(Lam *et al.*, 2019)
Thiolated HA – Thiolated gelatin	Photocrosslinking PEG crosslinker	Extrusion	Human liver stellate cells and Kupffer cells	(Skardal *et al.*, 2015)
HAMA	Photocrosslinking PEG crosslinker	Extrusion	-	(Ma *et al.*, 2020)

3.2.1 Agarose

Agarose is a polysaccharide which undergoes gelation at low temperatures (Hospodiuk *et al.*, 2017). Although agarose has good properties for printing, such as high viscosity, it does not have cell binding sites (Nadernezhad *et al.*, 2019), which makes it unpopular material alone. Agarose has been used as a support material in 3D bioprinting (Kucukgul *et al.*, 2015; Mirdamadi *et al.*, 2019), however, to increase its cell-friendliness, it has been blended with other hydrogels, such as ColI (Tan *et al.*, 2016; Kreimendahl *et al.*, 2017) or Matrigel (Fan *et al.*, 2016). The bioactivity and shear thinning behaviour of agarose can be increased for example by adding nanosilicate into the bioink (Nadernezhad *et al.*, 2019). Bioinks containing agarose have been used to bioprint for example hUVECs and human fibroblasts (Kreimendahl *et al.*, 2017), hiPSCs (Gu *et al.*, 2017) and human intestinal epithelial cells (Fan *et al.*, 2016).

3.2.2 Alginate

Alginate is a polysaccharide found in the cell walls of brown algae and some bacteria, and it consists of β-D-mannuronic acid and α-L-guluronic residues, which create a block-like structure (Abasalizadeh *et al.*, 2020). The advantages of alginate are its affordability and availability in addition to nontoxicity, biocompatibility and biodegradability (Y. Zhang *et al.*, 2019). The amount and ratio of these building blocks depend on the origin and growth conditions of the alginate. In addition, the molecular weigth and acetylation degree can vary, and for example, the viscosity of alginate increases, when the pH is decreased or the molecular weight is increased. (Abasalizadeh *et al.*, 2020) Therefore, the molecular weigth affects the bioprintability of the alginate-based bioink and mechanical properties of the bioprinted structure (Freeman and Kelly, 2017).

Alginate can form hydrogels in the presence of divalent cations, such as Ca^{2+} and Ba^{2+}, and typical method to create alginate gel is to add calcium chloride ($CaCl_2$) into alginate solution as crosslinker agent, resulting in ionic crosslinks (Abasalizadeh *et al.*, 2020). In addition to $CaCl_2$, for example calcium sulphate or calcium carbonate can be used, and the choice of the ionic crosslinker has been shown to affect the bioprintability and mechanical properties of the bioprinted structure (Freeman and Kelly, 2017). In addition to ionic crosslinking, alginate hydrogels can be created with chemical crosslinkers, such as glutaraldehyde. In addition, alginate can be methacrylated to create a photocrosslinkable hydrogel, or functionalized with thermosensitive polymer for thermal crosslinking or cell surface receptor -specific ligands to create cell crosslinked hydrogel. (Abasalizadeh *et al.*, 2020)

In 3D bioprinting, alginate has been studied as a bioink component for example in bioprinting cartilage tissue (Markstedt *et al.*, 2015; Nguyen *et al.*, 2017; Yang *et al.*, 2018; Henrionnet *et al.*, 2020), osteochondral tissue (Kilian *et al.*, 2020) and skin tissue (Zidarič *et al.*, 2020). In addition, alginate has been used to bioprint hiPSCs and differentiate them into neural tissue (Gu *et al.*, 2017). Its advantages are rapid crosslinking and affordability, however, the cell adhesion and mechanical strength are poor (Parak *et al.*, 2019).

3.2.3 Collagen

Collagen is the most abundant ECM protein, which can form biocompatible hydrogels with shear-thinning properties. In addition, it is sensitive to pH and temperature, as it undergoes physical crosslinking when the temperature is increased over 30 °C. Shear-thinning properties and the possibility to control its crosslinking with pH and temperature make collagen a potential component for bioinks, even though the mechanical properties are weak without further crosslinking. (Włodarczyk-Biegun and del Campo, 2017) There are several different collagen types, of which some are fibril-forming collagens whereas some form networks. Collagen types I, II and III are the most abundant, and they all form fibrils. ColIV is an example of a network-forming collagen, and it is typically present in basement membranes. (Mienaltowski and Birk, 2014)

ColI is the most widely studied type of collagen in 3D bioprinting, and for example, it has been used in engineering cartilage tissue (Yang *et al.*, 2018), cardiac tissue (Kim and Kim, 2019), small intestine (Kim and Kim, 2020) and liver tissue (Mazzocchi *et al.*, 2018). In addition, bioprinting bioinks containing collagen have been shown to promote stem cell differentiation of for example human adipose stem cells (Lee *et al.*, 2015) and mesenchymal stem cells (Duarte Campos *et al.*, 2016). Due to the tendency to form fibrils, ColI has been studied to bioprint aligned cells, such as myoblasts, preosteoblasts, cardiomyocytes and human adipose stem cells (Kim and Kim, 2019).

3.2.4 Decellularized tissue

ECM is produced by the cells to create a suitable environment for their adhesion, migration, differentiation and maturation. The interaction between the ECM and the cells is dynamic and mutual, as the cells produce the surrounding ECM, which again influences the behavior of the cells. The tissue-specificity of ECM is due to the composition of its components, including proteins, biomolecules and proteoglycans, as it varies between tissues. As ECM creates the required microenvironment for the cells in the native tissue, decellularized ECM derived from the native, tissue-specific ECM is a

promising material to provide appropriate, native-like biochemical cues and proteins for the 3D bioprinted cells. (Dzobo, Motaung and Adesida, 2019)

Decellularization is an important step to decrease the risk of inflammatory and immune response, leading to possible tissue rejection. However, decellularization needs to eliminate only the cellular components, and thus maintaining the native composition of the ECM. (Kabirian and Mozafari, 2020) Decellularization methods include various physical, chemical and enzymatic approaches (Kabirian and Mozafari, 2020), as were described previously.

Pig is the major source of decellularized ECM due to its availability, similarities in anatomy and physiology to humans and short gestation period (Kabirian and Mozafari, 2020). However, using xenogeneic ECM source can cause immunological reactions (Dzobo, Motaung and Adesida, 2019), and there is a change of xenozoonoses development (Kabirian and Mozafari, 2020). Human tissue is a better source for decellularized ECM, and for example, human adipose tissue is well available, as it produced as medical waste from liposuctions. Even though the biocompatibility and the native-like properties of decellularized ECM are its major advantages, the challenges in using decellularized ECM -based bioinks include difficulties in scalability, batch-to-batch variation and possible immune reaction. (Dzobo, Motaung and Adesida, 2019)

Decellularized ECM have been used to 3D bioprint adipose tissue (Pati *et al.*, 2015), cardiac tissue (Jang *et al.*, 2017; Yu *et al.*, 2019), liver tissue (Lee *et al.*, 2017; Yu *et al.*, 2019; Mao *et al.*, 2020), skeletal tissue (Choi *et al.*, 2016), skin tissue (B. S. Kim *et al.*, 2018), pancreatic tissue (J. Kim *et al.*, 2019), blood vessel -like structure (Gao *et al.*, 2017) and small intestine villus structure (Kim and Kim, 2020). In addition, decellularized ECM has been studied for bioprinting cornea (H. Kim *et al.*, 2019). If stem cells are used, their differentiation can be guided with the tissue-specific decellularized ECM -based bioink (Pati *et al.*, 2015; Choi *et al.*, 2016; Jang *et al.*, 2017; Lee *et al.*, 2017; H. Kim *et al.*, 2019; Yu *et al.*, 2019).

3.2.5 Fibrinogen and fibrin

Fibrinogen and fibrin are proteins found in ECM, and they have a key role in blood clotting and wound healing. Fibrinogen is synthetized in the liver, and a protease called thrombin causes it to hydrolyze and polymerize into fibrin. Fibrin is chemically crosslinked by calcium ions, which stabilizes its structure. They are derived from blood, which can be autologous. (Włodarczyk-Biegun and del Campo, 2017) The use of fibrinogen provides enhanced cell adhesion and integrity of printed structure, which is a major advantage in 3D bioprinting (Tröndle *et al.*, 2019; Henrionnet *et al.*, 2020). In addition, the advantages

of fibrin include the promotion of cell proliferation, differentiation and angiogenesis, good mechanical properties and fast gelation. However, fibrin is degraded fast by proteases, which is why protease inhibitors may be needed. (Włodarczyk-Biegun and del Campo, 2017)

Fibrinogen has been studied in 3D bioprinting for example hiPSC-derived neural tissue (de la Vega *et al.*, 2018; Abelseth *et al.*, 2019; Sharma *et al.*, 2020), hMSC-derived cartilage tissue (Henrionnet *et al.*, 2020) and hiPSC-derived cardiomyocytes (Anil Kumar *et al.*, 2019). In addition, human endothelial cells (Tröndle *et al.*, 2019) and human dermal fibroblasts (Freeman *et al.*, 2019) have been embedded in fibrinogen-based bioink in order to 3D bioprint vascular constructs.

3.2.6 Gelatin

Gelatin is derived from collagen through denaturation due to chemical treatment or change in temperature, and the denaturation is irreversible (Marques *et al.*, 2019). Gelatin contains innate adhesive peptide sequences, enhancing the adhesion and spreading of cells, and thus resulting in high biocompatibility (Lim *et al.*, 2020), which is important quality for bioink components. In addition, gelatin is widely studied in 3D bioprinting because it is cost-effective, well available and considered safe by the FDA (Van Hoorick *et al.*, 2019).

Gelatin is highly temperature-dependent, which affects its use as a bioink component. The dissociation temperature for gelatin is 30 – 35 °C, and whereas it dissolves at higher temperatures, hydrogels are formed at lower temperatures due to hydrogen bonding and physical crosslinking (Van Hoorick *et al.*, 2019). Subsequently, it liquifies at physiological temperatures (Parak *et al.*, 2019). By modifying gelatin, its properties, such as stability, can be altered, and typical crosslinking and modification methods for gelatin are methacrylation, thiolation and norbornene functionalization (Lim *et al.*, 2020). Photocrosslinkable gelatin, gelatin methacrylate (GelMA), has become the golden standard in bioinks (Van Hoorick *et al.*, 2019), and there are several commercially available GelMA-based bioinks (CELLINK; Sigma Aldrich; Allevi).

In 3D bioprinting, gelatin has been studied as a bioink component for example to bioprint hASCs (Sakai *et al.*, 2018) and hMSCs (Henrionnet *et al.*, 2020), and its methacrylated form has been studied for bone marrow stem cells (Yin *et al.*, 2018), osteoblasts (McBeth *et al.*, 2017), chondrocytes (Schuurman *et al.*, 2013), hUVECs (Jia, Selcan Gungor-Ozkerim, *et al.*, 2016; Liu *et al.*, 2017) and hMSCs (Gao *et al.*, 2015; Jia, Gungor-Ozkerim, *et al.*, 2016; J. Liu *et al.*, 2019). Moreover, GelMA has been studied in 3D

bioprinting tenocytes and myoblasts as co-culture to generate muscle-tendon tissues (Laternser *et al.*, 2018).

3.2.7 Hyaluronic acid

HA is a hydrohilic polymer and a common component in ECM, however, its concentration depends on the tissue type. It is a glycosaminoglycan composed of D-glucuronic acid and N-acetyl D-glucosamine linked via glycosidic bonds. In aqueous solutions, HA binds water molecules, forming a viscoelastic substance, and its major functions are to lubricate, hydrate and transport water in tissues. In addition, the large size of HA enables it to provide structural and biochemical support. HA is biologically synthesized in vertabrates by integral membrane proteins, which produce low- or high-molecular weigth HA. In addition, HA can be synthesized in laboratory from synthetic materials, which decreases the batch-to-batch variation. (Yazdani *et al.*, 2019)

HA can be used to create very soft hydrogels, however for 3D bioprinting applications, HA can be too soft to hold its 3D shape after printing (Serban and Skardal, 2019). Therefore, the possibility to chemically modify HA is essential for altering its physical properties and to enhance the printability. For example, it can be modified with metyhacrylate, norbornene, tyramine, thiol and acrylate groups (Lim *et al.*, 2020), and different crosslinking strategies, such as thiolation and photocrosslinking via methacrylation have been studied to increase the stiffness of HA (Lam *et al.*, 2019). Enzymatic crosslinking has been studied to pre-crosslink the HA-based bioink to make it extrudable (Petta *et al.*, 2018). In addition, combining HA with other bioink components can enhance the mechanical properties of the bioprinted structure (Skardal *et al.*, 2010; Schuurman *et al.*, 2013; Rajaram, Schreyer and Chen, 2014; Constantini *et al.*, 2016; Nguyen *et al.*, 2017; Kiyotake *et al.*, 2019; Lam *et al.*, 2019; Antich *et al.*, 2020). Chemical modification of HA and its combination with other polymers provide an attractive biomaterial for stem cell -based therapy and TE, and the number of clinical trials using HA-based materials with stem cells is increasing (Galvez-Martin *et al.*, 2019).

HA is a major component of native cartilage, and thus it has been widely studied as a bioink component for 3D bioprinting cartilage tissue (Constantini *et al.*, 2016; Nguyen *et al.*, 2017; Lam *et al.*, 2019; Antich *et al.*, 2020). HA has been used to bioprint stem cells, such as hiPSCs (Nguyen *et al.*, 2017), hMSCs (Constantini *et al.*, 2016) and hASCs (Sakai *et al.*, 2018). As examples of using modified HA, hyaluronic acid methacrylate (HAMA) has been used as a bioink component in 3D bioprinting cartilage (Duchi *et al.*, 2017; Lam *et al.*, 2019) and bone tissue (Michelle T. Poldervaart *et al.*, 2017), and thiolated HA to 3D bioprint liver tissue (Mazzocchi *et al.*, 2018).

3.2.8 Laminin

Laminins are heterotrimeric glycoproteins and abundant in basement membranes (Wilson, Torricelli and Marino, 2020), and shown to enhance cell adhesion and migration for example with hESC-derived neural stem cells (Barros *et al.*, 2019), hiPSC-derived spinal sheroids (Besser *et al.*, 2020) and human epithelial organoids (Broguiere *et al.*, 2018). However, there are quite few studies of laminin in bioinks, even though there are commercially available laminin products suitable for 3D bioprinting. Laminin is a primary component in Matrigel (Corning), which is a mixture of basement proteins from Engelbreth-Hol-Swarm mouse sarcoma (*Corning Matrigel Matrix*), and it has been used in 3D bioprinting of human breast cancer cells (Nerger, Brun and Nelson, 2019), human melanoma cells (Schmidt *et al.*, 2019) and human alveolar cells (Berg *et al.*, 2018). Sorkio et al. used human recombinant laminin to 3D bioprint hESC-LESCs (Sorkio *et al.*, 2018). In addition, laminin-based bioinks have been recently commercialized (*GelX LAMININK*; *CELLINK LAMININK*).

3.2.9 Nanocellulose

Cellulose is a polymer, which can be derived from plants or bacteria. Plant-based cellulose has a partially crystalline, micro- and nanofibril form, which main function is to act as a loadbearing structure. Thus, it has good mechanical strength and flexibility. The fibrils can be isolated, and the term nanocellulose is defined as the diameter of the fibrils in nanoscale. Nanocellulose can be categorized into bacterial nanocellulose, cellulose nanofibrils and cellulose nanocrystals, of which the two latter can be derived from biomass by breaking the bonds between fibrils with mechanical force, or combining the mechanical force with acidic, enzymatic or chemical oxidation. Whereas nanocrystals consists of the crystal regions alone, nanofibrils contain both crystalline and non-crystalline regions. Bacterial nanocellulose is synthezised via oxidative fermentation in microbial culture. (Wang, Wang and Xu, 2020)

Nanocellulose has gained attention in 3D bioprinting due to its porosity and interconnect framework within the hydrogel, as well as the shear-thinning properties for extrusion-based bioprinting. In addition, the nanocellulose fibrils seem to have similarities with collagen and fibronectin fibrils in native ECM. (Wang, Wang and Xu, 2020) Nanocellulose fibrils has been used in 3D bioprinting to enhance the properties of low viscosity bioinks by providing shear thinning behaviour (Markstedt *et al.*, 2015; Müller *et al.*, 2017; Shin *et al.*, 2017; Ojansivu *et al.*, 2019) and increasing the structural and mechanical support of the bioink (Nguyen *et al.*, 2017). It has been studied for example in 3D bioprinting of bone

(Ojansivu *et al.*, 2019) and cartilage tissue (Markstedt *et al.*, 2015; Nguyen *et al.*, 2017), and in wound healing applications (Xu *et al.*, 2019).

3.3 Crosslinking strategies of hydrogel based bioinks

Hydrogels are a widely studied material for 3D bioprinting as they provide an aqueous environment for the embedded cells (Chimene, Kaunas and Gaharwar, 2020). As any hydrogel, a hydrogel based bioink requires crosslinking for maintaining the stability of the printed structure (Cui *et al.*, 2020). There are almost unlimited possibilities to modify hydrogels, create new combinations and study different crosslinking strategies, which enables the discovery of new properties for bioinks.

Crosslinking can be done by creating physical or chemical interactions, and there are several different methods to crosslink the hydrogel based bioink (Figure 9). Physical crosslinking is non-covalent and reversible, and it includes electrostatic interactions (ionic crosslinking), hydrophobic interactions and hydrogen bonding interactions, of which the hydrophobic interactions and hydrogen bonding can depend on temperature. In chemical crosslinking, the network is created with covalent bonds, and the mechanical stability is usually better than with physical crosslinking. (Hospodiuk et al., 2017) The covalent bonding requires the presence of chemically reactive functional groups, which create chemical crosslinks with the polymer network (Cui et al., 2020). Chemical crosslinking includes for example different chemical crosslinkers and photocrosslinking. Moreover, enzymes can be used as crosslinkers for chemical crosslinking of hydrogels (Cui et al., 2020), however, it is not discussed in detail in this thesis.

Different cell types prefer different environments, and the mechanical properties of the bioink should mimic the natural environment of the cells (Williams et al., 2018). By increasing the crosslinking density, the strength and stiffness of the hydrogel can be increased because of the increase in the number of polymer chains and decrease in the length of individual chains. However, too high density can affect the cells due to decrease in porosity and permeability, which is why one of the key aspects in designing bioinks is to find a balance in the crosslinking density. (Chimene, Kaunas and Gaharwar, 2020) Thus, the optimization of the crosslinking strategy and parameters has a considerable effect on the bioprinted cells. Usually multiple components or modifications are combined to design hybrid bioinks, which enables the use of different crosslinking methods to utilize their advantages and develop novel, tunable bioinks (Ouyang et al., 2016; Petta et al., 2018; Zhu et al., 2018; Kajave et al., 2020; Shin et al., 2020).

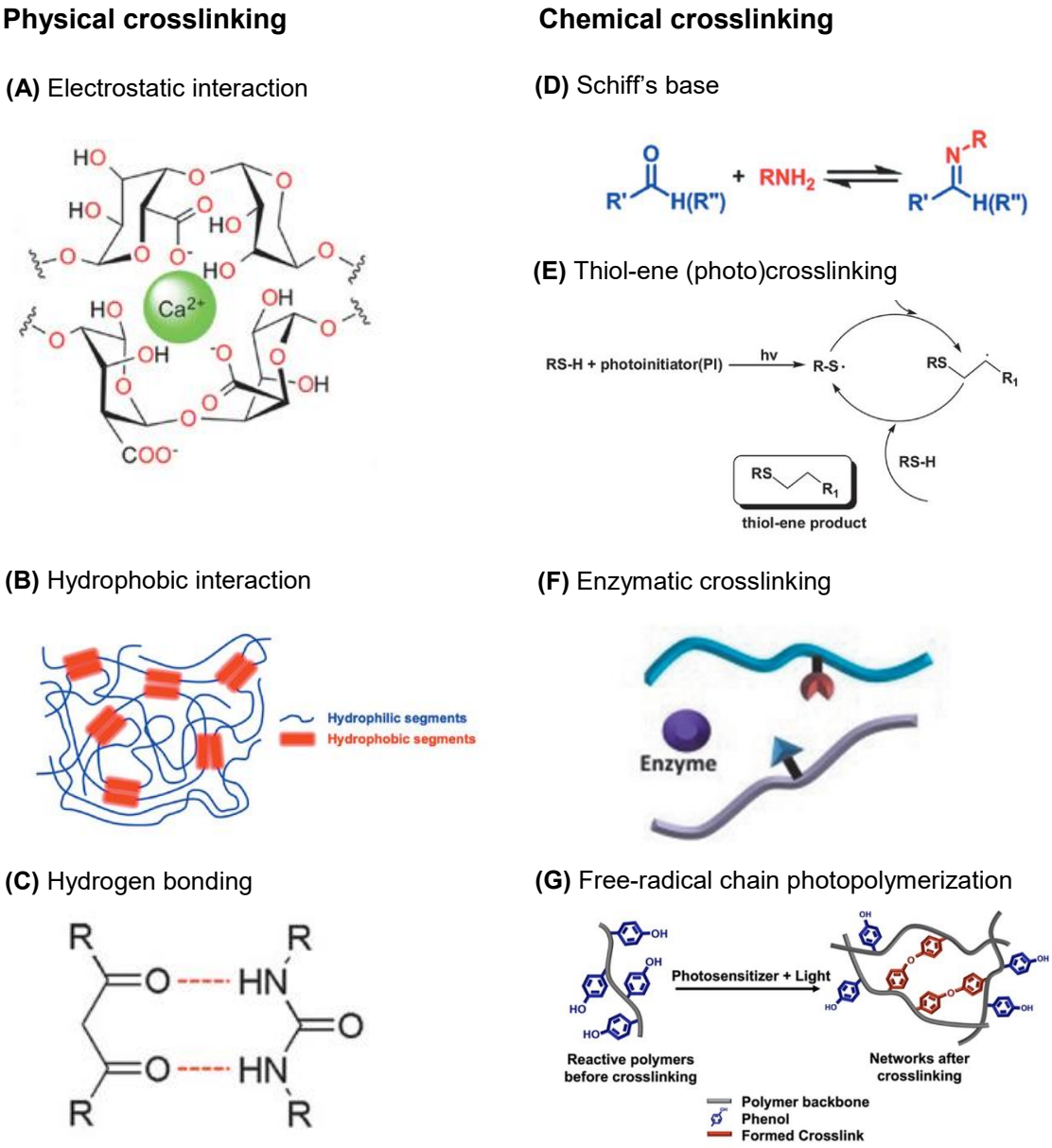

Figure 9. Schematic of the typical crosslinking methods used in hydrogel bioinks, including physical crosslinking **(A-C)** and chemical crosslinking **(D-G)**. Modified from (Cui *et al.*, 2020) and (Lim *et al.*, 2020).

3.3.1 Chemical crosslinkers

Chemical crosslinkers are used to create covalent bonds between the polymer chains, and the crosslinking density depends for example on the concentration of the crosslinker. Schiff's base formation is one of the most studied chemical crosslinking methods (Figure 9 D). There, the crosslink is formed between an amine containing and an aldehyde containing polymers. This crosslinking method results in hydrogels with shear thinning behaviour, however, the aldehyde groups can react with the amine groups in the ECM. (Cui et al., 2020)

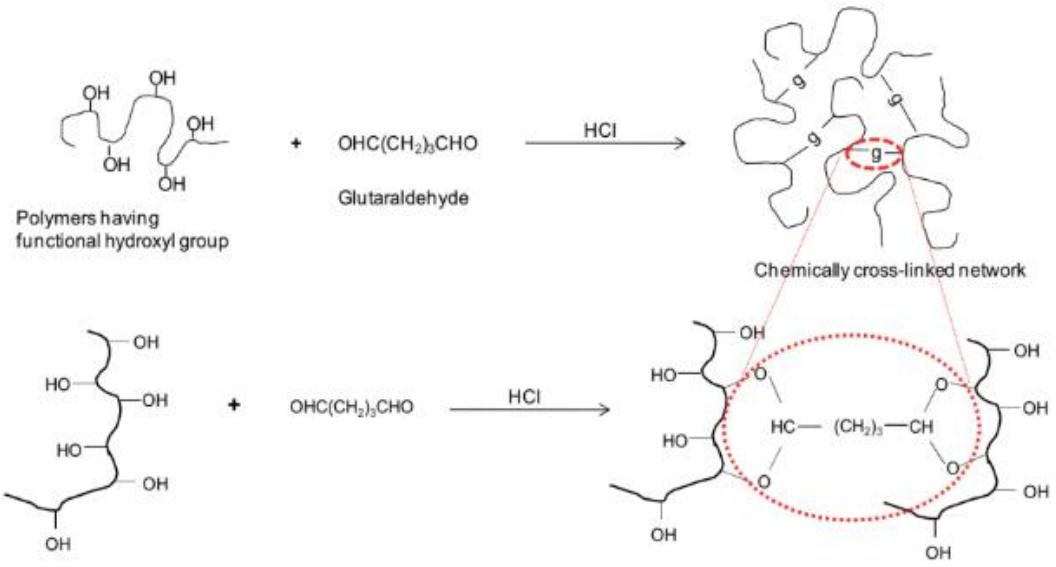

Figure 10. Illustration of a chemical crosslinking of a polymer containing hydroxyl groups by using glutaraldehyde as a crosslinker, resulting in covalent crosslinks. (Capri, 2011)

A common crosslinker is glutaraldehyde, however, as it might induce cytotoxicity, other crosslinkers have been studied (Hospodiuk *et al.*, 2017). Sodium bicarbonate has been used to crosslink collagen type I (Ng *et al.*, 2018), and genipin has been used to crosslink for example gelatin (Zhu *et al.*, 2018) and collagen type I (Kim, Lee and Kim, 2016; Kajave *et al.*, 2020). Figure 10 illustrates the chemical crosslinking and formation of a covalent bond between a polymer with hydroxyl functional groups and glutaraldehyde crosslinker.

In addition to previously mentioned crosslinkers, polyethylene glycol (PEG) -based crosslinkers have been studied. For example, PEG crosslinker containing an acrylate group, can be used to crosslink HAMA (Ma *et al.*, 2020) or GelMA (Jia, Selcan Gungor-Ozkerim, *et al.*, 2016). In addition, a thiolated polymer can be crosslinked with PEG crosslinkers (Rutz *et al.*, 2019), or PEG-based crosslinkers, such as polyethylene glycol diacrylate (PEGDA) and 8-arm PEG alkyne (Skardal *et al.*, 2016). Rutz et al. used PEG crosslinkers to create crosslink gelatin, and Skardal et al. used both PEGDA and 8-arm PEG with thiolated HA and thiolated gelatin together with tissue-specific ECM digest solution to bioprint liver spheroids. With PEGDA, a spontaneous crosslinking reaction between the thiol and acrylate groups, resulting a soft gel. With 8-arm PEG alkyne, a thiolated polymer needs UV irradiation to activate photocrosslinking, resulting a stiffer gel. (Skardal *et al.*, 2016)

3.3.2 Crosslinking based on thiolation

A thiolated polymer is a polymer with covalently attached thiol groups (Leichner, Jelkmann and Bernkop-Schnürch, 2019). Thiolated polymers can be utilized in hydrogel crosslinking in disulfide bond formation (Figure 11 A) (Gajendiran, Rhee and Kim, 2018), free-radical thiol-ene reaction (Figure 11 B) or Michael-type addition reaction (Figure 11 C). The most common polymers for thiolation are gelatin, collagen and HA (Holmes et al., 2017), and there are two approaches to fabricate thiolated polymers, ring-opening addition of thiolactone-based reagents and N-(3-dimethylaminopropyl)-N'-ethylcarboiimide/N-hydroxysuccinimide (EDC/NHS) coupling reaction. In EDC/NHS, the carboxylic acid and the amine groups react, and the reaction occurs between the thiolating agent and the selected polymer. The most widely used thiolating agent is 2-iminothiolane, also known as Traut's reagent. (Gajendiran, Rhee and Kim, 2018) In addition to Traut's reagent, there are several other thiolating agents (Leichner, Jelkmann and Bernkop-Schnürch, 2019). The thiolation via ring-opening of ColI is presented in Figure 12.

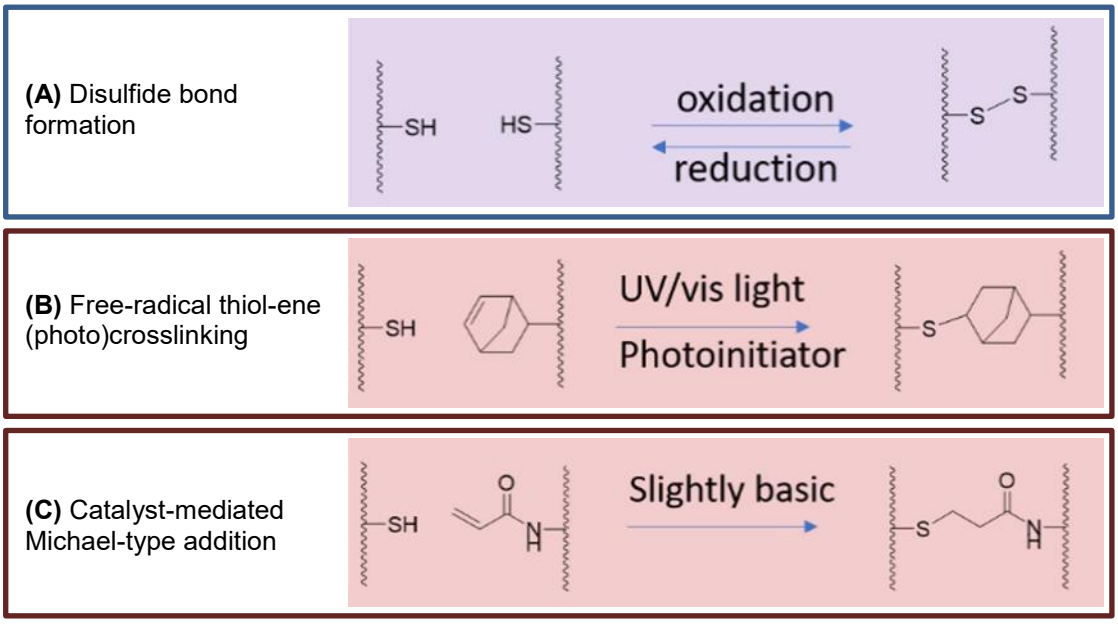

Figure 11. Overview of the crosslinking chemistries for thiolated polymers. **(A)** Disulfide bond formation **(purple)**, and thiol-ene crosslinking **(red)**: **(B)** Free-radical thiol-ene photocrosslinking and **(C)** catalyst-mediated Michael-type addition. Modified from (Van Hoorick *et al.*, 2019).

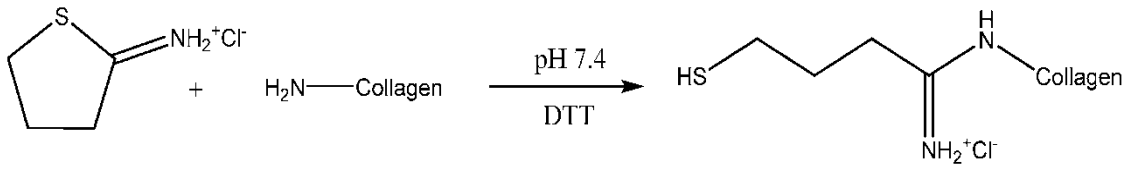

Figure 12. Thiolation reaction of collagen type I with Traut's reagent and dithiothreitol (DTT). (Holmes *et al.*, 2017)

Thiolated polymers form disulfide bonds (C-S-S-C) (Figure 11 A) between the thiol groups in oxidative environment, which is reversible process depending on oxidation and reduction (Van Hoorick et al., 2019). The polymer chain length, flexibility and charged substructrures affect the ability of the reactive groups to come close to each other, and subsequently the bond formation and crosslinking (Leichner, Jelkmann and Bernkop-Schnürch, 2019). In addition, the degree of thiolation affects the crosslinking (Leichner, Jelkmann and Bernkop-Schnürch, 2019), and the degree of thiolation and the number of thiol groups can be determined with Ellman's reaction (Gajendiran, Rhee and Kim, 2018).

Thiol-ene reaction is a chemical crosslinking method, where the thiolated polymer undergoes thiol-ene coupling due to reaction between a thiol and a carbon-carbon double bond ('ene') (Stichler et al., 2017), and is also referred as a thiol click reaction (Hoyle and Bowman, 2010). Thiol-ene reactions can be divided into a free-radical thiol-ene reaction (Figure 11 B) and Michael-type addition (Figure 11 C) (Holmes et al., 2017). The free radical thiol-ene reaction is usually initiated by light in thiol-ene photocrosslinking (Figure 13) (Van Hoorick *et al.*, 2019). Both of these reactions result in the formation of thioether linkage (C-S-C) (Holmes *et al.*, 2017), and the advantages relatively mild conditions, controllability, high chemical yield and relative inertness (Nguyen *et al.*, 2015).

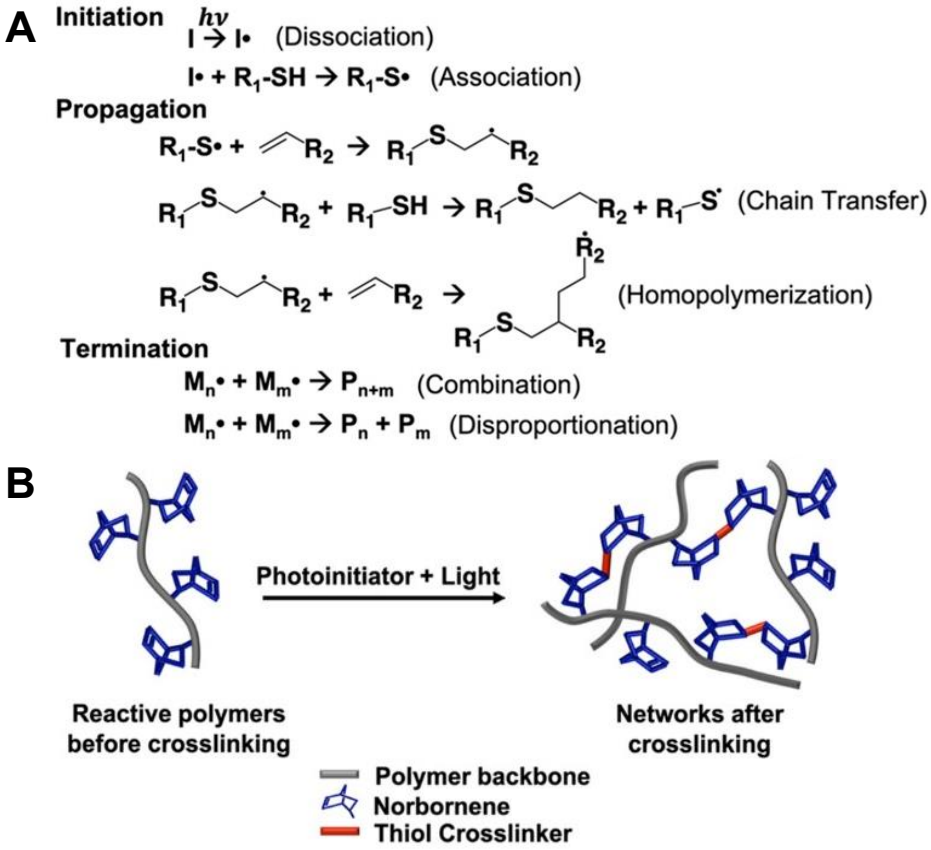

Figure 13. Thiol-ene (photo)crosslinking. **(A)** General mechanism and **(B)** schematic for radical-mediated thiol-ene photocrosslinking. Modified from (Lim *et al.*, 2020).

Michael-type addition reaction is catalyst-mediated, and there the thiol reacts with an electron-deficient ‘ene’, such as (meth)acrylate. The catalysts can be for example amines, acting as a nucleophiles. (Hoyle and Bowman, 2010) The reaction can occur at physiological pH, however, there is no spatiotemporal control due to fast reaction profile (Van Hoorick *et al.*, 2019).

In a free-radical thiol-ene reaction, a thiyl radical propagates across the ‘ene’ functional group, resulting a chain-transfer reaction, abstraction of a hydrogen radical from the thiol and step growth polymerization. As a net reaction, the thiol and ‘ene’ functional groups are combined in a exothermic reaction, which can be initiated by light in radical-mediated thiol-ene photocrosslinking. (Holmes *et al.*, 2017) There, the formation of the free radical is light-induced in the presence of a photoinitiator. Figure 13 A presents the steps in the thiol-ene (photo)crosslinking, where the reactive thiyl radical reacts with the ‘enes’ after initiation, which can result in chain transfer and step growth polymerization or homopolymerization. The reaction is terminated when all the reactive groups are consumed. (Lim *et al.*, 2020) The thiol-ene reaction can occur either between an ‘ene’-functionalized polymer (e.g. norbornene-functionalized gelatin) and a thiolated crosslinker (e.g. dithioretinol, DTT), as it shown in Figure 13 B, or between a thiolated polymer and a ‘ene’ crosslinker (e.g. PEGDA). The advantages of this method are the higher conversion of the functional groups, the possibility to control the time and location of the light-mediated activation, rapid reaction rate and low polymer shrinkage. (Van Hoorick *et al.*, 2019) In addition, the thiol-ene photo click crosslinking is not oxygen inhibited and requires lower concentration of free radicals (Stichler *et al.*, 2017).

In 3D bioprinting, thiol-ene crosslinking has been done for example by crosslinking thiolated HA with PEGDA, and combining the crosslinked HA-PEGDA with type I and II collagens and human fibroblasts (Walimbe *et al.*, 2019), and it has been applied for example to bioprint hMSCs (Galarraga, Kwon and Burdick, 2019; Xin *et al.*, 2019), hASCs (Tytgat *et al.*, 2019) and human articular chondrocytes (Soliman *et al.*, 2020). Galarraga et al. used norbornene functionalized HA, combined it with a photoinitiator and a crosslinker DTT, and used visible light to activate the thiol-ene photocrosslinking reaction. Xin et al. used norbornene-functionalized PEG and a thiolated PEG as a crosslinker, and applied UV light after printing. Tytgat et al. combined norbornene-functionalized and thiolated gelatin with a photoinitiator under UV light. Soliman et al. used DTT and thiolated PEG as crosslinkers for thiol-ene crosslinking of allyl-functionalized gelatin. They used this primary crosslinking before bioprinting and applied thiol-ene photocrosslinking after printing.

3.3.3 Ionic crosslinking

In ionic crosslinking, the opposite charges of the mixed materials attract each other, which creates the non-covalently crosslinked network (Figure 9 A) (Hospodiuk *et al.*, 2017). This interaction can occur either between two polyelectrolytes with opposite charges, or between a polyelectrolyte and a small charged molecule. Electrostatic interactions in ionic crosslinking can be affected with controlling the pH of the solution, as the pH affects the protonation of the charged functional groups. (Cui *et al.*, 2020) One advantage of ionic crosslinking is its reversible nature, which enables the possibility to use the physically crosslinkable component as a structural support for the 3D structure and remove it after bioprinting. Therefore, the desired polymer with relatively weak mechanical properties, such as gelatin, can be used to create a stable 3D structure with the help of ionically crosslinked template polymer. (Zhu *et al.*, 2018)

Typically, ionic crosslinking is utilized by crosslinking alginate with $CaCl_2$ (Pan *et al.*, 2016; Gu *et al.*, 2017; Raddatz *et al.*, 2018; Sarker *et al.*, 2018; Zhu *et al.*, 2018), as alginate contains negatively charged carboxylic acid groups (Hospodiuk *et al.*, 2017). There, alginate acts as a polyelectrolyte with negative charge. When using divalent calcium ions together with a negatively charged groups of the polymer, they form a bridge due to the electrical attraction (Hospodiuk *et al.*, 2017). The ionic crosslinking between a calcium ion and the carboxylic acid groups of alginate is shown in Figure 14. Often alginate-based structure is immersed in $CaCl_2$ after printing (MacCallum *et al.*, 2020). However, the $CaCl_2$ concentration and dispersion time can have negative effects on the cells, which is why fast completion of the process and careful wash are required (W. Liu *et al.*, 2018).

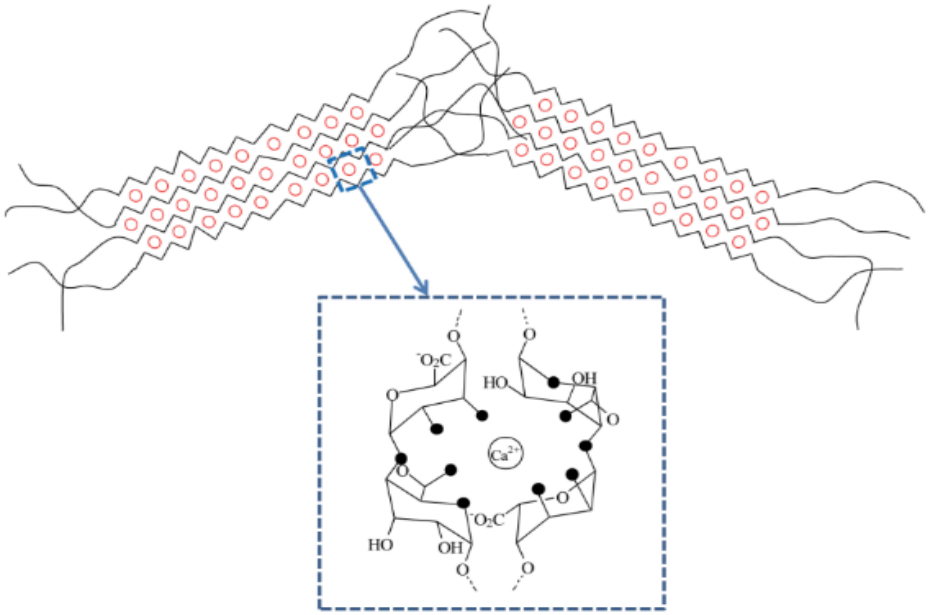

Figure 14. Illustration of ionic crosslinking between the carboxylic acid groups of alginate and a calcium ion. (Capri, 2011)

3.3.4 Photocrosslinking

Photocrosslinking is a chemical crosslinking method, and it is initiated by a photoinitiator when precursor bioink containing the photoinitiator is exposed to light (Lim et al., 2020). Photocrosslinking is irreversible, covalent and can be coupled with other crosslinking methods, such as reversible thermal crosslinking (Yin et al., 2018). There are three main photocrosslinking mechanisms, free-radical chain polymerization, thiol-ene and photomediated redox. (Lim et al., 2020) The thiol-ene (photo)polymerization is discussed later in a separate chapter. The biggest advantage of photocrosslinking is the spatiotemporal control over the reactions and the possibility to crosslink the bioink before, after or during printing, which enables precise building of the 3D structure (Lim et al., 2020). The main disadvantage of photocrosslinking is oxygen inhibition, which causes incomplete crosslinking. When the photoinitiator undergoes photolysis caused by light, radicals reacting with photocrosslinkable groups are formed. However, due to oxygen inhibition, some of these radicals are modified into peroxyl radicals due to oxygen molecules, which do not react with the photocrosslinkable groups. (Knowlton et al., 2017) Therefore, oxygen inhibition decreases polymerization rate and final conversion ratio (Choi et al., 2019).

Free-radical chain polymerization (Figure 9 G) has three stages (Figure 15 A). In the initiation stage, the photoinitiator is transformed into a reactive radical due light exposure.

(A) Free-radical chain polymerization

1. **Initiation**
   - $I \xrightarrow{h\nu} I\bullet$ (Dissociation)
   - $I\bullet + M \rightarrow M\bullet$ (Association)
2. **Propagation**
   - $M\bullet + M \rightarrow M_1\bullet$
   - $M_1\bullet + M \rightarrow M_2\bullet$
3. **Termination**
   - $M_n\bullet + M_m\bullet \rightarrow P_{n+m}$ (Coupling)
   - $M_n\bullet + M_m\bullet \rightarrow P_n + P_m$ (Disproportionation)
   - $M_n\bullet + HX \rightarrow P_n\text{-}H + X\bullet$ (Chain transfer)

(B) Photomediated redox crosslinking

Photo-oxidation and crosslinking

- $I \xrightarrow{h\nu} I^*$ (Photosensitization)
- $I^* + \text{R-OH} \leftrightarrow I^{\bullet-} + \text{R-O}\bullet + H^+$ (Oxidation)
- $R_1\text{-O}\bullet + R_2\text{-O}\bullet \rightarrow R_1\text{-O-}R_2$ (Crosslinking)

Oxygen-mediated side reactions

- $I^* + {}^3O_2 \rightarrow I + {}^1O_2$ (Energy transfer)
- $I^{\bullet-} + {}^3O_2 \rightarrow I + O_2^{\bullet-}$
- $2\ I^{\bullet-} + 2\ H^+ \rightarrow I + I\text{-}H_2$
- $I\text{-}H_2 + {}^3O_2 \rightarrow I + H_2O_2$ (Coupling)

Figure 15. General mechanisms of **(A)** free-radical chain polymerization and **(B)** photomediated redox crosslinking. **(A)** Free-radical chain polymerization includes three stages, initiation, propagation and termination. **(B)** Photomediated rexod crosslinking includes exication of oxygen by a photosensitizer and its pairing with another free radical oxygen. There are different possible side reactions: energy transfer between an exited photosensitizer and a ground state oxygen, a reaction of the radical derivatives of a photosensitizer, resulting in a superoxide, or photosensitizer intermediate radical species coupling, resulting in hydrogen peroxide. Based on figures from (Lim *et al.*, 2020).

The rate of the transformation depends for example on the efficiency and concentration of the photoinitiator. The photoinitiator, now as a free radical, reacts with the functional groups of the selected polymer, creating covalent bonds and reactive radical intermediates. In the propagation stage, these intermediates react with the subsquent reactive groups, propagating the radical species through unreacted carbon-carbon double bonds. The most common functional groups crosslinking via free-radical chain polymerization are (meth)acrylate and N-vinyl amide. Finally, the reaction progresses in the termination stage, where there are three termination options. The free radicals can be coupled to result in combination of two polymer chain ends. Another option is the disproportionation, which results in two polymer chains, one with a saturated terminal group and another with a nonsaturated terminal group. The third option is the chain transfer, where radicals are transferred away from the polymer chain. (Lim et al., 2020)

The main aspects to consider in photocrosslinking are the selection of the photoinitiator, the wavelength and intensity of the light and exposure time (Lim et al., 2020). The used wavelength of light depends on the absorption peak of the selected photoinitiator, as it affects the efficiency of the photoinitiator (Knowlton et al., 2017), and higher intensity or exposure time increases the photocrosslinking rate and density (Lim et al., 2020). Moreover, the concentration of the photoinitiator and the reactive groups of the photocurable polymer affect the photocrosslinking efficiency, and by increasing either of the concentrations, the photocrosslinking rate and density can be increased (Lim et al., 2020). Since the crosslinking density affects the mechanical properties of the hydrogel (Chimene, Kaunas and Gaharwar, 2020), the desired mechanical properties of a photocurable hydrogel bioink can be achieved by optimizing these parameters, which are summarized in Figure 16.

The typical light sources are ultraviolet (UV) light (200 – 400 nm) and visible light (400 – 800 nm) (Choi et al., 2019). In addition, possible cell cytotoxicity and the penetration efficiency affect the selection of the wavelength (Knowlton et al., 2017), and it has been shown that both UV A (320 – 400 nm) and UV B (290 – 320 nm) radiation can cause

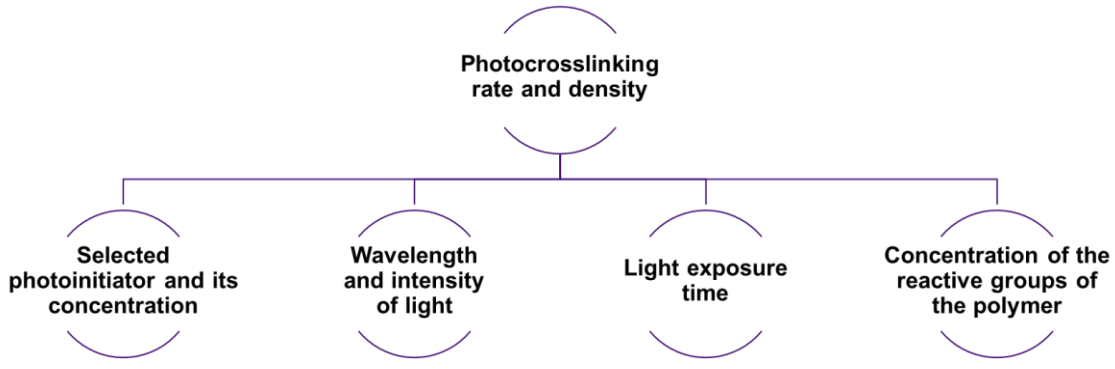

Figure 16. Parameters affecting the photocrosslinking efficiency.

genomic instability in the cells (Dahle, Kvam and Stokke, 2005). Usually the used wavelength in photocrosslinking is 365 nm, which is close to the visible light range, and thus the cytotoxicity and genotoxicity are minimized (Lim et al., 2020). Due to the limited penetration depth of UV, the photocrosslinking efficiency of larger constructs might be affected (Lim et al., 2016). Moreover, the photoinitiator concentration and addition of a photoabsorber decrease the penetration depth (Lim et al., 2020).

There are several photoinitiators, and two most widely used commercially available ones are 2-hydroxy-1-[4-hydroxyethoxyphenyl]-2-methyl-L-propanone (Igracure 2959) and lithium phenyl-2,4,6-trimethylbenzoylphosphinate (LAP) (Lim et al., 2020). There are other Igracure photoinitiators in addition to 2959, however, Igracure 2959 has shown the best cytocompatibility, and thus it is the most used Igracure to fabricate cell-laden hydrogels (Bryant, Nuttelman and Anseth, 2000). Lim et al. have made an extensive review of research done using Igracure 2959 and LAP as photoinitiators in 3D bioprinting, where the photoinitiator concentration range is 0.01 – 1 wt%, and the UV exposure time varies from 2 s per layer (Stichler et al., 2017) to 10 min after bioprinting (Shi et al., 2017) or to continuous exposure during bioprinting (Tigner et al., 2020). Both Igracure 2959 and LAP are type I photoinitiators, which go through homolytic cleavage caused by light, resulting in free radicals, and therefore photopolymerization process described previously. There are type II photoinitiators as well, however, their photocrosslinking mechanism is more complex. (Lim et al., 2020) Type II photoinitiators are not as widely used, and they are not discussed further in this thesis.

Igracure 2959 is hydrophilic, however, it absorbs light within the range of 200-370 nm, 254 nm being the most efficient (Van Hoorick et al., 2019). Thus, at higher wavelengths, its efficiency decreases. Lower wavelengths are not used due to the mutageneicity and phototoxicity for the cells, and thus the options for increasing the polymerization efficiency are to increase the Igracure 2959 concentration, light intensity or light exposure time to compensate the low efficiency at higher wavelengths. (Lim et al., 2020) Compared to Igracure 2959, LAP absorbs more light at 365 nm, resulting in more rapid polymerization, is able to absorb light within the visible light range (> 400 nm) and has greater water solubility (Fairbanks et al., 2009). Moreover, LAP has been shown to result better stability of the 3D bioprinted structure (Tigner et al., 2019).

Photomediated redox crosslinking (Figure 15 B) is used with polymers containing phenol groups. A photosensitizer is used, and they are usually light-absorbing dyes or additives, such as eosin-Y or rose bengal. The photosensitizer oxidates the reactive group of the selected polymer, which then can react with another oxidized group, creating crosslinks. Side reactions can occur in the presence of oxygen, such as energy transfer between an

exited photosensitizer and a ground state oxygen, which results in electrophilic, excited singlet oxygen spieces, possible to oxidize hydroxyl, sulfide and amine groups. Another possible side reaction is the electron transfer or hydrogen abstraction, which results in radical derivatives of a photosensitizer. These radical derivatives can undergo a reaction resulting in a superoxide, or coupling, resulting in hydrogen peroxide. (Lim et al., 2020)

Methacrylation is a widely studied method to modify the properties of the bioink and make the bioink photocrosslinkable (Skardal et al., 2010; Pereira and Bártolo, 2015; Michelle T Poldervaart et al., 2017; Yin et al., 2018; Xu et al., 2019; Ma et al., 2020). Many hydrogels can be methacrylated by adding methacrylate functional groups to the backbone of the polymer, such as gelatin or HA (Chimene, Kaunas and Gaharwar, 2020). Figure 17 illustrates the methacrylation and photocrosslinking of HA and gelatin.

GelMA and HAMA are synthesized by using for example methacrylic anhydride to substitute the amine side groups of gelatin (Figure 17 A) (Choi *et al.*, 2019) or hydroxyl

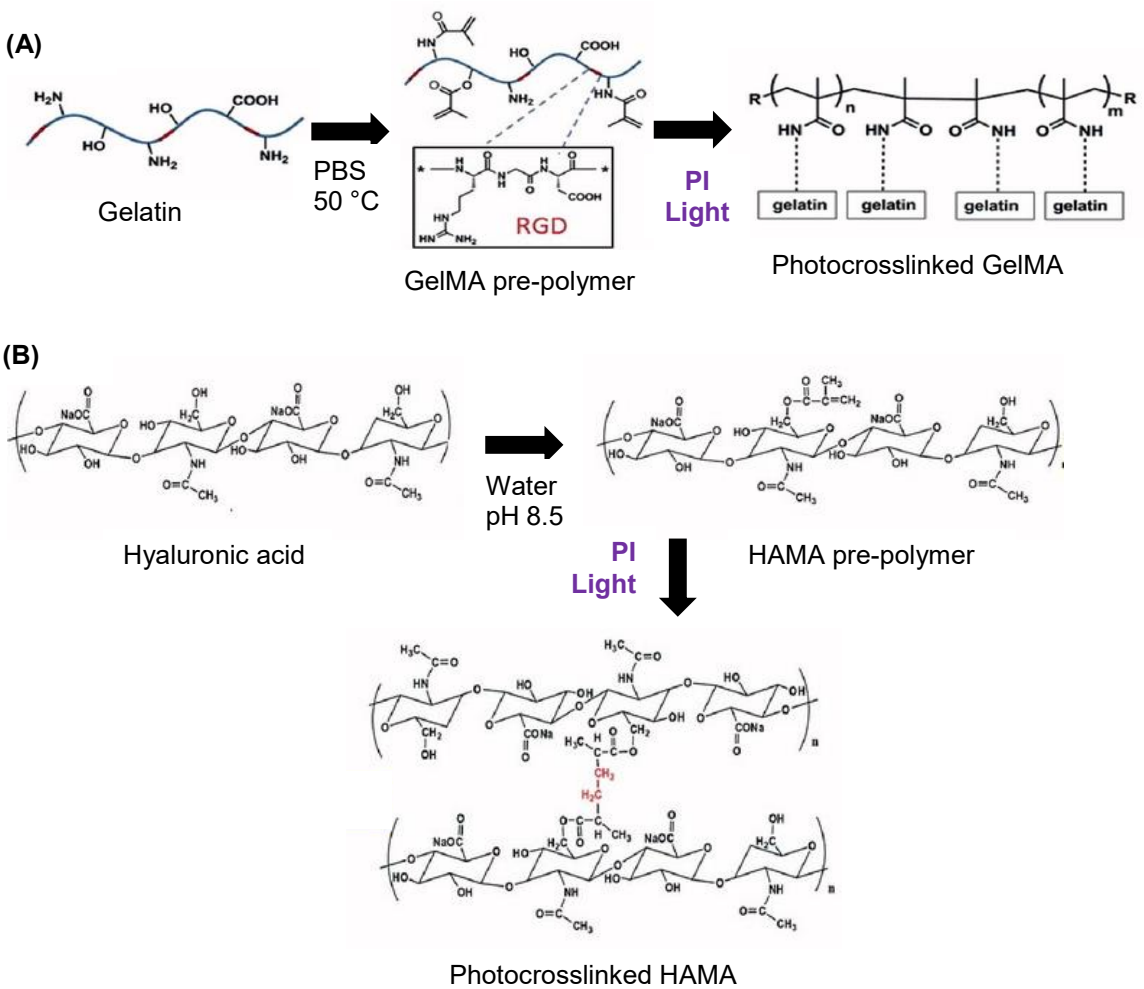

Figure 17. Methacrylation and photocrosslinking via free-radical chain polymerization of gelatin **(A)** and hyaluronic acid **(B)**. Briefly, the methacrylated gelatin (GelMA) or hyaluronic acid (HAMA) is photocrosslinked by a photoinitiator (PI) in the presence of light. Modified from (Choi *et al.*, 2019).

groups of HA (Figure 17 B) (Michelle T Poldervaart *et al.*, 2017) with methacrylate groups. By increasing the methacrylation degree or the GelMA/HAMA concentration, more crosslinking sites are created. The modulus in mechanical properties is increased and thus, it is possible to adjust the mechanical properties of the material. (Choi *et al.*, 2019; Spearman *et al.*, 2020) The compressive or elastic modulus of the hydrogel can be increased and the decradation rate decreased, when the methacrylation degree, polymer concentration or light exposure time is increased (Choi *et al.*, 2019). In addition, the viscosity of the material is affected (Spearman *et al.*, 2020) which affects the printability of the bioink.

3.3.5 Thermal crosslinking

Temperature-induced crosslinking is a reversible non-covalent crosslinking method and can be used for thermo-sensitive polymers, such as collagen type I (Drzewiecki *et al.*, 2017; Moncal *et al.*, 2019), gelatin (Pan *et al.*, 2016; Gu *et al.*, 2018; Luo *et al.*, 2020) or methylcellulose (Shin *et al.*, 2020). It is based on temperature-dependent hydrophobic interactions (Figure 9 B) and hydrogen bonding (Figure 9 C), which create the crosslinked network. Hydrogen bonds are formed between oxygen and hydrogen atoms, and thus they occur between polymer chains containing for example hydroxyl or carboxyl groups (Cui *et al.*, 2020). Hydrogen bonding is strongly affected by temperature and pH, which influences the crosslinking density (Wang *et al.*, 2018). In the case of hydrophobic interactions, an increase in temperature can cause the hydrophobic domains in the polymer to aggregate, as the contact area between hydrophobic domains and water is minimized (Cui *et al.*, 2020). For some hydrogels, the crosslinking occurs at low temperatures, as the polymer chains have more ordered conformations and form junctions (crosslinks) between the chains (Hospodiuk *et al.*, 2017).

Because 3D bioprinting uses living cells, it is important to keep the temperature between 1 °C and 37 °C (Eswaramoorthy, Ramakrishna and Rath, 2019). In thermal crosslinking, there is no need to use additional, possibly cytotoxic crosslinking agents (Moncal *et al.*, 2019), however, the mechanical properties of a thermally crosslinked hydrogel are usually too weak (Shin *et al.*, 2020). Therefore, another crosslinking method, such as photocrosslinking, is usually combined to create dual-crosslinked hydrogel. This enables the possibility to use both physical and chemical crosslinking and change between the crosslinking methods flexibly. (Shin *et al.*, 2020)

4. 3D BIOPRINTING OF OCULAR TISSUE

Traditional techniques, where cells are seeded afterwards on the prefabricated scaffold, do not provide homogenous cell seeding or appropriate adhesion (K. W. Kim *et al.*, 2018). The characteristics of the cornea include high cell density, a structure with multiple layers and cell types as well as curved shape, and therefore the fabrication of corneal substitutes require a technique capable of controlling the shape and structure of the produced tissue. Even though the curved shape still remains a challenge, 3D bioprinting has the possibility to fabricate precise shapes with the desired 3D structure. Moreover, it is a presice, repeatable and customizable fabrication technique, and offers a possibility to overcome issues of using donor tissue, such as tissue shortage and risk of rejection. In addition, various different materials and cells can be integrated by 3D bioprinting to mimic the complexity of the native tissue, which enables building an accurate 3D model of the cornea. (B. Zhang, Xue, Li, *et al.*, 2019)

Due to accessibility and immune priviledge, meaning that the normal inflammatory reponse is limited (Boyd, 2018), the eye has attracted attention in developing and implementing 3D bioprinting solutions in ophtalmology (Sommer and Blumenthal, 2019). Especially, the characteristics of the cornea, including the absence of vascularization, relatively homogenous cellular level and low metabolic demand, have made it an appeling tissue for 3D bioprinting (Sommer and Blumenthal, 2019), and there is an increasing number of studies (B. Zhang, Xue, Hu, *et al.*, 2019; H. Kim *et al.*, 2019) and newsarticles done in 3D bioprinting cornea (*Biomedical Research Team in Spain Working on 3D Printed Corneas to Make Up for Lack of Donors*, 2017; *Corneas Could Be the First Mainstream Application of Bioprinting*, 2018). In addition, different parts of the cornea has been studied in 3D bioprinting, such as endothelium (K. W. Kim *et al.*, 2018), stroma (Isaacson, Swioklo and Connon, 2018; Sorkio *et al.*, 2018; Duarte Campos *et al.*, 2019; Kilic Bektas and Hasirci, 2020; Kutlehria *et al.*, 2020; Mahdavi, Abdekhodaie, Kumar, *et al.*, 2020) and epithelium (Wu *et al.*, 2016; Sorkio *et al.*, 2018). The research done in 3D bioprinting corneal tissues is summarized in Table 4. In addition to cornea, retina has been studied in 3D bioprinting of ocular tissues, however, the number of studies is smaller and mainly biomaterial-free approaches are used (Shi *et al.*, 2018; Masaeli and Marquette, 2020; Masaeli *et al.*, 2020), and therefore 3D bioprinting retina is not discussed futher in this thesis.

Table 4. Summary of research in the field of 3D bioprinting cornea. hCKs = Human corneal keratocytes, hCSCs = Human corneal stromal cells, hCEnCs = Human corneal endothelial cells, hCEpCs = Human corneal epithelial cells

Target tissue	3D bioprinting technique	Cell type	Main bioink components	Reference
Corneal endothelium	Extrusion	hCEnCs	Gelatin	(K. W. Kim *et al.*, 2018)
Corneal stroma	DOD	hCKs	ColI with agarose	(Duarte Campos *et al.*, 2019)
Corneal stroma	Pneumatic extrusion	hCKs	Alginate with methacrylated ColI	(Isaacson, Swioklo and Connon, 2018)
Corneal stroma	Pneumatic extrusion	hCKs	GelMA	(Kilic Bektas and Hasirci, 2020)
Corneal stroma	Pneumatic extrusion	hCKs	ColI – Gelatin - Alginate	(Kutlehria *et al.*, 2020)
Corneal stroma	SLA	hCSCs	GelMA	(Mahdavi, Abdekhodaie, Kumar, *et al.*, 2020)
Corneal epithelium	Extrusion	hCEpCs	ColI – Gelatin – Alginate	(Wu *et al.*, 2016)
Corneal epithelium and corneal stroma	LIFT	hESC-LESCs	Laminin-521 with HA	(Sorkio *et al.*, 2018)
		hASCs	ColI with human plasma and thrombin	
Cornea	Extrusion	hCEpCs	Alginate – Gelatin	(B. Zhang, Xue, Hu, *et al.*, 2019)
Cornea	Pneumatic extrusion	hMSCs	Cornea-derived decellularized ECM	(H. Kim *et al.*, 2019)
Cornea	Not mentioned	hMSC-derived cells	Collagen	(*Biomedical Research Team in Spain Working on 3D Printed Corneas to Make Up for Lack of Donors*, 2017)
Cornea	LIFT	hCEpCs	Collagen	(*Corneas Could Be the First Mainstream Application of Bioprinting*, 2018)

All the main 3D bioprinting techniques have been used in 3D bioprinting corneal tissues, inkjet-based DOD bioprinting (Duarte Campos *et al.*, 2019), laser-based LIFT bioprinting (Sorkio *et al.*, 2018), lithography-based SLA bioprinting (Mahdavi, Abdekhodaie, Kumar, *et al.*, 2020) and pneumatic extrusion-based bioprinting (Isaacson, Swioklo and Connon, 2018; Kilic Bektas and Hasirci, 2020; Kutlehria *et al.*, 2020). Several different bioink components have been used, such as agarose (Duarte Campos *et al.*, 2019), alginate (Wu *et al.*, 2016; Isaacson, Swioklo and Connon, 2018; Kutlehria *et al.*, 2020), ColI (Wu *et al.*, 2016; Isaacson, Swioklo and Connon, 2018; Sorkio *et al.*, 2018; Duarte Campos *et al.*, 2019; Kutlehria *et al.*, 2020), decellularized cornea (H. Kim *et al.*, 2019), gelatin (Wu *et al.*, 2016; K. W. Kim *et al.*, 2018; Kutlehria *et al.*, 2020), GelMA (Kilic Bektas and Hasirci, 2020; Mahdavi, Abdekhodaie, Kumar, *et al.*, 2020) and laminin (Sorkio *et al.*, 2018).

The crosslinking of the 3D bioprinted ocular structures after printing have been made with temperature (Duarte Campos *et al.*, 2019; H. Kim *et al.*, 2019) and $CaCl_2$ (Wu *et al.*, 2016; Isaacson, Swioklo and Connon, 2018; Kutlehria *et al.*, 2020), or via photocrosslinking (K. W. Kim *et al.*, 2018; Kilic Bektas and Hasirci, 2020; Mahdavi, Abdekhodaie, Kumar, *et al.*, 2020). In addition, 3D bioprinting has been done without further crosslinking for epithelial cells and with fibrin-thrombin coagulation for stromal cells (Sorkio *et al.*, 2018). Kilic Bektas and Hasirci used UV light at 365 nm for 15% GelMA bioink with 0.5% Igracure 2959 photoinitiator to photocrosslink the 3D bioprinted structure. K. W. Kim et al. used Gel4Cell (Bioink Solutions, Inc., Sout Korea) bioink kit, which contains gelatin-based hydrogel and a photosensitive Gel-linker, and is photocrosslinked with UV light at 365 nm. The UV exposure times were 5 s (Kilic Bektas and Hasirci, 2020) and 15 s (K. W. Kim *et al.*, 2018), and in both studies, photocrosslinking was done after bioprinting all the layers. Mahdavi et al. used visible light instead of UV light and eosin Y with triethanolamine as a photoinitiator. The photocrosslinking was done layer-by-layer with the exposure time of 5 min.

Most of the current research in 3D bioprinting corneal tissues use low cell density in the bioink, from 1 million cells per ml (Wu *et al.*, 2016; Duarte Campos *et al.*, 2019; H. Kim *et al.*, 2019) to 2 (Isaacson, Swioklo and Connon, 2018), three (K. W. Kim *et al.*, 2018; Kutlehria *et al.*, 2020) or 8 (Mahdavi, Abdekhodaie, Kumar, *et al.*, 2020) million cells per ml. Since viscosity increases when the cell density in the bioink is increased (Chimene, Kaunas and Gaharwar, 2020), inkjet-based bioprinting cannot be used for high cell density bioinks (Hölzl *et al.*, 2016). Instead, laser-based LIFT bioprinting has been used to bioprint bioink with 30 million cells per ml (Sorkio *et al.*, 2018), however, it is costly technology and not as well available. Whereas extrusion-based bioprinting can be used

to bioprint high cell density bioinks, higher viscosity can cause the nozzle to clog and increases the shear stress, which can harm the cells and decrease cell viability (Cui *et al.*, 2020). However, native-like cell density is essential for biologically functional corneal tissue equivalents, and for example, the cell density in corneal epithelium is high due to stratified epithelial cells connected through tight junctions (Sridhar, 2018). Therefore, to 3D bioprint corneal tissues, suitable bioprinting technology and bioink with native-like cell density are needed.

The cell viability has been shown to be high after printing with all four 3D bioprinting technologies (Wu *et al.*, 2016; Isaacson, Swioklo and Connon, 2018; Sorkio *et al.*, 2018; Duarte Campos *et al.*, 2019; H. Kim *et al.*, 2019; Kilic Bektas and Hasirci, 2020; Kutlehria *et al.*, 2020). Typically, the cell morphology has been round-shaped after printing (Wu *et al.*, 2016; Isaacson, Swioklo and Connon, 2018; K. W. Kim *et al.*, 2018; Sorkio *et al.*, 2018; Duarte Campos *et al.*, 2019; Kutlehria *et al.*, 2020), and depending on the cell type, the morphology has changed into elongated (Duarte Campos *et al.*, 2019; Mahdavi, Abdekhodaie, Kumar, *et al.*, 2020), hexagonal (K. W. Kim *et al.*, 2018) or polygonal (Sorkio *et al.*, 2018) during culture. However, also round-shaped morphology has been reported after 7 days (Isaacson, Swioklo and Connon, 2018) and 14 days (Kutlehria *et al.*, 2020) post-printing, which is not desired for corneal cells.

One challenge in bioprinting cornea is its curved shape, and that has been tried to accomplish in some of the studies. Isaacson et al. used 3D printed plastic support structure to mimic the curvature of the cornea, and filled it with gelatine slurry to facilitate the printing of low viscosity bioink. The gelatin slurry was aspirated after incubation and crosslinking of the printed structure at 37 °C. Mahdavi et al. used also gelatin as a supportive sacrificial material during bioprinting. This was done layer-by-layer by removing the uncrosslinked bioink after photocrosslinking and adding sacrificial gelatin to the hollow part of the layer. Kutlehria et al. used SLA-based bioprinting to fabricate a supportive 6-well scaffold from clear resin and bioprinted corneal stromal structures in the curved wells. With DOD based bioprinting, Duarte Campos et al. were able to bioprint a curved structure without additional support. Other research has been done on flat surfaces, resulting in a flat 3D structure without curved shape. Typically the bioprinting has been done on a cell culture dish without any specific coating (Wu *et al.*, 2016; H. Kim *et al.*, 2019; Kilic Bektas and Hasirci, 2020), however, printing on bovine AM (K. W. Kim *et al.*, 2018), ColIV and laminin coated polyethylene terephthalate (PET) film, Corning Matrigel™ and Matriderm (Sorkio *et al.*, 2018) have been studied.

5. MATERIALS AND METHODS

This chapter describes on the experimental part of the thesis, and Figure 18 illustrates the iterative workflow of the experiments. First, hPSC-LESCs were produced for bioprinting, and the bioink components were prepared. On the printing day, the bioink was prepared and printed with an extrusion-based bioprinter. Later, the cell viability, proliferation, differentation and maturation were analyzed from the bioprinted samples. The bioprinting parameters and conditions were optimized based on the response of the bioprinted hPSC-LESCs. After finding the most suitable parameters, the bioink without cells was characterized.

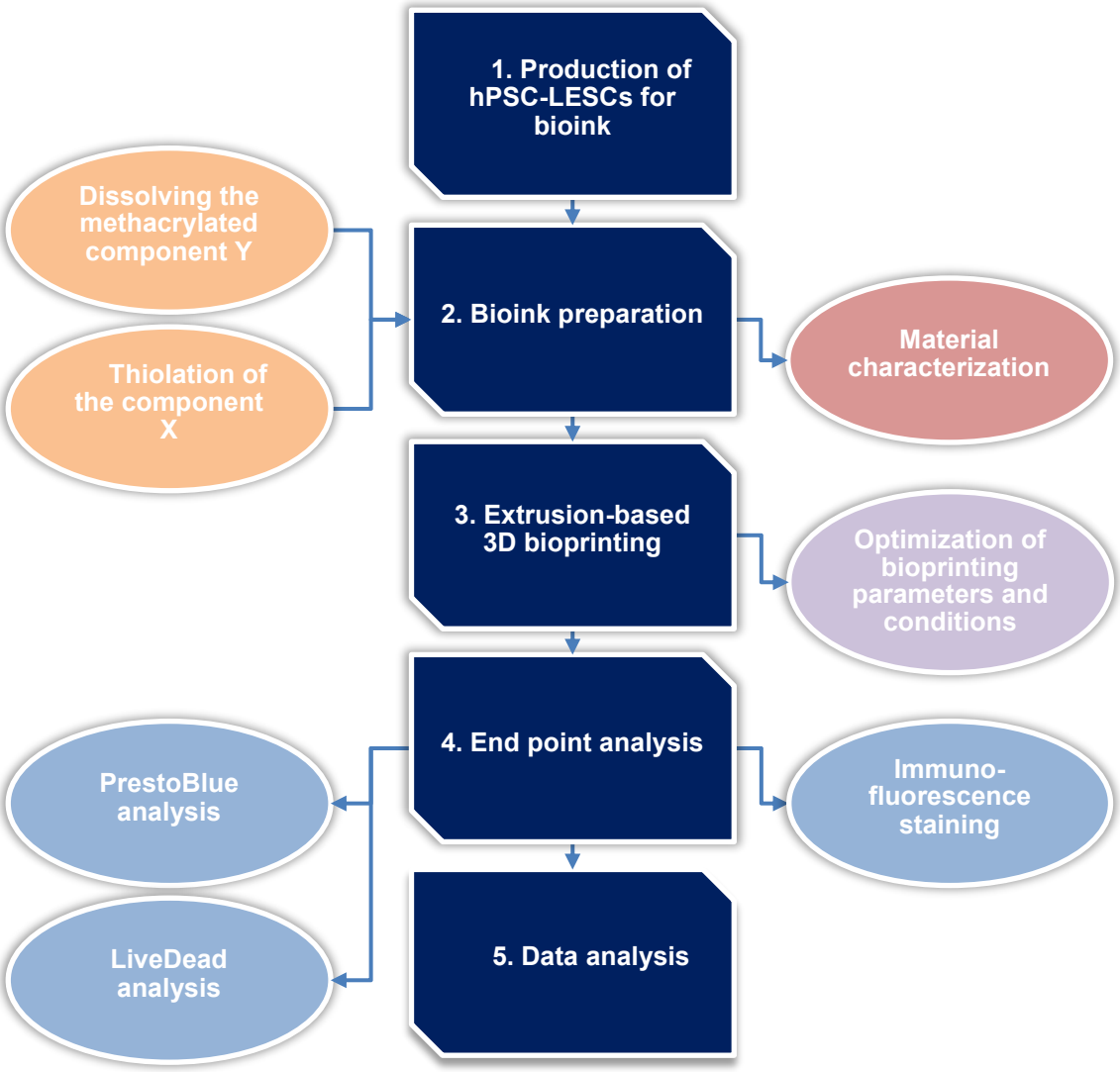

Figure 18. The iterative workflow of the thesis. **1:** First, the hPSC-LESCs used in the bioink were produced. **2:** The bioink was prepared and characterized. **3:** The bioprinting was done by using a extrusion-based 3D bioprinter, and the printing step included the optimization of the printing parameters. **4:** The bioprinted samples were analyzed with PrestoBlue, LiveDead and immunofluorescence staining. **5:** Finally, the gathered data was analyzed.

5.1 Preparation of the materials

Next, the materials needed in bioprinting and their preparation are described, including the production of hPSC-LESCs and the protocols for different coatings of the printing substrates. In addition, the preparation of the bioink and its components is described. The bioink composition is confidental, and thus its components are described in detail in Appendix A. Finally, the chapter represents the preparation of the 3D bioprinter and the 3D model used in the bioprinting.

5.1.1 Cell culturing

The cells used in this thesis were hPSC-LESCs from two different cell lines, hESC-line Regea 08/017 (46, XX) and hiPSC-line 001b B2 HT (46, XX). The research group has an approval to derive hESC-lines from surplus embryos not used in infertility treatments (R05116) and to produce hiPSC lines for ophthalmic research (R14023) from the ethics committee of the Pirkanmaa hospital district. This thesis was carried out under the approval from the local ethics committee of the Pirkanmaa hospital district, Finland, that allows the derivation and expanding of hESC-lines from surplus embryos donated by couples undergoing infertility treatments and to use these cell lines for research purposes (R05116). New cell lines were not derived for this study.

The differentiation of hPSC-LESCs is described elsewhere (Hongisto *et al.*, 2017), and the differentiated hPSC-LESCs were provided for the thesis by the research group. The hPSC-LESCs were either fresh or from frozen-stock. The fresh hPSC-LESCs were used for the analysis of cell viability, proliferation, maturation and differentiation after bioprinting, and hPSC-LESCs from frozen-stock were used for the UV exposure studies and as a control for immunofluorescence. The different batches of hPSC-LESCs used for bioprinting, the cell densities of the bioinks and the analyses they were used are summarized in Table 5.

Table 5. The summary of the used cell lines, their stocks and densities in the bioink.

Cell line	Stock	Cell density (cells/ml)	Used for
hESC-line 08/017	Frozen	-	Immunofluorescence control
hESC-line 08/017	Frozen	15 million	UV exposure and printing substrate studies
hESC-line 08/017	Fresh	3 million	Printing substrate studies
hESC-line 08/017	Fresh	9 million	Cell viability, proliferation, maturation and differentiation analysis
hiPSC-line 001b B2 HT	Fresh	8.8 million	Cell viability, proliferation, maturation and differentiation analysis

The differentiated hPSC-LESCs were cultured on 100 mm culture dishes (CellBIND Culture Dish, surface area 55 cm^2, Corning) in serum-free Cnt-30 medium (CELLnTEC Advanced Cell Systems AG, Switzerland) in an incubator at 37 °C 5% CO_2. The cells were fed every other day with 8 ml of fresh, pre-warmed medium. The hPSC-LESCs from frozen-stock used for bioprinting were thawed on the 100 mm culture dishes with the seeding density of 13 000 cells/cm^2. The hPSC-LESCs for the immunofluroescence control, pre-coated 24-well plates (CellBIND Multiple Well Plate, surface area 1.9 cm^2, Corning) were used with a seeding density of 29 000 cells/cm^2. The fresh hPSC-LESCs were dissociated for bioprinting on Day 28 after starting the differentiation process, and the hPSC-LESCs from frozen-stock used for bioprinting were dissociated on Day 8 after thawing. The hPSC-LESCs used for the immunofluroescence control were fixed with 4% paraformaldehyde (PFA) on Day 6 after thawing. The fixing protocol is described in Chapter 5.5.2.

The coating of the cell culture dishes and well plates used for hPSC-LESC expansion was done with laminin and ColIV to help the cells to attach the bottom of the dish. The native EBM beneath the corneal epithelium consists mainly of ColIV and laminins (Wilson, Torricelli and Marino, 2020), and subsequently, the coating composed of 5 µg/cm^2 of human recombinant laminin 521 (LN521, 100 µg/ml, BioLamina, Sweden) and 0.5 µg/cm^2 of collagen type IV from human placenta (ColIV C5533, 1 mg/ml, Sigma Aldrich, USA) diluted in phosphate buffered saline containing magnesium chloride and $CaCl_2$ (PBS ++, Gibco). The coating solution was prepared by using the equation 1

$$V_{Stock} = \frac{C_{Desired}}{C_{Stock}} \cdot A, \qquad (1)$$

where V_{Stock} means the needed volume of either ColIV or LN521, $C_{Desired}$ means the desired concentration of ColIV or LN521 in the coating solution, C_{Stock} means the initial concentration of ColIV or LN521, and A means the area of the coated surface. 3.5 ml of the coating solution was added onto the 100 mm culture dishes and 300 µl for the 24-well plates. The dishes and plates were covered with Parafilm to prevent evaporation, and left over night at 4 °C. Before seeding the cells, the solution was removed and the dishes and plates were warmed in the incubator at 37 °C 5% CO_2.

Dissociation of the hPSC-LESCs for bioprinting was done with TrypLE (1X, Gibco). First, the medium was removed and 2 ml of warm TrypLE was added onto each dish for 5 minutes. After this, TrypLE was removed and 2 ml Defined Trypsin Inhibitor (DTI, Gibco) was added to inactivate the enzyme and stop the cells to dissociate completely from the bottom of the dish. Then, the cells were scraped with a cell scraper from the bottom of the plates, transferred into centrifuge tubes through a filter, and the dish was rinsed with 2 ml of medium. The cell suspension was centrifuged at 300 g for 5 minutes, and the cells were resuspended in the culture medium. The cells were counted by using a Bürker chamber. Thereafter, the cells were centrifuged and resuspended in 400 µl of Cnt-30 medium for the bioink preparation. 15 µl of RevitaCell (100X, Gibco) was added into the cell suspension to help the cells to recover from the upcoming bioprinting process.

5.1.2 Coating of the printing substrates

Different coatings for the culture dishes (Falcon® 35 mm TC-treated Easy-Grip Tissue Culture Dish, Corning) were tested as printing substrates. The coatings were ColIV with LN521, Matrigel™ (Growth Factor Reduced Basement Membrane Matrix, Corning), LinkCell™ ColI membranes (LinkoCare Life Sciences AB, Sweden) or nonporous polyethylene terephthalate (PET) membranes (ipCELLCULTURE™ Track Etched Membrane, thickness 12 µm, it4ip, Belgium) coated with Matrigel™ or with ColIV and LN521. The coatings and the UV exposure times they were used with are presented in Table 6.

Matrigel™ was chosen to provide better adhesion for the printed cells due to its transparency, hydrophilicity and previous use in 3D bioprinting of hASCs (Sorkio *et al.*, 2018). LinkCell™ membranes have previously been used in culturing hPSC-LESCs (Mikhailova *et al.*, 2016), and porous PET membranes have been studied as a substrate in 3D bioprinting hPSC-LESCs (Sorkio *et al.*, 2018). The ColI and LN521 coating was used in hPSC-LESC culture and expansion, and subsequently selected as a coating option for bioprinting as well.

Table 6. Different substrates which were tested for 3D bioprinting of the bioink and which UV exposure times were used. Matrigel™ coating of the culture dish and PET membrane as well as LinkCell™ membrane were tested with bioprinted hPSC-LESCs.

Coating and printing substrate	**Tested printing conditions (UV exposure time, s/layer)**	**Used with cells**
Coll and LN521	0; 2; 5	No
Nonporous PET membrane coated with Coll and LN521	0; 2; 5	No
Nonporous PET membrane coated with Matrigel™	0; 2; 5	Yes
Matrigel™ coating	0; 2; 5; 15	Yes
LinkCell™ collagen membrane	0; 2	Yes

The ColIV with LN521 coating was done as described in Chapter 5.1.1. 150 µl of the ColIV-LN521 solution was used for each 35 mm dish, and the dishes were left over night at 4 °C. Before use, the solution was removed. Matrigel™ coating was prepared by melting it quickly from the freezer, and diluting it in Cnt-30 medium as a 2:1 dilution. 150 µl of the solution was used for each 35 mm dish, and the solution was quickly spread with a cell scraper (Greiner Bio-One GmbH, Germany). For the LinkCell™ and PET substrates, the membranes were punched into 15 mm pieces with a puncher (OmniCutter, NuVision Biotherapies Ltd.) and placed at the bottom of the dishes (Figure 19). With the PET membranes, one drop of PBS was added to the bottom of the dish before placing the PET membrane to keep it in place. The coating of the PET membrane either with Matrigel™ or ColIV and LN521 coating was done as described previously. The coated dishes were left to warm up at 37 °C for 0.5 – 1.5 hours before printing.

Figure 19. Nonporous PET membrane as a printing substrate. The membrane was punched with a 15 mm puncher and placed onto a culture dish. After printing, 300 – 400 µl of Cnt-30 medium or 1X PBS was added to the edges of the dish to provide humid environment for the hydrogel and prevent it from drying.

5.1.3 Preparation of the bioink

The bioink consisted of the hPSC-LESCs, a thiolated component X, methacrylated component Y and rheological modifiers increasing the biocompatibility and bioprintability of the bioink. The native cornea was used as a source for inspiration when choosing the bioink components. The bioink components, their dissolutions and volumes are described in confidental Appendix A. Other bioink components were ready for use without further preparation, except the methacrylated and thiolated components. The thiolation protocol is described next, and the more detailed description can be found from Appendix A.

The component X was thiolated with Pierce Traut's reagent (ThermoFisher Scientific). 5 mM of ethylenediaminetetraacetic acid (UltraPure EDTA, ThermoFischer Scientific) was added to the component X solution, and its pH was adjusted to 8 – 9 with 10X PBS (pH 8) and 1 M sodium hydroxide (NaOH, AnalaR NORMAPUR® ACS, Reag. Ph. Eur analytical reagent, VWR Chemicals). Traut's reagent was dissolved in 1X PBS (pH 8.5) containing 2 mM of EDTA to prepare 112 mM solution. 26.4 µl/ml of Traut's reagent solution was allowed to react with the component X solution for 1 h at room temperature

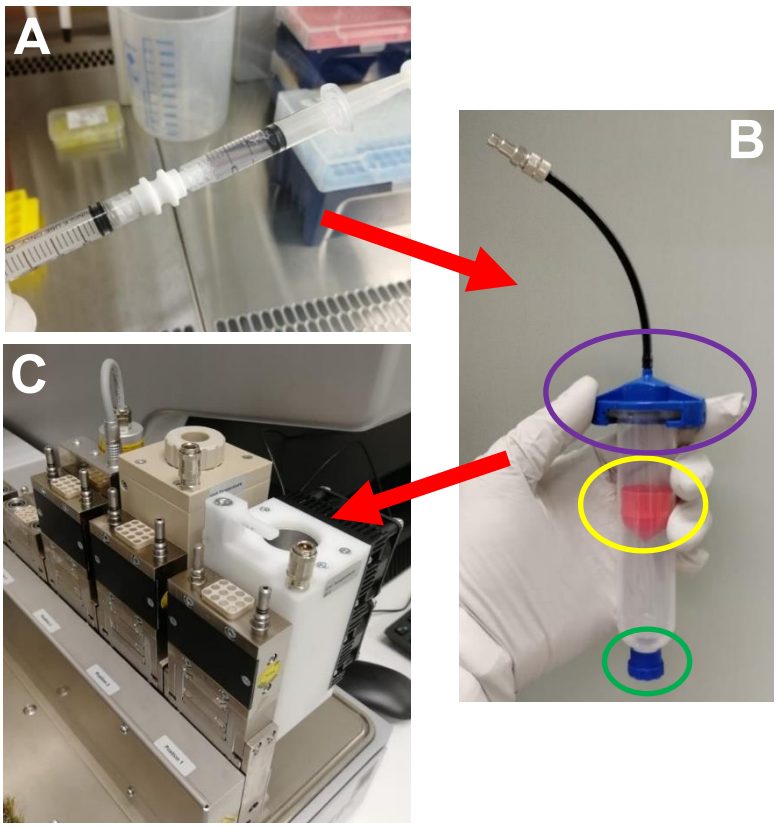

Figure 20. The preparation of the bioink. **(A)** The bioink components were mixed with two syringes attached with a luer-lock. **(B)** The bioink was transferred into a printing cartridge with a piston (yellow), a tip cap (green) and an air lock adapter (purple). **(C)** The cartridge was placed into the low-temperature dispensing head (far right). The UV head is also shown on far left.

before purifying the component X with Zeba spin desalting columns (ThermoFischer Scientific). After removing and discarding the storage solution, spin columns were purified with 1X PBS (pH 8.5) three times by centrifuging at 1000 g for 2 minutes. Next, the component X solution was applied into the column and centrifuged at 1000 g until most of the component X had been collected. The purified component X was aliquoted, some of the aliquots were stored at +4 °C to be used within 48 hours and some at -20 °C for later use.

The bioink was prepared in a laminar hood with lights out due to light-sensitivity of the methacrylated component Y. The printing consumables are listed in Table 7. First, all the components and consumables were cleaned with 70% ethanol and gathered into the laminar hood. First, the methacrylated component Y was slowly pulled into a 2.5 ml syringe with a luer lock tip (Terumo, Belgium) by using a needle (20 G, 1 ½ ‘’, KD-FINE, KD Medical GmbH Hospital Products, Germany). The medium containing the cells and other components of the bioink were pulled into another syringe. Needles were removed, excess air was pushed out and a luer-lock was attached in between the syringes (Figure 20 A). Then, the bioink was carefully mixed by pushing the plungers alternately at least 10 times. Finally, the bioink was transferred into the barrel with a tip cap on the bottom, and a piston was pushed in the middle of the syringe (Figure 20 B). The tip cap was changed into a printer needle, air lock adapter was attached, and the barrel was placed into the low-temperature printer head (Figure 20 C).

Table 7. Printing consumables used in the 3D bioprinting

Printing consumable	**Manufacturer**
32 G blunt needles, 0.50’’	CELLINK, Sweden
Optimum® Syringe Barrels, clear, 30cc	Nordson EFD
Optimum® Pistons, red	Nordson EFD
Optimum® Tip Caps, blue	Nordson EFD
Optimum® Adapter	Nordson EFD
Female-Female Luer Locks	Health Care Logistics, USA

5.2 The bioprinter and 3D model

The extrusion-based 3D bioprinter used was 3D-Bioplotter Manufacturer Series (EnvisionTEC GmbH, Germany) shown in Figure 21. The bioprinter had two dispensing-heads, with high (up to 250 °C) or low temperatures (2 – 70 °C), and a UV curing head (wavelength 365 nm). The 3D structure was designed with Perfactory RP software as a STL file. After determining the dimensions and placing the 3D structure, it was sliced in correspondece to the layer thickness, which was 80% of the inner diameter of the needle tip (80% of 100 µm). Finally, the STL file was saved as *Bordland Package Library (BPL)* file for the VisualMachines software, which is the executing software for controlling the material parameters, pattern design and the 3D bioprinter. In VisualMachines software, a new project was created and the 3D model as a BPL file was loaded in the Project Editor tab. The material parameters were selected in the Material Editor tab, and the UV program was designed in the UV Programs tab. Subsequently, the desired material was assigned for the low-temperature dispensing head in the Project Editor, and if using a UV program, it was assigned also in the Project Editor.

Before preparing the bioink, the printing platform was cleaned with 70% ethanol, and the low-temperature dispensing head was heated at 37 °C in advance by selecting the correct material. The printing platform was cooled at 8 °C to prevent the printed structure to spread. This was done by using a separate temperature controller (Minichiller 300, Huber) shown in Figure 22 A. After the barrel containing the bioink was in place, the

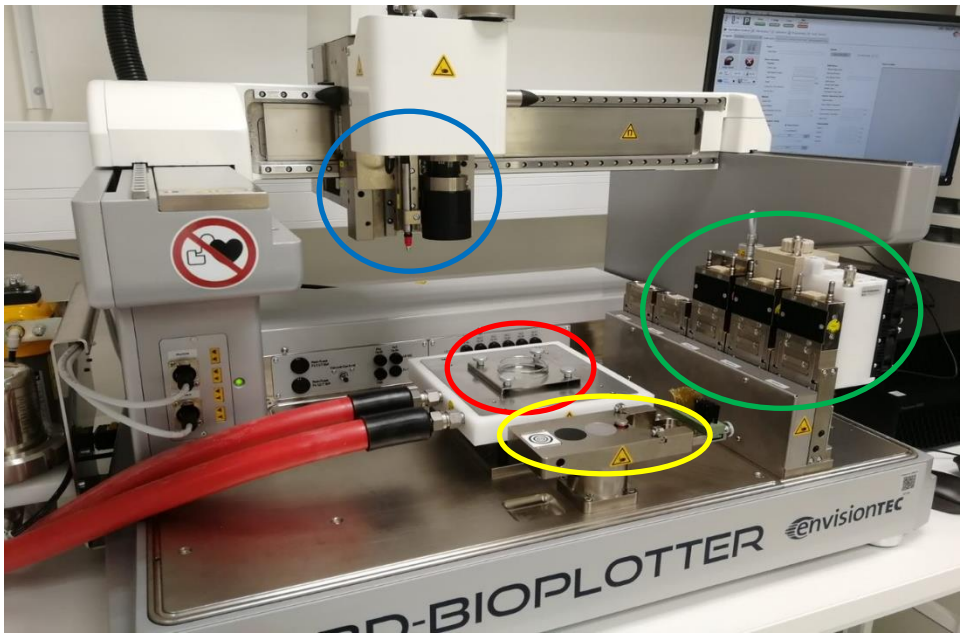

Figure 21. The 3D bioprinter used in this thesis (3D-Bioplotter, EnvisionTEC GmbH, Germany). The printing platform and base plate (red), the motor head with the camera and platform height control (blue), the purge station and needle calibration station (yellow) and printing heads (green) with the low-temperature head on far right.

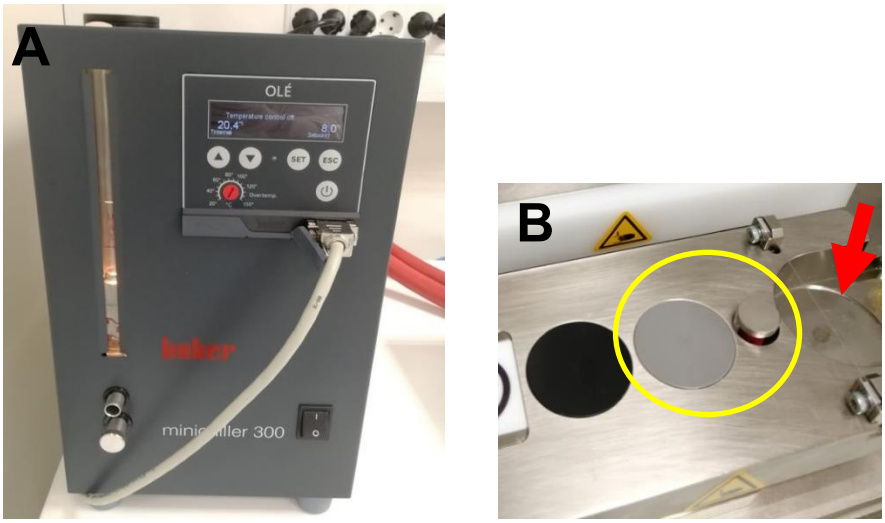

Figure 22. The additional printing equipment. (A) The temperature controller of the printing platform. (B) The purge station (red) and the needle calibration station (yellow).

needle was calibrated according to the instructions given by the manufacturer. Before printing, it was ensured that the bioink could come out through the needle by using the purging protocol. The bioprinter head was driven on top of the purge station (Figure 22 B) and pressure was applied to make the material come out from the nozzle.

5.3 Extrusion-based 3D bioprinting

The bioprinting was done on the 35 mm culture dishes with different coatings described in Chapter 5.1.2. After bioink preparation and needle calibration, the dish was placed on the printing platform to cool down, and the previously created project was selected to start the print. If an UV program was selected, the printer changed the dispensing head to the UV head automatically after printing each layer. Two layers were printed with the printing speed of 15 mm/s, the pressure 0.6 bar and the distance between strands 0.2 mm. The inner diameter of the 32G needle used for printing was 100 µm. Figure 23 shows the bioprinter in action.

Figure 23. 3D-Bioplotter bioprinting a corneal epithelium mimicking structure on a small culture dish. The cartridge containing the cell-laden bioink is inside the low-temperature dispensing head, set at 37 °C. Coated, empty dishes (right) are cooling before bioprinting on the printing platform set at 8 °C.

After printing was done, 300 – 400 µl of Cnt-30 medium was added to the edges of the dish as demonstrated in Figure 19, and the cell-laden structure was placed in an incubator at 37 °C 5% CO_2. 2 ml of the medium was added 3 h later to cover the printed structure, or in case of the PET membranes, medium was added beneath the membrane. This was done to prevent the printed gel to be washed away, which occurred, if a larger amount of medium was added right after the printing directly on top of the structure. During these 3 h the cells had enough time to attach at the bottom of the dish and the structure was not washed away during cell culture. The medium was changed every other day during the culture of the bioprinted samples until fixing, described in Chapter 5.5.2. If the printing was done without cells, PBS was used instead of Cnt-30 medium.

5.4 Printability of the bioink

The printability of the bioink was studied by printing the material without cells and UV exposure as two-layered filament structure and analyzing the effect of different pressures and printing speeds. In addition, the effect of the temperature of the printing plate was studied by testing printing of the filament on warm (23 °C) or cooled (8 °C) plate with constant pressure and speed (0.6 bar, 35 mm/s) and calculating the filament thickness and the distance between strands after printing two layers. The effects of the pressure, speed and platform temperature on the filament structure were analyzed visually by using the 3D-Bioplotter Manufacturer Series camera attached to the dispensing head mount to take a photo of the filament structure immediately after each layer was printed. This was done by setting the Image Taking Interval in the Project Editor at 1, meaning that the camera takes an image of the printing platform per one printed layer. The distance between strands was set at 1.5 mm for printing, and other printing parameters for printability tests are shown in Table 8.

Table 8. The parameters for printing filaments and studying the bioink printability. The filament was printed with either changing the printing speed, printing pressure or the temperature of the printing platform.

Parameter to be optimized	Printing pressure (bar)	Printing speed (mm/s)	Printing platform temperature (°C)
Printing speed	Constant 0.6	10; 15; 20; 25; 30; 35	8.0
Printing pressure	0.2; 0.4; 0.8; 1.0	Constant 15	8.0
Platform temperature	Constant 0.6	Constant 35	8.0; 23.0

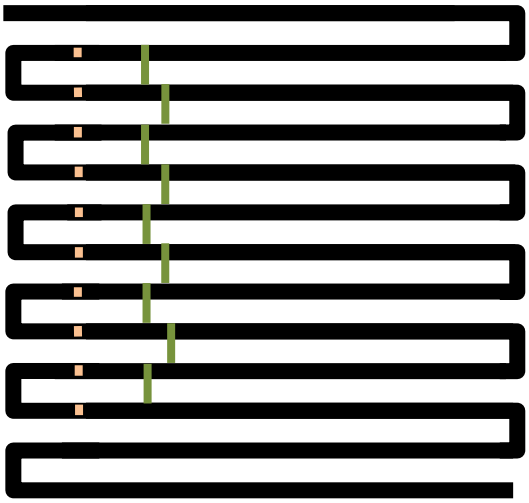

Figure 24. The printed filament structure for the printability test. Thickness was measured from the filaments shown in **light orange**, and the distance between strands was measured from the points shown in **olive green**.

To study the effect of the platform temperature, the filament thickness and the distance between strands was calculated from the photos taken with the 3D-Bioplotter camera. The filament thickness was calculated as an average of 10 individual filaments and the distance between strands as an average of 9 individual points. Figure 24 shows the printed filament structure with 13 individual filaments altogether. There, the filaments of which thicknesses were measured are shown in light orange and the points where the distance between strands was measured is shown in light green.

5.5 Optimization of the bioprinting conditions

After testing the printability of the bioink and selecting the optimal parameters and platform temperature, the bioprinting conditions were optimized for the hPSC-LESCs with substrate and UV exposure studies. They were performed with three experiments, which are summarized in Figure 25. The studies began by printing the bioink without cells on four different substrates and continued with bioprinting cells on the most promising substrates with different UV exposures. All the coatings and substrates were prepared as described previously. The first substrate tests (Figure 25 A) were done with Matrigel™ and ColIV and LN521 coatings, either by coating the plain culture dish or the PET membrane. No cells were used in this phase, and the UV exposures per printed layer were 0, 2 and 5 s. PBS was added after printing on top of the printed gels (samples without PET membrane) or beneath the PET membrane. On the next day, the analysis of the adhesion and stability of the gel was done visually and by gently moving the gel around inside the dish with a plastic pipette tip.

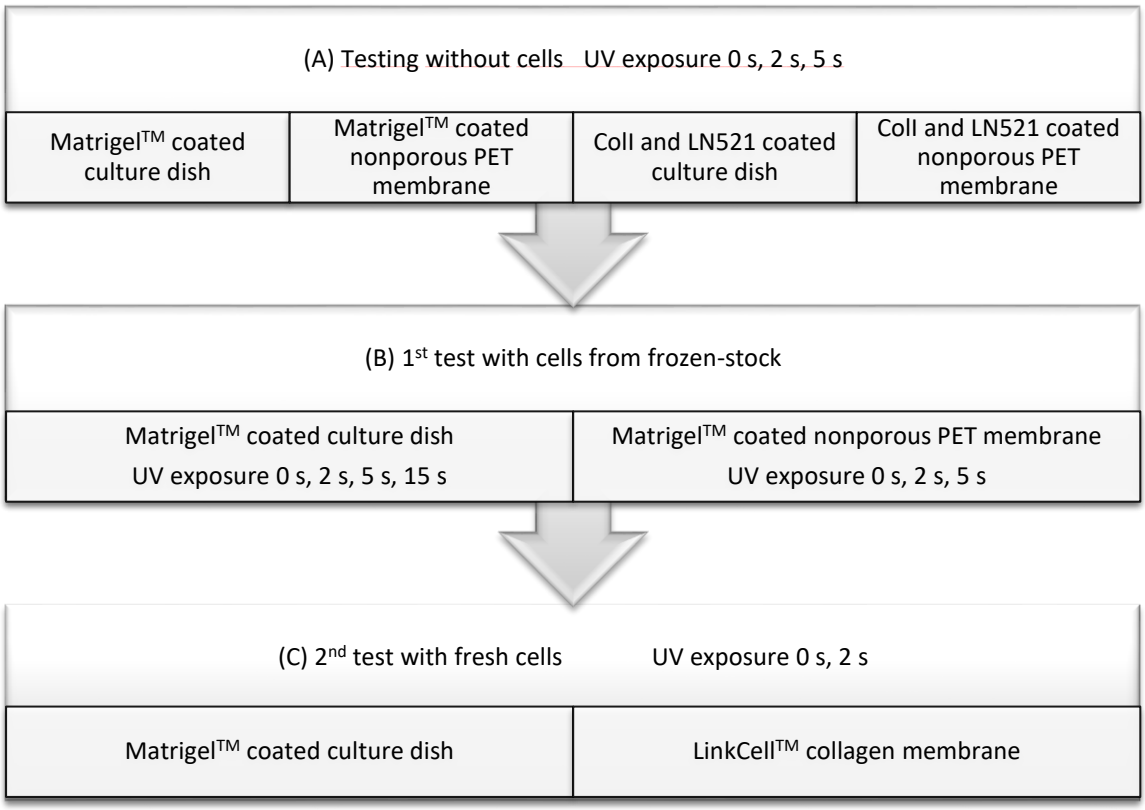

Figure 25. The three experiments with different printing substrates and UV exposures to optimize the suitable conditions for the final test series. **(A)** Four different substrates were tested with the same UV exposures and without cells. **(B)** Two substrates were selected from the first experiment for UV exposure studies. **(C)** Two substrates were studied with two UV exposure times to reduce the parameters further.

Two substrates from first substrate experiments without cells (Matrigel™ coated culture dish and Matrigel™ coated nonporous PET membrane) were selected for the second substrate and UV exposure study (Figure 25 B). Here, the hPSC-LESCs from frozen-stock with cell density of 15 million cells/ml in the bioink were used. The goal of the UV exposure studies was to observe the effect of different UV exposure times on the cell viability and proliferation, and to find the most suitable UV exposure for the cells and the 3D bioprinting. The performance of the coatings was observed meanwhile the bioprinted cells were cultured and analyzed until fixing on Day 6.

For bioprinting on Matrigel™ coated culture dish, four different UV exposure times (0 s, 2 s, 5 s, 15 s) were used to study if it influenced the cell viability. Two parallel samples of each UV exposure were bioprinted, and LIVE/DEAD analysis was performed for one of the two parallel samples. For the Matrigel™ coated PET membranes, three different UV exposure times (0 s, 2 s, 5 s) were studied, and one parallel sample of each UV exposure was bioprinted. No LIVE/DEAD analysis was performed for the samples bioprinted on PET membranes. The cell viability and proliferation on both substrates

were observed visually with the phase contrast microscope in timepoints 1 h, 3 h and on Day 1 after printing.

The third substrate and UV exposure study (Figure 25 C) included the comparison of Matrigel™ coated culture dish and the LinkCell™ membrane with UV exposure times 0 s and 2 s. The bioprinting was done with fresh hPSC-LESCs with the cell density of 3 million cells/ml, and the number of parallel samples per printing condition was 2-3. LIVE/DEAD analysis was done for the samples bioprinted on the LinkCell™ by analyzing one parallel sample. PrestoBlue analysis was done for both substrate options by analyzing one parallel sample per printing condition on Days 1, 3 and 6.

5.6 Bioink characterization

The bioink was characterized with Ellman's reaction and by analyzing the swelling, transparency and rheological properties. The Ellman's reaction, the swelling tests and the rheological measurements were done by using bioink containing the thiolated component X. Transparency analysis was performed for two different bioinks, either containing the fresh thiolated component X or the nonthiolated component X. No UV exposure or cells were used with any of the characterization methods.

5.6.1 Ellman's reaction

Ellman's reaction was used to quantitate the thiol groups from the thiolated component X. Ellman's reagent (D8130, Sigma Aldrich) was dissolved in 10X PBS (pH 8) containing 1 mM of EDTA to prepare 4 mg/ml solution. 1.25 ml of the same buffer and 25 µl of the Ellman's reagent solution was pipetted into two tubes. 125 µl of the thiolated component X solution was added to the first tube and 125 µl of the buffer solution to the other. The solutions were mixed, incubated for 15 minutes at room temperature and transferred into cuvettes (polystyrene semi-micro cuvette, Sarstedt, Germany). Absorbance was measured with Lambda 35 UV/VIS spectrophotometer (PerkinElmer) with wavelength of 412 nm. From the absorbance, *the concentration of thiol groups (c_{-SH})* in the thiolated component X was calculated according to the equation 2

$$C_{-SH} = \frac{\frac{A}{1\ cm \cdot 14\ 150\ cm^{-1}M^{-1}} \cdot 1.4 \cdot 10^{-3} l}{0.125 \cdot 10^{-3} l} \qquad (2)$$

where A is the measured absorbance.

5.6.2 Swelling behaviour

The swelling behaviour of the bioprinted structure was studied by recording changes in the weight of the printed gels. Four different UV exposure times to see, how the crosslinking density affected the stability and swelling of the printed structure. The exposure times were 0 s, 2 s, 15 s and 30 s for each layer, and two layers were printed in each 3D structure. Three parallel replicates of each UV exposure time were prepared. The printing was done on pre-weighed culture dishes without additional coating. After printing, the gels were immediately weighed to determine the initial weigth. After weighing, the gels were immersed in 2 ml of 1X PBS and stored in an incubator at 37 °C 5% CO_2. The printed gel was weighed after 1, 3 and 24 hours post-printing, and before weighing, PBS was removed and excess liquid was gently wiped from the corners of the dish. The weighing was performed immediately after the removal of PBS to prevent evaporation and inaccurate results. After weighing, the gel was immediately immersed in PBS and placed back in the incubator at 37 °C 5% CO_2. *The swelling ratio (SR)* was determined as relative water absorption with the equation 3

$$SR = \frac{w_{swollen} - w_{initial}}{w_{initial}} \cdot 100\% \qquad (3)$$

where $w_{initial}$ is the initial weight of the printed gel and $w_{swollen}$ is the gel weight after incubation in PBS.

5.6.3 Transparency

Bioink containing the fresh thiolated component X and bioink without the thiolated component X were used for transparency studies to determine if the thiolation affected the transparency of the bioink. The transparency was analyzed by measuring transmittance, which describes the ability of the material to transmit light. The higher the transmittance, the closer the passed intensity is to the intensity of the incident light. The transmittance measurement was performed by preparing 800 µl of the three bioink alternatives in the semi-micro cuvettes and measuring the transmittance with the Lamda 35 UV/VIS spectophotometer. The same cuvettes and spectrophotometer were used to measure absorbance as in the Ellman's reaction. The wavelengths used were ranging from 380 to 900 nm, and a cuvette filled with Milli-Q water (Milli-Q Advantage A10 Water Purification System, Merck) was used as blank. In addition, the transparency of the bioprinted sample was analyzed visually by evaluating the visibility and distortion of text, when the sample was placed on top of it.

5.6.4 Rheology

For the rheological measurements, the bioink containing the fresh thiolated component X was used to study the microstructure of the bioink without UV exposure, which the cells sense immediately after extrusion. The rheological measurements were performed with a Discovery HR-2 hybrid rheometer (TA Instruments) by using a 20 mm parallel-plate geometry measuring system with 1450 µm and 1180 µm gaps with fills of 350 µl and 300 µl, respectively. The rheometer was set at 25 °C. The bioink was prepared as described previously, and from one batch of bioink, four parallel samples were used for rheology in order to determine *the storage modulus (G')* and *the loss modulus (G")*. G' describes the elastic properties and the solid-state behaviour of the material, and G'' describes the viscosity and the liquid-state behaviour of the material (Anton Paar GmbH, 2020b).

The rheological measurements were done by performing the amplitude sweep and frequency sweep for the four samples. Amplitude sweeps were performed with 1 Hz frequency with the oscillation strain ranging from 0.01% to 100% to determine the maximum oscillation strain at *the linear viscoelastic region (LVE).* LVE region describes the strain range the experiment can be performed without breaking the microstructure of the material, and the maximum strain is typically determined at the point where G' begins to decrease (Anton Paar GmbH, 2020a). The maximum oscillation strain based on the amplitude sweep was 0.6%, and it was used in frequency sweeps. The frequency range in frequency sweeps was 1 Hz to 10 Hz. With weak gels, it has previously been reported that phase seperation between gel parts with different densities can occur, and to obtain more accurate data, the highest frequency has been selected as the initial frequency (Bui *et al.*, 2012). Therefore, the frequency was set to start from 10 Hz.

5.7 Analysis of the bioprinted cells

The viability, proliferation, maturation and differentiation was analyzed from the bioprinted hPSC-LESCs with different methods at different timepoints. The analyses included LIVE/DEAD on Day 1, PrestoBlue on Days 1, 3 and 6 and immunofluorescence on Day 3 and 6. For one sample type, immunofluorescence was done on Day 10. In addition, phase contrast microscope was used to visualize the cells at different timepoints to analyze their proliferation and migration. The viability and proliferation studies as well as the immunofluorescence staining with positive and negative controls are described next in detail.

5.7.1 LIVE/DEAD, PrestoBlue and phase contrast microscopy

For cell viability studies, LIVE/DEAD Viability/Toxicity Kit for mammalian cells and PrestoBlue cell viability reagent (both from Thermo Fischer Scientific) were used. PrestoBlue reagent changes color in red due to the reducing environment of viable cells, and thus the change in fluorescence can be measured. The higher the fluorescence, the higher the cell proliferation. In LIVE/DEAD, the amount of live and dead cells is determined with a two-color assay, where the green-fluorescent calcein-AM indicates live cells and the red-fluorescent ethidium homodimer-1 indicates dead cells.

LIVE/DEAD analysis was done on Day 1 to analyse the cell viability after bioprinting. LIVE/DEAD was done for 08/017 hESC-LESCs from frozen-stock and for fresh 001b B2 HT hiPSC-LESCs. The staining solution for the analysis was done by mixing 1.25 µl of ethidium homodimer-1 (2 mM) and calcein AM (4 mM) into 10 ml of 1X PBS. The cell samples were incubated in 1 ml of the staining solution at 37 °C for 30 min and immediately imaged with Olympus IX51 fluorescence microscope with 4x and 10 x augmentations. The images were analyzed with ImageJ Fiji (2.0.0-rc-69/1.52p; Java 1.8.0_172 [64-bit]), and the percentage of live cells was analyzed from 6-7 images per sample with ImageJ Fiji macro “live dead quantification” by Allevi3D (available at https://www.allevi3d.com/livedead-assay-quantification-fiji/). The average and standard deviation of the live cell percents were calculated and displayed in a bar graph.

PrestoBlue staining was done on Day 1, 3 and 6 after bioprinting to analyse the cell viability. In addition, PrestoBlue was done for hESC-LESCs on Day 9 and for hiPSC-LESCs on Day 10. PrestoBlue was performed for fresh bioprinted cells, and one sample per bioprinting condition was used. The staining solution was prepared by mixing PrestoBlue reagent and 1X PBS at 1:10 dilution. The culture medium was removed from the sample, 1 ml of the staining solution was added on each of the samples. In addition, one empty 35 mm dish without cells was used to determine the background fluorescence. The control was prepared the same way as the bioprinted samples.

After adding the reagent solution, the samples were incubated for 30 min at 37 °C 5% CO_2. The specimens were gathered on a 96 microwell plate (Nunc™ MicroWell™, Nunclon™ Delta-Treated, Flat-Bottom, Thermo Fisher Scientific) by taking three parallel specimens from each sample, including the control. The microwell plate was covered with aluminium foil to prevent light from influencing the results until the fluorescence was measured. Wallac 1429 VICTOR2 plate reader (Perkin Elmer) with 0.1 s exposure time was used to measure the fluorescence from the specimens. The average of the three fluorescence values from the parallel specimens was calculated, and the average fluorescence of the control was subtracted to get the value without the background. In

addition, the standard deviation of the fluorescence was calculated for each sample, and the data was presented in a bar graph.

In addition to LIVE/DEAD and PrestoBlue analyses, phase contrast microscopy was used as a simple and fast method to visualize the proliferation and migration of the bioprinted cells. Two different phase contrast microscopes were used, Nikon Eclipse TE2000-S and Zeiss Axio Vert A1 (Carl Zeiss AG, Germany). The first one was used to image the 3D bioprinted structures used for UV exposure studies, and the latter was used for the rest of the optical imaging. For the UV exposure studies, the bioprinted samples were imaged after 1 and 3 hours and again on Day 1 after bioprinting. The other samples were imaged on Days 1, 3 and 6, however, they were inspected daily with the phase contrast microscope. The images were analyzed with ImageJ Fiji.

5.7.2 Immunofluorescence

The proliferation, differentiation and maturation of the bioprinted samples was studied with immunofluroescence. In addition, hPSC-LESCs from frozen-stock were used as a control for immunofluorescence. Immunofluorescence utilizes fluroescent-labeled antibodies to detect specific target antigens, and in this thesis, primary antibodies and fluorescent-labeled secondary antibodies were used. The primary and secondary antibodies, other stainings and the mounting medium used in immunofluorescence analysis as well as their manufacturers and dilutions are presented in Table 9.

Before the staining, the cells were fixed, which means they were killed to stop the morphological and chemical changes. In this thesis, fixing was done on Day 3, 6 or 10, depending on the bioprinting condition of the sample and the cell batch used for the bioprinting. The fixing of the bioprinted samples and well plates with the control was done with 4% PFA, which was prepared from 20% PFA (Electron Microscopy Sciences) and 1X PBS. The culture medium was removed from the culture dishes/wells, and the cells were washed once with PBS before pipetting 1 ml 4% PFA onto the culture dishes/wells. PFA was left to affect for 10 minutes in room temperature before removing it and washing the cells twice with fresh PBS. Finally, 1 ml of PBS was pipetted per well/dish, parafilm was wrapped around the plates/dishes to prevent evaporation. The fixed bioprinted samples/well plates were stored at +4 °C before staining.

Table 9. The primary and secondary antibodies, other stainings and the mounting medium used in the thesis to analyze the hPSC-LESCs after bioprinting.

Staining		Manufacturer	Dilution	Purpose
Primary antibodies	Rabbit anti-p63α	Cell Signaling Tech	1:200	Corneal progenitor marker
	Mouse anti-p40	BioCare Medical	1:200	Corneal progenitor marker
	Rabbit anti-CK12	Abcam	1:200	Maturation marker
	Mouse anti-CK14	R&D Systems	1:300	Stratified epithelium marker
	Mouse anti-CK3	Abcam	1:200	Maturation marker
	Rabbit anti-Ki67	Millipore	1:500	Proliferation marker
Secondary antibodies	Alexa Fluor 488 donkey anti-rabbit IgG	Molecular Probes	1:500	Visualization of the primary antibody from rabbit
	Alexa Fluor 568 donkey anti-mouse IgG	Molecular Probes	1:500	Visualization of the primary antibody from mouse
Other	AlexaFluor 647 phalloidin	Molecular Probes	1:150	Actin cytoskeleton visualization
	Hoecst 33342	Molecular Probes	1:3000	Nucleic acid stain
	ProLong Gold Antifade Mountant with DAPI	Invitrogen		Mounting medium

For immunofluroescence, the fixed cells were first permeabilized with Triton™ X-100 (Sigma Aldrich) for 15 min to enable the antibodies to cross the cellular membrane. Next, the samples were blocked with 3% BSA (Bovine Serum Albumin heat shock fraction, Sigma Aldrich) for 1 h to reduce the unspecific binding of the antibodies. After permeabilization and blocking, primary antibody solution was prepared in 0.5% BSA in PBS, and the samples were left in the solution over night at +4 °C. On the next day, the samples were washed with PBS for 5 min three times, and the secondary antibody solution was prepared to match the primary antibody solution (anti-rabbit secondary antibody with primary antibody from rabbit and anti-mouse secondary antibody with primary antibody from mouse). The actin cytoskeleton stain and nucleic acid stain were added to the secondary antibody solution, since they did not bind to any primary antibody and contained the fluorescent label. The samples were left in the secondary antibody

solution for 1 h at room temperature, and after that, the samples were washed again with 1X PBS three times. Finally, the samples were mounted with the mounting medium by pipetting 40 µl of the reagent on top of the bioprinted sample and covering it with a 30 mm cover glass (VWR International).

The immunofluroescence control was prepared as a positive and negative control to determine the immunofluroescence results for hPSC-LESCs in normal cell culturing conditions (positive) and how much background immunofluorescence there is (negative). The staining was done as described previously, however, for the negative control, only the solution with secondary antibodies was used. Hence, theoretically, there should not be seen anything in the negative control due to the absence of the primary antibodies. After staining and washing, the control samples were mounted with 30 µl of the mounting medium and covered with a 15 mm cover glass (Thermo Scientific).

The stained and mounted samples/well plates were covered with aluminium foil, storaged at room temperature for 24 hours and visualized with Olympus IX51 fluroescence microscope. Every sample/well was imaged with 4x and 10x augmentations from at least three areas, and different filters were used to visualize different fluorescent dyes. Later, the images were analyzed and merged with ImageJ Fiji.

5.8 Statistical analysis

The statistical significance of data from printability, swelling behaviour, LIVE/DEAD and PrestoBlue analyses was determined with Mann-Whitney U test, and p-values ≤ 0.05 were considered statistically significant. The statistical data analysis was done with IBM SPSS Statistics software V25.0.

6. RESULTS

6.1 Printability of the bioink

Overall, the bioink extruded well without clogging the nozzle even after 30 min of printing. The printability of the bioink was further studied by printing the bioink without cells in filaments with different pressures and speeds (Figure 26) according to the parameter information in Table 8. In addition, the effect of the printing platform temperature was studied by measuring the filament thickness and the distance between strands as shown in Figure 24. The differences between the platform temperatures 8 °C and 23 °C are illustrated in Figure 27.

The filament thickness decreased when the speed was increased (Figure 26 A-F), and there was less bulging in the filament. The lowest speed (10 mm/s, Figure 26 A) caused extensive spreading of the printed filament and merging of the individual filaments. With the speeds 25, 30 and 35 mm/s (Figure 26 D-F), the starting point of the structure delayed and the filament structure was incomplete. This phenomenon is called lag on (O'Connell *et al.*, 2020) and is not desired.

With the pressure of 0.2 bar, the filament did not extrude at all. When the pressure was increased, filament bulging occurred with pressures 0.4 and 0.6 bar (Figure 26 B and G, respectively), however, there was less bulging with 0.4 bar. When increasing the pressure up to 0.8 and 1.0 bar (Figure 26 H and I, respectively), the same phenomenon causing the merging of the filaments occurred as with the lowest printing speed.

When studying the effect of the platform temperature on the filament, the difference in thickness was statistically significant ($p \leq 0.05$). The filament thickness was bigger on the warmer platform (0.72 mm) compared to the cooled platform (0.62 mm) (Figure 27 E). However, the distance between strands was not affected by the platform temperature, as it was 1.47 mm with both temperatures. In addition, it was close to the set distance (1.5 mm) with a difference of 30 µm.

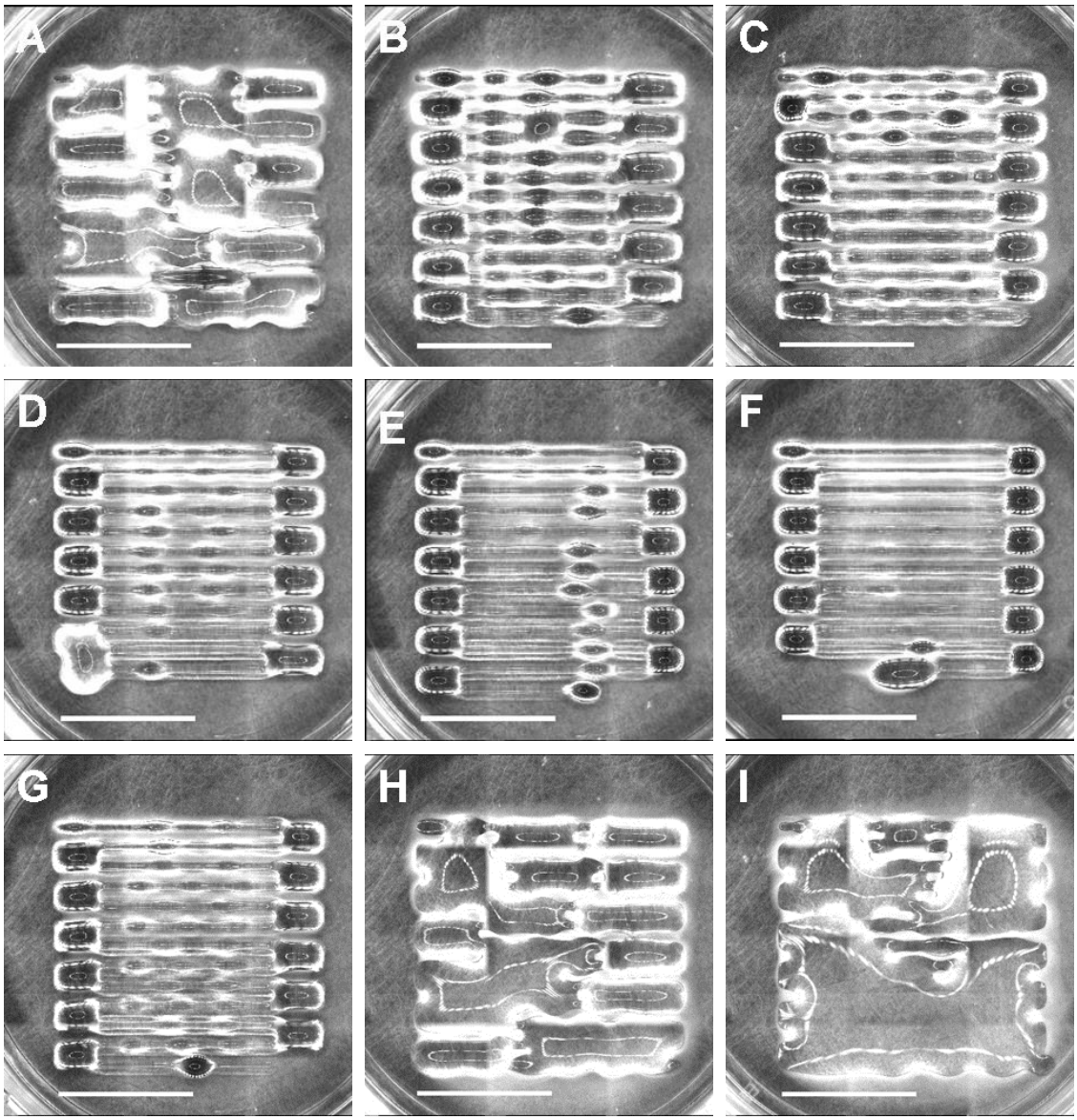

Figure 26. The effect of printing speed and pressure on the printability. **(A-F)** Constant pressure 0.6 bar. Printing speed **(A)** 10 mm/s, **(B)** 15 mm/s, **(C)** 20 mm/s, **(D)** 25 mm/s, **(E)** 30 mm/s, **(F)** 35 mm/s. **(G-H)** Constant speed 15 mm/s. Printing pressure **(G)** 0.4 bar, **(H)** 0.8 bar, **(I)** 1.0 bar. Scale bars 10 mm. Platform temperature 8 °C

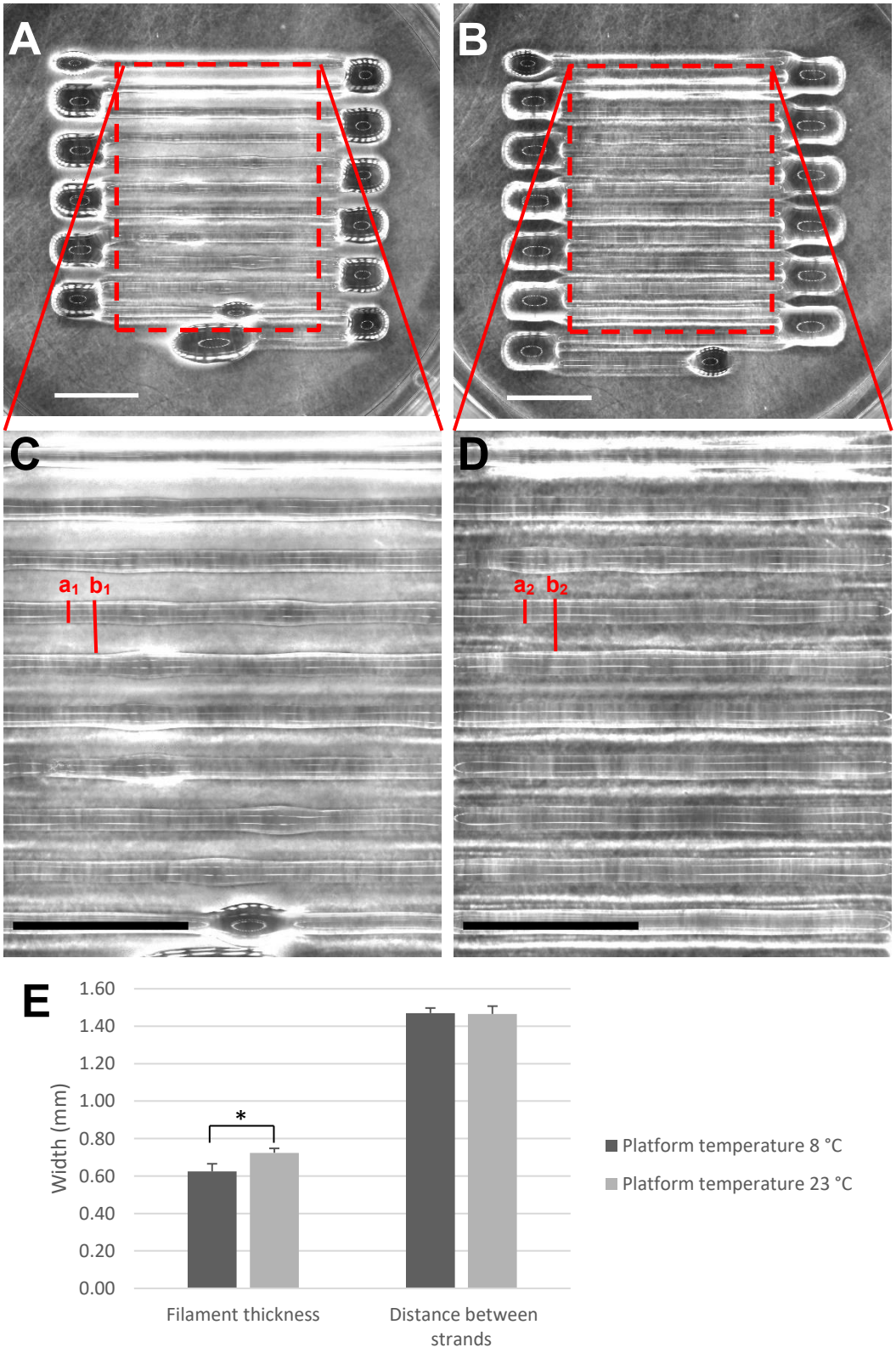

Figure 27. The effect of the temperature of the printing platform. Bioink was printed with printing speed of 35 mm/s and pressure 0.6 bar. **(A, C)** Platform temperature 8 °C. **(B, D)** Platform temperature 23 °C. **(E)** Average filament thickness ($p^* \leq 0.05$) and distance between strands ($n_{filament} = 10$, $n_{strand} = 9$) with platform temperatures 8 °C and 23 °C. The distance between strand was set at 1.5 mm for printing. **(a_1)** Filament thickness and **(b_1)** distance between strands with platform temperature 8 °C. **(a_2)** Filament thickness and **(b_2)** distance between strands with platform temperature 23 °C. Scale bars 5 mm.

6.2 Optimization of the bioprinting conditions

Different printing substrates and UV exposure times were tested to determine the optimal bioprinting conditions for hPSC-LESCs as described in Figure 25. The first substrate experiments were done without cells, and the UV experiments were carried out with the most promising substrates. In the UV experiments, hPSC-LESCs from frozen-stocks were used and their viability and proliferation was analyzed with LIVE/DEAD and PrestoBlue.

6.2.1 Substrate and UV studies without cells

The first substrate experiments were performed without cells, and the coating types were ColI and LN521 coating of the culture dish or PET membrane and Matrigel™ coating of the culture dish or PET membrane (Figure 25 A). The two coatings were selected to enhance the adhesion and biocompatibility of the plain culture dish surface or PET membrane. The PET membrane was tested due to the possibility to remove the 3D structure out from the culture dish for further analysis, since the membrane could be detached from the bottom of the dish. Moreover, the detachment enabled the addition of PBS or culture medium beneath the membrane. Subsequently, the PET membrane floated on the liquid surface, which resulted in better attachment of the printed structure compared to the structures printed onto the coated culture dish and immersed in PBS. Moving the membrane out from the culture dish did not disturb the printed structure, and it stayed attached on the membrane. When immersing the membrane with the structure in PBS, the gel printed with 0 s UV disappeared from the membranes. With 2 s and 5 s UV exposures, the gels stayed attached to the membrane even after the immersion.

When comparing the two coatings, the combined ColI and LN521 coating seemed to cause the bioink to spread more after printing. The spreading occurred with all UV exposure times, and the results were the same with or without the PET membrane in between the culture dish and the coating. Hence, ColI and LN521 coating was not tested further with cells. When printing on Matrigel™, there was not as significant spreading after printing, and the printed structure stayed in place after one day immersion in PBS. Therefore, Matrigel™ coated culture dishes were selected as one substrate for further studies, including the UV exposure studies. Even though the structures printed on Matrigel™ coated PET membranes showed some spreading of the bioink, the membranes were selected as the second substrate type for bioprinting hPSC-LESCs in the UV exposure studies to see, if the cell adhesion could decrease the spreading of the structure.

6.2.2 Substrate and UV studies with cells

Based on the results from the substrate studies done without cells, the substrate and UV exposure studies with hPSC-LESCs from frozen-stock began with testing the selected two substrate types and different UV exposures as described previously (Figure 25 B). When comparing the printing substrates, Matrigel™ coated nonporous PET membranes showed promising results as the bioprinted structure was not washed away immediately after printing, enabling more time for the cells to attach the substrate. However, when the bioprinted hPSC-LESCs were observed with the phase contrast microscope, the cell adhesion and proliferation on Matrigel™ coated PET membranes did not seem to be as good as in the samples printed on Matrigel™ coated culture dishes. Subsequently, the samples printed on the PET membranes were not further studied, and the LIVE/DEAD analysis and imaging with the phase contrast microscope were performed only for the samples printed on Matrigel™ coated culture dish.

The increased UV exposure time did not affect the cell viability significantly, and almost equal amounts of live and dead cells were detected with all the UV exposures (Figure 28). The average cell viability was above 90% in samples with UV exposures of 2, 5 and 15 s. However, the number of cells attached to the bottom of the dish was lower in the 5 s and 15 s samples (Figure 29 C-D). The average viability in the 0 s sample (87.5%) was slightly lower than with the other sample types, however, the number of attached cells was higher (Figure 29 A).

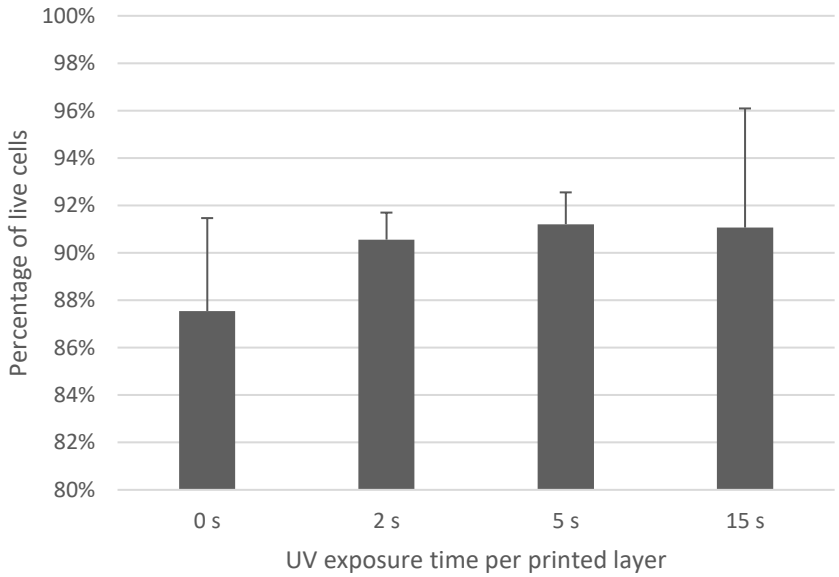

Figure 28. The effect of UV exposure time on cell viability. hPSC-LESCs from frozen-stock were 3D bioprinted on Matrigel™ coated culture dishes with four different UV exposure times (0 s, 2 s, 5 s, 15 s), and the cell viability was analyzed on Day 1 with LIVE/DEAD. The average percentages and standard deviation of live cells were analyzed from 6-7 images per UV exposure time ($n_{UV\ exposure\ time}$ = 6 or 7).

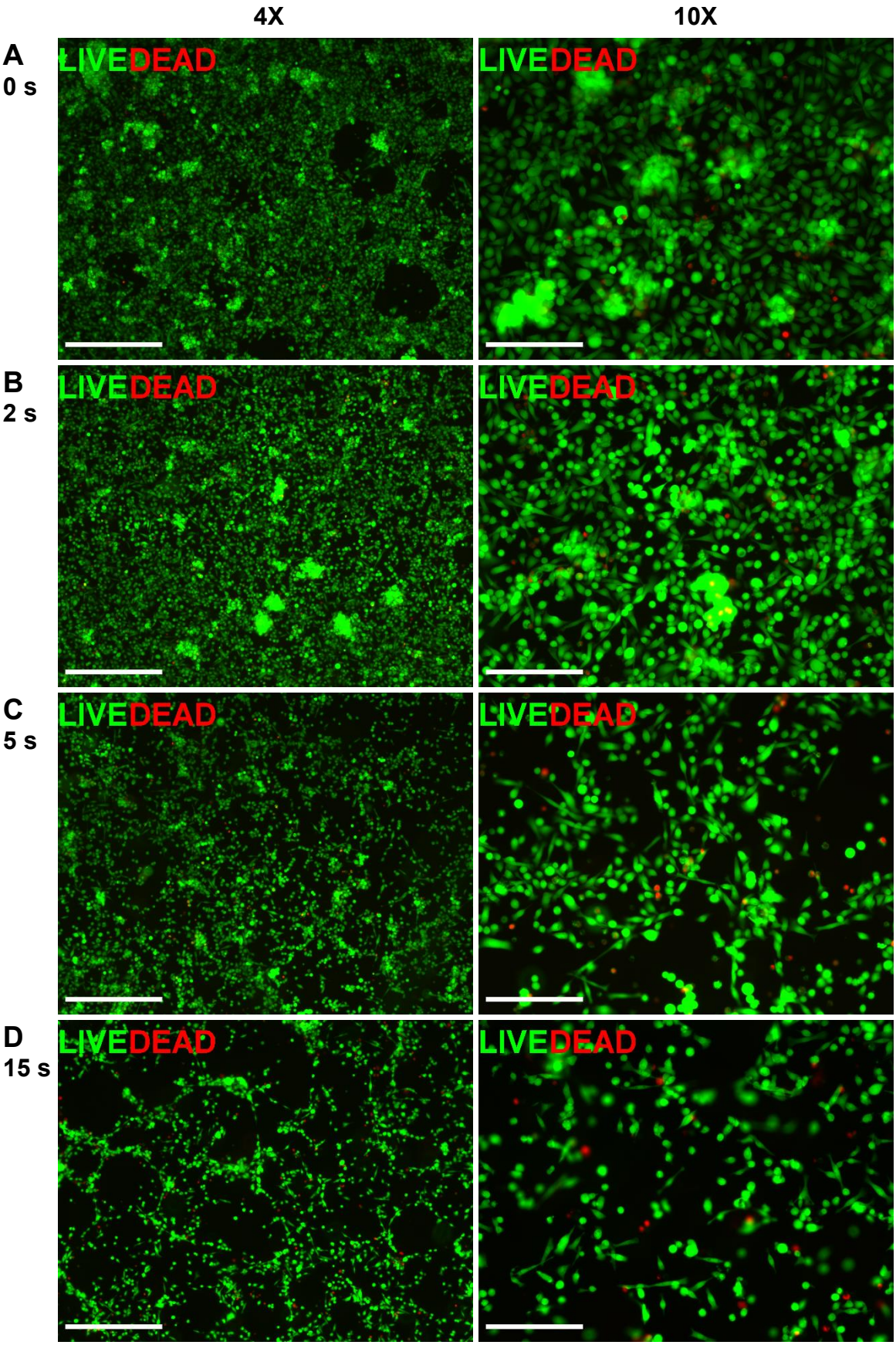

Figure 29. The effect of UV exposure time on the hPSC-LESC viability on Day 1 after bioprinting on Matrigel™ coated culture dish. UV exposure times: **(A)** 0 s, **(B)** 2 s, **(C)** 5 s, **(D)** 15 s. Scale bars 500 µm **(left column)** and 200 µm **(right column)**.

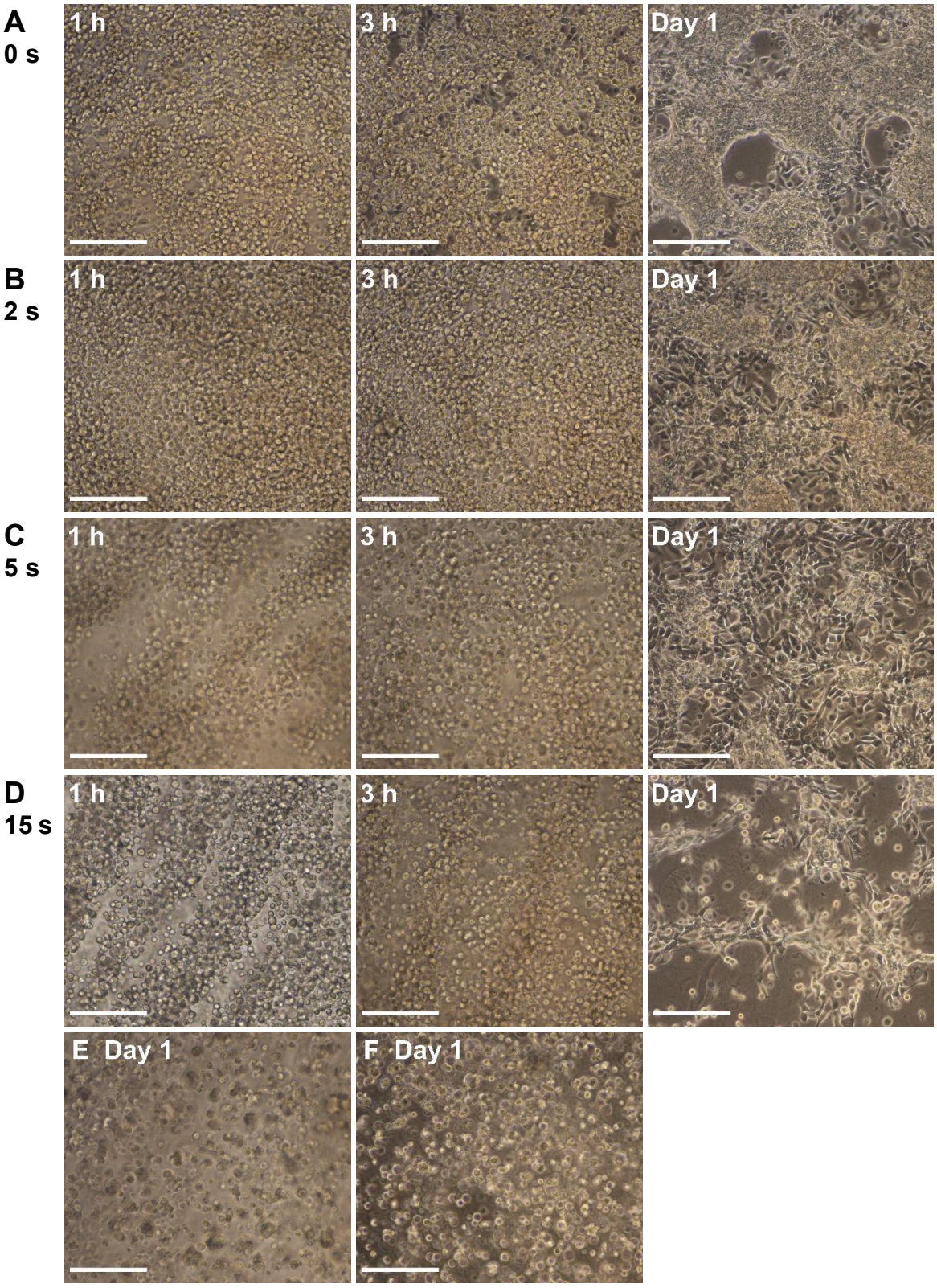

Figure 30. The effect of UV exposure time on the gel stiffness when bioprinting on Matrigel™ coated culture dish. UV exposure times **(A)** 0 s, **(B)** 2 s, **(C)** 5 s, **(D)** 15 s. **(E-F)** Gels were detached from the printing substrate: **(E)** 5 s, **(F)** 15 s. Scale bars 200 µm.

The stiffness of the printed structure was increased due to longer UV exposure and affected the cell migration and proliferation (Figure 30). The increase in stiffness was especially clear with the UV exposure times of 5 s and 15 s per printed layer. Due to stiffer material, the cells were not able to migrate or interact with each other, the printed filaments were visible 1 h after printing and the cells remained circular (Figure 30 C-D). The printed structure detached from the bottom of the printing substrate with higher UV exposure times (5 s and 15 s) during cell culture on Day 1. The cells in the detached structure remained circular (Figure 30 E-F), whereas the cells attached on the bottom could deform and migrate (Figure 30 C-D, Day 1). The detaching structure resulted in lower number of cells on the bottom of the dish compared to the samples with lower UV exposure.

Matrigel™ coating was used to enhance the cell adherence on the printing substrate, and the bioprinted hPSC-LESCs on Matrigel™ showed significantly high cell proliferation ($p \leq 0.05$) at all timepoints (Figure 31). However, already on Day 1, holes were seen in the formed epithelium (Figure 30 A, Day 1). The clustering and shrinkage of the Matrigel™ was observed especially with lower UV exposure times due to lower crosslinking density and softer structure. Due to the high proliferation and shrinkage of the Matrigel™, the cells were able to rip the coating, which resulted in Matrigel™ surface

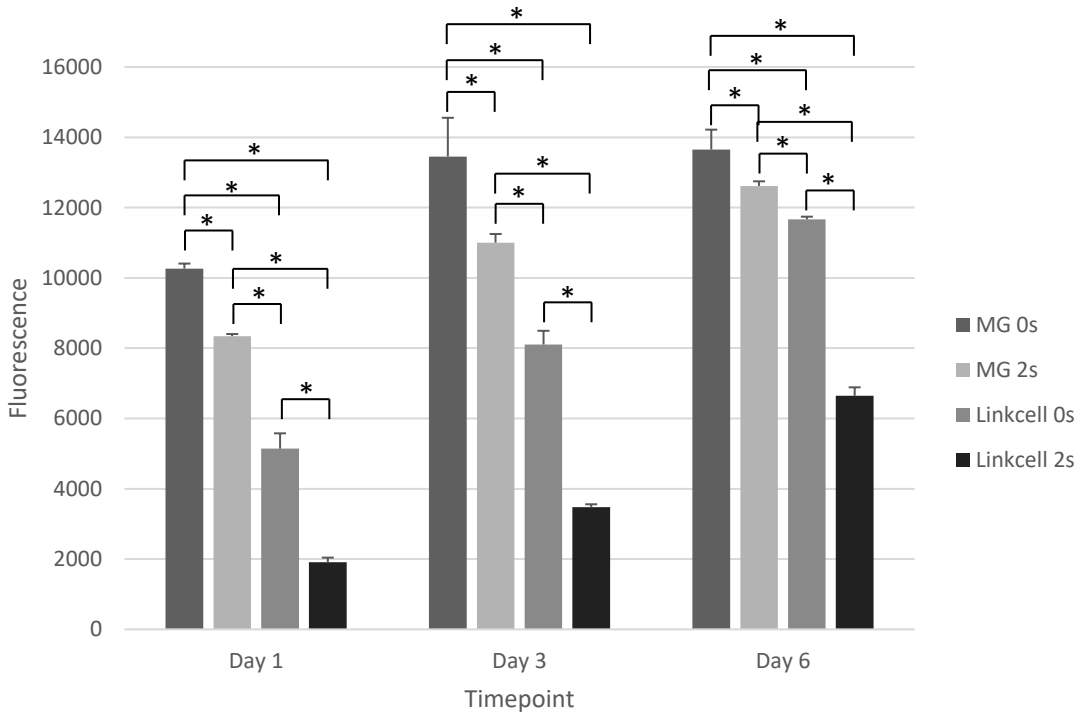

Figure 31. PrestoBlue data from bioprinted hPSC-LESCs (cell line 08/017) with four different conditions ($n_{condition} = 3$, $p^* \leq 0.05$): printing on Matrigel without UV exposure and with 2 s UV exposure per printed layer (MG 0s, MG 2s) and printing on Linkcell collagen membrane without UV exposure and with 2 s UV exposure (Linkcell 0s, Linkcell 2s).

with holes. Since the cells were not able to adhere and proliferate on the noncoated parts of the dish, this finally resulted in nonhomogenous epithelium.

Since the Matrigel™ coated nonporous PET membranes were not suitable as a printing substrate, LinkCell™ collagen membranes were tested in the third substrate study (Figure 25 C). The membranes were tested as a solution for the detaching masses from Matrigel™ due to higher stiffness of LinkCell™ membranes. Here, fresh hPSC-LESCs were used instead of the frozen-stock. The LinkCell™ membrane was stored in a liquid, resulting in firm attachment to the bottom of the dish, and thus the addition of the medium beneath the film was not possible. Even though the cell proliferation on Matrigel™ was significantly higher ($p \leq 0.05$) than on LinkCell memrbane, the proliferation of the bioprinted fresh hPSC-LESCs increased during cell culture with all the conditions (Figure 31). Moreover, the cell proliferation on LinkCell™ with 0 s UV at Day 6 was close to the proliferation on Matrigel™. However, UV exposure in combination with LinkCell™ membrane seemed to result too stiff structure where cells were not able to migrate or proliferate as well, which explains the significantly lower fluorescence value from PrestoBlue analysis compared to other printing conditions. Subsequently, LinkCell™ membranes without UV exposure were selected as a second substrate option together with Matrigel™ coated culture dishes with UV exposures of 0 s and 2 s. Importantly, when using fresh hPSC-LESCs, there was not as significant detaching of the cell masses in the samples bioprinted on either Matrigel™ or LinkCell™, which is why only fresh hPSC-LESCs were used in the final tests and Matrigel™ was selected as the other coating option despite the previously described challenges with it.

6.3 Bioink characterization

After optimizing the bioprinting conditions for the hPSC-LESCs, the bioink was further characterized with Ellman's reaction, swelling and transparency analysis as well as rheology, which included amplitude and frequency sweeps.

6.3.1 Ellman's reaction

Ellman's reaction was used to determine the concentration of the thiol groups for the thiolated component X in the bioink according to the equation 2. The concentration of the thiolated groups was 44.64 µM.

6.3.2 Swelling behaviour

The swelling behaviour of the bioink and the printed 3D structure without cells was studied visually and by weighing the structure after 1, 3 and 24 hours after printing and calculating the SR according to the equation 3. Significant swelling behaviour could already be detected visually after 3 h and 24 h from all the samples with different UV exposure times, and Figure 32 shows the visual swelling of the sample with 15 s UV exposure. The recordings of the weigths of the printed gels are shown in Figure 33. When weighing the gels after 1 h, there was a significant decrease in weight of the 0 s and 2 s gels ($p \leq 0.05$, Figure 33 A), which indicated low crosslinking degree and stability. Thus, the weights of the 0 s and 2 s samples at the timepoints 3 h and 24 h were not be measured. However, gels with 15 s and 30 s UV exposure were stabile enough and weighing was possible even after 24 h in PBS.

No significant swelling of the 15 s and 30 s gels was observed after 1 h (Figure 33). In fact, there was a slight decrease in weight in the 15 s sample compared to the initial weight (Figure 33 B), which indicated that some of the gel could have been washed away due to the removal of PBS. However, the decrease was minimal and the weight increased after 1 h. Even though the water absorption of the 30 s sample was higher after 3 h, the difference was not significant anymore after 24 h.

Figure 32. The swelling of printed structure with 15 s UV exposure **(A)** 3 h after printing and **(B)** 24 h after printing. The gel is inside the red dashed line.

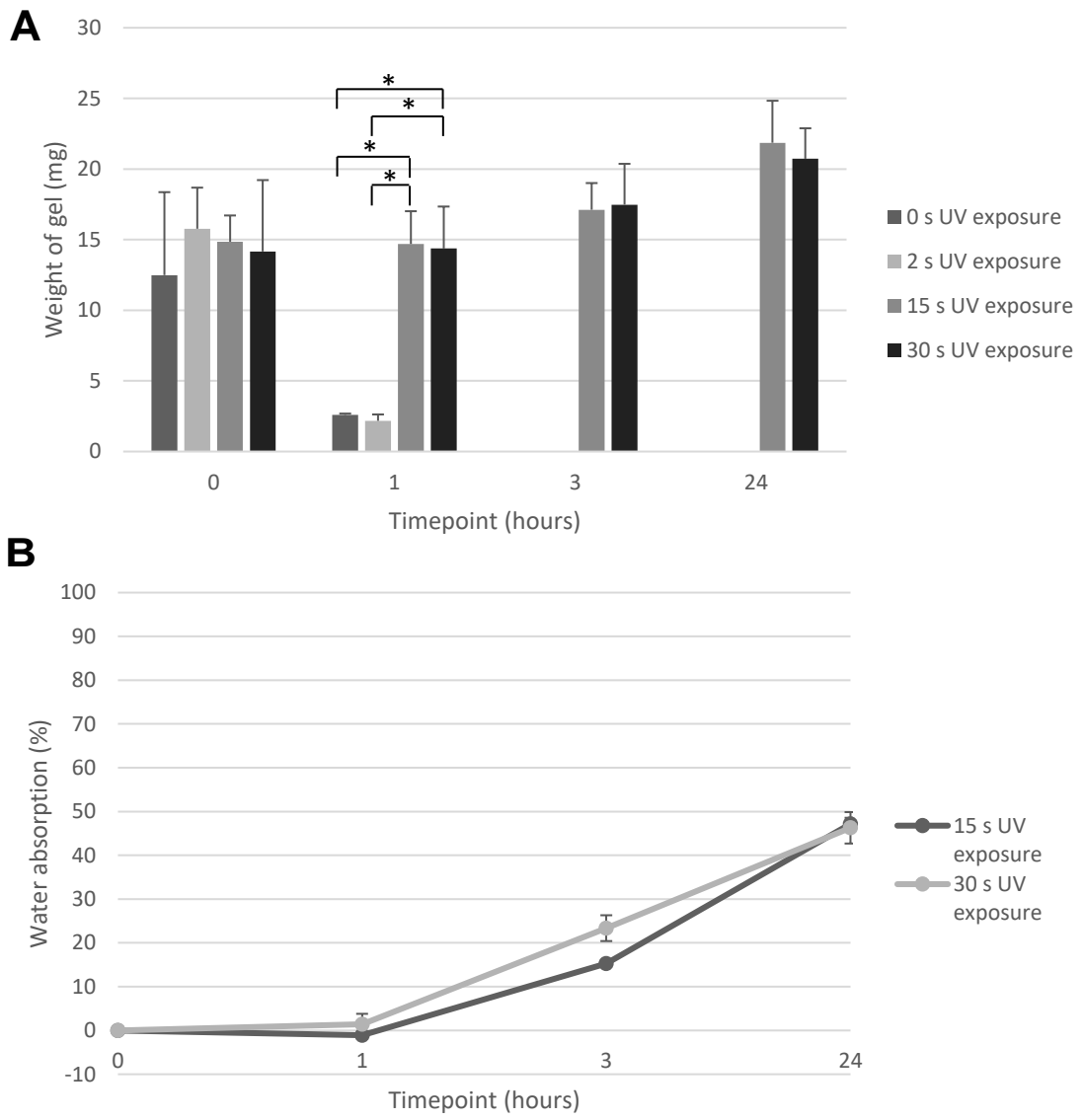

Figure 33. The swellin behaviour of the printed structures. **(A)** The change in weight ($p^* \leq 0.05$) and **(B)** the swelling ratio as relative water absorption of the printed structure after 1, 3 and 24 hours. Printing was done without coating of the dish and four different UV exposure times were used (0, 2, 15 and 30 s, $n_{condition} = 3$). During timepoints the printed structure was immersed in 1X PBS at 37 °C. With two lowest UV exposure values, the structure was washed away during PBS change after 1 h, and thus the timepoints at 3 and 24 h were not measured.

6.3.3 Transparency

The transparency of the bioprinted sample was analyzed visually by placing it on top text (Figure 34 A). The text was readible, clear and no distrotion was observed. In addition to visual analysis, transparency was analyzed by measuring the transmittance at wavelengths ranging from 380 to 900 nm with Milli-Q water as blank (Figure 34 B). The transmittance was measured from bioinks with the fresh thiolated component X and with the nonthiolated component X. The thiolation did not affect the transmittance except at the lower wavelengths. Ranging from 380 to 450 nm the transmittance of the bioink containing the nonthiolated component X was higher than the bioink containing the thiolated component X. At higher wavelengths, both bioinks acted similarly. At

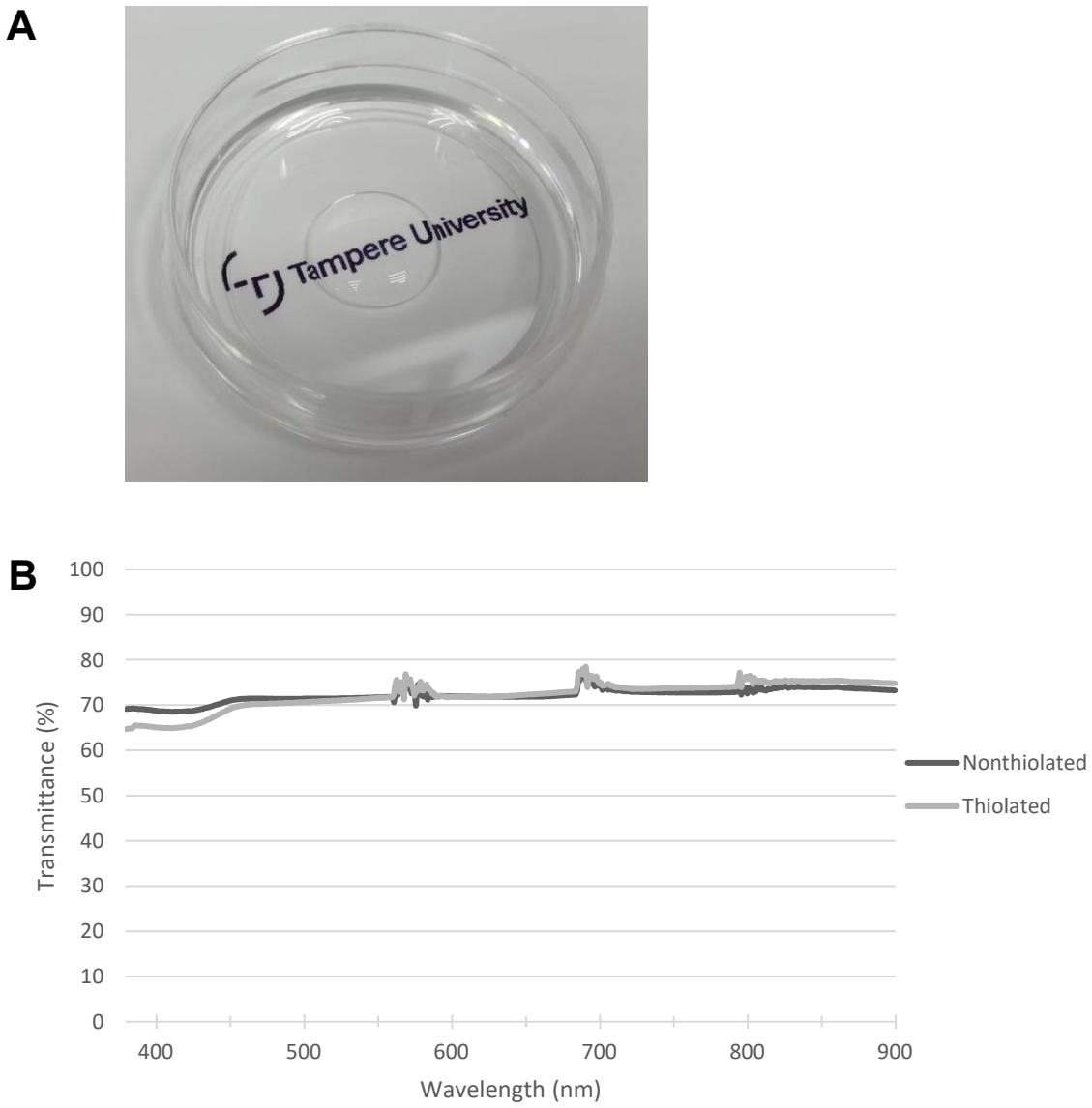

Figure 34. The transparency of the bioink was analyzed visually **(A)** and by measuring transmittance **(B)**. **(A)** Text was readible and shown without distortion through the printed gel, which indicates good transparency. **(B)** The transmittance of the bioink with and without the thiolated component X at wavelengths ranging from 380 to 900 nm was 65 – 75%.

wavelengths 560 – 590 nm, 685 – 715 nm and 795 – 805 nm, the transmittances were not aligned, however, this might be due to the bioink not being completely homogenous. Altogether, the bioink showed good transparency based on the visual analysis and the transparency ranging from 65 – 75%.

6.3.4 Rheology

Without UV exposure, the bioink was extremely difficult to handle due to its liquid-like properties and low crosslinking degree. Thus, the rheological measurements were challenging to perform. Moreover, the sufficient gap fill was challenging to achieve due to liquid-like nature of the bioink and the limited amount of material. Nevertheless, amplitude and frequency sweeps were performed from four parallel samples of the bioink, and they are presented in Figure 35.

From the amplitude sweeps, similar behaviour can be observed (Figure 35 A). At the beginning of the sweep, the G’ and G’’ values fluctuate, and after 0.2% strain they stabilize. After 0.6% strain, G’ begins to decrease, however, G’’ remains close to zero. Therefore, 0.6% strain was selected for the frequency sweeps, though a precise value for the maximum strain the material withstands without breaking could not be determined from the amplitude sweep due to the complexity of the material.

When performing the frequency sweep, the G’ increased after 1.5 Hz. The increase of G’’ was significantly lower. Subsequently, this suggests the material is more liquid-like at resting state, and when shear is applied, the elastic properties begin to dominate viscous properties. This indicates more solid-like behaviour, however, the G’ value is still very low, around 15 Pa with 10 Hz frequency.

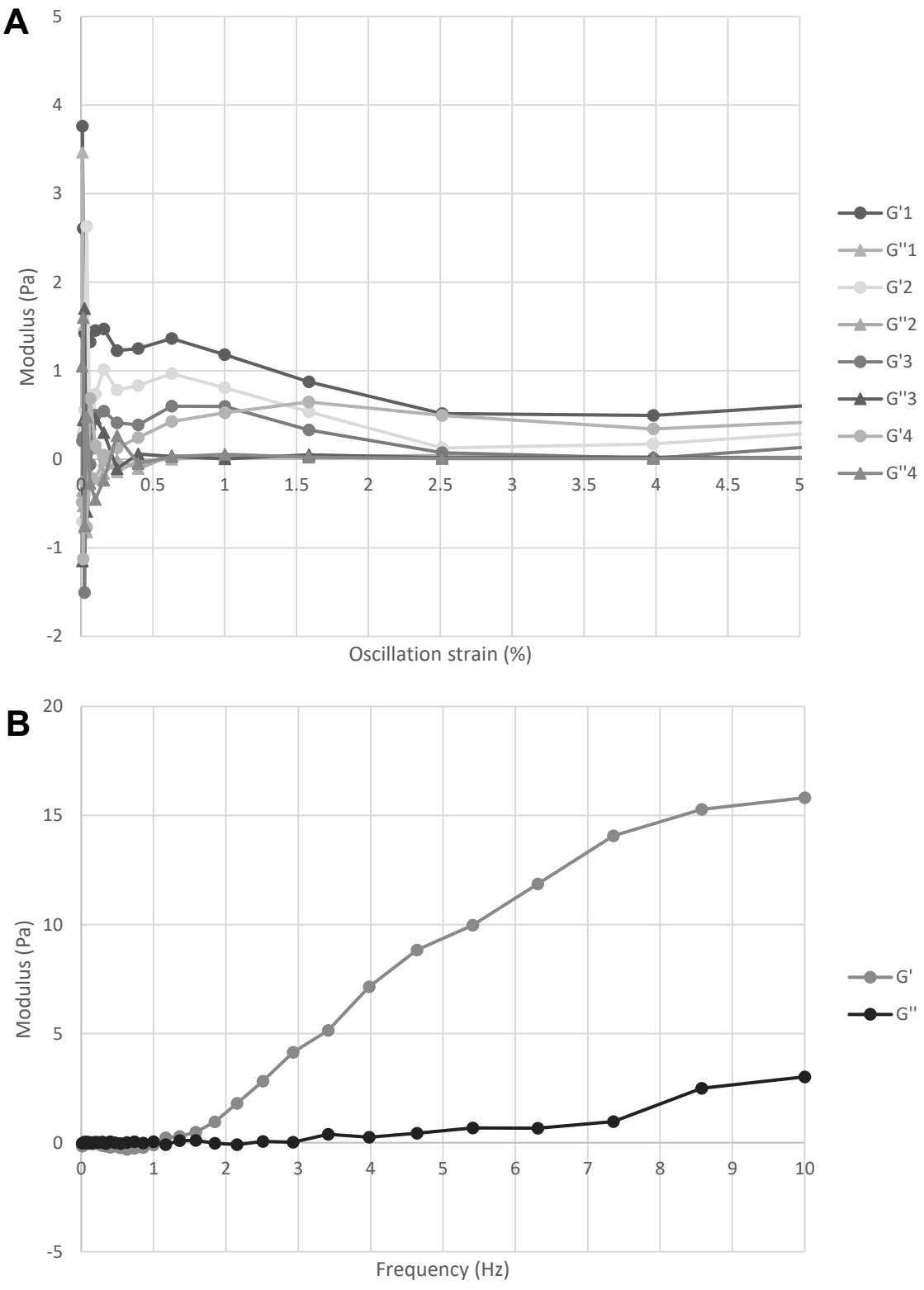

Figure 35. Amplitude **(A)** and frequency **(B)** sweeps for the bioink containing the thiolated component X. Both measurements were performed for four parallel samples. Amplitude sweeps were done with 1 Hz frequency, and frequency sweeps were done with 0.6% oscillation strain. Amplitude sweeps are shown from every measurement, and frequency sweep is shown from the measurement with the most optimal gap fill. Parallel plate geometry (20 mm) with 1450 or 1180 µm gap were used with 350 or 300 µl fills, respectively.

6.4 Cell viability, proliferation and maturation after 3D bioprinting

Based on the results from the preliminary substrate and UV exposure studies, the final experiments to study the viability, proliferation, maturation and differentiation of fresh hPSC-LESCs were performed with Matrigel™ coated culture dishes combined with 0 s and 2 s UV exposures and LinkCell™ membranes with 0 s UV exposure each layer. The 3D bioprinted structure consisted of total two layers. These conditions were used with two different fresh hPSC-LESC lines, hESC-line 08/017 and hiPSC-line 001b B2 HT. The cell viability on Day 1 was studied with LIVE/DEAD analysis from the cell line 001b B2 HT. When analyzing 6 or 7 images per bioprinted sample, the viabilities were above 90% for the Matrigel™ coated culture dishes with 2 s UV and the LinkCell™ membranes with 0 s UV, and above 88% for the Matrigel™ coated culture dishes with 0 s UV (Figure 36). Thus, no significant differences in the cell viabilities between the printing conditions were detected.

The cell proliferation was studied with PrestoBlue at several timepoints (Days 1, 3 and 6, and for LinkCell samples additional Day 9 or 10). The data from both cell lines (hESC-line 08/017 and hiPSC-line 001b B2 HT) is presented separately (Figure 37). When analysing the PrestoBlue data, Matrigel™ seemed to offer a suitable substrate for the bioprinting of hPSC-LESCs from both investigated cell lines. The hESC-LESCs seemed to prefer Matrigel™ over LinkCell™ since the fluoresence values on Day 1 were 1 – 2.5

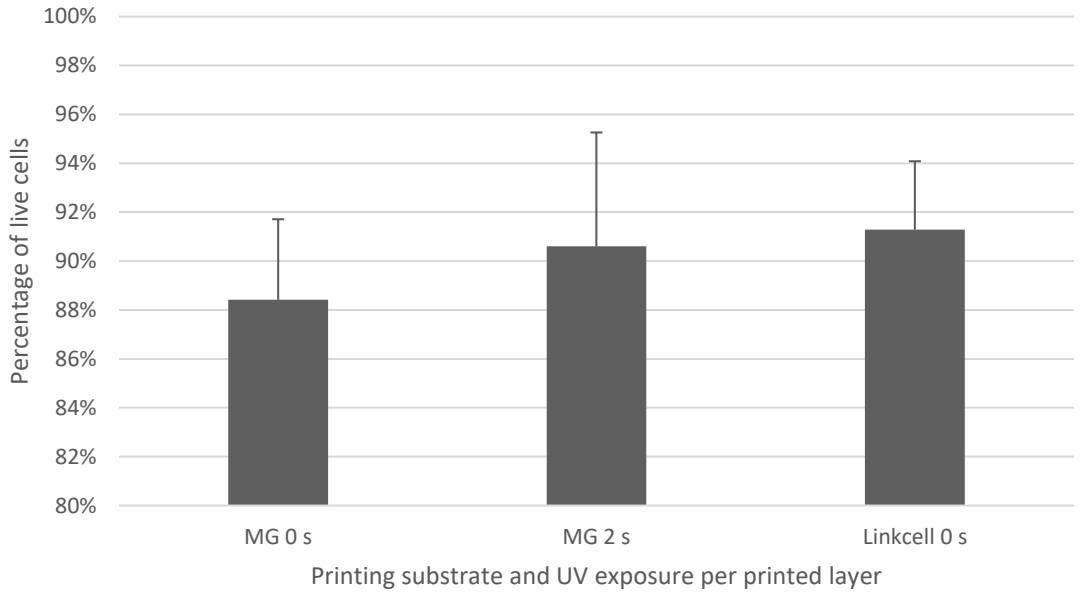

Figure 36. The cell viability of fresh hiPSC-LESCs after extrusion-based bioprinting on Day 1. Three different conditions were used: Matrigel™ (MG) coating with 0 s and 2 s UV exposure and LinkCell™ membranes with 0 s UV exposure. Cell line 001b B2 HT was used with the cell density of 8.8 million cells/ml in the bioink. The amount of live and dead cells was analyzed with ImageJ ($n_{condition}$ = 6 or 7).

times higher on the Matrigel™ samples ($p \leq 0.05$, Figure 37 A). At the later timepoints, the difference was slightly smaller, however, still significant. With the hiPSC-LESCs, the differences between Matrigel™ and LinkCell™ samples were not as considerable (Figure 37 B), suggesting there was not as high preference of the printing substrate.

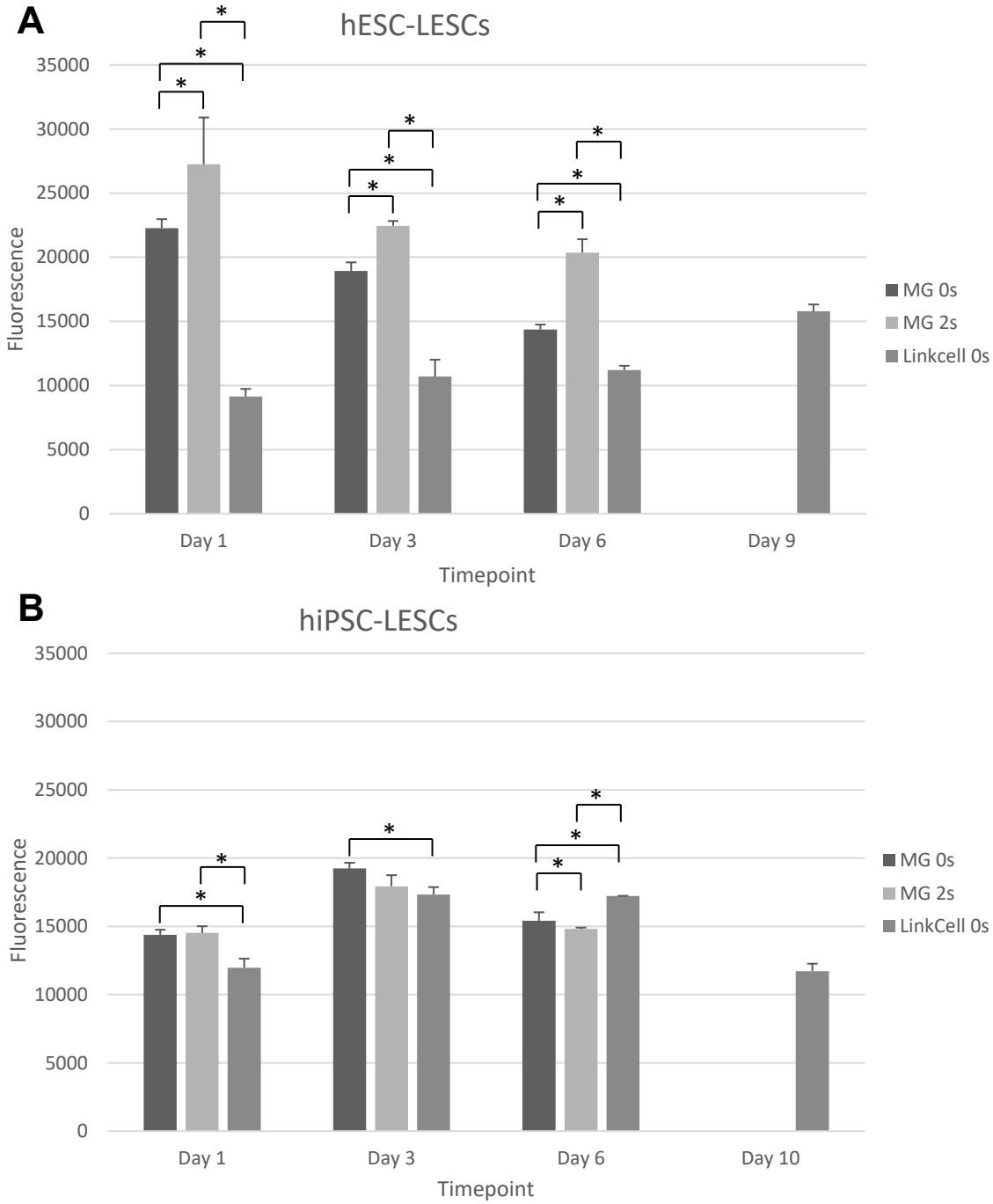

Figure 37. PrestoBlue data from the bioprinted fresh hPSC-LESCs from two cell lines with three different conditions ($n_{condition} = 3$, $p \leq 0.05$): printing on Matrigel without UV exposure (MG 0s), printing on Matrigel with 2 s UV exposure (MG 2s) and printing on LinkCell membrane without UV exposure (LinkCell 0s). **(A)** Cell line 08/017, cell density 9 million/ml. **(B)** Cell line 001b B2 HT, cell density 8.8 million/ml.

The proliferation of the samples bioprinted on Matrigel™ was generally higher with the hESC-LESCs, however, the proliferation of the hESC-LESCs decreased during timepoints with both UV exposure times (Figure 37 A). On the contrary, the proliferation of the hiPSC-LESCs bioprinted on Matrigel™ increased until Day 6 with both UV exposure times (Figure 37 B). When comparing the samples bioprinted on Matrigel™ with 0 s UV exposure, there was no significant difference in the proliferation of the two cell lines on Day 6. However, with 2 s UV, the proliferation was higher with the hESC-LESCs. Moreover, the 2 s UV resulted the highest proliferation of the hESC-LESCs on Day 1, 3 and 6. This did not occur with the hiPSC-LESCs, where the differences between printing conditions were generally smaller in all timepoints.

Overall, the proliferation on the LinkCell™ increased during timepoints with both cell lines, even though the proliferation and its increase was lower with the hESC-LESCs until the last timepoint. When comparing the proliferation of the samples bioprinted on LinkCell™, the value is higher with the hiPSC-line on Days 1, 3 and 6. In addition, whereas the difference between the cell lines is decreased on Day 6 when bioprinting on Matrigel with 0 s UV, the difference is increased in the case of the LinkCell™ samples. With the hiPSC-LESCs, the proliferation of the LinkCell™ sample on Day 6 is even higher than the proliferation of either of the Matrigel™ samples at the same timepoint, however, the difference is small. Though the hiPSC-LESCs showed higher proliferation at the earlier timepoints, the situation is the opposite at the last timepoint. There, the proliferation of the hESC-LESCs is higher, even though the timepoint of the analysis was one day earlier than with the hiPSC-LESCs. Moreover, there was no change between Days 3 and 6, when observing the proliferation of hESC-LESCs or hiPSC-LESCs.

The cell proliferation, maturation and differentiation were studied with immunofluorescence staining. Fresh hPSC-LESCs were 3D bioprinted on Matrigel™ or on LinkCell™ collagen membrane as described previously, and depending on the printing substrate and cell line, samples at Days 3 and 6, or Day 10 were studied in immunofluorescence. The results of the two cell lines used are presented seperately, where Figures 38, 40 and 42 show the results of hESC-LESCs and Figures 39, 41 and 43 show the results of hiPSC-LESCs. The results of the immunofluorescence control at Day 6 are shown in Figure 44, and the expression of the bioprinted samples is compared to the control.

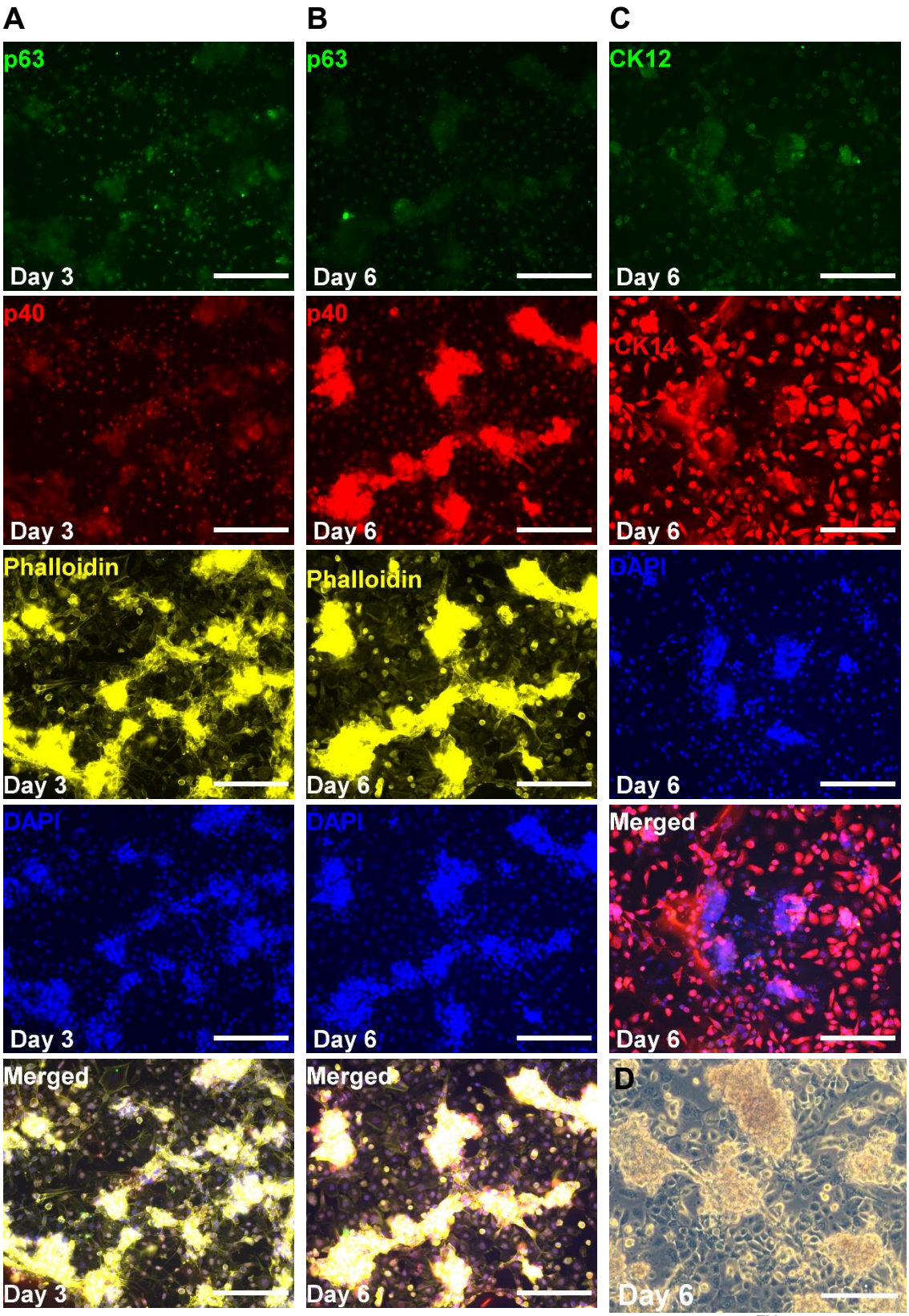

Figure 38. hESC-LESCs (9 million cells/ml) 3D bioprinted on Matrigel™ without UV exposure. **(A-B)** Immunofluorescence staining of corneal progenitor markers p63 (green) and p40 (red) and phalloidin (yellow) illustrating the cell morphology on Day 3 and Day 6 after printing. **(C)** Immunofluorescence staining of CK12 (green) and CK14 (red) illustrating the cell maturation on Day 6 after printing. **(D)** Phase contrast image of printed hPSC-LESCs on Day 6 after printing. **(A-C)** Nuclei stain DAPI (blue). Scale bars 200 µm.

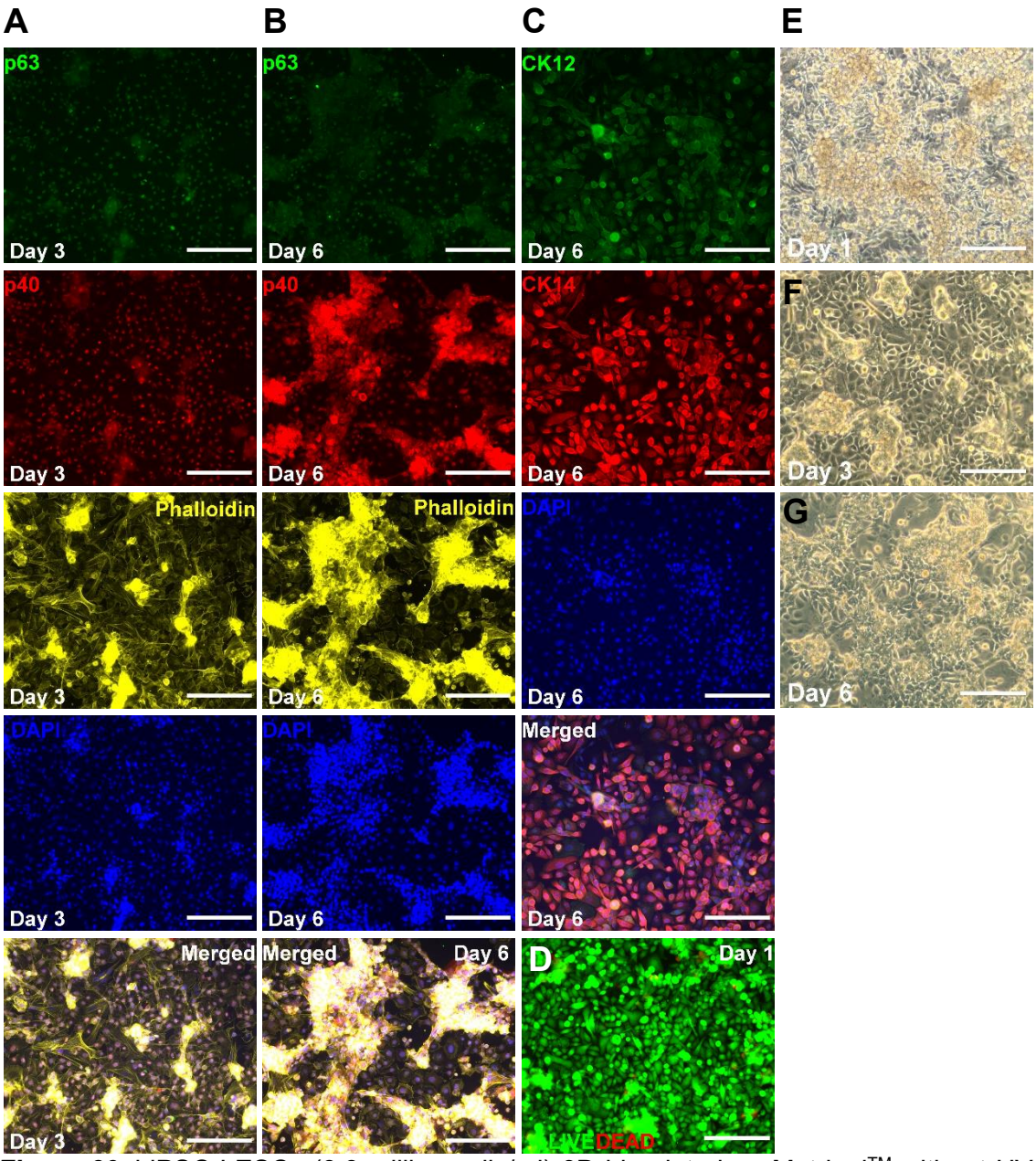

Figure 39. hiPSC-LESCs (8.8 million cells/ml) 3D bioprinted on Matrigel™ without UV exposure. **(A-B)** Immunofluorescence staining of corneal progenitor markers p63 (green) and p40 (red), and phalloidin (yellow) illustrating the cell morphology on Days 3 and 6 after printing. **(C)** Immunofluorescence staining of CK12 (green) and CK14 (red) illustrating the cell maturation on Day 6 after printing. **(D)** Cell viability on Day 1 after printing shown with LIVE/DEAD staining visualizing live cells with green and dead cells with red. **(E-G)** Phase contrast images of printed hPSC-LESCs on Day 1, 3 and 6 after printing. **(A-C)** Nuclei stain DAPI (blue). Scale bars 200 µm.

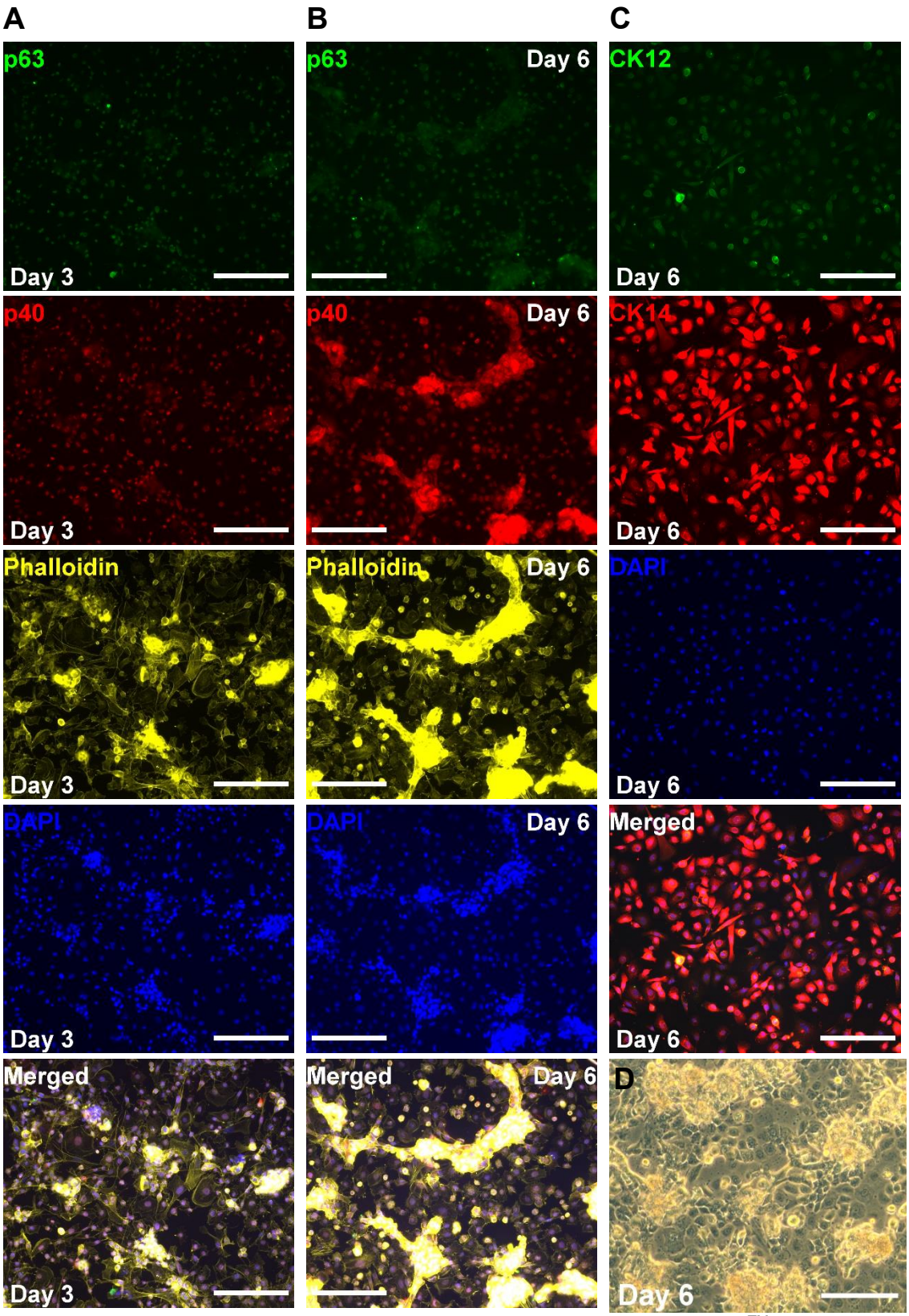

Figure 40. hESC-LESCs (9 million cells/ml) 3D bioprinted on Matrigel™ with 2 s UV exposure time. **(A-B)** corneal progenitor markers p63 (green) and p40 (red), and phalloidin (yellow) illustrating the cell morphology on Days 3 and 6 after printing. **(C)** Immunofluorescence staining of CK12 (green) and CK14 (red) illustrating the cell maturation on Day 6 after printing. **(D)** Phase contrast image of printed hPSC-LESCs on Day 6 after printing. **(A-C)** Nuclei stain DAPI (blue). Scale bars 200 µm.

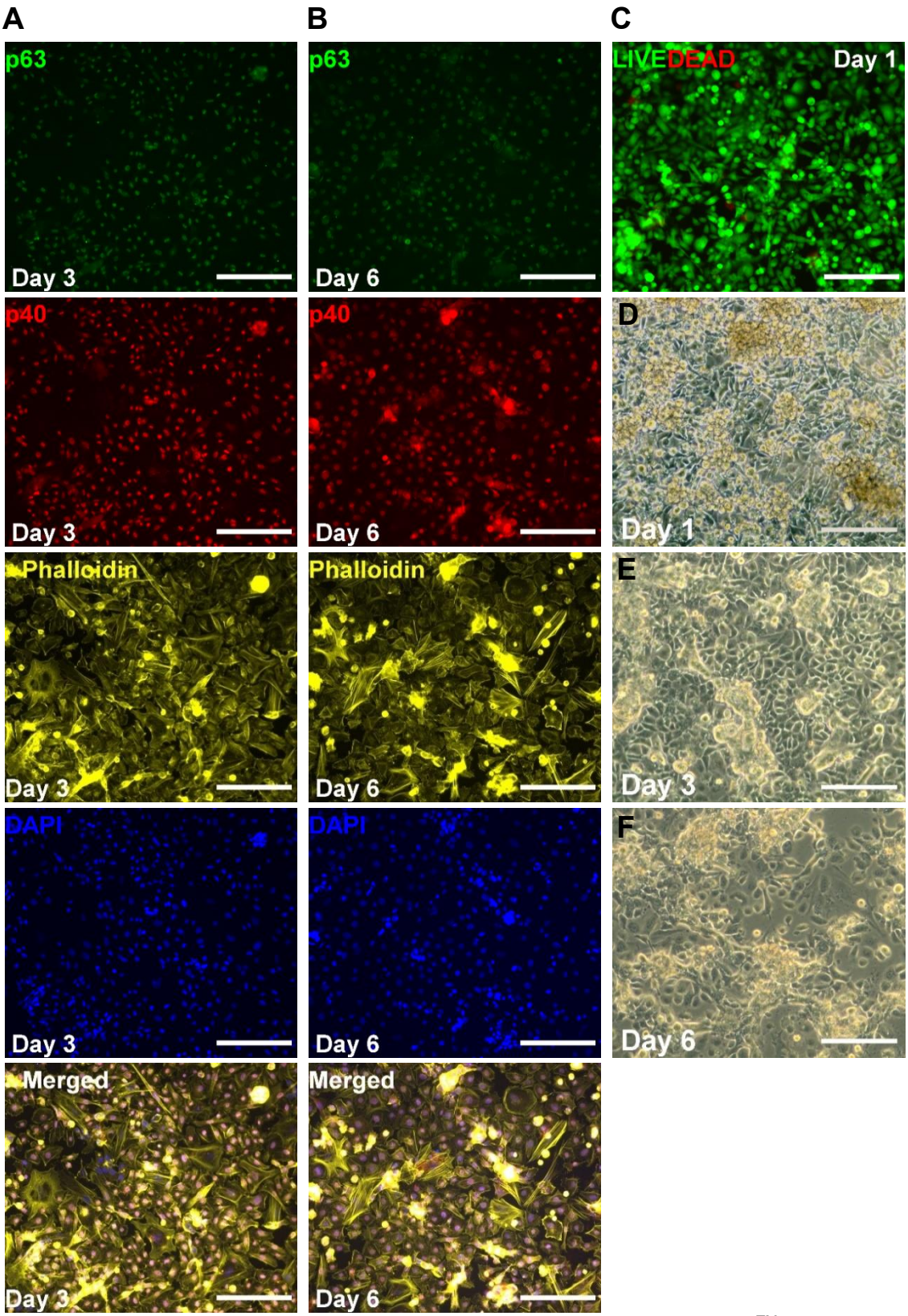

Figure 41. hiPSC-LESCs (8.8 million cells/ml) 3D bioprinted on Matrigel™ with 2 s UV exposure time. **(A-B)** corneal progenitor markers p63 (green) and p40 (red), and phalloidin (yellow) illustrating the cell morphology on Days 3 and 6 after printing. **(C)** Cell viability on Day 1 after printing. Live cells are shown in green and dead cells in red. **(D-F)** Phase contrast images of printed hPSC-LESCs on Day 1, 3 and 6 after printing. **(A-B)** Nuclei stain DAPI (blue). Scale bars 200 µm.

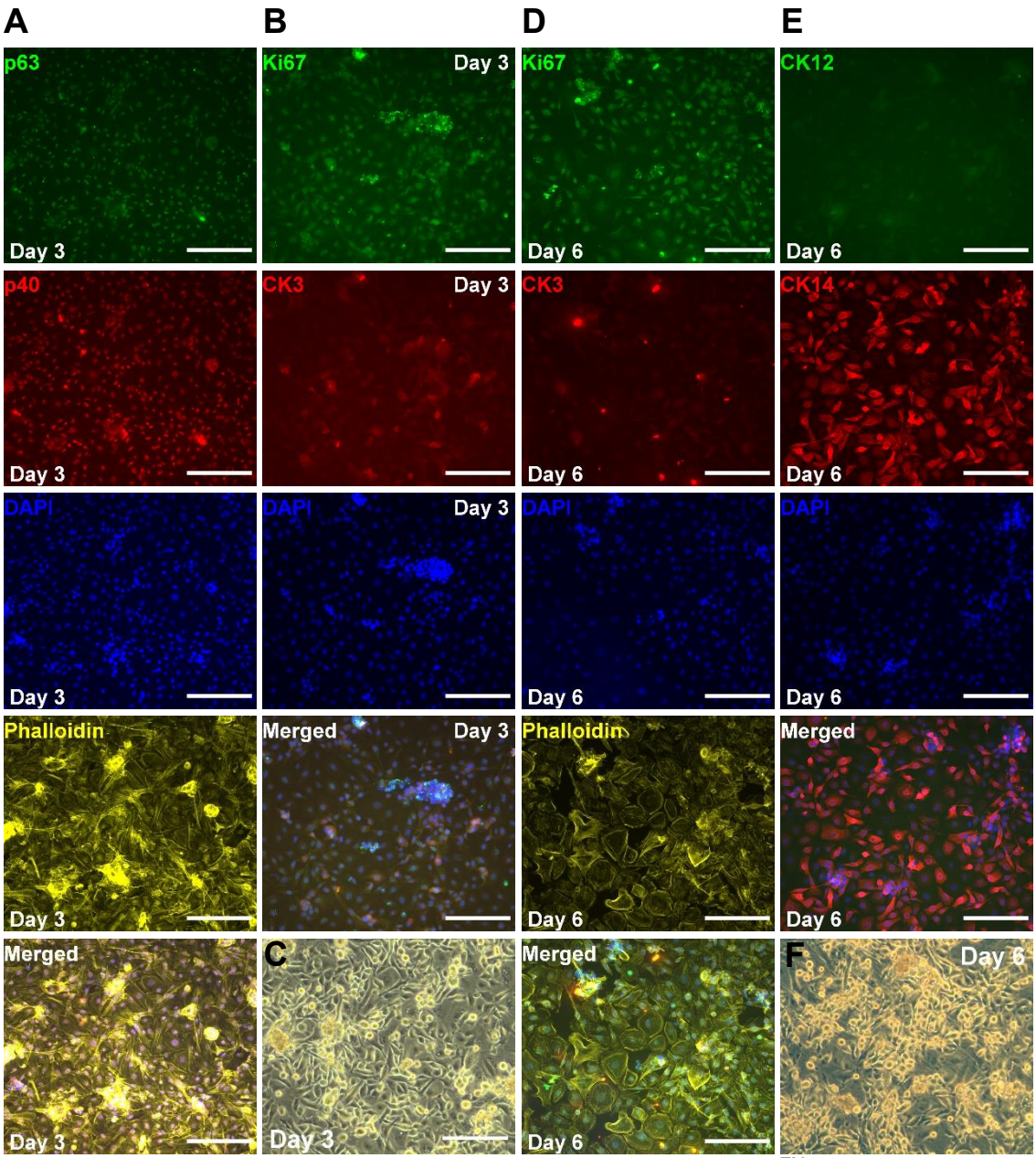

Figure 42. hESC-LESCs (9 million cells/ml) bioprinted on LinkCell™ membrane without UV exposure. **(A)** Corneal progenitor markers p63 (green) and p40 (red), and morphology with phalloidin (yellow) on Day 3 after printing. **(B)** Proliferation with Ki67 (green) and maturation with CK3 (red) on Day 3 after printing. **(C)** Phase contrast image of printed hLESCs on Day 3 after printing. **(D)** Proliferation with Ki67 (green), maturation with CK3 (red) and morphology with phalloidin (yellow) on Day 6 after printing. **(E)** Maturation with CK12 (green) and CK14 (red) on Day 6 after printing. **(F)** Phase contrast image on Day 6. **(A-B, D-E)** Nuclei stain DAPI (blue). Scale bars 200 μm.

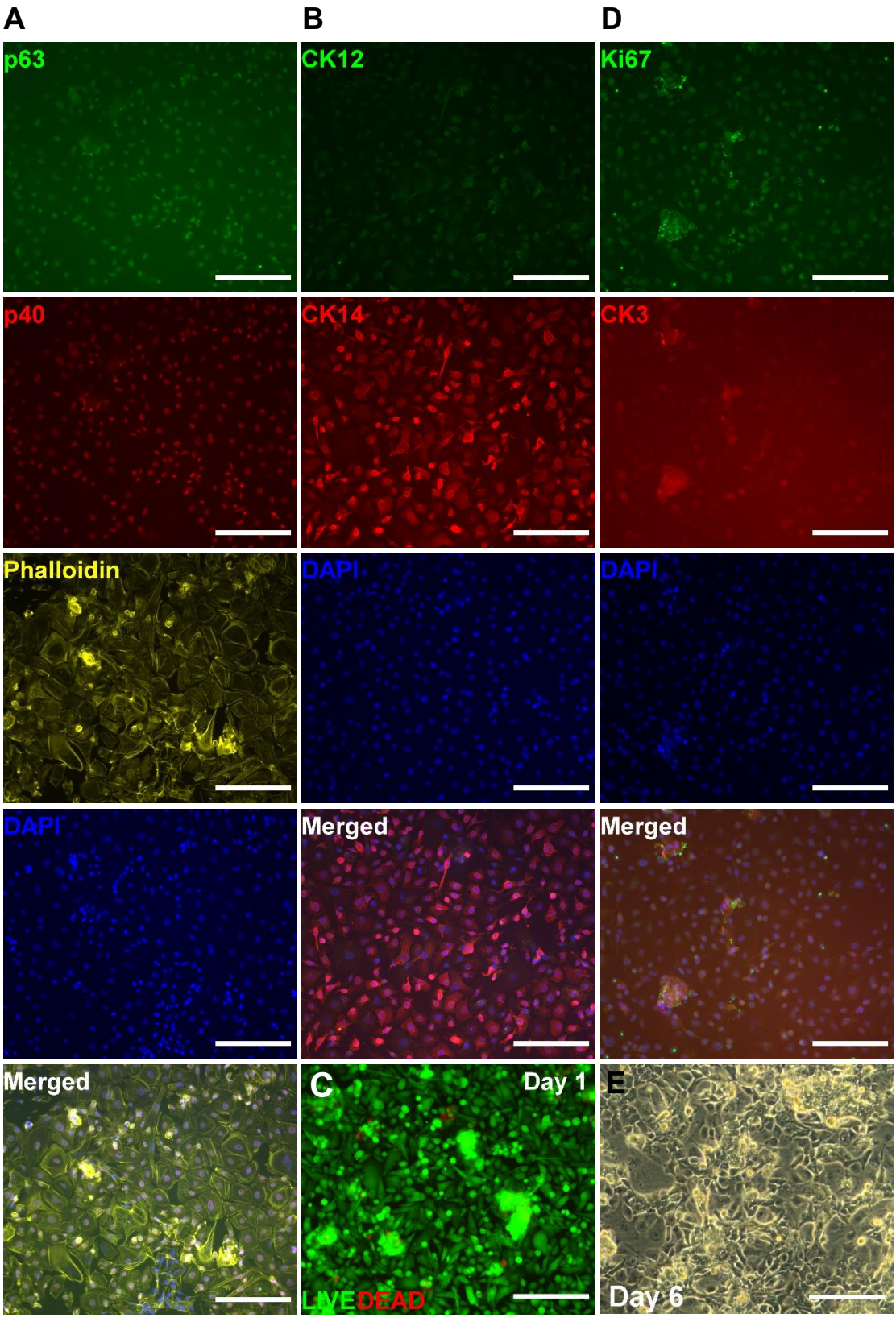

Figure 43. Maturation of hiPSC-LESCs (8.8 million cells/ml) on Day 10 after bioprinting on LinkCellTM membrane without UV exposure. **(A)** Corneal progenitor markers p63 (green) and p40 (red), morphology with phalloidin (yellow). **(B)** Maturation with CK12 (green) and CK14 (red). **(C)** Viability of printed hLESCs on Day 1. Live cells in green, dead cells in red. **(D)** Proliferation with Ki67 (green) and maturation with CK3 (red). **(E)** Phase contrast image on Day 6. **(A-B, D)** Nuclei stain DAPI (blue). Scale bars 200 µm.

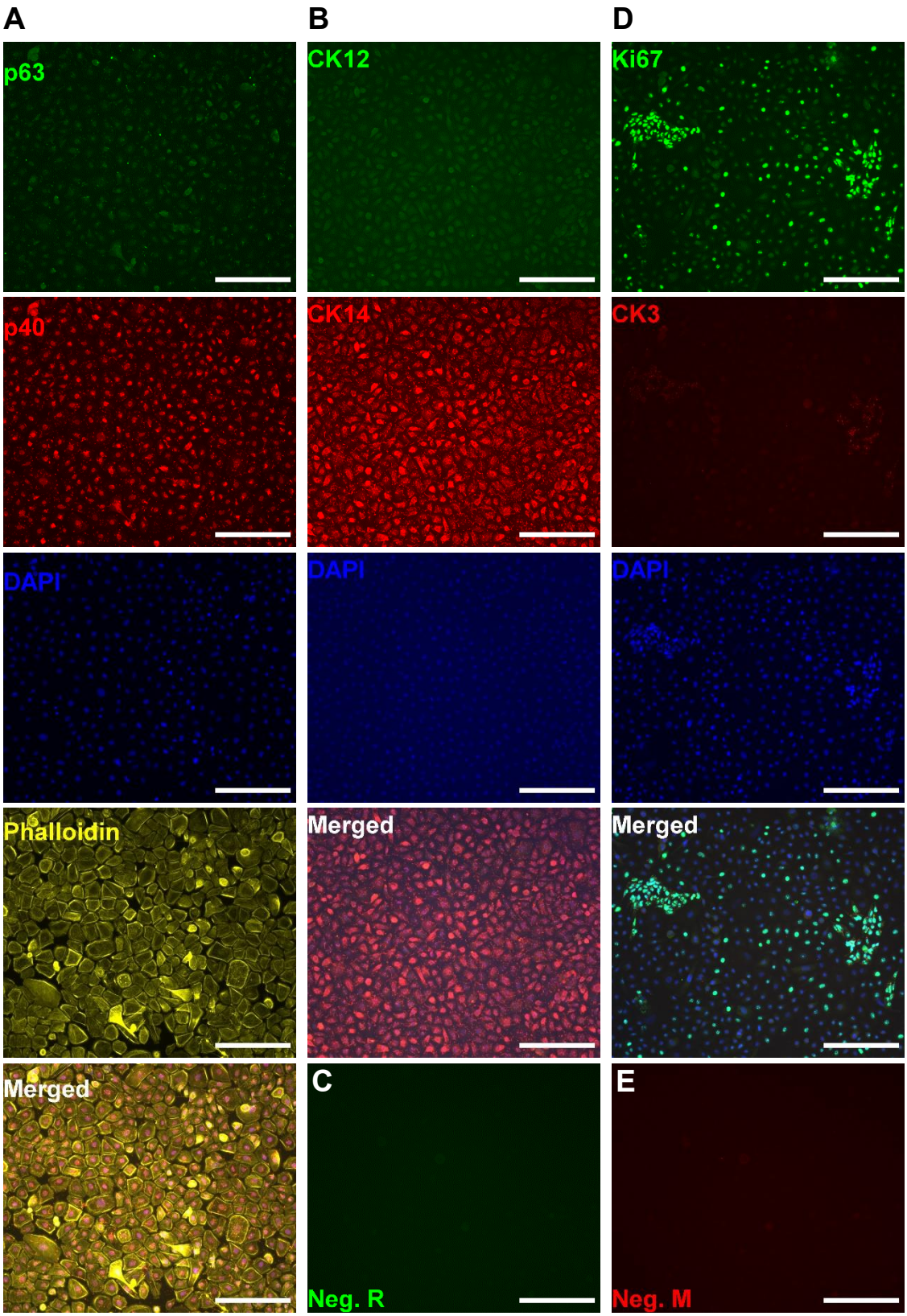

Figure 44. Immunofluorescence control of hPSC-LESCs at Day 6. **(A)** Corneal progenitor markers p63 (green) and p40 (red), morphology with phalloidin (yellow). **(B)** Matruation with CK12 (green) and CK14 (red). **(C)** Negative for primary antibodies originated from rabbit (p63, CK12, Ki67). **(D)** Proliferation with Ki67 (green) and maturation with CK3 (red). **(E)** Negative for primary antibodies derived from mouse (p40, CK14, CK3). **(A-B, D)** Nuclei stain DAPI (blue). Scale bars 200 µm.

Both cell lines express the corneal progenitor markers p63 and p40 in all the printing conditions (Figure 38 A-B, Figure 39 A-B, Figure 40 A-B, Figure 41 A-B, Figure 42 A and Figure 43 A). The increase in the expression of p40 between Day 3 and 6 can be seen in the samples bioprinted on Matrigel™ without UV expression (Figure 38-39) or with 2 s UV expression (Figure 40-41), and even after 10 days, the bioprinted hPSC-LESCs express p63 and p40 (Figure 43).

At Day 6, the bioprinted hPSC-LESCs show maturation towards corneal epithelial cells in all the printing conditions (Figure 38 C, Figure 39 C, Figure 40 C and Figure 42 E), however, the expression of the maturation markers CK12 and CK14 is not as strong on the LinkCell™ samples. Compared to the LinkCell™ sample at Day 6 (Figure 42 E), the expression of CK12 and CK14 has not changed at Day 10 (Figure 43 B). Moreover, the cells express the maturation marker CK3 (Figure 42 B, D and Figure 43 D) more strongly than the control (Figure 44 D), indicating maturation of the bioprinted cells towards mature corneal epithelium.

The hPSC-LESCs bioprinted on LinkCell™ express the proliferation marker Ki67, however, compared to the control (Figure 44 D), the the expression is not as strong. For maturing tissue, the decrease in proliferation is typical. There is no visible change in the expression of Ki67 between Day 3, 6 and 10 (Figure 42 B, D and Figure 43 D). However, the images at Days 3 and 6 are from hESC-LESCs and the Day 10 from hiPSC-LESCs. The proliferation data from PrestoBlue analyses support this observation, since the fluorescence values are similar between hESC-LESCs at Days 3 and 6 and hiPSC-LESCs at Day 10.

The bioprinted hPSC-LESCs showed epithelial cell morphology in all conditions (Figure 38 D, Figure 39 E-G, Figure 40 D, Figure 41 D-F, Figure 42 C, F and Figure 43 E). When examining the cell morphology illustrated with phalloidin, their nuclei stained with DAPI or the phase contrast microscope images, both investigated cell lines show areas of stratified epithelium on Matrigel™ without UV exposure (Figure 38-39). In addition, the cells proliferate and stratify more between the Day 3 and Day 6 (Figure 38 A-B and Figure 39 A-B). The hPSC-LESCs bioprinted on Matrigel™ with 2 s UV exposure have also stratified areas, however, they are not as large in size or in numbers. The same bioprinting condition with hiPSC-LESCs shows significantly less stratified areas, and both cell lines on LinkCell™ do not show any stratification.

7. DISCUSSION

Severe LSCD can lead to blindness, which is traditionally treated with corneal transplantation. However, there are not enough corneal transplants for every patient who needs one. Moreover, corneal transplantation is unsuitable treatment for LSCD due to lack of functional LESCs. Thus, there is a severe need for artificial corneas. 3D bioprinting provides a strategy to fabricate precise, pre-designed structures with different combinations of cell types and materials. Therefore, it offers a possible solution to fabricate patient-specific, artifical corneas with functional LESCs. Currently, the development of biocompatible and printable cell-laden bioinks is the main challenge in the field of 3D bioprinting. In this thesis, the aim was to design a novel bioink and optimize the printing conditions for extrusion-based 3D bioprinting of stratified corneal epithelial tissue by using hPSC-LESCs.

7.1 Printability of the bioink

Printability is one of the most important characteristics for a bioink (Morgan, Moroni and Baker, 2020). In this thesis, printability was studied by printing the filament structure without cells on a non-coated substrate. Printing speed and pressure are known to affect the printability (Van Hoorick *et al.*, 2019), which was demonstrated in this thesis by printing the filament with either increasing the speed or pressure. The filament thickness decreases when the printing speed is increased (Zhu *et al.*, 2017), and in this thesis, it was determined by analyzing the filament structure and thickness at different printing speeds. The change in the filament structure was clear, and more smooth filament was extruded with higher speed. However, the extruded filament and the substrate could not make a contact at the beginning of the filament print with higher speed. This resulted inaccurate starting point of the filament print and incorrect printing result. Therefore, lower speed was used for bioprinting the cell-laden 3D stuctures. Another option to decrease the lag of the starting point would be to increase preflow to begin the filament extrusion before the nozzle starts to move.

Higher pressure is needed if the bioink is highly viscous or the nozzle diameter is small (Kyle *et al.*, 2017). Since the 3D-Bioplotter uses pneumatic pressure as the force to extrude the bioink, the increase in pressure was expected to increase the flow rate of the bioink. As a consequence, by increasing the printing pressure, the filament thickness increased, merging the separate filaments together. An increase in the flow rate

increases the shear stress, and thus is damaging for the cells (Cui *et al.*, 2020). Therefore, the lowest pressure possible was desired, however, it was noticed that with too low pressure (0.2 bar), the filament did not extrude at all. When adding the cells, the viscosity of the bioink increased, and subsequently, higher pressure was required. Since it was not desired to increase the pressure considerably, the printing pressure was optimized to the lowest possible pressure for the extrusion of the cell-laden bioink (0.6 bar). Overall, since the bioink extruded well even with lower pressures, the viscosity of the bioink during extrusion was not high, which is know to be less damaging for the cells (Chimene, Kaunas and Gaharwar, 2020). Moreover, the low viscosity decreases the risk of nozzle clogging (Cui *et al.*, 2020), which is one of the challenges in extrusion based bioprinting. Low viscosity can decrease the shape fidelity of the bioprinted filament and to cause the structure to collapse (Cui *et al.*, 2020), however, this was not observed in this thesis. With sufficient printing parameters, the filament structure was clear and did not collapse after printing.

The temperature-sensitivity of the bioink can affect the printability (Gu *et al.*, 2018), and thus it was studied in this thesis by printing the bioink without cells on the platform, which temperature was either 8 °C or 23 °C (room temperature). The printing on a cooled platform was expected to enhance the shape fidelity of the bioink. The distance between strands in the filament structure did not depend on the platform temperature (average of 1.47 mm with both temperatures) and was close to the set strand width (1.5 mm). However, the filament thickness was higher when printing on the room temperature platfrom (0.72 mm) compared to the thickness of the print on the cooled platform (0.62 mm). Therefore, the bioink used in this thesis is temperature-sensitive, spreads due to decreased viscosity in higher temperatures, and thus requires cooled printing platform.

7.2 Optimization of the bioprinting conditions

In addition to printability, bioink requirements include supporting cell migration as well as tissue maturation and remodeling (Morgan, Moroni and Baker, 2020). The relevant mechanical properties of the bioink depend on the bioprinted cells, since they prefer different environments. Moreover, the mechanical stimuli provided by the bioink guides the proliferation and differentiation of the cells. (Williams *et al.*, 2018) This needs careful consideration when designing bioinks and the crosslinking strategies. The substrate stiffness have been showed to affect the migration, proliferation and phenotype of LESCs (Gouveia, Vajda, *et al.*, 2019). Softer substrate promotes the expression of limbal markers (Gouveia, Vajda, *et al.*, 2019), and hence the optimization of the bioink stiffness was the most fundamental step in optimizing the bioprinting conditions for hPSC-LESCs.

In this thesis, two main crosslinking strategies were used, photocrosslinking and thiolation. In photocrosslinking, several parameters affect the crosslinking density, such as photoinitiator concentration, the wavelength and intensity of light and light exposure time (Lim *et al.*, 2020), of which the latter was optimized in this thesis. UV is a common light source for photocrosslinking and the typically used wavelength is 365 nm (Lim *et al.*, 2020), which was also used in this thesis. Since UV irradiation can damage the cells (Dahle, Kvam and Stokke, 2005), it was essential to study the viability of the bioprinted hPSC-LESCs after UV exposure. Several different UV exposure times have been studied in 3D bioprinting photocurable bioinks (Lim *et al.*, 2020), and in this thesis, four different exposure times (0, 2, 5 and 15 s per layer) were chosen to examine the effect of the UV exposure time on the bioprinted cells. Due to bioprinting two layers and exposing each layer to UV after printing, the exposure for the bottom layer was increased by double. The cell viability studied with LIVE/DEAD staining at Day 1 did not show any significant differences in the viability between different UV exposure times. Even with the highest UV exposure (15 s per layer), the average viability was 91%, and thus the UV did not seem to damage the cells.

When the UV exposure time increases, the crosslinking density and therefore the stiffness of the hydrogel increases (Chimene, Kaunas and Gaharwar, 2020). The response of the hPSC-LESCs to the UV exposure and the crosslinking density was analyzed by imaging the bioprinted cells with a phase contrast microscope after 1 and 3 hours, and at Day 1 after printing. Already the increase in the UV exposure time to 5 s per layer had a visible effect on the hPSC-LESCs, as they remained circular and could not migrate in the printed structure. The increase of the UV exposure time to 15 s had similar effect. After 1 hour, the bioprinted filaments were visible in the 5 s and 15 s samples. After 3 hours, the filaments were still visible in the 15 s structure, however, they were not as visible in the 5 s structure. The cell morphology in both of the samples with higher exposure times was round-shape, which indicates that they cannot migrate well, and therefore UV exposures of 5 s or higher were not optimal for bioprinting corneal epithelium micking structures.

In addition to the visibility of the bioprinted filaments, the bioprinted structure detached from the substrate at Day 1 in both 5 s and 15 s samples, potentially indicating poor interaction with the crosslinked printed structure and the culture substrate. Some of the cells had been able to migrate and attach to the bottom of the culture dish and showed typical epithelial morphology in a monolayer with high viability. However, most of the cells had remained in the detached structure, where they stayed round-shaped and did not interact with each other. Hence, the hPSC-LESCs seemed to be sensitive to subtle

changes in the material stiffness caused by the UV exposure time, and therefore, the two lowest UV exposure times were used for the rest of the experiments in order to achieve an extremely soft, liquid-like material. This type of material was intended to provide short-term support for the bioprinted cells and enable them to form stratified epithelial tissue. By selecting another cell type with the preference for more rigid environments, longer UV exposure times could be used with this bioink to result in stiffer and more solid gel. In addition, UV exposure could be utilized in designing experimental environments for the cells to analyze how they behave in non-native environments. As the ECM stiffness is important for maintaining tissue homeostasis, abnormalities in the mechanical properties of the tissue can lead to different diseases (Handorf *et al.*, 2015). Thus, higher UV exposure could be used to bioprint stuctures that mimic the diseased environment and utilized in disease modeling. Moreover, the developed bioink with UV crosslinking could be potentially used for bioprinting stromal structures, where a stiffer environment is needed.

Since the UV exposure was observed to affect the crosslinking density considerably and resulting in unsuitable environment for hPSC-LESCs, other crosslinking strategies were considered. For better optimization and customization of the bioink properties, a combinations of different crosslinking strategies have been used previously (Petta *et al.*, 2018; Kajave *et al.*, 2020; Shin *et al.*, 2020; Soliman *et al.*, 2020). Thiolation is one option to make a hydrogel crosslinkable, and for example, thiol-ene photocrosslinking or Michael-type addition can be used as a crosslinking strategies for materials containing thiolated groups and ‘ene’s (Van Hoorick et al., 2019). In this thesis, the combination of the thiolated component X and methacrylated component Y was used for fine adjustment of the bioink stiffness. Subsequently, the addition of the thiolated component X seemed to provide the desired amount of increase in stiffness and resulted in soft, liquid-like material with enough viscosity to hold its shape after the extrusion even without UV exposure. To determine the actual crosslinking mechanism requires further research, however, the mechanisms could include the photocrosslinking between methacrylated groups and the thiol-ene photocrosslinking between the thiolated and methacrylated groups. Even though UV exposure was used to increase the crosslinking degree, the bioprinted structure was exposed to visible light after extrusion, which is likely to cause some crosslinking even without the UV exposure. Moreover, the concentration of the thiolated groups determined by Ellman’s reaction was low, which resulted in low crosslinking degree between thiolated and methacrylated groups. The crosslinking degree achieved in this thesis is not adequate by itself for bioprinting stabile 3D structures for long-term *in vitro* culture. Therefore, the role of the thiolated component X

in the crosslinking density of the bioink requires further research to obtain more stabile structure.

In addition to the UV exposure and the stiffness of the bioink, the printing substrate was optimized in this thesis. Matrigel™ has been shown to be applicable in 3D bioprinting of hPSC-LESCs, however, shrinkage of the Matrigel™ has been reported (Sorkio *et al.*, 2018). In this thesis, the shrinkage began to occur already at Day 1 after printing, however, there was a significant difference between fresh hPSC-LESCs and hPSC-LESCs from frozen-stock. Even though the shrinkage of the substrate and clustering of the cells occurred with both, the hPSC-LESCs from frozen-stock detached completely after clustering. The fresh hPSC-LESCs stayed attached in spite of the shrinkage and clustering, however, the end point analysis could not be done at late timepoints. Subsequently, at Day 6, the bioprinted hPSC-LESCs were not yet too clustered and the analyses were possible.

Different substrate options for Matrigel™ were studied, and the Matrigel™ coated PET membrane and LinkCell™ collagen membrane showed the most promising results. Porous PET membrane have been previously used in bioprinting of hPSC-LESCs (Sorkio *et al.*, 2018), and in this thesis, the PET membrane was nonporous. The cell adhesion and proliferation were not as good as with the Matrigel™ substrate. Since the PET membrane had Matrigel™ coating, the inferior performance of the PET membrane can be due to the nonporosity. Moreover, Sorkio et al. used a cell density of three times higher (30 million cells/ml), which increases the cells ability to form stratified tissue. Bioprinting on PET would have required more optimization of with the coating, and due to schedule limitations, it was discarded as a substrate option. Instead, LinkCell™ membrane was studied, since it has been used in hPSC-LESC culture (Mikhailova *et al.*, 2016). Their performance was better than the nonporous PET membranes, however, it was still not as good as with the Matrigel™ substrate. The reason for studying alternative substrates to maintain more stable substrate and avoid the shrinkage of Matrigel™, and LinkCell™ successfully provided considerabely more stable substrate than Matrigel™. However, the stratification of the bioprinted hPSC-LESCs was poor, and thus the Matrigel™ had the best performance of the studied alternatives. In the future, it would be beneficial to study more substrate and coating options to avoid the shrinkage of the substrate, provide more stable substrate and enhance the cell adhesion. Moreover, Matrigel™ is not optimal material for clinical applications since it is animal-derived.

Even though the extremely soft material with low crosslinking degree was beneficial for the bioprinted hPSC-LESCs, the culturing of the bioprinted structure developed another problem. The soft, liquid-like material could not attach to the substrate without cells since

it was washed away when the medium was added. The cells were capable of preventing the structure from washing away, however, the bioprinted hPSC-LESCs required time for migration and adhesion. Thus, the medium was not added on top of the bioprinted structure immediately after printing. Instead, the medium was added around the edges of the culture dish, and after 3 h, the structure was immersed in medium. This provided the cells sufficient time to migrate in the structure and adhere to the printing substrate. Moreover, the late immersion in medium did not seem to decrease the cell viability, since it was around 90% with all the selected bioprinting conditions. Subsequently, the bioink itself provided a sufficient environment for the hPSC-LESCs for the first 3 h after bioprinting to promote the formation of stratified corneal epithelium micking structure.

7.3 Bioink characterization

There are multiple different characterization methods for bioinks (O'Connell *et al.*, 2020), and previously, the bioink characterization in 3D bioprinting of ocular tissues has been done for example by analysing the water content (Kilic Bektas and Hasirci, 2020; Mahdavi, Abdekhodaie, Kumar, *et al.*, 2020) and the transparency of the material (H. Kim *et al.*, 2019; Kilic Bektas and Hasirci, 2020; Kutlehria *et al.*, 2020; Mahdavi, Abdekhodaie, Kumar, *et al.*, 2020), and with rheological measurements (Duarte Campos *et al.*, 2019; H. Kim *et al.*, 2019; Kutlehria *et al.*, 2020). These methods were selected in this thesis for bioink characterization after optimizing it for bioprinting hPSC-LESCs.

Hydrogels are highly hydrophilic, consist mainly of water and have the ability to swell (Chimene, Kaunas and Gaharwar, 2020). The swelling of the hydrogel bioink in this thesis was studied by immersing the 3D structure without cells in PBS and weighing it after 1, 3 and 24 hours without PBS. The weight of the material was expected to increase during timepoints due to the water absorption of the hydrogel. Four different UV exposure times were used (0, 2, 15 and 30 s per layer). However, the two lowest UV exposure times resulted in so soft and liquid-like structure that it washed away during the first weighing measurements, indicating low-degree crosslinking and poor stability in aqueous environment. Thus, only the results from the two highest UV exposure times were obtained from the later timepoints. After 1 hour, there was almost no change in weight compared to the intial weight. After 3 and 24 hours the weight was higher than the previous timepoint, as was expected.

Since the UV exposure increases the crosslinking density of the photocurable bioink, resulting in stiffer structure (Chimene, Kaunas and Gaharwar, 2020), the water absorption was expected to decrease with higher UV exposure. Moreover, the water absorption and swelling were expected to increase faster with lower crosslinking degree

due to lower crosslinking density. However, there was no significant difference in the relative water absorption between 15 and 30 s UV. In addition, the water absorption after 3 h was higher for the 30 s sample. This might be due to the fact that even the 30 s UV exposure per printed layer is relatively short time, even though the lower layer experiences 60 s UV altogether. Therefore, by increasing the photoinitiator concentration or the UV exposure up to minutes, the differencies in crosslinking density, stiffness and water absorption might be more distinguishable.

Corneal tissue is transparent (DelMonte and Kim, 2011), and transparency is one of the most important characteristic of corneal scaffolds (Ahearne *et al.*, 2020). In this thesis, the transparency of the bioink was analyzed visually and by measuring the transmittance with the UV/VIS spectrophotometer. The 3D bioprinted structure was visually transparent and did not show any hues, which has been a challenge in 3D bioprinting ocular tissues (B. Zhang, Xue, Hu, *et al.*, 2019; Duarte Campos *et al.*, 2019). Transmittance of the bioinks studied for corneal regeneration has been previously reported to be over 75% (H. Kim *et al.*, 2019), 60 – 90% (Kutlehria *et al.*, 2020; Mahdavi, Abdekhodaie, Kumar, *et al.*, 2020) and 70 – 90% (Kilic Bektas and Hasirci, 2020). The transparency of the bioink used in this thesis was 65 – 75%, which is close to the previously reported values, however, lower than the transmittance of native cornea (Beems and Van Best, 1990). In addition, the transmittance has increased at higher wavelengths (H. Kim *et al.*, 2019; Kilic Bektas and Hasirci, 2020; Kutlehria *et al.*, 2020; Mahdavi, Abdekhodaie, Kumar, *et al.*, 2020), which occurred during the transmittance measurements in this thesis. The transmittance of the bioink containing the thiolated component X was lower at wavelengths 380 – 450 nm, when compared to the nonthiolated bioink. Since the wavelength of visible light is 400 – 700 nm, this might be an issue when the bioink is used in clinical treatments. However, the difference was only 5%, and thus, the influence of the lower transparency would require in vivo studies.

To further study the microstructure of the bioink without UV exposure, rheological measurements including amplitude and frequency sweeps were performed. Typical hydrogel bioink is viscoelastic (Chimene, Kaunas and Gaharwar, 2020), with the viscosity resisting the flow, and the elasticity responding and recovering from stress. In rheology, the G’ represents the elastic portion and the G’’ the viscous portion (Anton Paar GmbH, 2020b). The rheological measurements done for the bioink in this thesis suggest, that the material behaves as a very weak viscoelastic liquid, because the G’ and G’’ values are close to zero. Typical G’ values for hydrogels used as cell matrices range from 100 Pa up to hundreds of KPa (Zhong *et al.*, 2020). However, lower G’ values have been reported for soft gels, such as 10 – 50 Pa for Matrigel™ with different

concentrations (Zaman *et al.*, 2006), 15 Pa for aldehyde-modified 1% HA (Lou *et al.*, 2018) and 50 Pa for alginate-ColI gels (Branco de Cunha *et al.*, 2014). The G' value of the studied bioink is not more than 15 Pa even after applying stress. Subsequently, it remains liquid-like after injecting it onto the measuring plate and does not become a solid hydrogel.

The bioink used in this thesis contains methacrylated and thiolated groups, and previously, thiolated and methacrylated components have been combined and crosslinked with Michael-type addition (Ravichandran *et al.*, 2016). Ravichandran et al. observed that the gelation time without the addition of a catalyst is slow (> 8 h), and they performed the rheological measurements after 24 h post gelation. In this thesis, the rheological measurements were done immediately after mixing the bioink, and thus, there was probably not enough time for the bioink to fully crosslink. Since the rheological measurements suggest the bioink is not a typical viscoelastic hydrogel and remains liquid-like, it would be valuable to perform the measurements again after at least 8 hours of rest. Moreover, the concentration of the thiolated groups measured with Ellman's reaction was low, which limits the crosslinking density and affects the rheological properties. Previously, the same thiolation protocol has been used with a new Traut's reagent. Then, a higher conversion of primary amines to thiol groups than the conversion for the thiolated component X used in this thesis has been reported. This suggests that the Traut's reagent used in this thesis might be ineffective, and the thiolation should be repeated with a new reagent.

The frequency sweep of the bioink suggests that the elastic properties of the material become progressively dominating as the frequency increases. This may be due to the loss of relaxation time with high frequencies (Janmey, Georges and Hvidt, 2007). Even though the bioink is liquid-like, due to an increase in the G' and G'' values after 1.5 Hz, the bioink is not a simple liquid. Subsequently, it could be considered as a heterogenic structured fluid with a liquid phase containing solid particles (TA Instruments, no date). Some parts of the bioink could be crosslinked for example due to visible light to create the solid-like particles, and the rest of the bioink remains in liquid phase. Moreover, this heterogenic microstructure of the bioink could generate the fluctuation in the beginning of amplitude sweep.

Structured fluids have complex flow behaviour, and to better understand the behaviour and rheology of the bioink used in this thesis, the rheological measurements require more repetition. In addition to letting the material set at least 8 hours before measuring in order to have higher crosslinking density, the rheological measurements should be repeated with a bioink containing the component thiolated with a new Traut's reagent.

Moreover, to obtain reproducible data, the constant sample volume and gap are required to maintain between measurements. Therefore, the sample loading requires optimization in the future. If the samples would be solid enough after a suitable curing time, this could be achieved by preparing samples in molds with the same size as the measuring geometry. In addition, even though the rheological measurements were performed only for the bioink without UV exposure due to the better stratification of the bioprinted hPSC-LESCs in that condition, the rheology of the bioink exposed to UV could be studied in the future. Nevertheless, the protocol used for the rheological measurements mimics the situation, which the bioprinted cells sense immediately after extrusion, as the bioprinting is done immediately after mixing the bioink.

7.4 Cell viability, proliferation and maturation after 3D bioprinting

The cell viability in extrusion-based bioprinting is known to be lower than in other 3D bioprinting techniques (Cui *et al.*, 2020), which is why high cell density of the bioink is important to obtain enough viable cells (Matai *et al.*, 2020). In this thesis, the cell density was higher than in several other research done in 3D bioprinting ocular tissues (Wu *et al.*, 2016; Isaacson, Swioklo and Connon, 2018; K. W. Kim *et al.*, 2018; Duarte Campos *et al.*, 2019; H. Kim *et al.*, 2019; Kutlehria *et al.*, 2020). Moreover, the cell viability after extrusion-based bioprinting of ocular tissues has been previously reported to be over 80% (B. Zhang, Xue, Hu, *et al.*, 2019) or over 90% (Wu *et al.*, 2016; Isaacson, Swioklo and Connon, 2018; Kilic Bektas and Hasirci, 2020; Kutlehria *et al.*, 2020), which correlates to the cell viability obtained in this thesis. Previously, only Wu et al. and Sorkio et al. have reported bioprinting of corneal epithelium mimicking structures. Moreover, Wu et al. have done it by extrusion-based bioprinting, as was done in this thesis as well.

Overall, the bioprinted hPSC-LESCs maintained good cell viability after extrusion-based bioprinting and showed high proliferation even with 100 µm nozzle. Wu et al. obtained over 90% cell viability of hCECs, however, the nozzle diameter is not reported. Moreover, they did not achieved any stratification of hCECs and the cell morphology remained rounded. Stratified corneal epithelial tissue has been successfully bioprinted with laser-based 3D bioprinting (Sorkio *et al.*, 2018), however, the cell density was over three times higher compared to this thesis. In addition, Sorkio et al. did not use any crosslinking strategy for the bioink, which requires high cell density. Due to high cost of producing hPSC-derived cells, it would be more optimal to need lower amount of hPSC-LESCs. To obtain stratified corneal epithelium mimicking structure with lower cell density, sufficient crosslinking degree of the bioink is required to provide support for the cell proliferation.

When further analyzing the viability and proliferation of the bioprinted hPSC-LESCs, the Matrigel™ seemed to be suitable substrate for the hPSC-LESCs, however, the culturing of the bioprinted samples could not be continued long-term due to the clustering and detaching of cells described previously. LinkCell™ membrane offered an alternative for long-term culture. In PrestoBlue, differences between the two cell lines could be observed. This might be due to the abnormal stem cell karyotype in the hiPSC-line at later passages, which was detected later during karyotyping of the cell line. In immunofluroescence analysis, there was no significant differences between the cell lines, and therefore the data was still used in this thesis. For further research, the cell line can be used only until passage 19.

The polygonal cell morphology of the bioprinted hPSC-LESCs was typical for epithelial cells, and the expression of corneal progenitor markers p63 and p40 was high. The cells bioprinted on Matrigel™ showed higher expression of maturation markers CK12 and CK14 than the cells bioprinted on LinkCell™, which contributes to the selection of Matrigel™ over LinkCell™ as a printing substrate. Stratified epithelium could be observed in Matrigel™ samples, and bioprinting without UV exposure resulted more and larger stratified areas. Sorkio et al. bioprinted stratified corneal epithelial tissue without additional crosslinking, which suggests the softness of the material achieved in this thesis was optimal for the hPSC-LESCs to form stratified epithelium. However, the softness of the Matrigel™ substrate remained a challenge as the cells were able to rip it during culture. Subsequently, the printing substrate requires further optimization to result better adhesion and suitable stiffness to maintain the stratified tissue. Moreover, with higher cell density, the cells would not have to migrate as far to interact with each other, which would support their ability to form stratified corneal epithelial tissue in the whole bioprinted structure. Yet, as was mentioned previously, production of hPSC-derived cells is costly. When developing clinical solutions for treating patients, higher production cost increases the price as well. Therefore, it would more beneficial to first optimize the printing substrate and the crosslinking degree to obtain stratified epithelium mimicking structure, without the need to produce more cells.

7.5 Future perspectives

The cornea has a curved shape, and culturing corneal epithelial cells on a curved substrate has been shown to support the adhesion, proliferation and stratification of the corneal epithelial cells (Gouveia, Koudouna, *et al.*, 2017). 3D bioprinting provides a possibility to create the curved shape, and it has been done previously in 3D bioprinting corneal tissue (Isaacson, Swioklo and Connon, 2018; Duarte Campos *et al.*, 2019;

Mahdavi, Abdekhodaie, Kumar, *et al.*, 2020). However, in this thesis the bioprinted 3D structure was flat due to the extremely soft bioink and bioprinting without any mold. To result in a curved shape of the cornea, a mold or supportive bath is needed to support the unstable material while printing. Moreover, much higher crosslinking degree is required to maintain the printed shape. Thus, a permanent supportive stroma-like structure with curvature could be a potential substrate for bioprinting corneal epithelium mimicking structures.

As a technology, 3D bioprinting enables dispensing multiple different materials and cell types into a same 3D structure (Matai *et al.*, 2020). However, different cell types require different culture conditions, which brings a challenge. Previously, hPSC-LESCs and hASCs have been bioprinted by using a laser-based 3D bioprinter to mimick the corneal epithelium and stroma, however, long-term co-culture conditions need further optimization (Sorkio *et al.*, 2018). Subsequently, the optimal co-culture conditions are required because it is essential to combine different cell types in order to 3D bioprint a full corneal mimicking structure.

8. CONCLUSIONS

The aim of this thesis was to design a novel bioink for extrusion-based 3D bioprinting of stratified corneal epithelium mimicking structures by using hPSC-LESCs. The hPSC-LESCs were observed to be very sensitive for the stiffness of the 3D environment and to prefer an extremely soft material with low crosslinking degree. In this thesis, this type of environment was fabricated by optimizing the composition of the photocurable bioink and the bioprinting conditions. The bioprinting conditions included the UV photocrosslinking degree, printing substrate and later addition of the culture medium. The soft material was intended to provide short-term support for the bioprinted cells and enable them to migrate, interact and form stratified epithelial tissue.

Typically, extrusion-based bioprinting does not have as high resolution when compared to other bioprinting techniques. In this thesis, high resolution was achieved with 100 µm nozzle. The bioink was well extrudable even with low pressures and the cell viability after extrusion was high. Moreover, the UV exposure did not decrease the viability. The bioink had good transparency, which is an important characteristic for cornea applications. The bioprinting process did not seem to affect the proliferation or differentiation capability of the stem cells. After optimizing the bioink composition and bioprinting conditions, stratified corneal epithelium mimicking structures were succesfully bioprinted. However, the cells were able to tear the coating material acting as the substrate during culture, which resulted areas without stratified epithelium. Therefore, the printing substrate still requires further optimization to enable long-term cell culture.

The rheological characterization of bioinks still remains a challenge and should be investigated in the future. In this thesis, the soft structure with low crosslinking degree was preferred by the hPSC-LESCs. However, it caused significant challenges in the sample loading of the rheological measurements. Subsequently, further optimization of the sample loading is required.

Even though 3D bioprinting of corneal tissues have been studied previously, most of the studies focus on bioprinting stromal structures. Corneal epithelium is an essential part of the cornea, and therefore, bioprinting native-like corneal epithelial tissue is required to fabricate a functional corneal mimicking structure. This was the first study in which the stratification of hPSC-LESCs was observed after extrusion-based 3D bioprinting. The novel bioink studied in this thesis showed great potential for 3D bioprinting corneal epithelium mimicking structures and should be further studied in ocular surface

reconstruction. However, the 3D bioprinting conditions studied in this thesis are not sufficient enough to maintain the stratified corneal epithelium mimicking structures in long-term. Thus, more research in 3D bioprinting cornea, especially corneal epithelial tissue, is still needed. In addition, the co-culturing of corneal tissues require more consideration and research in the future, when 3D bioprinted corneal tissues are combined. Furthermore, bioprinting stem cells is a promising approach to develop perzonalized treatments and to provide sufficient amounts of desired cell types. However, the sensitivity, variability and cost are challenges in the production and bioprinting of stem cells, and are required to overcome.

REFERENCES

Abasalizadeh, F., Moghaddam, S. V., Alizadeh, E., Akbari, E., Kashani, E., Fazljou, S. M. B., Torbati, M. and Akbarzadeh, A. (2020) “Alginate-based hydrogels as drug delivery vehicles in cancer treatment and their applications in wound dressing and 3D bioprinting,” *Journal of Biological Engineering*. BioMed Central Ltd., pp. 1–22. doi: 10.1186/s13036-020-0227-7.

Abelseth, E., Abelseth, L., De La Vega, L., Beyer, S. T., Wadsworth, S. J. and Willerth, S. M. (2019) “3D Printing of Neural Tissues Derived from Human Induced Pluripotent Stem Cells Using a Fibrin-Based Bioink,” *ACS Biomaterials Science and Engineering*. American Chemical Society, 5(1), pp. 234–243. doi: 10.1021/acsbiomaterials.8b01235.

Acosta-Vélez, G., Linsley, C., Craig, M. and Wu, B. (2017) “Photocurable Bioink for the Inkjet 3D Pharming of Hydrophilic Drugs,” *Bioengineering*. MDPI AG, 4(4), p. 11. doi: 10.3390/bioengineering4010011.

Ahearne, M., Fernández-Pérez, J., Masterton, S., Madden, P. W. and Bhattacharjee, P. (2020) “Designing Scaffolds for Corneal Regeneration,” *Advanced Functional Materials*. Wiley-VCH Verlag. doi: 10.1002/adfm.201908996.

Alexander, F. A., Johnson, L., Williams, K. and Packer, K. (2019) “A parameter study for 3D-printing organized nanofibrous collagen scaffolds using direct-write electrospinning,” *Materials*. MDPI AG, 12(24). doi: 10.3390/MA12244131.

Allevi *Allevi Protocols How to Prepare GelMA Bioink (Sterile-Solution)*, *2020*. Available at: https://www.allevi3d.com/prepare-gelma-sterile-solution/ (Accessed: June 1, 2020).

Anil Kumar, S., Alonzo, M., Allen, S. C., Abelseth, L., Thakur, V., Akimoto, J., Ito, Y., Willerth, S. M., Suggs, L., Chattopadhyay, M. and Joddar, B. (2019) “A Visible Light-Cross-Linkable, Fibrin-Gelatin-Based Bioprinted Construct with Human Cardiomyocytes and Fibroblasts,” *ACS Biomaterials Science and Engineering*. American Chemical Society, 5(9), pp. 4551–4563. doi: 10.1021/acsbiomaterials.9b00505.

Antich, C., de Vicente, J., Jiménez, G., Chocarro, C., Carrillo, E., Montañez, E., Gálvez-Martín, P. and Marchal, J. A. (2020) “Bio-inspired hydrogel composed of hyaluronic acid and alginate as a potential bioink for 3D bioprinting of articular cartilage engineering constructs,” *Acta Biomaterialia*. Acta Materialia Inc, 106, pp. 114–123. doi: 10.1016/j.actbio.2020.01.046.

Anton Paar GmbH (2020a) *Amplitude sweeps*. Available at: https://wiki.anton-paar.com/en/amplitude-sweeps/ (Accessed: July 28, 2020).

Anton Paar GmbH (2020b) *Basics of rheology: Oscillation tests and viscoelasticity*. Available at: https://wiki.anton-paar.com/en/basics-of-rheology/#oscilliation-tests-and-viscoelasticity (Accessed: July 27, 2020).

Applegate, M. B., Partlow, B. P., Coburn, J., Marelli, B., Pirie, C., Pineda, R., Kaplan, D. L. and Omenetto, F. G. (2016) "Photocrosslinking of Silk Fibroin Using Riboflavin for Ocular Prostheses," *Advanced Materials*. Wiley-VCH Verlag, 28(12), pp. 2417–2420. doi: 10.1002/adma.201504527.

Arabpour, Z., Baradaran-Rafii, A., Bakhshaiesh, N. L., Ai, J., Ebrahimi-Barough, S., Esmaeili Malekabadi, H., Nazeri, N., Vaez, A., Salehi, M., Sefat, F. and Ostad, S. N. (2019) "Design and characterization of biodegradable multi layered electrospun nanofibers for corneal tissue engineering applications," *Journal of Biomedical Materials Research Part A*. John Wiley and Sons Inc., 107(10), pp. 2340–2349. doi: 10.1002/jbm.a.36742.

Aslan, B., Guler, S., Tevlek, A. and Aydin, H. M. (2018) "Evaluation of collagen foam, poly(L-lactic acid) nanofiber mesh, and decellularized matrices for corneal regeneration," *Journal of Biomedical Materials Research Part B: Applied Biomaterials*. John Wiley and Sons Inc., 106(6), pp. 2157–2168. doi: 10.1002/jbm.b.34022.

Barros, D., Conde-Sousa, E., Gonçalves, A. M., Han, W. M., García, A. J., Amaral, I. F. and Pêgo, A. P. (2019) "Engineering hydrogels with affinity-bound laminin as 3D neural stem cell culture systems," *Biomaterials Science*. Royal Society of Chemistry, 7(12), pp. 5338–5349. doi: 10.1039/c9bm00348g.

Baylis, O., Figueiredo, F., Henein, C., Lako, M. and Ahmad, S. (2011) "13 Years of cultured limbal epithelial cell therapy: A review of the outcomes," *Journal of Cellular Biochemistry*. John Wiley & Sons, Ltd, pp. 993–1002. doi: 10.1002/jcb.23028.

Beems, E. M. and Van Best, J. A. (1990) "Light transmission of the cornea in whole human eyes," *Experimental Eye Research*. Academic Press, 50(4), pp. 393–395. doi: 10.1016/0014-4835(90)90140-P.

Berg, J., Hiller, T., Kissner, M. S., Qazi, T. H., Duda, G. N., Hocke, A. C., Hippenstiel, S., Elomaa, L., Weinhart, M., Fahrenson, C. and Kurreck, J. (2018) "Optimization of cell-laden bioinks for 3D bioprinting and efficient infection with influenza A virus," *Scientific Reports*. Nature Publishing Group, 8(1). doi: 10.1038/s41598-018-31880-x.

Besser, R. R., Bowles, A. C., Alassaf, A., Carbonero, D., Claure, I., Jones, E., Reda,

J., Wubker, L., Batchelor, W., Ziebarth, N., Silvera, R., Khan, A., MacIel, R., Saporta, M. and Agarwal, A. (2020) “Enzymatically crosslinked gelatin-laminin hydrogels for applications in neuromuscular tissue engineering,” *Biomaterials Science*. Royal Society of Chemistry, 8(2), pp. 591–606. doi: 10.1039/c9bm01430f.

Bhattacharjee, P., Fernández-Pérez, J. and Ahearne, M. (2019) “Potential for combined delivery of riboflavin and all-trans retinoic acid, from silk fibroin for corneal bioengineering,” *Materials Science and Engineering C*. Elsevier Ltd, 105, p. 110093. doi: 10.1016/j.msec.2019.110093.

Biazar, E., Baradaran-Rafii, A., Heidari-keshel, S. and Tavakolifard, S. (2015) “Oriented nanofibrous silk as a natural scaffold for ocular epithelial regeneration,” *Journal of Biomaterials Science, Polymer Edition*. Taylor and Francis Inc., 26(16), pp. 1139–1151. doi: 10.1080/09205063.2015.1078930.

Biomedical Research Team in Spain Working on 3D Printed Corneas to Make Up for Lack of Donors (2017) *3DPrint.com*. Available at: https://3dprintingindustry.com/news/idipaz-researchers-work-mit-3d-printed-cornea-replacements-120205/ (Accessed: May 15, 2020).

Boyd, K. (2018) *The Eye and Immune Privilege - American Academy of Ophtalmology*. Available at: https://www.aao.org/eye-health/tips-prevention/eye-immune-privilege (Accessed: June 5, 2020).

Bozdağ, S. C., Yüksel, M. K. and Demirer, T. (2018) “Adult stem cells and medicine,” in *Advances in Experimental Medicine and Biology*. Springer New York LLC, pp. 17–36. doi: 10.1007/5584_2018_184.

Branco de Cunha, C., Klumpers, D. D., Li, W. A., Koshy, S. T., Weaver, J. C., Chaudhuri, O., Granja, P. L. and Mooney, D. J. (2014) “Influence of the stiffness of three-dimensional alginate/collagen-I interpenetrating networks on fibroblast biology,” *Biomaterials*, 35(32). doi: 10.1016/j.biomaterials.2014.06.047.

Bravery, C. A. (2015) “Do Human Leukocyte Antigen-Typed Cellular Therapeutics Based on Induced Pluripotent Stem Cells Make Commercial Sense?,” *Stem Cells and Development*. Mary Ann Liebert Inc., 24(1), pp. 1–10. doi: 10.1089/scd.2014.0136.

Broguiere, N., Isenmann, L., Hirt, C., Ringel, T., Placzek, S., Cavalli, E., Ringnalda, F., Villiger, L., Züllig, R., Lehmann, R., Rogler, G., Heim, M. H., Schüler, J., Zenobi-Wong, M. and Schwank, G. (2018) “Growth of Epithelial Organoids in a Defined Hydrogel,” *Advanced Materials*. Wiley-VCH Verlag, 30(43), p. 1801621. doi: 10.1002/adma.201801621.

Bryant, S. J., Nuttelman, C. R. and Anseth, K. S. (2000) “Cytocompatibility of UV and visible light photoinitiating systems on cultured NIH/3T3 fibroblasts in vitro,” *Journal of Biomaterials Science, Polymer Edition*. Taylor & Francis Group , 11(5), pp. 439–457. doi: 10.1163/156856200743805.

Bui, B., Saasen, A., Ozbayoglu, E. M., Miska, S. Z., Yu, M. and Takach, N. E. (2012) “Viscoelastic Properties of Oil-Based Drilling Fluids,” *Annual Transactions of the Norvid Rheology Society*, 20. Available at: https://www.researchgate.net/publication/284668965.

Capri, A. (2011) “Methods to produce hydrogel,” in Smiljanic, T. (ed.) *Progress in Molecular and Environmental Bioengineering: From Analysis and Modeling to Technology Applications*. InTech, pp. 126–131. Available at: https://books.google.fi/books?hl=fi&lr=&id=MOaODwAAQBAJ&oi=fnd&pg=PA117&ots=_b_9zwbS57&sig=iijbMAHYKSgAWoXI0_DL3NGUc84&redir_esc=y#v=onepage&q&f=true (Accessed: May 5, 2020).

CELLINK (no date) *CELLINK GelMA*. Available at: https://www.cellink.com/product/cellink-gelma/ (Accessed: June 1, 2020).

CELLINK LAMININK (no date). Available at: https://www.cellink.com/global/product-tag/cellink-laminink/ (Accessed: May 4, 2020).

Cen, Y. J. and Feng, Y. (2018) “Constructing a novel three-dimensional biomimetic corneal endothelium graft by culturing corneal endothelium cells on compressed collagen gels,” *Chinese Medical Journal*. Wolters Kluwer Medknow Publications, 131(14), pp. 1710–1714. doi: 10.4103/0366-6999.235883.

Chae, J. J., McIntosh Ambrose, W., Espinoza, F. A., Mulreany, D. G., Ng, S., Takezawa, T., Trexler, M. M., Schein, O. D., Chuck, R. S. and Elisseeff, J. H. (2015) “Regeneration of corneal epithelium utilizing a collagen vitrigel membrane in rabbit models for corneal stromal wound and limbal stem cell deficiency,” *Acta Ophthalmologica*. Blackwell Publishing Ltd, 93(1), pp. e57–e66. doi: 10.1111/aos.12503.

Chakrabarty, K., Shetty, R. and Ghosh, A. (2018) “Corneal cell therapy: With iPSCs, it is no more a far-sight 11 Medical and Health Sciences 1113 Ophthalmology and Optometry 10 Technology 1004 Medical Biotechnology,” *Stem Cell Research and Therapy*. BioMed Central Ltd., pp. 1–15. doi: 10.1186/s13287-018-1036-5.

Chan, E. H., Chen, L., Rao, J. Y., Yu, F. and Deng, S. X. (2015) “Limbal Basal Cell Density Decreases in Limbal Stem Cell Deficiency,” *American Journal of Ophthalmology*. Elsevier Inc., 160(4), pp. 678-684.e4. doi: 10.1016/j.ajo.2015.06.026.

Chen, D., Qu, Y., Hua, X., Zhang, L., Liu, Z., Pflugfelder, S. C. and Li, D. Q. (2017) “A hyaluronan hydrogel scaffold-based xeno-free culture system for ex vivo expansion of human corneal epithelial stem cells,” *Eye (Basingstoke)*. Nature Publishing Group, 31(6), pp. 962–971. doi: 10.1038/eye.2017.8.

Chen, J., Yan, C., Zhu, M., Yao, Q., Shao, C., Lu, W., Wang, J., Mo, X., Gu, P., Fu, Y. and Fan, X. (2015) “Electrospun nanofibrous SF/P(LLA-CL) membrane: A potential substratum for endothelial keratoplasty,” *International Journal of Nanomedicine*. Dove Medical Press Ltd., 10, pp. 3337–3350. doi: 10.2147/IJN.S77706.

Chen, Y., Zhang, J., Liu, X., Wang, S., Tao, J., Huang, Y., Wu, W., Li, Y., Zhou, K., Wei, X., Chen, S., Li, X., Xu, X., Cardon, L., Qian, Z. and Gou, M. (2020) “Noninvasive in vivo 3D bioprinting,” *Science Advances*. American Association for the Advancement of Science (AAAS), 6(23), p. eaba7406. doi: 10.1126/sciadv.aba7406.

Chen, Z., You, J., Liu, X., Cooper, S., Hodge, C., Sutton, G., Crook, J. M. and Wallace, G. G. (2018) “Biomaterials for corneal bioengineering,” *Biomedical Materials*. IOP Publishing, 13(3), p. 032002. doi: 10.1088/1748-605X/AA92D2.

Chimene, D., Kaunas, R. and Gaharwar, A. K. (2020) “Hydrogel Bioink Reinforcement for Additive Manufacturing: A Focused Review of Emerging Strategies,” *Advanced Materials*, 32(1), p. 1902026. doi: 10.1002/adma.201902026.

Choi, J. R., Yong, K. W., Choi, J. Y. and Cowie, A. C. (2019) “Recent advances in photo-crosslinkable hydrogels for biomedical applications,” *BioTechniques*. Future Science, 66(1), pp. 40–53. doi: 10.2144/btn-2018-0083.

Choi, Y.-J., Kim, T. G., Jeong, J., Yi, H.-G., Park, J. W., Hwang, W. and Cho, D.-W. (2016) “3D Cell Printing of Functional Skeletal Muscle Constructs Using Skeletal Muscle-Derived Bioink,” *Advanced Healthcare Materials*. Wiley-VCH Verlag, 5(20), pp. 2636–2645. doi: 10.1002/adhm.201600483.

Constantini, M., Idaszek, J., Szöke, K., Jaroszewicz, J., Dentini, M., Barbetta, A., Brinchmann, J. E. and Święszkowski, W. (2016) “3D bioprinting of BM-MSCs-loaded ECM biomimetic hydrogels for in vitro neocartilage formation,” *Biofabrication*, 8(3). Available at: https://iopscience.iop.org/article/10.1088/1758-5090/8/3/035002 (Accessed: May 19, 2020).

Corneas Could Be the First Mainstream Application of Bioprinting (2018) *IEEE Spectrum*. Available at: https://spectrum.ieee.org/the-human-os/biomedical/devices/human-corneas-could-be-the-first-mainstream-application-of-bioprinting (Accessed: June 5, 2020).

Corning Matrigel Matrix (no date). Available at: https://www.corning.com/worldwide/en/products/life-sciences/products/surfaces/matrigel-matrix.html (Accessed: May 4, 2020).

Costantini, M., Colosi, C., Święszkowski, W. and Barbetta, A. (2019) "Co-axial wet-spinning in 3D bioprinting: state of the art and future perspective of microfluidic integration Co-axial wet-spinning in 3D bioprinting: state of the art and future perspective of microfluidic integration," *Biofabrication*, 11, p. 12001. doi: 10.1088/1758-5090/aae605.

Cui, W., Li, X., Zhou, S. and Weng, J. (2008) "Degradation patterns and surface wettability of electrospun fibrous mats," *Polymer Degradation and Stability*. Elsevier, 93(3), pp. 731–738. doi: 10.1016/j.polymdegradstab.2007.12.002.

Cui, X., Li, J., Hartanto, Y., Durham, M., Tang, J., Zhang, H., Hooper, G., Lim, K. and Woodfield, T. (2020) "Advances in Extrusion 3D Bioprinting: A Focus on Multicomponent Hydrogel-Based Bioinks," *Advanced Healthcare Materials*. John Wiley & Sons, Ltd, p. 1901648. doi: 10.1002/adhm.201901648.

Dahle, J., Kvam, E. and Stokke, T. (2005) "Bystander effects in UV-induced genomic instability: Antioxidants inhibit delayed mutagenesis induced by ultraviolet A and B radiation," *Journal of Carcinogenesis*. Medknow Publications and Media Pvt. Ltd., 4(1), p. 11. doi: 10.1186/1477-3163-4-11.

DelMonte, D. and Kim, T. (2011) "Anatomy and physiology of the cornea," *J Cataract Refract Surg*, 37(3). doi: 10.1016/j.jcrs.2010.12.037.

Derakhshanfar, S., Mbeleck, R., Xu, K., Zhang, X., Zhong, W. and Xing, M. (2018) "3D bioprinting for biomedical devices and tissue engineering: A review of recent trends and advances," *Bioactive Materials*. KeAi Communications Co., pp. 144–156. doi: 10.1016/j.bioactmat.2017.11.008.

Ding, H. and Chang, R. (2018) "Printability Study of Bioprinted Tubular Structures Using Liquid Hydrogel Precursors in a Support Bath," *Applied Sciences*. MDPI AG, 8(3), p. 403. doi: 10.3390/app8030403.

Drzewiecki, K. E., Malavade, J. N., Ahmed, I., Lowe, C. J. and Shreiber, D. I. (2017) "A thermoreversible, photocrosslinkable collagen bio-ink for free-form fabrication of scaffolds for regenerative medicine," *TECHNOLOGY*. World Scientific Pub Co Pte Lt, 05(04), pp. 185–195. doi: 10.1142/s2339547817500091.

Dua, H. S., Saini, J. S., Azuara-Blanco, A. and Gupta, P. (2000) "Limbal stem cell deficiency: Concept, aetiology, clinical presentation, diagnosis and management," *Indian Journal of Ophthalmology*. Medknow Publications and Media Pvt. Ltd., 48(2), pp. 83–92.

Duarte Campos, D. F., Blaeser, A., Buellesbach, K., Sen, K. S., Xun, W., Tillmann, W. and Fischer, H. (2016) “Bioprinting Organotypic Hydrogels with Improved Mesenchymal Stem Cell Remodeling and Mineralization Properties for Bone Tissue Engineering,” *Advanced Healthcare Materials*. Wiley-VCH Verlag, 5(11), pp. 1336–1345. doi: 10.1002/adhm.201501033.

Duarte Campos, D. F., Rohde, M., Ross, M., Anvari, P., Blaeser, A., Vogt, M., Panfil, C., Yam, G. H., Mehta, J. S., Fischer, H., Walter, P. and Fuest, M. (2019) “Corneal bioprinting utilizing collagen-based bioinks and primary human keratocytes,” *Journal of Biomedical Materials Research Part A*, 107(9), pp. 1945–1953. doi: 10.1002/jbm.a.36702.

Duchi, S., Onofrillo, C., O’Connell, C. D., Blanchard, R., Augustine, C., Quigley, A. F., Kapsa, R. M. I., Pivonka, P., Wallace, G., Di Bella, C. and Choong, P. F. M. (2017) “Handheld Co-Axial Bioprinting: Application to in situ surgical cartilage repair,” *Scientific Reports*. Nature Publishing Group, 7(1), pp. 1–12. doi: 10.1038/s41598-017-05699-x.

Dzobo, K., Motaung, K. S. C. M. and Adesida, A. (2019) “Recent trends in decellularized extracellular matrix bioinks for 3D printing: An updated review,” *International Journal of Molecular Sciences*. MDPI AG. doi: 10.3390/ijms20184628.

Eswaramoorthy, S. D., Ramakrishna, S. and Rath, S. N. (2019) “Recent advances in three-dimensional bioprinting of stem cells,” *Journal of Tissue Engineering and Regenerative Medicine*. John Wiley and Sons Ltd, pp. 908–924. doi: 10.1002/term.2839.

European Medicines Agency (2019) *Holoclar, INN - ex vivo expanded autologous human corneal epithelial cells containing stem cells*, *Annex I - Summary of product characteristics*.

Fagerholm, P., Lagali, N. S., Merrett, K., Jackson, W. B., Munger, R., Liu, Y., Polarek, J. W., Söderqvist, M. and Griffith, M. (2010) “A biosynthetic alternative to human donor tissue for inducing corneal regeneration: 24-Month follow-up of a phase 1 clinical study,” *Science Translational Medicine*. American Association for the Advancement of Science, 2(46), pp. 46ra61-46ra61. doi: 10.1126/scitranslmed.3001022.

Fairbanks, B. D., Schwartz, M. P., Bowman, C. N. and Anseth, K. S. (2009) “Photoinitiated polymerization of PEG-diacrylate with lithium phenyl-2,4,6-trimethylbenzoylphosphinate: polymerization rate and cytocompatibility,” *Biomaterials*. Elsevier, 30(35), pp. 6702–6707. doi: 10.1016/j.biomaterials.2009.08.055.

Fan, R., Piou, M., Darling, E., Cormier, D., Sun, J. and Wan, J. (2016) “Bio-printing cell-laden Matrigel–agarose constructs,” *Journal of Biomaterials Applications*. SAGE

Publications Ltd, 31(5), pp. 684–692. doi: 10.1177/0885328216669238.

Faulkner-Jones, A., Fyfe, C., Cornelissen, D.-J., Gardner, J., King, J., Courtney, A. and Shu, W. (2015) “Bioprinting of human pluripotent stem cells and their directed differentiation into hepatocyte-like cells for the generation of mini-livers in 3D,” *Biofabrication*, 7. doi: 10.1088/1758-5090/7/4/044102.

Fernández-Pérez, J., Kador, K. E., Lynch, A. P. and Ahearne, M. (2020) “Characterization of extracellular matrix modified poly(ε-caprolactone) electrospun scaffolds with differing fiber orientations for corneal stroma regeneration,” *Materials Science and Engineering C*. Elsevier Ltd, 108, p. 110415. doi: 10.1016/j.msec.2019.110415.

Fernández-Pérez, J. and Ahearne, M. (2020) “Decellularization and recellularization of cornea: Progress towards a donor alternative,” *Methods*. Academic Press Inc., pp. 86–96. doi: 10.1016/j.ymeth.2019.05.009.

Fiorica, C., Senior, R. A., Pitarresi, G., Palumbo, F. S., Giammona, G., Deshpande, P. and MacNeil, S. (2011) “Biocompatible hydrogels based on hyaluronic acid cross-linked with a polyaspartamide derivative as delivery systems for epithelial limbal cells,” *International Journal of Pharmaceutics*. Elsevier, 414(1–2), pp. 104–111. doi: 10.1016/j.ijpharm.2011.05.002.

Freeman, F. E. and Kelly, D. J. (2017) “Tuning alginate bioink stiffness and composition for controlled growth factor delivery and to spatially direct MSC Fate within bioprinted tissues,” *Scientific Reports*. Nature Publishing Group, 7(1), pp. 1–12. doi: 10.1038/s41598-017-17286-1.

Freeman, S., Ramos, R., Alexis Chando, P., Zhou, L., Reeser, K., Jin, S., Soman, P. and Ye, K. (2019) “A bioink blend for rotary 3D bioprinting tissue engineered small-diameter vascular constructs,” *Acta Biomaterialia*. Acta Materialia Inc, 95, pp. 152–164. doi: 10.1016/j.actbio.2019.06.052.

Frost, B., Sutliff, B. P., Thayer, P., Bortner, M. J. and Foster, E. J. (2019) “Gradient poly(Ethylene glycol) diacrylate and cellulose nanocrystals tissue engineering composite scaffolds via extrusion bioprinting,” *Frontiers in Bioengineering and Biotechnology*. Frontiers Media S.A., 7(OCT). doi: 10.3389/fbioe.2019.00280.

Gaebel, R., Ma, N., Liu, J., Guan, J., Koch, L., Klopsch, C., Gruene, M., Toelk, A., Wang, W., Mark, P., Wang, F., Chichkov, B., Li, W. and Steinhoff, G. (2011) “Patterning human stem cells and endothelial cells with laser printing for cardiac regeneration,” *Biomaterials*. Elsevier, 32(35), pp. 9218–9230. doi: 10.1016/j.biomaterials.2011.08.071.

Gain, P., Jullienne, R., He, Z., Aldossary, M., Acquart, S., Cognasse, F. and Thuret, G. (2016) “Global survey of corneal transplantation and eye banking,” *JAMA Ophthalmology*. American Medical Association, 134(2), pp. 167–173. doi: 10.1001/jamaophthalmol.2015.4776.

Gajendiran, M., Rhee, J.-S. and Kim, K. (2018) “Recent Developments in Thiolated Polymeric Hydrogels for Tissue Engineering Applications,” *Tissue Engineering Part B: Reviews*. Mary Ann Liebert Inc., 24(1), pp. 66–74. doi: 10.1089/ten.teb.2016.0442.

Galarraga, J. H., Kwon, M. Y. and Burdick, J. A. (2019) “3D bioprinting via an in situ crosslinking technique towards engineering cartilage tissue,” *Scientific Reports*. Nature Research, 9(1), pp. 1–12. doi: 10.1038/s41598-019-56117-3.

Galvez-Martin, P., López-Ruiz, E., Jiménez, G., Álvarez De Cienfuegos, L., Antich, C., Sabata, R., Marchal, J. A. and Gálvez-Martín, P. (2019) “ADVANCES OF HYALURONIC ACID IN STEM CELL THERAPY AND TISSUE ENGINEERING, INCLUDING CURRENT CLINICAL TRIALS,” *European Cells and Materials*, 37(2019), pp. 186–213. doi: 10.22203/eCM.v037a12.

Gao, G., Schilling, A. F., Hubbell, K., Yonezawa, T., Truong, D., Hong, Y., Dai, G. and Cui, X. (2015) “Improved properties of bone and cartilage tissue from 3D inkjet-bioprinted human mesenchymal stem cells by simultaneous deposition and photocrosslinking in PEG-GelMA,” *Biotechnology Letters*. Kluwer Academic Publishers, 37(11), pp. 2349–2355. doi: 10.1007/s10529-015-1921-2.

Gao, G., Lee, J. H., Jang, J., Lee, D. H., Kong, J.-S., Kim, B. S., Choi, Y.-J., Jang, W. B., Hong, Y. J., Kwon, S.-M. and Cho, D.-W. (2017) “Tissue Engineered Bio-Blood-Vessels Constructed Using a Tissue-Specific Bioink and 3D Coaxial Cell Printing Technique: A Novel Therapy for Ischemic Disease,” *Advanced Functional Materials*. Wiley-VCH Verlag, 27(33), p. 1700798. doi: 10.1002/adfm.201700798.

GelX LAMININK (no date). Available at: https://www.cellink.com/global/product-tag/gelx-laminink/ (Accessed: May 4, 2020).

Gesteira, T. F., Sun, M., Coulson-Thomas, Y. M., Yamaguchi, Y., Yeh, L. K., Hascall, V. and Coulson-Thomas, V. J. (2017) “Hyaluronan rich microenvironment in the limbal stem cell niche regulates limbal stem cell differentiation,” *Investigative Ophthalmology and Visual Science*. Association for Research in Vision and Ophthalmology Inc., 58(11), pp. 4407–4421. doi: 10.1167/iovs.17-22326.

Ghezzi, C. E., Marelli, B., Omenetto, F. G., Funderburgh, J. L. and Kaplan, D. L. (2017) “3D functional corneal stromal tissue equivalent based on corneal stromal stem

cells and multi-layered silk film architecture," *PLoS ONE*. Public Library of Science, 12(1). doi: 10.1371/journal.pone.0169504.

Gipson, I. K. (2007) "The ocular surface: The challenge to enable and protect vision. The Friedenwald lecture," in *Investigative Ophthalmology and Visual Science*. NIH Public Access, pp. 4391–4398. doi: 10.1167/iovs.07-0770.

Goodarzi, H., Jadidi, K., Pourmotabed, S., Sharifi, E. and Aghamollaei, H. (2019) "Preparation and in vitro characterization of cross-linked collagen–gelatin hydrogel using EDC/NHS for corneal tissue engineering applications," *International Journal of Biological Macromolecules*. Elsevier B.V., 126, pp. 620–632. doi: 10.1016/j.ijbiomac.2018.12.125.

Gouveia, R. M., González-Andrades, E., Cardona, J. C., González-Gallardo, C., Ionescu, A. M., Garzon, I., Alaminos, M., González-Andrades, M. and Connon, C. J. (2017) "Controlling the 3D architecture of Self-Lifting Auto-generated Tissue Equivalents (SLATEs) for optimized corneal graft composition and stability," *Biomaterials*. Elsevier Ltd, 121, pp. 205–219. doi: 10.1016/j.biomaterials.2016.12.023.

Gouveia, R. M., Koudouna, E., Jester, J., Figueiredo, F. and Connon, C. J. (2017) "Template Curvature Influences Cell Alignment to Create Improved Human Corneal Tissue Equivalents," *Advanced Biosystems*. Wiley, 1(12), p. 1700135. doi: 10.1002/adbi.201700135.

Gouveia, R. M., Lepert, G., Gupta, S., Mohan, R. R., Paterson, C. and Connon, C. J. (2019) "Assessment of corneal substrate biomechanics and its effect on epithelial stem cell maintenance and differentiation," *Nature Communications*. Nature Publishing Group, 10(1), pp. 1–17. doi: 10.1038/s41467-019-09331-6.

Gouveia, R. M., Vajda, F., Wibowo, J. A., Figueiredo, F. and Connon, C. J. (2019) "YAP, ΔNp63, and β-Catenin Signaling Pathways Are Involved in the Modulation of Corneal Epithelial Stem Cell Phenotype Induced by Substrate Stiffness," *Cells*. MDPI AG, 8(4), p. 347. doi: 10.3390/cells8040347.

Groll, J., Burdick, J. A., Cho, D.-W., Derby, B., Gelinsky, M., Heilshorn, S. C., Jüngst, T., Malda, J., Mironov, V. A., Nakayama, K., Ovsianikov, A., Sun, W., Takeuchi, S., Yoo, J. and Woodfield, T. B. F. (2018) "A definition of bioinks and their distinction from biomaterial inks," *Biofabrication*, 11. doi: 10.1088/1758-5090/aaec52.

Gruene, M., Pflaum, M., Hess, C., Diamantouros, S., Schlie, S., Deiwick, A., Koch, L., Wilhelmi, M., Jockenhoevel, S., Haverich, A. and Chichkov, B. (2011) "Laser printing of three-dimensional multicellular arrays for studies of cell-cell and cell-environment interactions," *Tissue Engineering - Part C: Methods*. Mary Ann Liebert Inc., 17(10), pp.

973–982. doi: 10.1089/ten.tec.2011.0185.

Gu, Q., Tomaskovic-Crook, E., Wallace, G. G. and Crook, J. M. (2017) “3D Bioprinting Human Induced Pluripotent Stem Cell Constructs for In Situ Cell Proliferation and Successive Multilineage Differentiation,” *Advanced Healthcare Materials*. Wiley-VCH Verlag, 6(17), p. 1700175. doi: 10.1002/adhm.201700175.

Gu, Y., Zhang, L., Du, X., Fan, Z., Wang, L., Sun, W., Cheng, Y., Zhu, Y. and Chen, C. (2018) “Reversible physical crosslinking strategy with optimal temperature for 3D bioprinting of human chondrocyte-laden gelatin methacryloyl bioink.,” *Journal of biomaterials applications*. SAGE Publications Ltd, 33(5), pp. 609–618. doi: 10.1177/0885328218805864.

Handorf, A. M., Zhou, Y., Halanski, M. A. and Li, W.-J. (2015) “Tissue Stiffness Dictates Development, Homeostasis, and Disease Progression,” *Organogenesis*. Taylor and Francis Inc., 11(1), pp. 1–15. doi: 10.1080/15476278.2015.1019687.

Henrionnet, C., Pourchet, L., Neybecker, P., Messaoudi, O., Gillet, P., Loeuille, D., Mainard, D., Marquette, C. and Pinzano, A. (2020) “Combining Innovative Bioink and Low Cell Density for the Production of 3D-Bioprinted Cartilage Substitutes: A Pilot Study,” *Hindawi Stem Cells International*, 2020, p. 16. doi: 10.1155/2020/2487072.

Higa, K., Takeshima, N., Moro, F., Kawakita, T., Kawashima, M., Demura, M., Shimazaki, J., Asakura, T., Tsubota, K. and Shimmura, S. (2011) “Porous silk fibroin film as a transparent carrier for cultivated corneal epithelial sheets,” *Journal of Biomaterials Science, Polymer Edition*. Taylor and Francis Inc., 22(17), pp. 2261–2276. doi: 10.1163/092050610X538218.

Holland, E. J. (2015) “Management of limbal stem cell deficiency: A historical perspective, past, present, and future,” *Cornea*. Lippincott Williams and Wilkins, pp. S9–S15. doi: 10.1097/ICO.0000000000000534.

Holmes, R., Yang, X.-B., Dunne, A., Florea, L., Wood, D. and Tronci, G. (2017) “Thiol-Ene Photo-Click Collagen-PEG Hydrogels: Impact of Water-Soluble Photoinitiators on Cell Viability, Gelation Kinetics and Rheological Properties,” *Polymers*, 9(12), p. 226. doi: 10.3390/polym9060226.

Hölzl, K., Lin, S., Tytgat, L., Van Vlierberghe, S., Gu, L. and Ovsianikov, A. (2016) “Bioink properties before, during and after 3D bioprinting,” *Biofabrication*. Institute of Physics Publishing. doi: 10.1088/1758-5090/8/3/032002.

Hongisto, H., Ilmarinen, T., Vattulainen, M., Mikhailova, A. and Skottman, H. (2017) “Xeno- and feeder-free differentiation of human pluripotent stem cells to two distinct

ocular epithelial cell types using simple modifications of one method," *Stem Cell Research and Therapy*. BioMed Central Ltd., 8(1), p. 291. doi: 10.1186/s13287-017-0738-4.

Van Hoorick, J., Tytgat, L., Dobos, A., Ottevaere, H., Van Erps, J., Thienpont, H., Ovsianikov, A., Dubruel, P. and Van Vlierberghe, S. (2019) "(Photo-)crosslinkable gelatin derivatives for biofabrication applications," *Acta Biomaterialia*. Acta Materialia Inc, pp. 46–73. doi: 10.1016/j.actbio.2019.07.035.

Hospodiuk, M., Dey, M., Sosnoski, D. and Ozbolat, I. T. (2017) "The bioink: A comprehensive review on bioprintable materials," *Biotechnology Advances*. Elsevier Inc., pp. 217–239. doi: 10.1016/j.biotechadv.2016.12.006.

Hoyle, C. E. and Bowman, C. N. (2010) "Thiol-Ene Click Chemistry," *Angewandte Chemie International Edition*. John Wiley & Sons, Ltd, 49(9), pp. 1540–1573. doi: 10.1002/anie.200903924.

ICTRP Search Portal (2020). Available at: https://apps.who.int/trialsearch/Trial2.aspx?TrialID=JPRN-UMIN000036539 (Accessed: April 26, 2020).

Ilic, D., Devito, L., Miere, C. and Codognotto, S. (2015) "Human embryonic and induced pluripotent stem cells in clinical trials." doi: 10.1093/bmb/ldv045.

Isaacson, A., Swioklo, S. and Connon, C. J. (2018) "3D bioprinting of a corneal stroma equivalent," *Experimental Eye Research*. Academic Press, 173, pp. 188–193. doi: 10.1016/j.exer.2018.05.010.

Iskratsch, T., Wolfenson, H. and Sheetz, M. P. (2014) *Appreciating force and shape — the rise of mechanotransduction in cell biology*, *Nat Rev Mol Cell Biol*. doi: 10.1038/nrm3903.

Jackson, C. J., Myklebust Ernø, I. T., Ringstad, H., Tønseth, K. A., Dartt, D. A. and Utheim, T. P. (2020) "Simple limbal epithelial transplantation: Current status and future perspectives," *Stem Cells Translational Medicine*. John Wiley and Sons Ltd., pp. 316–327. doi: 10.1002/sctm.19-0203.

Jang, J., Park, H. J., Kim, Seok Won, Kim, H., Park, J. Y., Na, S. J., Kim, H. J., Park, M. N., Choi, S. H., Park, S. H., Kim, Sung Won, Kwon, S. M., Kim, P. J. and Cho, D. W. (2017) "3D printed complex tissue construct using stem cell-laden decellularized extracellular matrix bioinks for cardiac repair," *Biomaterials*. Elsevier Ltd, 112, pp. 264–274. doi: 10.1016/j.biomaterials.2016.10.026.

Janmey, P. A., Georges, P. C. and Hvidt, S. (2007) "Basic Rheology for Biologists,"

Methods in Cell Biology, 83. doi: 10.1016/S0091-679X(07)83001-9.

Jester, J., Moller-Pedersen, T., Huan, J., Sax, C., Kays, W. T., Cavangh, H. D., Petroll, W. M. and Piatigorsky, J. (1999) “The cellular basis of corneal transparency: evidence for ‘corneal crystallins,’” *J Cell Sci*, 112.

Jia, W., Gungor-Ozkerim, P. S., Zhang, Y. S., Yue, K., Zhu, K., Liu, W., Pi, Q., Byambaa, B., Dokmeci, M. R., Shin, S. R. and Khademhosseini, A. (2016) “Direct 3D bioprinting of perfusable vascular constructs using a blend bioink,” *Biomaterials*. Elsevier Ltd, 106, pp. 58–68. doi: 10.1016/j.biomaterials.2016.07.038.

Jia, W., Selcan Gungor-Ozkerim, P., Zhang, Y. S., Yue, K., Zhu, K., Liu, W., Pi, Q., Byambaa, B., Dokmeci, R., Shin, S. R. and Khademhosseini, A. (2016) “Direct 3D bioprinting of perfusable vascular constructs using a blend bioink.” doi: 10.1016/j.biomaterials.2016.07.038.

Jirsova, K. and Jones, G. L. A. (2017) “Amniotic membrane in ophthalmology: properties, preparation, storage and indications for grafting—a review,” *Cell and Tissue Banking*. Springer Netherlands, pp. 193–204. doi: 10.1007/s10561-017-9618-5.

Kabirian, F. and Mozafari, M. (2020) “Decellularized ECM-derived bioinks: Prospects for the future,” *Methods*. Academic Press Inc., pp. 108–118. doi: 10.1016/j.ymeth.2019.04.019.

Kajave, N. S., Schmitt, T., Nguyen, T. U. and Kishore, V. (2020) “Dual crosslinking strategy to generate mechanically viable cell-laden printable constructs using methacrylated collagen bioinks,” *Materials Science and Engineering C*. Elsevier Ltd, 107, p. 110290. doi: 10.1016/j.msec.2019.110290.

Kang, L. H., Armstrong, P. A., Lee, L. J., Duan, B., Kang, K. H. and Butcher, J. T. (2017) “Optimizing Photo-Encapsulation Viability of Heart Valve Cell Types in 3D Printable Composite Hydrogels,” *Annals of Biomedical Engineering*. Springer New York LLC, 45(2), pp. 360–377. doi: 10.1007/s10439-016-1619-1.

Kasai, Y. *et al.* (2020) “A stable protocol for the fabrication of transplantable human oral mucosal epithelial cell sheets for clinical application,” *Regenerative Therapy*. Japanese Society of Regenerative Medicine, 14, pp. 87–94. doi: 10.1016/j.reth.2019.11.007.

Keivyon, K. R. and Tseng, S. C. G. (1989) “Limbal Autograft Transplantation for Ocular Surface Disorders,” *Ophthalmology*. Elsevier, 96(5), pp. 709–723. doi: 10.1016/S0161-6420(89)32833-8.

Kiiskinen, J. (2016) *Co-culture of corneal epithelial cells and adipose stem cells -*

towards the use of hydrogels in ocular surface reconstruction. University of Tampere.

Kilian, D., Ahlfeld, T., Akkineni, A. R., Bernhardt, A., Gelinsky, M. and Lode, A. (2020) “3D Bioprinting of osteochondral tissue substitutes – in vitro-chondrogenesis in multi-layered mineralized constructs,” *Scientific Reports*. Nature Publishing Group, 10(1), p. 8277. doi: 10.1038/s41598-020-65050-9.

Kilic Bektas, C., Burcu, A., Gedikoglu, G., Telek, H. H., Ornek, F. and Hasirci, V. (2019) “Methacrylated gelatin hydrogels as corneal stroma substitutes: *in vivo* study,” *Journal of Biomaterials Science, Polymer Edition*. Taylor and Francis Inc., 30(18), pp. 1803–1821. doi: 10.1080/09205063.2019.1666236.

Kilic Bektas, C. and Hasirci, V. (2020) “Cell loaded 3D bioprinted GelMA hydrogels for corneal stroma engineering,” *Biomaterials Science*. Royal Society of Chemistry, 8(1), pp. 438–449. doi: 10.1039/c9bm01236b.

Kim, B. S., Kwon, Y. W., Kong, J. S., Park, G. T., Gao, G., Han, W., Kim, M. B., Lee, H., Kim, J. H. and Cho, D. W. (2018) “3D cell printing of in vitro stabilized skin model and in vivo pre-vascularized skin patch using tissue-specific extracellular matrix bioink: A step towards advanced skin tissue engineering,” *Biomaterials*. Elsevier Ltd, 168, pp. 38–53. doi: 10.1016/j.biomaterials.2018.03.040.

Kim, H., Park, M.-N., Kim, J., Jang, J., Kim, H.-K. and Cho, D.-W. (2019) “Characterization of cornea-specific bioink: high transparency, improved in vivo safety,” *Journal of Tissue Engineering*. SAGE Publications Ltd, 10, p. 204173141882338. doi: 10.1177/2041731418823382.

Kim, J., Kim, M., Hwang, D. G., Shim, I. K., Kim, S. C. and Jang, J. (2019) “Pancreatic Tissue-Derived Extracellular Matrix Bioink for Printing 3D Cell-Laden Pancreatic Tissue Constructs,” *Journal of Visualized Experiments*. NLM (Medline), (154), p. e60434. doi: 10.3791/60434.

Kim, J. I., Kim, J. Y. and Park, C. H. (2018) “Fabrication of transparent hemispherical 3D nanofibrous scaffolds with radially aligned patterns via a novel electrospinning method,” *Scientific Reports*. Nature Publishing Group, 8(1). doi: 10.1038/s41598-018-21618-0.

Kim, K. W., Lee, S. J., Park, S. H. and Kim, J. C. (2018) “Ex Vivo Functionality of 3D Bioprinted Corneal Endothelium Engineered with Ribonuclease 5-Overexpressing Human Corneal Endothelial Cells,” *Advanced Healthcare Materials*. Wiley-VCH Verlag, 7(18), p. 1800398. doi: 10.1002/adhm.201800398.

Kim, W. J. and Kim, G. H. (2020) “An intestinal model with a finger-like villus structure

fabricated using a bioprinting process and collagen/SIS-based cell-laden bioink," *Theranostics*. Ivyspring International Publisher, 10(6), pp. 2495–2508. doi: 10.7150/thno.41225.

Kim, W. and Kim, G. (2019) "A functional bioink and its application in myoblast alignment and differentiation." doi: 10.1016/j.cej.2019.02.071.

Kim, Y. B., Lee, H. and Kim, G. H. (2016) "Strategy to Achieve Highly Porous/Biocompatible Macroscale Cell Blocks, Using a Collagen/Genipin-bioink and an Optimal 3D Printing Process," *ACS Applied Materials and Interfaces*. American Chemical Society, 8(47), pp. 32230–32240. doi: 10.1021/acsami.6b11669.

Kiyotake, E. A., Douglas, A. W., Thomas, E. E., Nimmo, S. L. and Detamore, M. S. (2019) "Development and quantitative characterization of the precursor rheology of hyaluronic acid hydrogels for bioprinting," *Acta Biomaterialia*. Elsevier, 95, pp. 176–187. doi: 10.1016/J.ACTBIO.2019.01.041.

Knowlton, S., Yenilmez, B., Anand, S. and Tasoglu, S. (2017) "Photocrosslinking-based bioprinting: Examining crosslinking schemes," *Bioprinting*. Elsevier B.V., 5, pp. 10–18. doi: 10.1016/j.bprint.2017.03.001.

Kobayashi, T., Kan, K., Nishida, K., Yamato, M. and Okano, T. (2013) "Corneal regeneration by transplantation of corneal epithelial cell sheets fabricated with automated cell culture system in rabbit model," *Biomaterials*. Elsevier, 34(36), pp. 9010–9017. doi: 10.1016/j.biomaterials.2013.07.065.

Koch, L., Kuhn, S., Sorg, H., Gruene, M., Schlie, S., Gaebel, R., Polchow, B., Reimers, K., Stoelting, S., Ma, N., Vogt, P. M., Steinhoff, G. and Chichkov, B. (2010) "Laser Printing of Skin Cells and Human Stem Cells," *Tissue Eng Part C*, 16(5).

Kolesky, D. B., Truby, R. L., Gladman, A. S., Busbee, T. A., Homan, K. A. and Lewis, J. A. (2014) "3D Bioprinting of Vascularized, Heterogeneous Cell-Laden Tissue Constructs," *Advanced Materials*. Wiley-VCH Verlag, 26(19), pp. 3124–3130. doi: 10.1002/adma.201305506.

Kong, B., Sun, W., Chen, G., Tang, S., Li, M., Shao, Z. and Mi, S. (2017) "Tissue-engineered cornea constructed with compressed collagen and laser-perforated electrospun mat," *Scientific Reports*. Nature Publishing Group, 7(1). doi: 10.1038/s41598-017-01072-0.

Kong, B. and Mi, S. (2016) "Electrospun scaffolds for corneal tissue engineering: A review," *Materials*. MDPI AG. doi: 10.3390/ma9080614.

Kreimendahl, F., Köpf, M., Thiebes, A. L., Duarte Campos, D. F., Blaeser, A., Schmitz-

Rode, T., Apel, C., Jockenhoevel, S. and Fischer, H. (2017) “Three-Dimensional Printing and Angiogenesis: Tailored Agarose-Type i Collagen Blends Comprise Three-Dimensional Printability and Angiogenesis Potential for Tissue-Engineered Substitutes,” *Tissue Engineering - Part C: Methods*. Mary Ann Liebert Inc., 23(10), pp. 604–615. doi: 10.1089/ten.tec.2017.0234.

Kucukgul, C., Ozler, S. B., Inci, I., Karakas, E., Irmak, S., Gozuacik, D., Taralp, A. and Koc, B. (2015) “3D bioprinting of biomimetic aortic vascular constructs with self-supporting cells,” *Biotechnology and Bioengineering*. John Wiley and Sons Inc., 112(4), pp. 811–821. doi: 10.1002/bit.25493.

Kutlehria, S., Dinh, T. C., Bagde, A., Patel, N., Gebeyehu, A. and Singh, M. (2020) “High-throughput <scp>3D</scp> bioprinting of corneal stromal equivalents,” *Journal of Biomedical Materials Research Part B: Applied Biomaterials*. John Wiley and Sons Inc., p. jbm.b.34628. doi: 10.1002/jbm.b.34628.

Kyle, S., Jessop, Z. M., Al-Sabah, A. and Whitaker, I. S. (2017) “‘Printability’’ of Candidate Biomaterials for Extrusion Based 3D Printing: State-of-the-Art,’” *Advanced Healthcare Materials*. Wiley-VCH Verlag, 6(16), p. 1700264. doi: 10.1002/adhm.201700264.

de la Vega, L., A. Rosas Gómez, D., Abelseth, E., Abelseth, L., Allisson da Silva, V. and Willerth, S. (2018) “3D Bioprinting Human Induced Pluripotent Stem Cell-Derived Neural Tissues Using a Novel Lab-on-a-Printer Technology,” *Applied Sciences*. MDPI AG, 8(12), p. 2414. doi: 10.3390/app8122414.

Lacorzana, J. (2020) “Amniotic membrane, clinical applications and tissue engineering. Review of its ophthalmic use,” *Archivos de la Sociedad Española de Oftalmología (English Edition)*. Elsevier BV, 95(1), pp. 15–23. doi: 10.1016/j.oftale.2019.09.008.

Lam, T., Dehne, T., Krüger, J. P., Hondke, S., Endres, M., Thomas, A., Lauster, R., Sittinger, M. and Kloke, L. (2019) “Photopolymerizable gelatin and hyaluronic acid for stereolithographic 3D bioprinting of tissue-engineered cartilage,” *Journal of Biomedical Materials Research - Part B Applied Biomaterials*. John Wiley and Sons Inc., 107(8), pp. 2649–2657. doi: 10.1002/jbm.b.34354.

Laternser, S., Keller, H., Leupin, O., Rausch, M., Graf-Hausner, U. and Rimann, M. (2018) “A Novel Microplate 3D Bioprinting Platform for the Engineering of Muscle and Tendon Tissues.,” *SLAS technology*. SAGE Publications Inc., 23(6), pp. 599–613. doi: 10.1177/2472630318776594.

Le, Q. and Deng, S. X. (2019) “The application of human amniotic membrane in the surgical management of limbal stem cell deficiency,” *Ocular Surface*. Elsevier Inc., pp. 221–229. doi: 10.1016/j.jtos.2019.01.003.

Lee, H., Han, W., Kim, H., Ha, D. H., Jang, J., Kim, B. S. and Cho, D. W. (2017) “Development of Liver Decellularized Extracellular Matrix Bioink for Three-Dimensional Cell Printing-Based Liver Tissue Engineering,” *Biomacromolecules*. American Chemical Society, 18(4), pp. 1229–1237. doi: 10.1021/acs.biomac.6b01908.

Lee, H. J., Kim, Y. B., Ahn, S. H., Lee, J.-S., Jang, C. H., Yoon, H., Chun, W. and Kim, G. H. (2015) “A New Approach for Fabricating Collagen/ECM-Based Bioinks Using Preosteoblasts and Human Adipose Stem Cells,” *Advanced Healthcare Materials*. Wiley-VCH Verlag, 4(9), pp. 1359–1368. doi: 10.1002/adhm.201500193.

Leichner, C., Jelkmann, M. and Bernkop-Schnürch, A. (2019) “Thiolated polymers: Bioinspired polymers utilizing one of the most important bridging structures in nature,” *Advanced Drug Delivery Reviews*. Elsevier B.V., pp. 191–221. doi: 10.1016/j.addr.2019.04.007.

Li, L., Lu, C., Wang, L., Chen, M., White, J., Hao, X., McLean, K. M., Chen, H. and Hughes, T. C. (2018) “Gelatin-Based Photocurable Hydrogels for Corneal Wound Repair,” *ACS Applied Materials and Interfaces*. American Chemical Society, 10(16), pp. 13283–13292. doi: 10.1021/acsami.7b17054.

Li, M., Ma, J., Gao, Y. and Yang, L. (2019) “Cell sheet technology: a promising strategy in regenerative medicine,” *Cytotherapy*. Elsevier B.V., pp. 3–16. doi: 10.1016/j.jcyt.2018.10.013.

Li, Y., Yang, Y., Yang, L., Zeng, Y., Gao, X. and Xu, H. (2017) “Poly(ethylene glycol)-modified silk fibroin membrane as a carrier for limbal epithelial stem cell transplantation in a rabbit LSCD model,” *Stem Cell Research and Therapy*. BioMed Central Ltd., 8(1). doi: 10.1186/s13287-017-0707-y.

Lim, K. S., Schon, B. S., Mekhileri, N. V., Brown, G. C. J., Chia, C. M., Prabakar, S., Hooper, G. J. and Woodfield, T. B. F. (2016) “New Visible-Light Photoinitiating System for Improved Print Fidelity in Gelatin-Based Bioinks,” *ACS Biomaterials Science and Engineering*. American Chemical Society, 2(10), pp. 1752–1762. doi: 10.1021/acsbiomaterials.6b00149.

Lim, K. S., Galarraga, J. H., Cui, X., Lindberg, G. C. J., Burdick, J. A. and Woodfield, T. B. F. (2020) “Fundamentals and Applications of Photo-Cross-Linking in Bioprinting,” *Chemical Reviews*. doi: 10.1021/acs.chemrev.9b00812.

Liu, H., Zhou, Z., Lin, H., Wu, J., Ginn, B., Choi, J. S., Jiang, X., Chung, L., Elisseeff, J. H., Yiu, S. and Mao, H. Q. (2018) “Synthetic Nanofiber-Reinforced Amniotic Membrane via Interfacial Bonding,” *ACS Applied Materials and Interfaces*. American Chemical Society, 10(17), pp. 14559–14569. doi: 10.1021/acsami.8b03087.

Liu, J., Lawrence, B. D., Liu, A., Schwab, I. R., Oliveira, L. A. and Rosenblatt, M. I. (2012) “Silk fibroin as a biomaterial substrate for corneal epithelial cell sheet generation,” *Investigative Ophthalmology and Visual Science*. Association for Research in Vision and Ophthalmology, 53(7), pp. 4130–4138. doi: 10.1167/iovs.12-9876.

Liu, J., Li, L., Suo, H., Yan, M., Yin, J. and Fu, J. (2019) “3D printing of biomimetic multi-layered GelMA/nHA scaffold for osteochondral defect repair,” *Materials and Design*. Elsevier Ltd, 171, p. 107708. doi: 10.1016/j.matdes.2019.107708.

Liu, W., Heinrich, M. A., Zhou, Y., Akpek, A., Hu, N., Liu, X., Guan, X., Zhong, Z., Jin, X., Khademhosseini, A. and Zhang, Y. S. (2017) “Extrusion Bioprinting of Shear-Thinning Gelatin Methacryloyl Bioinks,” *Advanced Healthcare Materials*. Wiley-VCH Verlag, 6(12). doi: 10.1002/adhm.201601451.

Liu, W., Zhong, Z., Hu, N., Zhou, Y., Maggio, L., Miri, A. K., Fragasso, A., Jin, X., Khademhosseini, A. and Zhang, Y. S. (2018) “Coaxial extrusion bioprinting of 3D microfibrous constructs with cell-favorable gelatin methacryloyl microenvironments,” *Biofabrication*, 10(2). Available at: https://iopscience.iop.org/article/10.1088/1758-5090/aa9d44 (Accessed: June 1, 2020).

Liu, Y., Liu, X., Wu, M., Ji, P., Lv, H. and Deng, L. (2019) “A collagen film with micro-rough surface can promote the corneal epithelization process for corneal repair,” *International Journal of Biological Macromolecules*. Elsevier B.V., 121, pp. 233–238. doi: 10.1016/j.ijbiomac.2018.10.026.

Lou, J., Stowers, R., Nam, S., Xia, Y. and Chaudhuri, O. (2018) “Stress relaxing hyaluronic acid-collagen hydrogels promote cell spreading, fiber remodeling, and focal adhesion formation in 3D cell culture,” *Biomaterials*, 154. doi: 10.1016/j.biomaterials.2017.11.004.

Luo, C., Xie, R., Zhang, J., Liu, Y., Zhang, Y., Li, Z., Zhang, X., Yan, T. and Fan, W. (2020) “Low temperature 3D printing of tissue cartilage engineered with gelatin methacrylamide,” *Tissue Eng Part C*. doi: 10.1089/ten.TEC.2020.0053.

Ma, K., Zhao, T., Yang, L., Wang, P., Jin, J., Teng, H., Xia, D., Zhu, L., Li, L., Jiang, Q. and Wang, X. (2020) “Application of robotic-assisted in situ 3D printing in cartilage regeneration with HAMA hydrogel: An in vivo study,” *Journal of Advanced Research*.

Elsevier B.V., 23, pp. 123–132. doi: 10.1016/j.jare.2020.01.010.

Ma, X., Qu, X., Zhu, W., Li, Y. S., Yuan, S., Zhang, H., Liu, J., Wang, P., Lai, C. S. E., Zanella, F., Feng, G. S., Sheikh, F., Chien, S. and Chen, S. (2016) "Deterministically patterned biomimetic human iPSC-derived hepatic model via rapid 3D bioprinting," *Proceedings of the National Academy of Sciences of the United States of America*. National Academy of Sciences, 113(8), pp. 2206–2211. doi: 10.1073/pnas.1524510113.

MacCallum, B., Naseri, E., Butler, H., MacNevin, W., Tasker, R. A. and Ahmadi, A. (2020) "Development of a 3D bioprinting system using a Co-Flow of calcium chloride mist," *Bioprinting*. Elsevier, p. e00085. doi: 10.1016/j.bprint.2020.e00085.

Madathil, B. K., Kumar, P. R. A. and Kumary, T. V. (2014) "N-Isopropylacrylamide-co-glycidylmethacrylate as a Thermoresponsive Substrate for Corneal Endothelial Cell Sheet Engineering," *BioMed Research International*. Hindawi Limited, 2014. doi: 10.1155/2014/450672.

Mahdavi, S. S., Abdekhodaie, M. J., Mashayekhan, S., Baradaran-Rafii, A. and Djalilian, A. R. (2020) "Bioengineering Approaches for Corneal Regenerative Medicine," *Tissue Engineering and Regenerative Medicine*. Korean Tissue Engineering and Regenerative Medicine Society, pp. 1–27. doi: 10.1007/s13770-020-00262-8.

Mahdavi, S. S., Abdekhodaie, M. J., Kumar, H., Mashayekhan, S., Baradaran-Rafii, A. and Kim, K. (2020) "Stereolithography 3D Bioprinting Method for Fabrication of Human Corneal Stroma Equivalent," *Annals of Biomedical Engineering*. Springer, 48(7), pp. 1955–1970. doi: 10.1007/s10439-020-02537-6.

Mao, Q., Wang, Y., Li, Y., Juengpanich, S., Li, W., Chen, M., Yin, J., Fu, J. and Cai, X. (2020) "Fabrication of liver microtissue with liver decellularized extracellular matrix (dECM) bioink by digital light processing (DLP) bioprinting," *Materials Science and Engineering C*. Elsevier Ltd, 109, p. 110625. doi: 10.1016/j.msec.2020.110625.

MarketsandMarkets™ INC (2017) *3D Bioprinting Market by Technology (Microextrusion, Inkjet, Laser, Magnetic), Material (Cells, Hydrogels, Extracellular Matrices, Biomaterials), Application (Clinical (Bone, Cartilage, Skin) & Research (Regenerative Medicine)) - Global Forecasts to 2021*. Available at: https://www.marketresearch.com/MarketsandMarkets-v3719/3D-Bioprinting-Technology-Microextrusion-Inkjet-10615970/ (Accessed: June 4, 2020).

Markstedt, K., Mantas, A., Tournier, I., Martínez Ávila, H., Hägg, D. and Gatenholm, P. (2015) "3D bioprinting human chondrocytes with nanocellulose-alginate bioink for cartilage tissue engineering applications," *Biomacromolecules*. American Chemical

Society, 16(5), pp. 1489–1496. doi: 10.1021/acs.biomac.5b00188.

Marques, C. F., Diogo, G. S., Pina, S., Oliveira, J. M., Silva, T. H. and Reis, R. L. (2019) “Collagen-based bioinks for hard tissue engineering applications: a comprehensive review,” *Journal of Materials Science: Materials in Medicine*. Springer New York LLC, pp. 1–12. doi: 10.1007/s10856-019-6234-x.

Masaeli, E., Forster, V., Picaud, S., Karamali, F., Nasr-Esfahani, M. H. and Marquette, C. (2020) “Tissue engineering of retina through high resolution 3-dimensional inkjet bioprinting,” *Biofabrication*, 12(2). Available at: https://iopscience.iop.org/article/10.1088/1758-5090/ab4a20 (Accessed: May 15, 2020).

Masaeli, E. and Marquette, C. (2020) “Direct-Write Bioprinting Approach to Construct Multilayer Cellular Tissues,” *Frontiers in Bioengineering and Biotechnology*. Frontiers Media S.A., 7. doi: 10.3389/fbioe.2019.00478.

Masterton, S. and Ahearne, M. (2018) “Mechanobiology of the corneal epithelium,” *Experimental Eye Research*, 177. doi: 10.1016/j.exer.2018.08.001.

Matai, I., Kaur, G., Seyedsalehi, A., McClinton, A. and Laurencin, C. T. (2020) “Progress in 3D bioprinting technology for tissue/organ regenerative engineering,” *Biomaterials*. Elsevier Ltd, p. 119536. doi: 10.1016/j.biomaterials.2019.119536.

Matthyssen, S., Van den Bogerd, B., Dhubhghaill, S. N., Koppen, C. and Zakaria, N. (2018) “Corneal regeneration: A review of stromal replacements,” *Acta Biomaterialia*. Acta Materialia Inc, pp. 31–41. doi: 10.1016/j.actbio.2018.01.023.

Mazzocchi, A., Devarasetty, M., Huntwork, R., Soker, S. and Skardal, A. (2018) “Optimization of collagen type I-hyaluronan hybrid bioink for 3D bioprinted liver microenvironments,” *Biofabrication*, 11(1). Available at: https://iopscience.iop.org/article/10.1088/1758-5090/aae543 (Accessed: June 11, 2020).

McBeth, C., Lauer, J., Ottersbach, M., Campbell, J., Sharon, A. and Sauer-Budge, A. F. (2017) “3D bioprinting of GelMA scaffolds triggers mineral deposition by primary human osteoblasts,” *Biofabrication*, 9(1). Available at: https://iopscience.iop.org/article/10.1088/1758-5090/aa53bd (Accessed: June 1, 2020).

Medicines Agency, E. (2015) *Public summary of opinion on orphan designation Ex vivo expanded autologous human corneal epithelium containing stem cells for the treatment of corneal lesions, with associated corneal (limbal) stem cell deficiency, due to ocular burns*. Available at: www.ema.europa.eu/contact (Accessed: April 19, 2020).

Mienaltowski, M. J. and Birk, D. E. (2014) “Structure, Physiology, and Biochemistry of

Collagens," in. Springer, Dordrecht, pp. 5–29. doi: 10.1007/978-94-007-7893-1_2.

Mikhailova, A., Jylhä, A., Rieck, J., Nättinen, J., Ilmarinen, T., Veréb, Z., Aapola, U., Beuerman, R., Petrovski, G., Uusitalo, H. and Skottman, H. (2015) "Comparative proteomics reveals human pluripotent stem cell-derived limbal epithelial stem cells are similar to native ocular surface epithelial cells," *Scientific Reports*. Nature Publishing Group, 5. doi: 10.1038/srep14684.

Mikhailova, A., Ilmarinen, T., Ratnayake, A., Petrovski, G., Uusitalo, H., Skottman, H. and Rafat, M. (2016) "Human pluripotent stem cell-derived limbal epithelial stem cells on bioengineered matrices for corneal reconstruction," *Experimental Eye Research*. Academic Press, 146, pp. 26–34. doi: 10.1016/j.exer.2015.11.021.

Miotto, M., Gouveia, R. M., Ionescu, A. M., Figueiredo, F., Hamley, I. W. and Connon, C. J. (2019) "4D Corneal Tissue Engineering: Achieving Time-Dependent Tissue Self-Curvature through Localized Control of Cell Actuators," *Advanced Functional Materials*. Wiley-VCH Verlag, 29(8), p. 1807334. doi: 10.1002/adfm.201807334.

Mirdamadi, E., Muselimyan, N., Koti, P., Asfour, H. and Sarvazyan, N. (2019) "Agarose Slurry as a Support Medium for Bioprinting and Culturing Freestanding Cell-Laden Hydrogel Constructs," *3D Printing and Additive Manufacturing*. Mary Ann Liebert Inc., 6(3), pp. 158–164. doi: 10.1089/3dp.2018.0175.

Mobaraki, M., Abbasi, R., Vandchali, S. O., Ghaffari, M., Moztarzadeh, F. and Mozafari, M. (2019) "Corneal repair and regeneration: Current concepts and future directions," *Frontiers in Bioengineering and Biotechnology*. Frontiers Media S.A. doi: 10.3389/fbioe.2019.00135.

Moldovan, L., Barnard, A., Gil, C.-H., Lin, Y., Grant, M. B., Yoder, M. C., Prasain, N. and Moldovan, N. I. (2017) "iPSC-Derived Vascular Cell Spheroids as Building Blocks for Scaffold-Free Biofabrication," *Biotechnology Journal*. Wiley-VCH Verlag, 12(12), p. 1700444. doi: 10.1002/biot.201700444.

Moncal, K. K., Ozbolat, V., Datta, P., Heo, D. N. and Ozbolat, I. T. (2019) "Thermally-controlled extrusion-based bioprinting of collagen," *Journal of Materials Science: Materials in Medicine*. Springer New York LLC, 30(5), pp. 1–14. doi: 10.1007/s10856-019-6258-2.

Montero, R. B., Vial, X., Nguyen, D. T., Farhand, S., Reardon, M., Pham, S. M., Tsechpenakis, G. and Andreopoulos, F. M. (2012) "BFGF-containing electrospun gelatin scaffolds with controlled nano-architectural features for directed angiogenesis," *Acta Biomaterialia*. Elsevier, 8(5), pp. 1778–1791. doi: 10.1016/j.actbio.2011.12.008.

Morgan, F. L. C., Moroni, L. and Baker, M. B. (2020) “Dynamic Bioinks to Advance Bioprinting,” *Advanced Healthcare Materials*. Wiley-VCH Verlag, p. 1901798. doi: 10.1002/adhm.201901798.

Müller, M., Öztürk, E., Arlov, Ø., Gatenholm, P. and Zenobi-Wong, M. (2017) “Additive Manufacturing of Biomaterials, Tissues, and Organs Alginate Sulfate-Nanocellulose Bioinks for Cartilage Bioprinting Applications,” *Annals of Biomedical Engineering*, 45(1). doi: 10.1007/s10439-016-1704-5.

Nadernezhad, A., Caliskan, O. S., Topuz, F., Afghah, F., Erman, B. and Koc, B. (2019) “Nanocomposite Bioinks Based on Agarose and 2D Nanosilicates with Tunable Flow Properties and Bioactivity for 3D Bioprinting,” *ACS Applied Bio Materials*. American Chemical Society, 2(2), pp. 796–806. doi: 10.1021/acsabm.8b00665.

Nahmias, Y., Schwartz, R. E., Verfaillie, C. M. and Odde, D. J. (2005) “Laser-guided direct writing for three-dimensional tissue engineering,” *Biotechnology and Bioengineering*. John Wiley & Sons, Ltd, 92(2), pp. 129–136. doi: 10.1002/bit.20585.

Nahmias, Y. K., Gao, B. Z. and Odde, D. J. (2004) “Dimensionless parameters for the design of optical traps and laser guidance systems,” *Applied Optics*. OSA - The Optical Society, 43(20), pp. 3999–4006. doi: 10.1364/AO.43.003999.

Nahmias, Y. and Odde, D. J. (2006) “Micropatterning of living cells by laser-guided direct writing: Application to fabrication of hepatic-endothelial sinusoid-like structures,” *Nature Protocols*. Nature Publishing Group, 1(5), pp. 2288–2296. doi: 10.1038/nprot.2006.386.

Nakamura, T., Inatomi, T., Sotozono, C., Amemiya, T., Kanamura, N. and Kinoshita, S. (2004) “Transplantation of cultivated autologous oral mucosal epithelial cells in patients with severe ocular surface disorders,” *British Journal of Ophthalmology*. BMJ Publishing Group, 88(10), pp. 1280–1284. doi: 10.1136/bjo.2003.038497.

Nerger, B. A., Brun, P. T. and Nelson, C. M. (2019) “Microextrusion printing cell-laden networks of type i collagen with patterned fiber alignment and geometry,” *Soft Matter*. Royal Society of Chemistry, 15(28), pp. 5728–5738. doi: 10.1039/c8sm02605j.

Ng, W. L., Goh, M. H., Yeong, W. Y. and Naing, M. W. (2018) “Applying macromolecular crowding to 3D bioprinting: Fabrication of 3D hierarchical porous collagen-based hydrogel constructs,” *Biomaterials Science*. Royal Society of Chemistry, 6(3), pp. 562–574. doi: 10.1039/c7bm01015j.

Nguyen, D., Hgg, D. A., Forsman, A., Ekholm, J., Nimkingratana, P., Brantsing, C., Kalogeropoulos, T., Zaunz, S., Concaro, S., Brittberg, M., Lindahl, A., Gatenholm, P.,

Enejder, A. and Simonsson, S. (2017) “Cartilage Tissue Engineering by the 3D Bioprinting of iPS Cells in a Nanocellulose/Alginate Bioink,” *Scientific Reports*. Nature Publishing Group, 7(1). doi: 10.1038/s41598-017-00690-y.

Nguyen, K. N., Bobba, S., Richardson, A., Park, M., Watson, S. L., Wakefield, D. and Di Girolamo, N. (2018) “Native and synthetic scaffolds for limbal epithelial stem cell transplantation,” *Acta Biomaterialia*. Acta Materialia Inc, pp. 21–35. doi: 10.1016/j.actbio.2017.10.037.

Nguyen, Q. V., Huynh, D. P., Park, J. H. and Lee, D. S. (2015) “Injectable polymeric hydrogels for the delivery of therapeutic agents: A review,” *European Polymer Journal*. Elsevier Ltd, 72, pp. 602–619. doi: 10.1016/j.eurpolymj.2015.03.016.

O’Connell, C., Ren, J., Pope, L., Li, Y., Mohandas, A., Blanchard, R., Duchi, S. and Onofrillo, C. (2020) “Characterizing Bioinks for Extrusion Bioprinting: Printability and Rheology,” in Crook, J. M. (ed.) *3D Bioprinting: Principles and Protocols*. Humana Press, pp. 111–133. Available at: http://www.springer.com/series/7651.

Odde, D. J. and Renn, M. J. (1999) “Laser-guided direct writing for applications in biotechnology,” *Trends in Biotechnology*. Elsevier Ltd, pp. 385–389. doi: 10.1016/S0167-7799(99)01355-4.

Ojansivu, M., Rashad, A., Ahlinder, A., Massera, J., Mishra, A., Syverud, K., Finne-Wistrand, A., Miettinen, S. and Mustafa, K. (2019) “Wood-based nanocellulose and bioactive glass modified gelatin-alginate bioinks for 3D bioprinting of bone cells,” *Biofabrication*. Institute of Physics Publishing, 11(3). doi: 10.1088/1758-5090/ab0692.

Oliva, J., Bardag-Gorce, F. and Niihara, Y. (2020) “Clinical trials of limbal stem cell deficiency treated with oral mucosal epithelial cells,” *International Journal of Molecular Sciences*. MDPI AG. doi: 10.3390/ijms21020411.

Ong, C. S., Fukunishi, T., Zhang, H., Huang, C. Y., Nashed, A., Blazeski, A., Disilvestre, D., Vricella, L., Conte, J., Tung, L., Tomaselli, G. F. and Hibino, N. (2017) “Biomaterial-Free Three-Dimensional Bioprinting of Cardiac Tissue using Human Induced Pluripotent Stem Cell Derived Cardiomyocytes,” *Scientific Reports*. Nature Publishing Group, 7(1), pp. 1–11. doi: 10.1038/s41598-017-05018-4.

Ong, C. S., Yesantharao, P., Huang, C. Y., Mattson, G., Boktor, J., Fukunishi, T., Zhang, H. and Hibino, N. (2018) “3D bioprinting using stem cells,” *Pediatric Research*. Nature Publishing Group, pp. 223–231. doi: 10.1038/pr.2017.252.

Ortega, Í., Ryan, A. J., Deshpande, P., Macneil, S. and Claeyssens, F. (2012) “Combined microfabrication and electrospinning to produce 3-D architectures for corneal

repair.” doi: 10.1016/j.actbio.2012.10.039.

Ortuño-Costela, M. D. C., Cerrada, V., García-López, M. and Gallardo, M. E. (2019) “The challenge of bringing iPSCs to the patient,” *International Journal of Molecular Sciences*. MDPI AG. doi: 10.3390/ijms20246305.

Osei-Bempong, C., Figueiredo, F. C. and Lako, M. (2013) “The limbal epithelium of the eye - A review of limbal stem cell biology, disease and treatment,” *BioEssays*. John Wiley & Sons, Ltd, 35(3), pp. 211–219. doi: 10.1002/bies.201200086.

Ouyang, L., Highley, C. B., Rodell, C. B., Sun, W. and Burdick, J. A. (2016) “3D Printing of Shear-Thinning Hyaluronic Acid Hydrogels with Secondary Cross-Linking.” doi: 10.1021/acsbiomaterials.6b00158.

Ovsianikov, A., Khademhosseini, A. and Mironov, V. (2018) “The Synergy of Scaffold-Based and Scaffold-Free Tissue Engineering Strategies,” *Trends in Biotechnology*. Elsevier Ltd, pp. 348–357. doi: 10.1016/j.tibtech.2018.01.005.

Pan, T., Song, W., Cao, X. and Wang, Y. (2016) “3D Bioplotting of Gelatin/Alginate Scaffolds for Tissue Engineering: Influence of Crosslinking Degree and Pore Architecture on Physicochemical Properties,” *Journal of Materials Science and Technology*. Chinese Society of Metals, 32(9), pp. 889–900. doi: 10.1016/j.jmst.2016.01.007.

Parak, A., Pradeep, P., du Toit, L. C., Kumar, P., Choonara, Y. E. and Pillay, V. (2019) “Functionalizing bioinks for 3D bioprinting applications,” *Drug Discovery Today*. Elsevier Ltd, pp. 198–205. doi: 10.1016/j.drudis.2018.09.012.

Pati, F., Ha, D. H., Jang, J., Han, H. H., Rhie, J. W. and Cho, D. W. (2015) “Biomimetic 3D tissue printing for soft tissue regeneration,” *Biomaterials*. Elsevier Ltd, 62, pp. 164–175. doi: 10.1016/j.biomaterials.2015.05.043.

Pellegrini, G., Traverso, C. E., Franzi, A. T., Zingirian, M., Cancedda, R. and De Luca, M. (1997) “Long-term restoration of damaged corneal surfaces with autologous cultivated corneal epithelium,” *Lancet*. Lancet Publishing Group, 349(9057), pp. 990–993. doi: 10.1016/S0140-6736(96)11188-0.

Pellegrini, G., Ardigò, D., Milazzo, G., Iotti, G., Guatelli, P., Pelosi, D. and De Luca, M. (2018) “Navigating Market Authorization: The Path Holoclar Took to Become the First Stem Cell Product Approved in the European Union,” *STEM CELLS Translational Medicine*. John Wiley and Sons Ltd., 7(1), pp. 146–154. doi: 10.1002/sctm.17-0003.

Pereira, R. F. and Bártolo, P. J. (2015) “3D bioprinting of photocrosslinkable hydrogel constructs,” *Journal of Applied Polymer Science*, 132(48), p. n/a-n/a. doi:

10.1002/app.42458.

Petta, D., Armiento, A. R., Grijpma, D., Alini, M., Eglin, D. and D'Este, M. (2018) "3D bioprinting of a hyaluronan bioink through enzymatic-and visible light-crosslinking," *Biofabrication*. Institute of Physics Publishing, 10(4). doi: 10.1088/1758-5090/aadf58.

Poldervaart, Michelle T., Goversen, B., de Ruijter, M., Abbadessa, A., Melchels, F. P. W., Öner, F. C., Dhert, W. J. A., Vermonden, T. and Alblas, J. (2017) "3D bioprinting of methacrylated hyaluronic acid (MeHA) hydrogel with intrinsic osteogenicity," *PLOS ONE*. Edited by M. Yamamoto. Public Library of Science, 12(6), p. e0177628. doi: 10.1371/journal.pone.0177628.

Poldervaart, Michelle T, Goversen, B., de Ruijter, M., Abbadessa, A., W Melchels, F. P., Cumhur, F. O., A Dhert, W. J., Vermonden, T. and Alblas, J. (2017) "3D bioprinting of methacrylated hyaluronic acid (MeHA) hydrogel with intrinsic osteogenicity," *PLoS One*, 12(6). doi: 10.1371/journal.pone.0177628.

Prabhasawat, P., Ekpo, P., Uiprasertkul, M., Chotikavanich, S., Tesavibul, N., Pornpanich, K. and Luemsamran, P. (2016) "Long-term result of autologous cultivated oral mucosal epithelial transplantation for severe ocular surface disease," *Cell and Tissue Banking*. Springer Netherlands, 17(3), pp. 491–503. doi: 10.1007/s10561-016-9575-4.

Prendergast, M. E. and Burdick, J. A. (2020) "Recent Advances in Enabling Technologies in 3D Printing for Precision Medicine," *Advanced Materials*. Wiley-VCH Verlag, 32(13), p. 1902516. doi: 10.1002/adma.201902516.

Priyadarsini, S., Nicholas, S. E. and Karamichos, D. (2018) "3D stacked construct: A novel substitute for corneal tissue engineering," in *Methods in Molecular Biology*. Humana Press Inc., pp. 173–180. doi: 10.1007/7651_2017_23.

Raddatz, L., Lavrentieva, A., Pepelanova, I., Bahnemann, J., Geier, D., Becker, T., Scheper, T. and Beutel, S. (2018) "Development and application of an additively manufactured calcium chloride nebulizer for alginate 3D-bioprinting purposes," *Journal of Functional Biomaterials*. MDPI AG, 9(4). doi: 10.3390/jfb9040063.

Rafat, M., Xeroudaki, M., Koulikovska, M., Sherrell, P., Groth, F., Fagerholm, P. and Lagali, N. (2016) "Composite core-and-skirt collagen hydrogels with differential degradation for corneal therapeutic applications," *Biomaterials*. Elsevier Ltd, 83, pp. 142–155. doi: 10.1016/j.biomaterials.2016.01.004.

Rajaram, A., Schreyer, D. and Chen, D. (2014) "Bioplotting Alginate / Hyaluronic Acid Hydrogel Scaffolds with Structural Integrity and Preserved Schwann Cell Viability," *3D*

Printing and Additive Manufacturing, 1(4). doi: 10.1089/3dp.2014.0006.

Ravichandran, R., Islam, M. M., Alarcon, E. I., Samanta, A., Wang, S., Lundström, P., Hilborn, J., Griffith, M. and Phopase, J. (2016) “Functionalised type-I collagen as a hydrogel building block for bio-orthogonal tissue engineering applications,” *Journal of Materials Chemistry B*. Royal Society of Chemistry, 4(2), pp. 318–326. doi: 10.1039/c5tb02035b.

Rehakova, D., Souralova, T. and Koutna, I. (2020) “Clinical-Grade Human Pluripotent Stem Cells for Cell Therapy: Characterization Strategy,” *International Journal of Molecular Sciences*. MDPI AG, 21(7), p. 2435. doi: 10.3390/ijms21072435.

Rodríguez-Salvador, M., Rio-Belver, M. R. and Garechana-Anacabe, G. (2017) “Scientometric and patentometric analyses to determine the knowledge landscape in innovative technologies: The case of 3D bioprinting,” *PLoS ONE*, 12(6). doi: 10.1371/journal.pone.0180375.

Rutz, A. L., Gargus, E. S., Hyland, K. E., Lewis, P. L., Setty, A., Burghardt, W. R. and Shah, R. N. (2019) “Employing PEG crosslinkers to optimize cell viability in gel phase bioinks and tailor post printing mechanical properties,” *Acta Biomaterialia*, 99, pp. 121–132. doi: 10.1016/j.actbio.2019.09.007.

Saeed, H. N., Shanbhag, S. and Chodosh, J. (2017) “The Boston keratoprosthesis,” *Current Opinion in Ophthalmology*. Lippincott Williams and Wilkins, 28(4), pp. 390–396. doi: 10.1097/ICU.0000000000000373.

Sahle, F. F., Kim, S., Niloy, K. K., Tahia, F., Fili, C. V., Cooper, E., Hamilton, D. J. and Lowe, T. L. (2019) “Nanotechnology in regenerative ophthalmology,” *Advanced Drug Delivery Reviews*. Elsevier B.V., pp. 290–307. doi: 10.1016/j.addr.2019.10.006.

Sakai, S., Ohi, H., Hotta, T., Kamei, H. and Taya, M. (2018) “Differentiation potential of human adipose stem cells bioprinted with hyaluronic acid/gelatin-based bioink through microextrusion and visible light-initiated crosslinking,” *Biopolymers*, 109(2), p. e23080. doi: 10.1002/bip.23080.

Salaris, Colosi, Brighi, Soloperto, Turris, Benedetti, Ghirga, Rosito, Di Angelantonio and Rosa (2019) “3D Bioprinted Human Cortical Neural Constructs Derived from Induced Pluripotent Stem Cells,” *Journal of Clinical Medicine*. MDPI AG, 8(10), p. 1595. doi: 10.3390/jcm8101595.

Salaris, F. and Rosa, A. (2019) “Construction of 3D in vitro models by bioprinting human pluripotent stem cells: Challenges and opportunities,” *Brain Research*. Elsevier B.V., p. 146393. doi: 10.1016/j.brainres.2019.146393.

Salehi, S., Czugala, M., Stafiej, P., Fathi, M., Bahners, T., Gutmann, J. S., Singer, B. B. and Fuchsluger, T. A. (2017) “Poly (glycerol sebacate)-poly (ε-caprolactone) blend nanofibrous scaffold as intrinsic bio- and immunocompatible system for corneal repair,” *Acta Biomaterialia*. Elsevier Ltd, 50, pp. 370–380. doi: 10.1016/j.actbio.2017.01.013.

Samoila, O. and Gocan, D. (2020) “Clinical Outcomes From Cultivated Allogenic Stem Cells vs. Oral Mucosa Epithelial Transplants in Total Bilateral Stem Cells Deficiency,” *Frontiers in Medicine*. Frontiers Media S.A. doi: 10.3389/fmed.2020.00043.

Sangwan, V. S., Basu, S., Macneil, S. and Balasubramanian, D. (2012) “Simple limbal epithelial transplantation (SLET): a novel surgical technique for the treatment of unilateral limbal stem cell deficiency,” *Br J Ophthalmol*, 96(7). doi: 10.1136/bjophthalmol-2011-301164.

Sanie-Jahromi, F., Eghtedari, M., Mirzaei, E., Jalalpour, M. H., Asvar, Z., Nejabat, M. and Javidi-Azad, F. (2020) “Propagation of limbal stem cells on polycaprolactone and polycaprolactone/gelatin fibrous scaffolds and transplantation in animal model,” *BioImpacts*. Tabriz University of Medical Sciences, 10(1), pp. 44–54. doi: 10.15171/bi.2020.06.

Sarker, M., Izadifar, M., Schreyer, D. and Chen, X. (2018) “Influence of ionic crosslinkers (Ca^{2+} /Ba^{2+} /Zn^{2+}) on the mechanical and biological properties of 3D Bioplotted Hydrogel Scaffolds,” *Journal of Biomaterials Science, Polymer Edition*. Taylor and Francis Inc., 29(10), pp. 1126–1154. doi: 10.1080/09205063.2018.1433420.

Schmidt, S. K., Schmid, R., Arkudas, A., Kengelbach-Weigand, A. and Bosserhoff, A. K. (2019) “Tumor Cells Develop Defined Cellular Phenotypes After 3D-Bioprinting in Different Bioinks,” *Cells*. MDPI AG, 8(10), p. 1295. doi: 10.3390/cells8101295.

Schuurman, W., Levett, P. A., Pot, M. W., van Weeren, P. R., Dhert, W. J. A., Hutmacher, D. W., Melchels, F. P. W., Klein, T. J. and Malda, J. (2013) “Gelatin-Methacrylamide Hydrogels as Potential Biomaterials for Fabrication of Tissue-Engineered Cartilage Constructs,” *Macromolecular Bioscience*, 13(5), pp. 551–561. doi: 10.1002/mabi.201200471.

Selcan Gungor-Ozkerim, P., Inci, I., Zhang, Y. S., Khademhosseini, A. and Dokmeci, M. R. (2018) “Biomaterials Science REVIEW Bioinks for 3D bioprinting: an overview,” *Biomaterials Science*, 6, p. 915. doi: 10.1039/c7bm00765e.

Serban, M. A. and Skardal, A. (2019) “Hyaluronan chemistries for three-dimensional matrix applications,” *Matrix Biology*. Elsevier B.V., pp. 337–345. doi: 10.1016/j.matbio.2018.02.010.

Shanbhag, S. S., Saeed, H. N., Paschalis, E. I. and Chodosh, J. (2018) “Boston keratoprosthesis type 1 for limbal stem cell deficiency after severe chemical corneal injury: A systematic review,” *Ocular Surface*. Elsevier Inc., pp. 272–281. doi: 10.1016/j.jtos.2018.03.007.

Shanbhag, S. S., Hall, L., Chodosh, J. and Saeed, H. N. (2020) “Long-term outcomes of amniotic membrane treatment in acute Stevens-Johnson syndrome/toxic epidermal necrolysis,” *Ocular Surface*. Elsevier Inc. doi: 10.1016/j.jtos.2020.03.004.

Sharma, R., Smits, I. P. M., De La Vega, L., Lee, C. and Willerth, S. M. (2020) “3D Bioprinting Pluripotent Stem Cell Derived Neural Tissues Using a Novel Fibrin Bioink Containing Drug Releasing Microspheres,” *Frontiers in Bioengineering and Biotechnology*. Frontiers Media S.A., 8. doi: 10.3389/fbioe.2020.00057.

Sharma, S., Mohanty, S., Gupta, D., Jassal, M., Agrawal, A. K. and Tandon, R. (2011) “Cellular response of limbal epithelial cells on electrospun poly-ε- caprolactone nanofibrous scaffolds for ocular surface bioengineering: A preliminary in vitro study,” *Molecular Vision*. Emory University, 17, pp. 2898–2910.

Shi, L., Carstensen, H., Hölzl, K., Lunzer, M., Li, H., Hilborn, J., Ovsianikov, A. and Ossipov, D. A. (2017) “Dynamic Coordination Chemistry Enables Free Directional Printing of Biopolymer Hydrogel,” *Chemistry of Materials*. American Chemical Society, 29(14), pp. 5816–5823. doi: 10.1021/acs.chemmater.7b00128.

Shi, P., Tan, Y. S. E., Yeong, W. Y., Li, H. Y. and Laude, A. (2018) “A bilayer photoreceptor-retinal tissue model with gradient cell density design: A study of microvalve-based bioprinting,” *Journal of Tissue Engineering and Regenerative Medicine*. John Wiley and Sons Ltd, 12(5), pp. 1297–1306. doi: 10.1002/term.2661.

Shin, J. Y., Yeo, Y. H., Jeong, J. E., Park, S. A. and Park, W. H. (2020) “Dual-crosslinked methylcellulose hydrogels for 3D bioprinting applications,” *Carbohydrate Polymers*. Elsevier Ltd, 238, p. 116192. doi: 10.1016/j.carbpol.2020.116192.

Shin, S., Park, S., Park, M., Jeong, E., Na, K., Youn, H. J. and Hyun, J. (2017) “Cellulose Nanofibers for the Enhancement of Printability of Low Viscosity Gelatin Derivatives | Shin | BioResources,” *BioResources*, 12(2). Available at: https://ojs.cnr.ncsu.edu/index.php/BioRes/article/view/BioRes_12_2_2941_Shin_Cellulose_Nanofiber_Enhancement_Printability/5159 (Accessed: March 16, 2020).

Sigma Aldrich (no date) *TissueFab® - GelMA-UV bioink*. Available at: https://www.sigmaaldrich.com/catalog/product/aldrich/905429?lang=fi&region=FI (Accessed: June 1, 2020).

Skardal, A., Zhang, J., Mccoard, L., Xu, X., Oottamasathien, S. and Prestwich, G. D. (2010) “Photocrosslinkable Hyaluronan-Gelatin Hydrogels for Two-Step Bioprinting,” *Tissue Engineering Part A*, 16(8). doi: 10.1089/ten.tea.2009.0798.

Skardal, A., Devarasetty, M., Kang, H. W., Mead, I., Bishop, C., Shupe, T., Lee, S. J., Jackson, J., Yoo, J., Soker, S. and Atala, A. (2015) “A hydrogel bioink toolkit for mimicking native tissue biochemical and mechanical properties in bioprinted tissue constructs,” *Acta Biomaterialia*. Elsevier Ltd, 25, pp. 24–34. doi: 10.1016/j.actbio.2015.07.030.

Skardal, A., Devarasetty, M., Kang, H. W., Seol, Y. J., Forsythe, S. D., Bishop, C., Shupe, T., Soker, S. and Atala, A. (2016) “Bioprinting cellularized constructs using a tissue-specific hydrogel bioink,” *Journal of Visualized Experiments*. Journal of Visualized Experiments, 2016(110). doi: 10.3791/53606.

Soliman, B. G., Lindberg, G. C. J., Jungst, T., Hooper, G. J., Groll, J., Woodfield, T. B. F. and Lim, K. S. (2020) “Stepwise Control of Crosslinking in a One-Pot System for Bioprinting of Low-Density Bioinks,” *Advanced Healthcare Materials*. Wiley-VCH Verlag, p. 1901544. doi: 10.1002/adhm.201901544.

Sommer, A. C. and Blumenthal, E. Z. (2019) “Implementations of 3D printing in ophthalmology,” *Graefe’s Archive for Clinical and Experimental Ophthalmology*. Springer Verlag, pp. 1815–1822. doi: 10.1007/s00417-019-04312-3.

Song, J. E., Sim, B. R., Jeon, Y. S., Kim, H. S., Shin, E. Y., Carlomagno, C. and Khang, G. (2019) “Characterization of surface modified glycerol/silk fibroin film for application to corneal endothelial cell regeneration,” *Journal of Biomaterials Science, Polymer Edition*. Taylor and Francis Inc., 30(4), pp. 263–275. doi: 10.1080/09205063.2018.1535819.

Sorkio, A., Koch, L., Koivusalo, L., Deiwick, A., Miettinen, S., Chichkov, B. and Skottman, H. (2018) “Human stem cell based corneal tissue mimicking structures using laser-assisted 3D bioprinting and functional bioinks,” *Biomaterials*, 171, pp. 57–71. doi: 10.1016/j.biomaterials.2018.04.034.

Spearman, B. S., Agrawal, N. K., Rubiano, A., Simmons, C. S., Mobini, S. and Schmidt, C. E. (2020) “Tunable methacrylated hyaluronic acid-based hydrogels as scaffolds for soft tissue engineering applications,” *Journal of Biomedical Materials Research Part A*, 108(2), pp. 279–291. doi: 10.1002/jbm.a.36814.

Sridhar, M. S. (2018) “Anatomy of cornea and ocular surface,” *Indian Journal of Ophthalmology*. Medknow Publications, pp. 190–194. doi: 10.4103/ijo.IJO_646_17.

Stafiej, P., Küng, F., Thieme, D., Czugala, M., Kruse, F. E., Schubert, D. W. and Fuchsluger, T. A. (2017) “Adhesion and metabolic activity of human corneal cells on PCL based nanofiber matrices,” *Materials Science and Engineering C*. Elsevier Ltd, 71, pp. 764–770. doi: 10.1016/j.msec.2016.10.058.

Stichler, S., Bertlein, S., Tessmar, J., Jüngst, T. and Groll, J. (2017) “Thiol-ene Cross-Linkable Hydrogels as Bioinks for Biofabrication,” *Macromolecular Symposia*. Wiley-VCH Verlag, 372(1), pp. 102–107. doi: 10.1002/masy.201600173.

Syed-Picard, F. N., Du, Y., Hertsenberg, A. J., Palchesko, R., Funderburgh, M. L., Feinberg, A. W. and Funderburgh, J. L. (2018) “Scaffold-free tissue engineering of functional corneal stromal tissue,” *Journal of Tissue Engineering and Regenerative Medicine*. John Wiley and Sons Ltd, 12(1), pp. 59–69. doi: 10.1002/term.2363.

TA Instruments (no date) *Understanding Rheology of Structured Fluids - AAN016*. Available at: https://www.tainstruments.com/applications-library-search/ (Accessed: July 24, 2020).

Takahashi, K., Tanabe, K., Ohnuki, M., Narita, M., Ichisaka, T., Tomoda, K. and Yamanaka, S. (2007) “Induction of Pluripotent Stem Cells from Adult Human Fibroblasts by Defined Factors,” *Cell*. Cell Press, 131(5), pp. 861–872. doi: 10.1016/j.cell.2007.11.019.

Tan, Y. J., Tan, X., Yeong, W. Y. and Tor, S. B. (2016) “Hybrid microscaffold-based 3D bioprinting of multi-cellular constructs with high compressive strength: A new biofabrication strategy,” *Scientific Reports*. Nature Publishing Group, 6(1), pp. 1–13. doi: 10.1038/srep39140.

Thayer, P. S., Orrhult, L. S. and Martínez, H. (2018) “Bioprinting of cartilage and skin tissue analogs utilizing a novel passive mixing unit technique for bioink precellularization,” *Journal of Visualized Experiments*. Journal of Visualized Experiments, 2018(131). doi: 10.3791/56372.

Thoft, R. A. and Friend, J. (1983) “The X, Y, Z hypothesis of corneal epithelial maintenance,” *Investigative Ophtalmology & Visual Science*, 24(10). Available at: https://iovs.arvojournals.org/article.aspx?articleid=2159583 (Accessed: May 20, 2020).

Thomson, J. A., Itskovitz-Eldor, J., Shapiro, S. S., Waknitz, M. A., Swiergiel, J. J., Marshall, V. S. and Jones, J. M. (1998) “Embryonic stem cell lines derived from human blastocysts,” *Science*. American Association for the Advancement of Science, 282(5391), pp. 1145–1147. doi: 10.1126/science.282.5391.1145.

Tigner, T. J., Rajput, S., Gaharwar, A. K. and Alge, D. L. (2019) “Comparison of Photo

Cross Linkable Gelatin Derivatives and Initiators for Three-Dimensional Extrusion Bioprinting.” doi: 10.1021/acs.biomac.9b01204.

Tigner, T. J., Rajput, S., Gaharwar, A. K. and Alge, D. L. (2020) “Comparison of Photo Cross Linkable Gelatin Derivatives and Initiators for Three-Dimensional Extrusion Bioprinting,” *Biomacromolecules*. American Chemical Society, 21(2), pp. 454–463. doi: 10.1021/acs.biomac.9b01204.

Tonsomboon, K., Strange, D. G. T. and Oyen, M. L. (2013) “Gelatin nanofiber-reinforced alginate gel scaffolds for corneal tissue engineering,” in *Proceedings of the Annual International Conference of the IEEE Engineering in Medicine and Biology Society, EMBS*, pp. 6671–6674. doi: 10.1109/EMBC.2013.6611086.

Torras, N., García-Díaz, M., Fernández-Majada, V. and Martínez, E. (2018) “Mimicking epithelial tissues in three-dimensional cell culture models,” *Frontiers in Bioengineering and Biotechnology*. Frontiers Media S.A. doi: 10.3389/fbioe.2018.00197.

Trampe, E., Koren, K., Akkineni, A. R., Senwitz, C., Krujatz, F., Lode, A., Gelinsky, M. and Kühl, M. (2018) “Functionalized Bioink with Optical Sensor Nanoparticles for O_2 Imaging in 3D-Bioprinted Constructs,” *Advanced Functional Materials*. Wiley-VCH Verlag, 28(45), p. 1804411. doi: 10.1002/adfm.201804411.

Tröndle, K., Koch, F., Finkenzeller, G., Stark, G. B., Zengerle, R., Koltay, P. and Zimmermann, S. (2019) “Bioprinting of high cell-density constructs leads to controlled lumen formation with self-assembly of endothelial cells,” *Journal of Tissue Engineering and Regenerative Medicine*. John Wiley and Sons Ltd, 13(10), pp. 1883–1895. doi: 10.1002/term.2939.

Tse, C., Whiteley, R., Yu, T., Stringer, J., MacNeil, S., Haycock, J. W. and Smith, P. J. (2016) “Inkjet printing Schwann cells and neuronal analogue NG108-15 cells,” *Biofabrication*, 8(1). Available at: https://iopscience.iop.org/article/10.1088/1758-5090/8/1/015017 (Accessed: June 16, 2020).

Tytgat, L., Van Damme, L., Van Hoorick, J., Declercq, H., Thienpont, H., Ottevaere, H., Blondeel, P., Dubruel, P. and Van Vlierberghe, S. (2019) “Additive manufacturing of photo-crosslinked gelatin scaffolds for adipose tissue engineering,” *Acta Biomaterialia*. Acta Materialia Inc, 94, pp. 340–350. doi: 10.1016/j.actbio.2019.05.062.

Utheim, T. P. (2013) “Limbal Epithelial Cell Therapy: Past, Present, and Future,” in. Humana Press, Totowa, NJ, pp. 3–43. doi: 10.1007/978-1-62703-432-6_1.

Vaidyanathan, U., Hopping, G. C., Liu, H. Y., Somani, A. N., Ronquillo, Y. C., Hoopes, P. C. and Moshirfar, M. (2019) “Persistent Corneal Epithelial Defects: A Review Article.,”

Medical hypothesis, discovery & innovation ophthalmology journal. Middle East Persian Teb International Co, 8(3), pp. 163–176. Available at: http://www.ncbi.nlm.nih.gov/pubmed/31598519 (Accessed: May 4, 2020).

Vázquez, N., Rodríguez-Barrientos, C. A., Aznar-Cervantes, S. D., Chacón, M., Cenis, J. L., Riestra, A. C., Sánchez-Avila, R. M., Persinal, M., Brea-Pastor, A., Fernández-Vega Cueto, L., Meana, Á. and Merayo-Lloves, J. (2017) "Silk fibroin films for corneal endothelial regeneration: Transplant in a rabbit descemet membrane endothelial keratoplasty," *Investigative Ophthalmology and Visual Science*. Association for Research in Vision and Ophthalmology Inc., 58(9), pp. 3357–3365. doi: 10.1167/iovs.17-21797.

Venugopal, B., Shenoy, S. J., Mohan, S., Anil Kumar, P. R. and Kumary, T. V. (2020) "Bioengineered corneal epithelial cell sheet from mesenchymal stem cells—A functional alternative to limbal stem cells for ocular surface reconstruction," *Journal of Biomedical Materials Research Part B: Applied Biomaterials*. John Wiley and Sons Inc., 108(3), pp. 1033–1045. doi: 10.1002/jbm.b.34455.

Vijayavenkataraman, S., Yan, W. C., Lu, W. F., Wang, C. H. and Fuh, J. Y. H. (2018) "3D bioprinting of tissues and organs for regenerative medicine," *Advanced Drug Delivery Reviews*. Elsevier B.V., pp. 296–332. doi: 10.1016/j.addr.2018.07.004.

Walimbe, T., Calve, S., Panitch, A. and Sivasankar, M. P. (2019) "Incorporation of types I and III collagen in tunable hyaluronan hydrogels for vocal fold tissue engineering," *Acta Biomaterialia*. Acta Materialia Inc, 87, pp. 97–107. doi: 10.1016/j.actbio.2019.01.058.

Wang, S., Ghezzi, C. E., Gomes, R., Pollard, R. E., Funderburgh, J. L. and Kaplan, D. L. (2017) "In vitro 3D corneal tissue model with epithelium, stroma, and innervation," *Biomaterials*. Elsevier Ltd, 112, pp. 1–9. doi: 10.1016/j.biomaterials.2016.09.030.

Wang, X., Wang, Q. and Xu, C. (2020) "Nanocellulose-Based Inks for 3D Bioprinting: Key Aspects in Research Development and Challenging Perspectives in Applications—A Mini Review," *Bioengineering*. MDPI AG, 7(2), p. 40. doi: 10.3390/bioengineering7020040.

Wang, Y. J., Li, C. Y., Wang, Z. J., Zhao, Y., Chen, L., Wu, Z. L. and Zheng, Q. (2018) "Hydrogen bond-reinforced double-network hydrogels with ultrahigh elastic modulus and shape memory property," *Journal of Polymer Science Part B: Polymer Physics*. John Wiley and Sons Inc., 56(19), pp. 1281–1286. doi: 10.1002/polb.24620.

Williams, D., Thayer, P., Martinez, H., Gatenholm, E. and Khademhosseini, A. (2018)

"A perspective on the physical, mechanical and biological specifications of bioinks and the development of functional tissues in 3D bioprinting," *Bioprinting*. Elsevier B.V., pp. 19–36. doi: 10.1016/j.bprint.2018.02.003.

Wilson, S. E., Torricelli, A. A. M. and Marino, G. K. (2020) "Corneal epithelial basement membrane: Structure, function and regeneration," *Experimental Eye Research*. Academic Press, p. 108002. doi: 10.1016/j.exer.2020.108002.

Włodarczyk-Biegun, M. K. and del Campo, A. (2017) "3D bioprinting of structural proteins," *Biomaterials*. Elsevier Ltd, pp. 180–201. doi: 10.1016/j.biomaterials.2017.04.019.

Wu, J., Rnjak-Kovacina, J., Du, Y., Funderburgh, M. L., Kaplan, D. L. and Funderburgh, J. L. (2014) "Corneal stromal bioequivalents secreted on patterned silk substrates," *Biomaterials*. Elsevier, 35(12), pp. 3744–3755. doi: 10.1016/j.biomaterials.2013.12.078.

Wu, Z., Su, X., Xu, Y., Kong, B., Sun, W. and Mi, S. (2016) "Bioprinting three-dimensional cell-laden tissue constructs with controllable degradation," *Scientific Reports*. Nature Publishing Group, 6. doi: 10.1038/srep24474.

Xin, S., Chimene, D., Garza, J. E., Gaharwar, A. K. and Alge, D. L. (2019) "Clickable PEG hydrogel microspheres as building blocks for 3D bioprinting," *Biomaterials Science*. Royal Society of Chemistry, 7(3), pp. 1179–1187. doi: 10.1039/c8bm01286e.

Xu, W., Wang, Z., Liu, Y., Wang, L., Jiang, Z., Li, T., Zhang, W. and Liang, Y. (2018) "Carboxymethyl chitosan/gelatin/hyaluronic acid blended-membranes as epithelia transplanting scaffold for corneal wound healing," *Carbohydrate Polymers*. Elsevier Ltd, 192, pp. 240–250. doi: 10.1016/j.carbpol.2018.03.033.

Xu, W., Molino, B. Z., Cheng, F., Molino, P. J., Yue, Z., Su, D., Wang, X., Willför, S., Xu, C. and Wallace, G. G. (2019) "On Low-Concentration Inks Formulated by Nanocellulose Assisted with Gelatin Methacrylate (GelMA) for 3D Printing toward Wound Healing Application," *ACS Applied Materials and Interfaces*. American Chemical Society, 11(9), pp. 8838–8848. doi: 10.1021/acsami.8b21268.

Yang, X., Lu, Z., Wu, H., Li, W., Zheng, L. and Zhao, J. (2018) "Collagen-alginate as bioink for three-dimensional (3D) cell printing based cartilage tissue engineering," *Materials Science and Engineering C*. Elsevier Ltd, 83, pp. 195–201. doi: 10.1016/j.msec.2017.09.002.

Yazdani, M., Shahdadfar, A., Jackson, C. J. and Utheim, T. P. (2019) "Hyaluronan-Based Hydrogel Scaffolds for Limbal Stem Cell Transplantation: A Review," *Cells*. MDPI

AG, 8(3), p. 245. doi: 10.3390/cells8030245.

Yazdanpanah, G., Haq, Z., Kang, K., Jabbehdari, S., Rosenblatt, M. I. and Djalilian, A. R. (2019) “Strategies for reconstructing the limbal stem cell niche,” *Ocular Surface*. Elsevier Inc., pp. 230–240. doi: 10.1016/j.jtos.2019.01.002.

Ye, J., Shi, X., Chen, X., Xie, J., Wang, C., Yao, K., Gao, C. and Gou, Z. (2014) “Chitosan-modified, collagen-based biomimetic nanofibrous membranes as selective cell adhering wound dressings in the treatment of chemically burned corneas,” *Journal of Materials Chemistry B*. Royal Society of Chemistry, 2(27), pp. 4226–4236. doi: 10.1039/c3tb21845g.

Yin, J., Yan, M., Wang, Y., Fu, J. and Suo, H. (2018) “3D Bioprinting of Low-Concentration Cell-Laden Gelatin Methacrylate (GelMA) Bioinks with a Two-Step Cross-linking Strategy,” *ACS Appl. Mater. Interfaces*, 10(8). doi: 10.1021/acsami.7b16059.

Yu, C., Ma, X., Zhu, W., Wang, P., Miller, K. L., Stupin, J., Koroleva-Maharajh, A., Hairabedian, A. and Chen, S. (2019) “Scanningless and continuous 3D bioprinting of human tissues with decellularized extracellular matrix,” *Biomaterials*. Elsevier Ltd, 194, pp. 1–13. doi: 10.1016/j.biomaterials.2018.12.009.

Yu, J., Vodyanik, M. A., Smuga-Otto, K., Antosiewicz-Bourget, J., Frane, J. L., Tian, S., Nie, J., Jonsdottir, G. A., Ruotti, V., Stewart, R., Slukvin, I. I. and Thomson, J. A. (2007) “Induced pluripotent stem cell lines derived from human somatic cells,” *Science*. American Association for the Advancement of Science, 318(5858), pp. 1917–1920. doi: 10.1126/science.1151526.

Zaman, M. H., Trapani, L. M., Sieminski, A. L., MacKellar, D., Gong, H., Kamm, Alan Wells, R. D., Lauffenburger, D. A. and Matsudaira, P. (2006) “Migration of tumor cells in 3D matrices is governed by matrix stiffness along with cell-matrix adhesion and proteolysis,” *PNAS*, 103(29). doi: 10.1073/pnas.0604460103.

Zhang, B., Gao, L., Gu, L., Yang, H., Luo, Y. and Ma, L. (2017) “High-resolution 3D Bioprinting System for Fabricating Cell-laden Hydrogel Scaffolds with High Cellular Activities | Elsevier Enhanced Reader,” *Procedia CIRP*. Available at: https://reader.elsevier.com/reader/sd/pii/S2212827117305255?token=E37F485B05D36A6E7C88A6CA4156562986B51C812CE86EC96F82C5CA768BE0A03A43DFE4AB2D69A8EC0B4242369F6B9C (Accessed: May 11, 2020).

Zhang, B., Xue, Q., Li, J., Ma, L., Yao, Y., Ye, H., Cui, Z. and Yang, H. (2019) “3D bioprinting for artificial cornea: Challenges and perspectives,” *Medical Engineering and Physics*, 71, pp. 68–78. doi: 10.1016/j.medengphy.2019.05.002.

Zhang, B., Xue, Q., Hu, H. yi, Yu, M. fei, Gao, L., Luo, Y. chen, Li, Y., Li, J. tao, Ma, L., Yao, Y. feng and Yang, H. yong (2019) “Integrated 3D bioprinting-based geometry-control strategy for fabricating corneal substitutes,” *Journal of Zhejiang University: Science B*. Zhejiang University Press, 20(12), pp. 945–959. doi: 10.1631/jzus.B1900190.

Zhang, Y., Zhou, D., Chen, J., Zhang, X., Li, X., Zhao, W. and Xu, T. (2019) “Biomaterials based on marine resources for 3D bioprinting applications,” *Marine Drugs*. MDPI AG, p. 555. doi: 10.3390/md17100555.

Zhang, Y. S., Arneri, A., Bersini, S., Shin, S. R., Zhu, K., Goli-Malekabadi, Z., Aleman, J., Colosi, C., Busignani, F., Dell’Erba, V., Bishop, C., Shupe, T., Demarchi, D., Moretti, M., Rasponi, M., Dokmeci, M. R., Atala, A. and Khademhosseini, A. (2016) “Bioprinting 3D microfibrous scaffolds for engineering endothelialized myocardium and heart-on-a-chip,” *Biomaterials*. Elsevier Ltd, 110, pp. 45–59. doi: 10.1016/j.biomaterials.2016.09.003.

Zhong, J., Yang, Y., Liao, L. and Zhang, C. (2020) “Matrix stiffness-regulated cellular functions under different dimensionalities,” *Biomaterials Science*, 8(10), pp. 2734–2755. doi: 10.1039/C9BM01809C.

Zhou, H., Wang, Z., Cao, H., Hu, H., Luo, Z., Yang, X., Cui, M. and Zhou, L. (2019) “Genipin-crosslinked polyvinyl alcohol/silk fibroin/nano-hydroxyapatite hydrogel for fabrication of artificial cornea scaffolds—a novel approach to corneal tissue engineering,” *Journal of Biomaterials Science, Polymer Edition*. Taylor and Francis Inc., 30(17), pp. 1604–1619. doi: 10.1080/09205063.2019.1652418.

Zhou, Z., Long, D., Hsu, C. C., Liu, H., Chen, L., Slavin, B., Lin, H., Li, X., Tang, J., Yiu, S., Tuffaha, S. and Mao, H. Q. (2019) “Nanofiber-reinforced decellularized amniotic membrane improves limbal stem cell transplantation in a rabbit model of corneal epithelial defect,” *Acta Biomaterialia*. Acta Materialia Inc, 97, pp. 310–320. doi: 10.1016/j.actbio.2019.08.027.

Zhu, K., Chen, N., Liu, X., Mu, X., Zhang, W., Wang, C. and Zhang, Y. S. (2018) “A General Strategy for Extrusion Bioprinting of Bio-Macromolecular Bioinks through Alginate-Templated Dual-Stage Crosslinking,” *Macromolecular Bioscience*. Wiley-VCH Verlag, 18(9), p. e1800127. doi: 10.1002/mabi.201800127.

Zhu, W., Qu, X., Zhu, J., Ma, X., Patel, S., Liu, J., Wang, P., Lai, C. S. E., Gou, M., Xu, Y., Zhang, K. and Chen, S. (2017) “Direct 3D bioprinting of prevascularized tissue constructs with complex microarchitecture,” *Biomaterials*. Elsevier Ltd, 124, pp. 106–115. doi: 10.1016/j.biomaterials.2017.01.042.

Zidarič, T., Milojević, M., Gradišnik, L., Kleinschek, K. S., Maver, U. and Maver, T. (2020) “Polysaccharide-based bioink formulation for 3D bioprinting of an in vitro model of the human dermis,” *Nanomaterials*. MDPI AG, 10(4). doi: 10.3390/nano10040733.

Zimmerman Jones, A. (2019) *What Is Viscosity in Physics?* Available at: https://www.thoughtco.com/viscosity-2699336 (Accessed: March 8, 2020).